# DESIGN AND PERFORMANCE ANALYSIS OF IMPROVED FREE SPACE OPTICAL COMMUNICATION SYSTEM FOR TURBULENT ATMOSPHERE

A Thesis Submitted
In Partial Fulfillment of the Requirements
for the Degree of

## **DOCTOR OF PHILOSOPHY**

by

Rekha Rani (Roll No. 2K19/PHDEC/507)

**Under the Supervision of** 

Dr. N. Jayanthi Associate Professor, ECE Delhi Technological University

Dr. Anup Mandpura Assistant Professor, EE Delhi Technological University



**Department of Electronics and Communication Engineering** 

#### **DELHI TECHNOLOGICAL UNIVERSITY**

(Formerly Delhi College of Engineering) Shahbad Daulatpur, Main Bawana Road, Delhi-110042, India

June, 2025



# **DELHI TECHNOLOGICAL UNIVERSITY**

(Formerly Delhi College of Engineering) Shahbad Daulatpur, Main Bawana Road, Delhi-42

#### CANDIDATE'S DECLARATION

I Rekha Rani, Roll No. 2K19/PHDEC/507 hereby certify that the work which is being presented in the thesis titled "Design and Performance Analysis of Improved Free Space Optical Communication System for Turbulent Atmosphere" in partial fulfilment of the requirement for the award of the Degree of Doctor of Philosophy, submitted in the Department of Electronics and Communication Engineering, Delhi Technological University is an authentic record of my own work carried out during the period from January 2020 to June 2025 under the supervision of Dr. N. Jayanthi and Dr. Anup Mandpura.

The matter presented in the thesis has not been submitted by me for the award of any other degree of this or any other institute.

Candidate's Signature

This is to certify that the student has incorporated all the corrections suggested by the examiners in the thesis and the statement made by the candidate is correct to the best of our knowledge.

**Signature of Supervisor(s)** 

**Signature of External Examiner** 



# **DELHI TECHNOLOGICAL UNIVERSITY**

(Formerly Delhi College of Engineering) Shahbad Daulatpur, Main Bawana Road, Delhi-42

#### **CERTIFICATE BY THE SUPERVISOR(s)**

Certified that <u>Rekha Rani</u> (2K19/PHDEC/507) has carried out her search work presented in this thesis entitled <u>"Design and Performance Analysis of Improved Free Space Optical Communication System for Turbulent Atmosphere"</u> for the award of <u>Doctor of Philosophy</u> from Department of Electronics and Communication Engineering, Delhi Technological University, Delhi, under our supervision. The thesis embodies results of original work, and studies are carried out by the student herself and the contents of the thesis do not form the basis for the award of any other degree to the candidate or to anybody else from this or any other University/Institution.

Signature	Signature
(Dr. N. Jayanthi)	(Dr. Anup Mandpura)
(Associate Professor)	(Assistant Professor
Place: Delhi	Place: Delh
Date:	

#### **ABSTRACT**

With the proliferation of mobile devices, the demand for bandwidth has surged, while radio frequency (RF) spectrum resources are limited leading to a bottleneck in the traditional RF cellular networks. Additionally, existing backhaul network infrastructure often struggles to support the increased data traffic. Researchers have proposed to use optical fibers as a potential solution for alleviating the backhaul load congestion. However, as the number of cells becomes very large, networks can still suffer from the limited optical fiber installations which are very costly and sometimes even restricted. To support these challenges, free space optics (FSO) technology emerges as an alternative solution to the RF links and optical fiber, since it is more flexible, license-free, power efficient, cost effective, and most importantly it increases the capacity of networks. However, its performance is affected by the atmospheric turbulence, adverse weather, and pointing errors. To improve reliability, dual-hop RF-FSO system and hybrid FSO/RF system are employed. In the dual-hop RF-FSO system, relays act as intermediate nodes between the source and the destination to extend coverage. In the hybrid FSO/RF system, both links operate simultaneously to transmit the same signal. Since if one link is degraded, ensuring continuous communication even if one link degrades.

Multiuser (MU) diversity has been widely exploited to alleviate the performance loss due to atmospheric turbulence induced fading. However, to efficiently allocate resources to multiple users, effective scheduling schemes are required to achieve substantial system performance. In the event, where users experience lower average signal-to-noise ratio (SNR), accessing channel resources becomes problematic, particularly in the presence of users enjoying comparatively higher average SNR levels. Consequently, the system may allocates resources to users with weaker channels to ensure their requirements are satisfied. However, such allocations do not contribute favorably to achieving optimum system performance. This situation introduces a conflict between the objectives of meeting fairness in user channel access and optimizing overall system performance.

Further, to enhance network capacity in next-generation systems, one way is to reduce the cell size. This reduction in cell dimensions brings about the challenge of co-channel interference (CCI), which can adversely affect system performance within these smaller cells. Another challenging problem in the wireless networks is assuming the perfect channel state information (CSI) of channel between the transmitter and receiver which is not possible to get perfect CSI in real time scenario. Therefore, this motivates the work done to address these technical challenges in this thesis.

The first part of this thesis analyzes the impact of turbulence on the performance of FSO system over Inverse Gaussian Gamma (IGG) distribution. The analytical formulations derives closed-form expressions for the outage probability (OP) and average bit error rate (ABER). The proposed work also provides valuable insights to enhance the system performance.

In the second part, the performance analysis of MU dual-hop RF-FSO systems is analyzed for cumulative distribution function based scheduling (CDFS) scheme under perfect CSI at both RF and FSO links. The performance is evaluated by deriving the closed-form expression for OP considering independent and non-identically distributed (i.n.i.d) CCI at relay. Moreover, expression for optimum power allocation and channel

access ratio (CAR) are evaluated to enhance outage performance. The CDFS scheme is used to promotes fairness and precise control over the CAR to improve the system performance.

In the third part, performance analysis of MU dual-hop RF-FSO systems is analyzed employing CDFS scheme under imperfect CSI at both RF and FSO links. The performance is evaluated by deriving the closed-form expression for OP. Moreover, expression for optimum power allocation and CAR are evaluated to enhance outage performance. We also compare the performance of the CDFS based system against greedy scheduling (GS), and proportional fairness scheduling (PFS) schemes.

In the fourth part, performance analysis of dual-hop MU RF-hybrid FSO/RF system is presented. Closed-form expressions for OP and ABER are derived under the influence of CCI at the relay. Moreover, expressions for optimum power allocation and CAR are evaluated to enhance outage performance.

In the final part of this thesis, performance of MIMO FSO and WDM FSO systems is presented in terms of BER and Quality factor. Since the involvement of complex function such as Meijer-G function and Fox-H function in the derivations, asymptotic expressions at high SNR are derived using elementary functions to provide engineering insights into system performance. The frameworks proposed in this work can be efficiently utilized in various wireless standards. It will be helpful for a communication engineer to design a wireless systems without performing extensive simulations or tedious experiments.

## DELHI TECHNOLOGICAL UNIVERSITY

DEL TECH \*

(Formerly Delhi College of Engineering) Shahbad Daulatpur, Main Bawana Road, Delhi-42

#### **ACKNOWLEDGEMENTS**

I would like to express my sincere gratitude to my supervisor, Dr. N. Jayanthi, for her invaluable guidance, insightful comments, and unwavering support throughout my research work. Her enthusiasm for research and thoughtful suggestions made the entire process both stimulating and enriching. Her encouragement and ability to remove hurdles along the way inspired me to strive for excellence and stay ahead of schedule. I am also deeply thankful for the excellent research environment she provided, which significantly contributed to the success of my work.

I am equally grateful to my Jt. supervisor, Dr. Anup Mandpura, whose invaluable support and enlightening guidance made this journey possible. His extensive knowledge, steadfast encouragement, and positive outlook greatly enhanced my research experience. Working under his mentorship has been an absolute pleasure, and I deeply appreciate his warm-heartedness, dedication, and continuous support throughout every step of my work. His energy, insights, and constructive suggestions have been truly inspiring.

I extend my sincere regards to HoD for his constant support. I wish to express my gratitude towards the DRC chairperson, the distinguished DRC members, and the esteemed faculty members for their valuable time and efforts throughout this journey.

I extend my heartfelt appreciation to my parents, my husband, my adorable son, and my entire family for their patience, love, and unwavering belief in me throughout this journey. Their sacrifices and understanding sustained me during my research work. Thank you for your unconditional support and for making this possible.

Finally, and most importantly, I offer my deepest gratitude to God Almighty for His favor, grace, and protection throughout my research work. His boundless blessings and wonderful grace carried me through every challenge and enabled me to complete this research successfully.

Rekha Rani

# TABLE OF CONTENTS

De	eclara	tion	i
C	ertific	ate	ii
Al	bstrac	t	iii
A	cknow	eledgments	v
Тa	able o	f Contents	vi
Li	ist of '	Tables	ix
Li	ist of l	Figures	X
Li	ist of S	Symbols	xiii
Al	bbrev	iations	xiv
1	CH	APTER 1: INTRODUCTION	1
	1.1	RF Communication	1
		1.1.1 Challenges of RF communication	1
	1.2	FSO Communication System	2
		1.2.1 Challenges of FSO communication system	3
	1.3	Channel Model	5
		1.3.1 Channel Models for RF link	5
		1.3.2 Channel Models for FSO link	6
	1.4	Mitigation Techniques	9
		1.4.1 Dual-hop System	9
		1.4.2 Hybrid System	11
		1.4.3 Multiuser Diversity	13
		1.4.4 Different Diversity Schemes	14
	1.5	Research Motivation	16
	1.6	Thesis Organization	17
2	CH	APTER 2: LITERATURE SURVEY	19
	2.1	Literature Survey on FSO communication System	19

	2.2	Literature Survey on MU Dual-hop RF-FSO system with Perfect CSI	21
	2.3	Literature Survey on MU Dual-hop RF-FSO system with Imperfect CSI	23
	2.4	Literature Survey on hybrid FSO/RF Communication System	25
	2.5	Research Gaps	26
	2.6	Objectives and Scope of the Work	27
3	CHA	APTER 3: PERFORMANCE ANALYSIS OF FSO SYSTEM OVER	
	INV	ERSE GAUSSIAN GAMMA TURBULENCE CHANNEL	28
	3.1	System Model and Statistical Characteristics	28
	3.2	Amount of Fading	30
	3.3	Comparison with Previous Models and Experimental Data	31
	3.4	Performance Metrics	33
		3.4.1 Exact and Asymptotic Outage Probability	33
		3.4.2 Upper Bound on Outage Probability	34
		3.4.3 Exact and Asymptotic Average Bit Error Probability	34
	3.5	Results and Discussion	37
4	CHA	APTER 4: PERFORMANCE ANALYSIS OF MULTIUSER DUAL-	
	HO	P RF-FSO SYSTEMS WITH PERFECT CSI	43
	4.1	System and Channel Model	43
		4.1.1 System Model	43
		4.1.2 Channel Model	45
	4.2	Performance Metrics	46
		4.2.1 Outage Probability	46
		4.2.2 Asymptotic Outage Performance	48
	4.3	Optimum Performance Analysis	50
		4.3.1 Optimal Power Allocation	50
		4.3.2 Optimal CAR Allocation	51
	4.4	Simulation Results	52
5	CHA	APTER 5: PERFORMANCE ANALYSIS OF MULTIUSER DUAL-	
	HO	P RF/FSO SYSTEMS WITH IMPERFECT CSI	57
	5.1	System and Channel Model	57
	5.2	Outage Probability	61
	5.3	Optimum Performance Analysis	65
		5.3.1 Optimal Power Allocation	65
		5.3.2 Optimal CAR Allocation	66
	5.4	Simulation Results	67
6	CHA	APTER 6:PERFORMANCE ANALYSIS OF DUAL-HOP MULTIUSEI	R
	RF-	HYBRID FSO/RF SYSTEM	72
	6.1	System and Channel Model	72
		6.1.1 Channel Model	74
	6.2	Performance Metrics	76
		6.2.1 Outage Probability	76
		6.2.2 Asymptotic Outage Probability	77

Li	st of 1	Publications 1	118
Aj	pend	lices 1	113
Re	eferen	ces 1	100
	8.3	Social Impact	100
	8.2	Future Scope	99
	8.1	Conclusion	98
8	CHA	APTER 8: CONCLUSION, FUTURE SCOPE AND SOCIAL IMPACT	98
	7.2	Results and Discussion	94
	7.1	System Model	90
	TEN		90
7	_	APTER 7: MIMO-FSO AND WDM-FSO COMMUNICATION SYS-	
	6.4	Simulation Results	84
		6.3.2 Optimum Power Allocation	83
		6.3.1 Optimal CAR Assignments	82
	6.3	Optimum Performance Analysis	81
		6.2.3 Average Bit Error Rate	79

# LIST OF TABLES

2.1	Literature survey on FSO communication system	20
2.2	Literature Survey for Dual-hop System with Perfect Channel Estima-	
	tion and Scheduling Schemes	23
2.3	Literature Survey for Dual-hop System with Imperfect Channel Esti-	
	mation and Scheduling Schemes	24
2.4	Literature survey for Hybrid FSO/RF Communication System	26
3.1	Comparison with Previous Models and Experimental Data	33
3.2	Truncation Accuracy of Summation Limits for OP and ABER	37
5.1	Truncation accuracy of summation limit	68
7.1	Real-Time data for Leh, Ladakh for the year 2020 [134]	91
7.2	Parameters Values for Proposed Systems	92
7.3	Measured rainfall attenuation, fog attenuation, dry snow attenuation,	
	total attenuation, and refractive index structure parameter, $C_n^2$ for Leh,	
	Ladakh during the year 2020	93
7.4	Measured parameters such as geometric loss ( $L_{\rm geo\ loss}$ ), Rytov variance	
	$(\sigma^2)$ , and scintillation loss with varying channel length $R$	94
7.5	BER of MIMO FSO and WDM FSO communication systems	97

# LIST OF FIGURES

1.1	FSO Communication System	3
1.2	Dual-hop RF-FSO system for uplink scenario	10
1.3	Dual-hop FSO-RF system for downlink scenario	10
1.4	Hybrid FSO/RF system	12
1.5	Relay-assisted hybrid RF/dual-hop RF-FSO system	12
1.6	Relay-assisted hybrid FSO/dual-hop RF-FSO system	13
1.7	Relay-assisted hybrid dual-hop RF-FSO/dual-hop FSO-RF system	13
3.1	System model of the considered communication system	29
3.2	Comparison between IGG distribution, $\mathcal F$ distribution, and IGGG dis-	
	tribution in the context of experimental data provided in [115, Figure	
	19]	32
3.3	Comparison between IGG distribution, $\mathcal{F}$ distribution, and IGGG dis-	
	tribution in the context of experimental data provided in [ [115, Figure	20
2.4	21]	32
3.4	turbulence conditions	38
3.5	OP for different atmospheric turbulence conditions with $\gamma_{th} = 0$ dB and	30
5.5	D = 10mm	38
3.6	OP for different thresholds, $\gamma_{th}$ under strong turbulence conditions	39
3.7	OP for different aperture, D under strong turbulence conditions with	
	$\gamma_{th}$ = 0 dB	39
3.8	ABER for different atmospheric turbulence conditions with BPSK mod-	
• •	ulation and $D = 10$ mm	40
3.9	ABER for different aperture, $D$ under strong turbulence conditions with	4.0
2.10	BPSK modulation.	40
3.10	ABER for various modulation schemes under strong turbulence condi-	11
3.11	tions with $D = 10$ mm	41
3.11	tions with $D = 10$ mm	41
4.1	System model of MU relay system with i.n.i.d CCI	44
4.2	OP versus $\gamma_t$ over i.n.i.d CCI and data rates considering GS based sys-	<i></i>
4.2	tem under strong turbulence condition fixed $\beta = 0.5.$	53
4.3	OP versus $\gamma_t$ over i.n.i.d CCI considering PFS based system under strong turbulence condition for $\rho = 2$ , $\beta = 0.5$	53
	strong turbulence condition for $\rho = 2, \rho = 0.5$	33

4.4	OP versus $\gamma_t$ over i.n.i.d CCI considering CDFS based system under	
	strong turbulence condition fixed at $\rho$ = 1, $\beta=0.5$ and $\upsilon_m=[0.6,0.3,0.1]$	. 54
4.5	OP versus $\gamma_t$ under different turbulence conditions considering CDFS	
	based system fixed at $P_t/P_{I_{n,r}}$ = [20, 25, 30] (dB), $\rho$ = 1, $\beta$ = 0.5 and	
	$v_m = [0.6, 0.3, 0.1]$	54
4.6	OP versus power allocation coefficient considering CDFS based system	
	under moderate turbulence condition fixed at $v_m = [1/3, 1/3, 1/3]$ .	55
4.7	OP versus $\gamma_t$ over equal power and optimized power allocation, consid-	
	ering CDFS based system under moderate turbulence condition fixed	
4.0	at $v_m = [1/3, 1/3, 1/3]$	55
4.8	OP versus $\gamma_t$ over equal channel access ratio and optimized channel	
	access ratios for both GS and CDFS based systems under moderate	~ ~
4.0	turbulence condition fixed at $\beta = 0.5$	56
4.9	Comparison of channel access ratio, $\boldsymbol{v}_m$ for different scheduling schemes.	56
5.1	System model of a MU dual-hop RF-FSO system in the presence of	
	interferers under channel imperfection	58
5.2	OP versus $\gamma_t$ over different values of $\zeta_{\rm SR}$ considering CDFS based sys-	
	tem fixed at $P_t/P_{I_{n,r}}$ = [20, 25, 30] (dB) under strong turbulence con-	
	dition fixed at $\rho=1, \zeta_{\rm RD}=0.8, \sigma_{\epsilon}^2=0.5, \beta=0.5,$ and $\upsilon_m=0.5$	
	[0.6, 0.3, 0.1]	68
5.3	OP versus $\gamma_t$ over different values of $\zeta_{RD}$ considering CDFS based	
	system fixed at $P_t/P_{I_{n,r}}$ = [20, 25, 30] (dB) under strong turbulence	
	condition fixed at $\rho = 1$ , $\zeta_{RF} = 0.98$ , $\sigma_{\epsilon}^2 = 0.5$ , $\beta = 0.5$ , and	
	$v_m = [0.6, 0.3, 0.1]$	69
5.4	OP versus $\gamma_t$ under different turbulence conditions considering CDFS	
	based system fixed at $P_t/P_{I_{n,r}}$ = [20, 25, 30] (dB), $\rho=1,\sigma_\epsilon^2=0.5,$	
	$\beta=0.5$ and $\upsilon_m=[0.6,0.3,\overset{\text{a.i.}}{0}.1].$	69
5.5	OP versus power allocation coefficient considering CDFS based sys-	
	tem under moderate turbulence condition fixed at $\sigma_{\epsilon}^2=0.5$ and $\upsilon_m=$	
	[1/3, 1/3, 1/3]	70
5.6	OP versus $\gamma_t$ over equal power and optimized power allocation, consid-	
	ering CDFS based system under moderate turbulence condition fixed	
	at $\sigma_{\epsilon}^2 = 0.5$ and $v_m = [1/3, 1/3, 1/3]$	71
5.7	OP versus $\gamma_t$ with equal and optimized channel access ratio for both GS	
	and CDFS based systems under moderate turbulence condition fixed at	71
	$\sigma_{\epsilon}^2=0.5$ and $\beta=0.5$	71
6.1	Dual-hop MU RF and hybrid FSO/RF system with i.n.i.d CCI	73
6.2	OP versus $\gamma_t$ over i.n.i.d CCI considering CDFS based system under	
	strong turbulence condition fixed at $P_I$ = 5 dB, $\beta$ = 0.5, $\omega$ = 1.33 and	
	$v_m = [0.6, 0.3, 0.1]$	85
6.3	OP versus $\gamma_t$ over i.n.i.d CCI considering CDFS based system under	
	strong turbulence conditions fixed at $\gamma_{th}$ = 0 dB, $\beta$ = 0.5, $\omega$ = 1.33 and	
	$v_m = [0.6, 0.3, 0.1]$	85

6.4	OP versus $\omega$ over i.n.i.d CCI considering CDFS based system under	
	different turbulence conditions fixed at $\gamma_{th}$ = 0 dB, $P_I$ = 5 dB, $\beta$ = 0.5,	
	and $v_m = [0.6, 0.3, 0.1]$	86
6.5	OP versus $\gamma_t$ under strong turbulence conditions fixed at $\gamma_{th}$ = 0 dB,	
	$P_I$ = 5 dB, $\beta = 0.5$ , $\omega = 1.33$ and $v_m = [0.6, 0.3, 0.1]$ . We have	
	set, $m_{1,r}=2, m_{2,r}=3, m_{3,r}=3, m_{\rm r,d}=2, m_I=6.23027, \Omega_I=6.23027$	
	$0.4664$ for i.n.i.d Nakagami- $m$ fading, $m_{1,r}=2, m_{2,r}=3, m_{3,r}=1$	
	$3, m_{\rm r.d}=2, m=2.5, \Omega=0.2624$ for i.i.d Nakagami- <i>m</i> fading and	
	$m_{1,r}=m_{2,r}=m_{3,r}=m_{\mathrm{r,d}}=m=1, \Omega=0.2624$ for i.i.d Rayleigh	
	fading	86
6.6	ABER versus $\gamma_t$ for different modulations under strong turbulence con-	
	ditions fixed at $\beta=0.5, \omega=1.33$ and $\upsilon_m=[0.6,0.3,0.1].$	87
6.7	OP versus power allocation coefficient considering CDFS based system	
	under different turbulence conditions and pointing errors at $\gamma_{th} = 0$ dB,	
	$P_I$ = 10 dB, and $v_m = [1/3, 1/3, 1/3]$	87
6.8	OP versus $\gamma_t$ over equal power and optimized power allocation con-	
	sidering CDFS based system under different turbulence conditions and	
	pointing errors at $\gamma_{th}$ = 0 dB, $P_I$ = 10 dB, and $v_m = [1/3, 1/3, 1/3]$ .	88
6.9	OP versus $\gamma_t$ over equal channel access ratio and optimized channel ac-	
	cess ratios for CDFS based systems under strong turbulence condition	
	fixed at $\beta = 0.5$ , $\omega = 1.33$ . We have set, $m_{1,r} = 2, m_{2,r} = 3, m_{3,r} =$	
	$3, m_{\rm r,d}=5, m_I=6.23027, \Omega_I=0.4664$ for i.n.i.d Nakagami- $m$ fading.	88
7.1	Proposed MIMO-FSO communication system	91
7.2	Proposed WDM-FSO communication system	91
7.3	Bit error rate versus channel length	95
7.4	Bit error rate versus data rate	95
7.5	Quality factor versus data rate	95
7.6	Bit error rate versus channel length at a data rate of 5Gb/s	96
7.7	Bit error rate versus data rate at channel length of 4km	96
7.8	Quality factor versus data rate at channel length of 4km	97
7.9	BER versus transmitted power at channel length of 3km	97

## **List of Symbols**

 $C\mathcal{N}(0,\sigma^2)$  Complex Gaussian Distribution with 0 mean and  $\sigma^2$  variance

 $\Gamma(.)$  Gamma Function

 $K_v(.)$  Second kind Modified Bessel Function with order v

 $G_{p,q}^{m,n}$  Meijer-G function

U(.;.;.) KummerU Function

 $\mathbb{E}(.)$  Expectation Operator

 $F^S$  CDF for Scheduling Scheme

 $F^C$  Complementary CDF

W(.) Lambert W Function

ln(.) Natural Logrithmic Function

Ψ Tricomi Confluent Hypergeometric Function

 $H^{m_1,n_1:m_2,n_2:m_3,n_3}_{p_1,q_1:p_2,q_2;p_3,q_3}$  Bivariate Fox-H Function

#### **List of Abbreviations**

5G Fifth Generation

ABEP Average Bit Error Probability

ABER Average Bit Error Rate

AF Amplify and Forward

AOF Amount of Fading

AWGN Additive White Gaussian Noise

B5G Beyond 5G

BPSK Binary Phase Shift Keying

CAR Channel Access Ratio

CBFSK Coherent Binary Frequency Shift Keying

CCI Co-channel Interference

CDF Cumulative Distribution Function

CDFS Cumulative Distribution function based Scheduling

CSI Channel State Information

DD Direct detection

DF Decode and Forward

DFSK Differential Frequency Shift Keying

DGG Double Generalized Gamma

DW Double Weibull

DPSK Differential Phase Shift Keying

EC Ergodic Capacity

EGC Equal Gain Combining

EW Exponentiated Weibull

FSO Free-space optics

GG Gamma-Gamma

GS Greedy Scheduling

HD Heterodyne Detection

HS Hard Switching

IG Inverse Gaussian

IGG Inverse Gaussian Gamma

IGGG Inverted Gamma Gamma- Gamma

IGIGG Inverse Gamma/Inverse Gamma/Gamma

IGIGGG Inverse Gamma/Inverse Gamma/Gamma/Gamma

IM/DD Intensity Modulation Direct-Detection

i.n.i.d Independent but not Identically Distributed

IoT Internet of Things

IR Infrared

LED Light Emitting Diode

LN Log-Normal

LO Local Oscillator

LoS Line-of-Sight

MIMO Multi-Input Multi-output

MPSK Minimum Phase Shift Keying

MRC Maximum Ratio Combining

MSE Mean Squared Error

MU Multi-User

NOMA Non-Orthogoanl Multi-Access

OFDM Orthogonal Frequency-Division Multiplexing

OOK On-Off Keying

OP Outage Probability

PD Photodiode

PDF Probability Density Function

PFS Proportional Fairness Scheduling

PPM Pulse Position Modulation

PSK Phase Shift Keying

QAM Quadrature Amplitude Modulation

QPSK Quadrature Phase Shift Keying

RF Radio Frequency

RV Random Variable

SC Selection Combining

SIC Successive Interference Cancellation

SIM Subcarrier Intensity Modulation

SIMO Single-Input Multi-output

SINR Signal-to-Interference-Noise Ratio

SNR Signal-to-Noise Ratio

# Chapter 1

# Introduction

This chapter briefly explained the overview of wireless communication systems, outlines the key challenges, discusses various mitigation techniques followed by motivation.

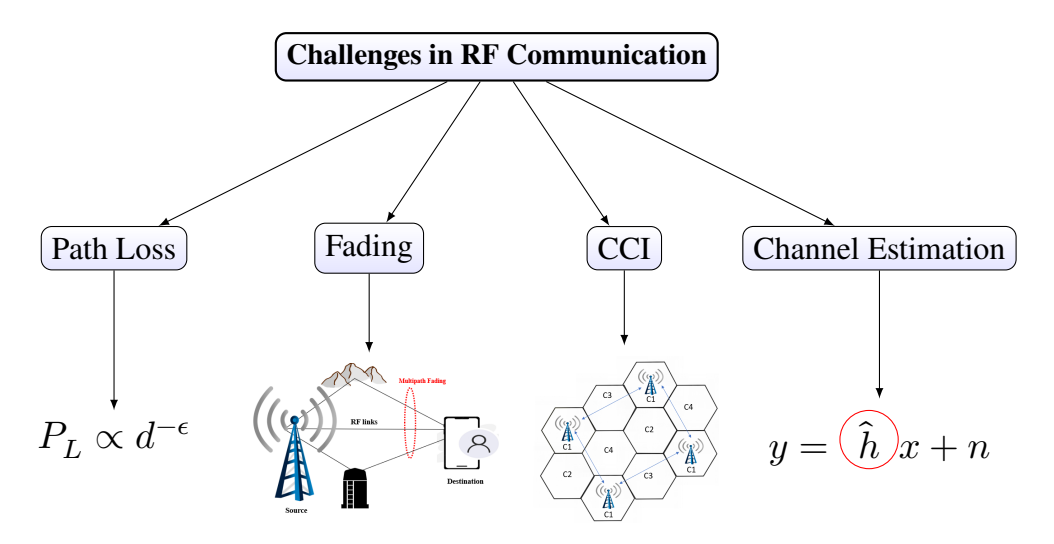
#### 1.1 RF Communication

The rapid advancement of wireless technology has increased pressure on the already scarce RF spectrum, necessitating the exploration of alternative solutions. As per the Cisco Annual Internet Report (2018–2023), there were 3.9 billion internet users globally (51% of the population) in 2018, which is projected to increase to 5.3 billion(66%) by 2023 [1]. This surge in telecom network data traffic has exacerbated radio frequency (RF) spectrum congestion. Further, RF signals are highly affected by unpredicatable wireless channel characteristics such as pathloss, multipath fading, interference and channel estimation error.

## 1.1.1 Challenges of RF communication

- 1. Pathloss is a large-scale propagation phenomenon that describe the reduction in the signal power over long distances. It is a deterministic function, typically modeled based on distance d with a general expression  $P_L \propto d^{-\epsilon}$ , where  $\epsilon$  denotes the path loss exponent. As distance increases, signal power reduces significantly due to path loss.
- 2. RF links are susceptible to multipath fading, which occurs when transmitted signals reflect off objects like buildings, the ground, or trees and arrive at the receiver via multiple paths. These signal may have different delays and phases, causing constructive or destructive interference that results to rapid fluctuations in the received signal strength. The statistical behaviour of such fading depends on the environment. Rayleigh distribution is used in scenarios with rich scattering and no direct line-of-sight (LoS), while Rician distribution models environment where a dominant LoS component is present.

- 3. Co-channel interference (CCI) arises when multiple transmitters share the same frequency band, leading to a reduction in the signal-to-interference-plus-noise ratio (SINR) and a subsequent degradation in overall system performance.
- 4. Channel estimation error is the deviation between the true channel parameters and their estimates derived through channel estimation techniques. It results from factors such noise, interference, fading, and inherent limitations of estimation algorithms, ultimately leading to degrading performance in wireless communication systems.



## **1.2** FSO Communication System

Wireless communication has emerged as a basic life commodity for everyone and has taken a prime spot in connecting the entire world across the borders under its own limitations. With continuous technological advancements and the fast-growing demand for high data rates, wireless communication often faces scarcity of RF spectrum and reaching out its limits. Hence, the replenishment of spectrum scarcity has become a primary research concern in the wireless communication domain. In an attempt to overcome the spectrum crunch and provide high data throughput, free-space optics (FSO) technology has been introduced as a possible solution for 5G and beyond cellular networks with a cost-efficient framework. FSO technology, akin to fiber optics, transmits data via a narrow optical beam powered by a laser or light-emitting diode (LED) through a LoS path between transmitter and receiver across several kilometers. Unlike RF technology, FSO deployment does not require government licensing. Once LoS is established, the FSO transceiver can be easily installed without the need for intermediate devices, enabling seamless and interference-free transmission Also, FSO technology supports high data rates similar to fiber technology but at a meager cost as digging up of fiber is not required in FSO. Operating at wavelengths between 850 nm to 1550 nm, FSO systems offers benefits such as license-free operation, high data rates, rapid deployment, low maintenance cost, and high security [2]. FSO applications include fiber backup, interbuilding connectivity, drone-assisted emergency links, border surveillance and disaster recovery [3]. It is also deployed in satellite communications, and deep-space missions due to its compact and power-efficient transceivers [4]. For instance, the United Kingdom-based television broadcaster BBC has deployed FSO connections between studios established in South Africa to live telecast of FIFA football World Cup 2010. At present, several companies worldwide including Canon (Japan), Cassidian (Germany), fSONA (Canada), GeoDesy (Hungary), Laser ITC (Russia), LightPointe Communications (USA), MRV (USA), Northern Hi-Tec (UK), Novasol (USA), Omnitek (Turkey), Plaintree Systems (Canada), and Wireless Excellence (UK) have developed commercial FSO products.

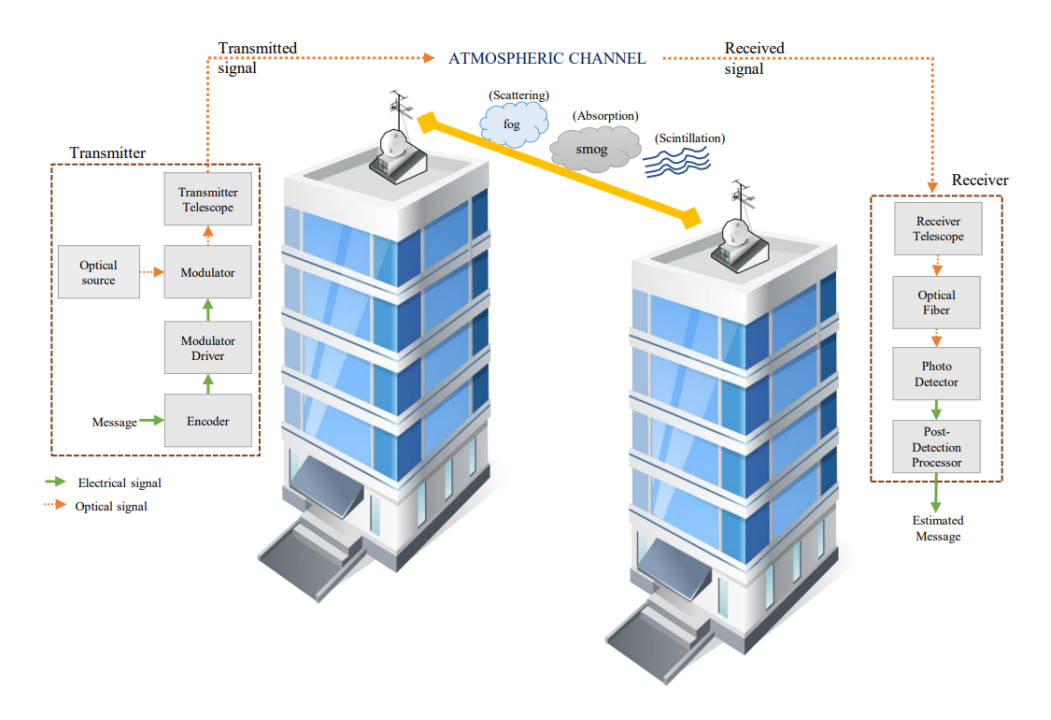


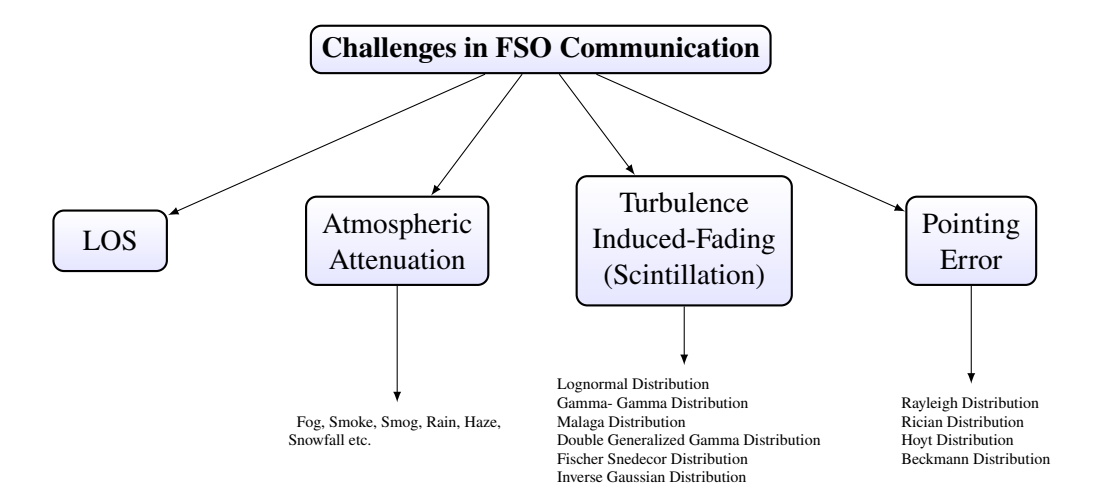
Figure 1.1: FSO Communication System.

As depicted in Fig. 1.1, a laser source transmits information to the optical receiver equipped with a photo-detector, through a channel affected by atmospheric turbulence. The photo-detector measures the instantaneous power of received laser beam using intensity modulation/direct detection (IM/DD) or heterodyne detection (HD). In IM/DD, the photo-detector directly senses the instantaneous power of the modulated optical signals, while, in HD, received signal is mixed with the local oscillator before detection, enabling enhanced sensitivity and performance.

### 1.2.1 Challenges of FSO communication system

1. Atmospheric losses: Atmospheric constituents such as gases, fog, smoke, and suspended particles significantly impair the visibility of the optical propagation path. These elements interact with the optical beam through absorption and scattering mechanism, leading to substantial attenuation and degradation of signal strength during transmission [5], [6].

- 2. Atmospheric turbulence: It, also known as scintillation, arises from random fluctuations in the refractive index due to variation in temperature, pressure, humidity, altitude and wind. These inhomogeneities form turbulent air pockets, or eddies, of varying sizes and refractive indices, through which an optical beam propagates. As a result, the beam experiences random temporal and spatial intensity and phase variations, leading to severe signal fading. The turbulence medium is typically characterized by three parameters: the inner scale (smallest eddy size), outer scale, and the refractive index structure parameter. These lead to fluctuations in irradiance i.e., the received optical signal power across the transmission path. To model these random irradiance variations, several statistical fading distribution have been proposed including log-Normal (LN) [7], Inverse Gaussian (IG) distribution [8], Gamma-Gamma (GG) distribution [9], [10],  $\alpha - \mu$  distribution [11], Double Weibull (DW) distribution [12], Exponentiated Weibull (EW) distribution [13], Log-normal Rician distribution (also, known as Beckmann) [14], Double Generalized Gamma (DGG) distribution [15], Malaga distribution ( $\mathcal{M}$ ) distribution [16], Fischer Snedecor ( $\mathcal{F}$ ) distribution [17], Inverted Gamma Gamma- Gamma (IGGG) distribution [18] and Inverse Gaussian Gamma (IGG) distribution [19].
- 3. Pointing Error: It significantly degrade the performance of FSO system due to misalignment between the transmitter and receiver apertures. These misalignments can arise from environmental factors such as wind, thermal expansion, and seismic activity. One approach to mitigate misalignment is by increasing the optical beam radius but it also lowers received power, increases bit error rate, and compromises link security. Hence, optimal beam width is crucial to balance geometric losses and system performance. Pointing errors are generally characterized by two components: Boresight Error: A fixed offset between the beam center and the detector center. Jitter: A random displacement in the position of the beam at the detector plane, typically modeled as a Gaussian process. Several statistical models have been proposed to describe pointing error effects in FSO systems, including the Rayleigh, Rician, and Hoyt distributions. These models consider factors such as non-zero boresight errors, beam width, detector aperture size, and i.i.d. Gaussian jitter in both elevation and horizontal directions [20], [21].



#### 1.3 Channel Model

Various statistical models are used to characterize the random fluctuations in both the RF link and FSO link, as brief discussed below.

#### 1.3.1 Channel Models for RF link

• Rayleigh Model: This model is commonly used to characterize the signal envelope in the NLoS conditions, where transmitted signal reaches the receiver through multiple scattered paths. This model is particularly suitable for dense urban environments with significant obstructions, such as buildings, that cause severe multipath propagation [22]. It is written as:

$$f(x) = \frac{x}{\Omega} e^{-\frac{x^2}{2\Omega}}, x \ge 0 \tag{1.1}$$

where,  $\Omega$  represents the average power (i.e. variance of x).

• **Rician Model:** This model applies to line-of-sight (LoS) scenarios, where a dominant direct signal path exists along with multiple scattered paths. It is suitable for environments with minimal obstructions, such as open rural or suburban areas, and accurately models situations where the direct component significantly contributes to the received signal [23]. It is represented as:

$$f(x) = \frac{2(K+1)x}{\Omega}e^{(-k-\frac{(K+1)x^2}{\Omega})}I_0\left(2\sqrt{\frac{K(K+1)}{\Omega}}x\right), x \ge 0, K \ge 0, \tag{1.2}$$

where, K is shape parameters,  $I_0(.)$  is the modified Bessel function of first kind with zero order.

 Nakagami-m Model: It is a flexible and generalized fading model that accurately represents both LoS and NLoS propagation scenarios. It can model various fading environments by adjusting the shape parameter m. It is provided in [24]:

$$f(x) = \frac{2m^m x^{2m-1}}{\Omega^m \Gamma(m)} e^{\left(-\frac{mx^2}{\Omega}\right)}, x \ge 0$$
(1.3)

where,  $m \ge 0.5$  represents the fading parameter. Special cases include the one-sided Gaussian distribution when  $m = \frac{1}{2}$ , and the Rayleigh distribution when m = 1.

•  $\kappa - \mu$  **Model:** This distribution models small-scale fading in LoS conditions where the signal consists of clusters of multipath waves, each having a dominant component. It is well-suited for non-homogeneous propagation environments with LoS scenarios and provides greater modeling flexibility compared to traditional fading models [25, Eq. (10)]. It is represented as:

$$f(x) = \frac{\mu(1+\kappa)^{\frac{\mu+1}{2}}}{\bar{x}\kappa^{\frac{\mu-1}{2}}e^{-\mu\kappa}} \left(\frac{x}{\bar{x}}\right)^{\frac{\mu-1}{2}} e^{-\left(\frac{\mu(1+\kappa)x}{\bar{x}}\right)} I_{\mu-1} \left(2\mu\sqrt{\frac{\kappa(1+\kappa)x}{\bar{x}}}\right) \tag{1.4}$$

where, parameter  $\kappa$  denotes the ratio of the power of the dominant component to that of the scattered waves within each cluster, whereas  $\mu$  signifies the number of multipath clusters.

#### 1.3.2 Channel Models for FSO link

• Log-Normal (LN) Model: It is a widely used statistical model for characterizing weak turbulence in FSO systems, where the received signal intensity exhibits a log-normal behavior due to small fluctuations in the refractive index. It is provided in [26]:

$$f(I) = \frac{1}{\sqrt{2\pi}\sigma I} e^{-\frac{(\ln(I) + \frac{\sigma^2}{2})^2}{2\sigma^2}}$$
(1.5)

where,  $\sigma^2$  is the log-irradiance variance of I.

• Negative Exponential(NE) Model: It is commonly used to model strong atmospheric turbulence in FSO systems. It represents the irradiance fluctuations under saturated turbulence conditions, where the received signal experiences deep fading due to severe scattering effects [27]. It is represented as:

$$f(I) = \frac{1}{\bar{I}}e^{-\frac{I}{\bar{I}}} \tag{1.6}$$

where,  $\bar{I}$  is the mean intensity.

• Inverse Gaussian(IG) Model: It is used to model irradiance fluctuations in FSO links, particularly under moderate turbulence conditions. It offers a flexible and accurate fit for intensity variations caused by random refractive index fluctuations

in the atmosphere [8] and expressed as:

$$f(I) = \sqrt{\frac{\alpha}{2\pi I^3}} e^{-\frac{\alpha(I-\mu)^2}{2\mu^2 I}},$$
 (1.7)

where,  $\mu$  is the mean intensity and  $\alpha$  is the fading parameter.

• **K distribution:** It is well-suited for strong turbulence in FSO links as it accurately reflects the effects of severe irradiance fading and its PDF is provided by [28]:

$$f(I) = \frac{2}{\Gamma(\alpha)} \alpha^{(\frac{\alpha+1}{2})} I^{(\frac{\alpha-1}{2})} K_{\alpha-1}(2\sqrt{\alpha I}) \tag{1.8}$$

where,  $K_a(.)$  denotes the modified Bessel function of second kind with order a.

• Gamma-Gamma Turbulence Model: it is widely used to characterize moderate to strong atmospheric turbulence for FSO links. It is expressed as [29]:

$$f(I) = \frac{2(\alpha\beta)^{\frac{\alpha+\beta}{2}}}{\Gamma(\alpha)\Gamma(\beta)} I^{\frac{\alpha+\beta}{2}-1} K_{\alpha-\beta} \left(2\sqrt{\alpha\beta I}\right), \quad I > 0$$
 (1.9)

where,  $\alpha$  and  $\beta$  are the turbulence parameters.

• Double Generalized Gamma distribution (DGG): The DGG model characterizes composite atmospheric turbulence by modeling the irradiance as the product of two independent Generalized Gamma-distributed random variables (RVs). It provides greater flexibility in fitting experimental data over a wide range of turbulence regimes. Its PDF is given by [15]:

$$\begin{split} f(I) &= \frac{\gamma_2 p p^{m_2 - 1/2} q^{m_1 - 1/2} (2\pi)^{1 - \frac{p + q}{2}}}{\Gamma(m_1) \Gamma(m_2)} I^{-1} \\ &\times G_{p + q, \, 0}^{0, \, p + q} \left[ \left( \frac{\Omega_2}{I^{\gamma_2}} \right)^p \frac{p^p q^q \Omega_1^q}{m_1^q m_2^p} \left| \begin{array}{c} \Delta(q:1 - m_1), \Delta(p:1 - m_2) \\ - \end{array} \right] \end{split} \tag{1.10}$$

where,  $G_{n,\,2}^{m,\,p}(.)$  is the MeijerG- function,  $rac{p}{q}=rac{\gamma_1}{\gamma_2}$  and  $\Delta(j:x)=rac{x}{j},rac{x+j}{j}..rac{x+j-1}{j}.$ 

• Exponentiated Weibull (EW) Model: The EW distribution is a flexible threeparameter model that extends the Weibull distribution to better fit irradiance fluctuations caused by atmospheric turbulence. It effectively models a wide range of fading conditions by adjusting its shape and scale parameters. This model captures both light and heavy tails of the distribution, making it suitable for various turbulence scenarios [13]. It is written as:

$$f(I) = \frac{\alpha\beta}{\eta} \left(\frac{I}{\eta}\right)^{\beta-1} \exp\left(-\left(\frac{I}{\eta}\right)^{\beta}\right) \left[1 - \exp\left(-\left(\frac{I}{\eta}\right)^{\beta}\right)\right]^{\alpha-1} \tag{1.11}$$

• **Double Weibull distribution:** It is a statistical model developed to characterize irradiance fluctuations caused by atmospheric turbulence in FSO systems. It is particularly useful under moderate to strong turbulence conditions, where single-component models like LN or Gamma-Gamma may not offer sufficient flexibility. Its PDF is given by [12]:

$$f(I) = \frac{\beta_2 k \sqrt{(kl)}}{(2\pi)^{\frac{l+k}{2}-1}} I^{-1} G_{k+l,0}^{0,k+l} \left[ \left( \frac{\Omega_2}{I^{\beta_2}} \right)^k k^k l^l \Omega_1^l \right] \frac{\Delta(l;0), \Delta(k;0)}{-}$$
(1.12)

where, 
$$\frac{l}{k} = \frac{\beta_2}{\beta_1}$$

• Malaga,  $\mathcal{M}$  Turbulence Model: It is a versatile statistical model which is suitable for weak to strong turbulence regimes. It encompasses several models, including LN, GG, and K-distribution. It is characterized by a combination of LoS and scattered components, It is provided by [30]:

$$f(I) = A \sum_{k=1}^{\beta} a_k I^{\frac{\alpha+k}{2}-1} K_{\alpha-k} \left( 2\sqrt{\frac{\alpha\beta I}{\gamma\beta + \Omega'}} \right), \quad I_a > 0 \tag{1.13}$$

where, 
$$A = \frac{2\alpha^{\alpha/2}}{\gamma^{1+\alpha/2}\Gamma(\alpha)} \left(\frac{\gamma\beta}{\gamma\beta+\Omega'}\right)^{\beta+\alpha/2}$$
 and  $a_k = \binom{\beta-1}{k-1} \frac{(\gamma\beta+\Omega')^{1-k/2}}{(k-1)!} \left(\frac{\Omega'}{\gamma}\right)^{k-1} \left(\frac{\alpha}{\beta}\right)^{k/2}$ 

• **Fisher Snedecor,**  $\mathcal{F}$  **Turbulence Model:** This model is suitable for modeling moderate to strong turbulence and provides a good fit to measured data due to its flexible structure. Its PDF is given by [17, Eq. (6)]:

$$f(I) = \frac{a^a (b-1)^b I^{a-1}}{\beta(a,b) \left(aI + (b-1)\right)^{a+b}}.$$
 (1.14)

where,  $\beta(.,.)$  denotes the beta function.

• **IGG distribution:** This model is a composite statistical model proposed to capture the irradiance fluctuations of optical signals propagating through moderate to strong atmospheric turbulence in FSO. It combines an IG distribution (modeling large-scale fluctuations) with a Gamma distribution (representing small-scale effects), providing a more flexible and accurate fit to empirical data than traditional models under certain turbulence conditions [19]. The PDF is written as:

$$f(I) = \sqrt{\frac{2\alpha}{\pi}} \frac{\beta^{\beta} I^{\beta - 1} e^{\alpha}}{\Gamma \beta} \left( 1 + \frac{2\beta I}{\alpha} \right)^{-\frac{\beta}{2} - \frac{1}{4}} K_{\beta + \frac{1}{2}} \left( \alpha \sqrt{1 + \frac{2\beta I}{\alpha}} \right), \quad h_{\text{IGG}} \ge 0$$

$$(1.15)$$

• **IGGG Distribution:** This model is introduced to characterize strong atmospheric turbulence. It represents large-scale irradiance fluctuations using the IG distribution and small-scale fluctuations using the GG distribution, making it well-suited

for modeling highly turbulent atmospheric conditions. The IGGG distribution provides better fitting accuracy over traditional models like GG or LN in certain turbulent regimes. Its PDF is given as [18, Eq. (31)]:

$$f(I) = \left(\frac{\sigma\mu}{\psi - 1}\right)^{\sigma} \frac{\Gamma(\sigma + \psi)\Gamma(\mu + \psi)}{\Gamma\sigma\Gamma\mu\Gamma\psi} I^{\sigma - 1} \ U(\sigma + \psi; 1 + \sigma - \mu; \frac{\sigma\mu}{\psi - 1}I) \tag{1.16}$$

where, U(.;.;.) is the confluent hypergeometric function of second kind.

## 1.4 Mitigation Techniques

To address the challenges in RF and FSO communication systems, several mitigation techniques have been employed, including relay-assited dual-hop system, hybrid FSO/RF system, multiuser diversity, and different diversity schemes (MIMO, combining schemes and aperture averaging).

## 1.4.1 Dual-hop System

FSO communication is an promising solution aimed at fulfilling the target date rate requirements for future 5G and beyond wireless networks. It provides a significantly high optical bandwidth, enabling communication with high data rates and operates within license-free bands [31]. Despite these features of FSO communication, its widespread adoption has been hindered by the unreliability of link, particularly in communication over large distances due to atmospheric turbulence [2]. RF based wireless communication system are commonly utilized as the primary means of connection but face challenges like limited spectrum, interference from frequency reuse, and significant propagation loss in the transmission medium [32]. Therefore, the combined RF and FSO systems indeed offer a promising solution by uniting the strength of both technologies. The combination of these two links provides a robust and reliable communication system that can operate in diverse environments. This hybrid approach leverages the strengths of both technologies to overcome the limitations typically encountered in wireless communication systems [33]. One outstanding feature is the enhanced speed compared to traditional RF/RF communication systems. This speed improvement is achieved by aggregating multiple RF data onto a single FSO link, thereby utilizing the maximum capacity available [34]. Additionally, both links operate on entirely different sets of frequencies, with inherent interference avoidance [35]. Several combined RF and FSO communication system are there such as Relay-assisted dual-hop RF-FSO, dual-hop FSO-RF systems, and a triple-hop RF-FSO-RF system. In an uplink scenario, an RF link in the backbone network transmits information to the relay, where the RF signal is multiplexed, converted to optical signal, and then forwarded to the destination via an FSO link. Conversely, in a downlink scenario, signal is transmitted via FSO link to base station, where it is demultiplexed, converted into RF signals, and then forwarded to the destination node. Such systems are applicable in emerging technologies like Google's Loon and Facebook's Aquila projects. Different relaying protocols have been created according to how the signal is carried from the relay such as amplify and forward (AF) [36], [37], decode and forward (DF) [38], [39], quantize-and-forward [40] and quantize-and-encode [41].

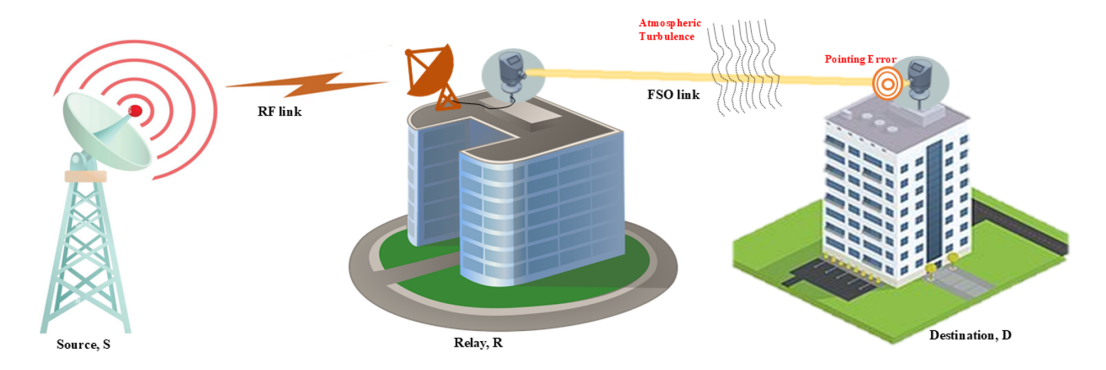


Figure 1.2: Dual-hop RF-FSO system for uplink scenario.

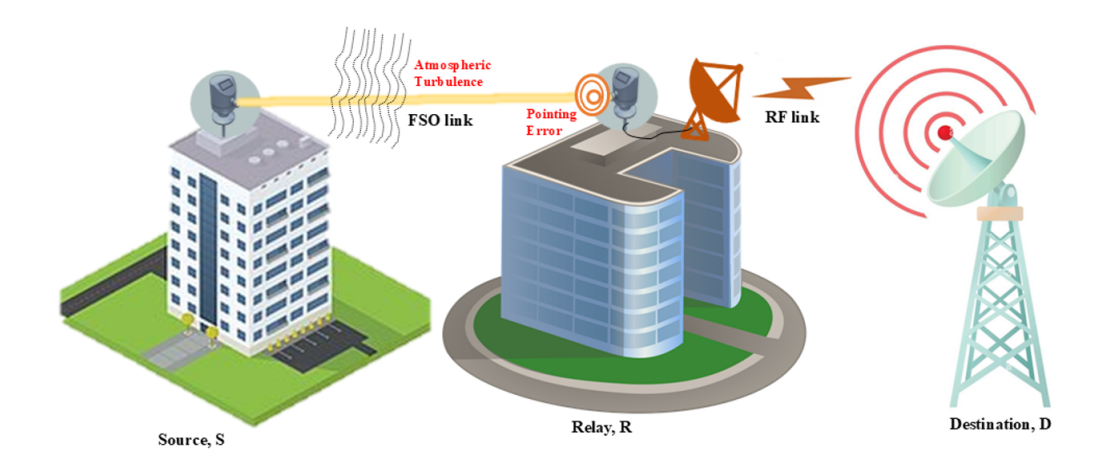
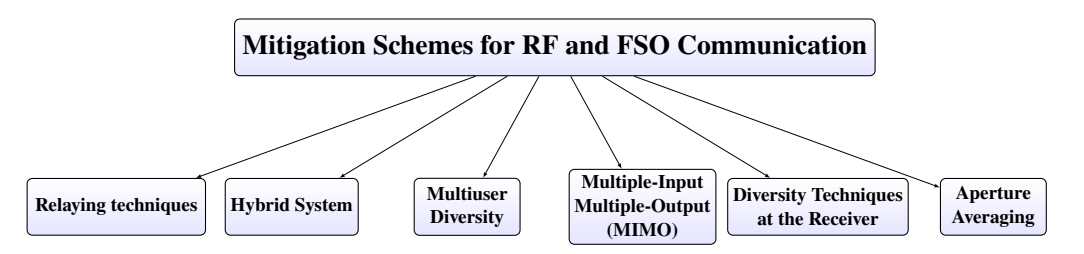


Figure 1.3: Dual-hop FSO-RF system for downlink scenario.

- Amplify and Forward (AF): In AF relaying, the relay amplifies and forwards the received signal from the source to the next node. However, this process also amplifies the noise along with the signal [42]. AF relays are classified into two types: Fixed Gain where relay gain remains constant throughout the transmission, regardless of channel variations [35] and Variable Gain in which relay gain adapts dynamically based on the instantaneous channel state of the source-to-relay link.
- **Decode and Forward:** The noise amplification issue in AF protocol led to the development of DF protocol. In DF protocol, the relay decodes the received signal, re-encodes it, and forwards it to the destination. By breaking the noise propagation chain, DF protocol provide more reliable communication. Although this protocol introduces additional complexity, the decoding step at the relay significantly enhances performance compared to AF protocol [39].

- Quantize-and-Forward: Under the Quantize-and-Forward protocol, firstly relay quantizes the received signal, and then forwards it over the FSO link to the destination [40].
- **Quantize-and-Encode:** Under this protocol, relay processes the received signal by first quantizing and then encoding it before transmission, which improves system robustness and performance [41].

Further, relay-assisted communication can be realized through serial relaying, parallel relaying, or a hybrid of both. Serial relaying is employed to extend link distance when LoS path is unavailable. In this approach, relays are located in series between the source and destination, enabling multi-hop transmission. In contrast, parallel relaying involves multiple independent serial relay paths operating simultaneously between the source and destination to enhance reliability.



## 1.4.2 Hybrid System

The hybrid system presents a compelling solution for next-generation wireless networks, leveraging the complementary strengths of both to provide high-capacity, robust, and resilient communication while mitigating their individual limitations. These systems are well-suited to meet the diverse and demanding requirements of 5G and beyonds, delivering enhanced connectivity and improved reliability across a broad range of applications. A major advantage of RF technology over FSO is its adaptability to mobile communications scenarios. FSO performance deteriorates significantly when one or both transceivers are in motion, primarily due to the challenge of maintaining accurate beam alignment. Although this can be addressed using advanced optical components such as gimbals, mirrors, or adaptive optics, the solution adds complexity and cost. Additionally, RF and FSO links exhibits differently sensitivities to atmospheric and weather conditions. FSO links are highly susceptible to fog, which can drastically impair signal quality, whereas RF links remain largely unaffected. Conversely, RF links, especially in the higher frequency bands, experience significant attenuation attenuation in the heavy rain, while rain has a relatively minor impact on FSO links compared to fog and haze [43].

A review of the literature on the hybrid FSO/RF systems reveals a variety of design strategies employed by researchers to motivate their combinations of FSO and RF. These include hybrid FSO/RF system [44], relay-assisted hybrid RF/dual hop RF-FSO system [45] [46], relay-assisted hybrid FSO/dual-hop RF-FSO system [47], relay-assisted hybrid RF/dual-hop RF-FSO system [46], relay-assisted hybrid dual- hop-RF-FSO/dual-hop FSO-RF [48] etc.

In Fig. 1.4, the FSO and RF links transmit data in parallel from source to destination.

The same information is modulated separately onto optical and RF carriers, producing two distinct signals that are transmitted via a light-emitting diode (LED) and an RF antenna, respectively. At the receiver, these signals are combined using various diversity techniques such as Selection Combining (SC), Maximal Ratio Combining (MRC), Equal Gain Combining (EGC), or Adaptive Combining. These methods significantly enhance link reliability and offer diversity gains by adapting to dynamic channel and weather conditions.

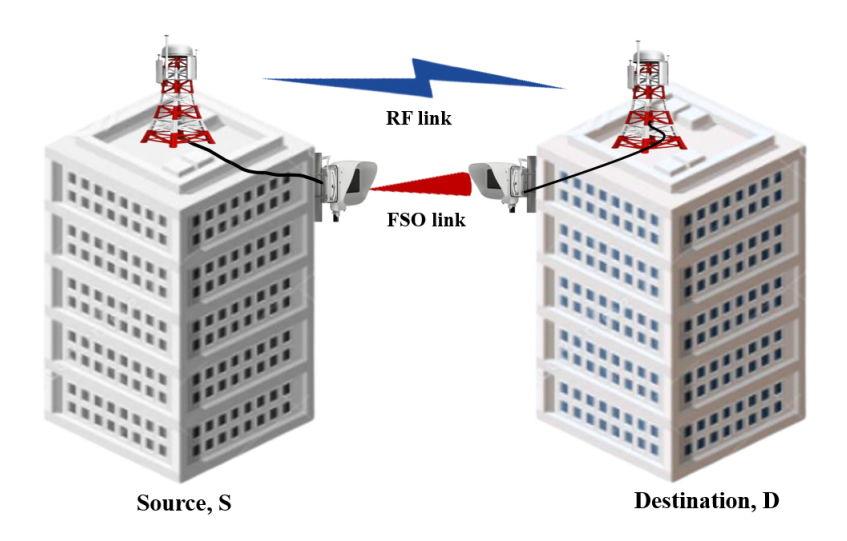


Figure 1.4: Hybrid FSO/RF system.

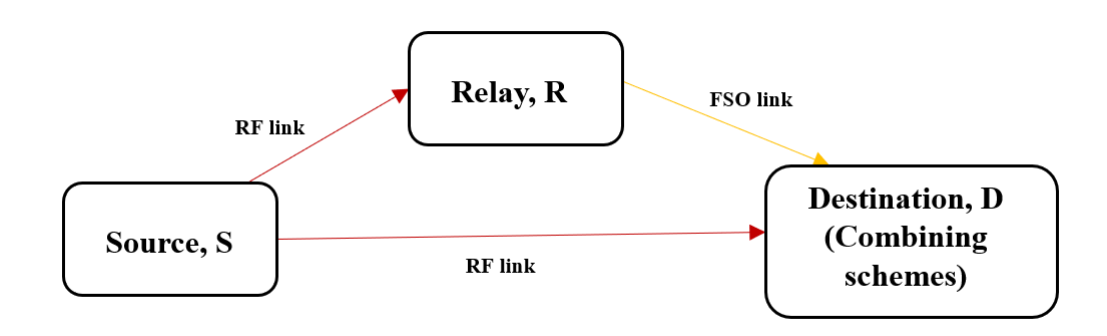


Figure 1.5: Relay-assisted hybrid RF/dual-hop RF-FSO system.

Fig.1.5, mobile users establish communication with the base station either via direct RF link or through dual-hop RF–FSO path. Conversely, Alternatively, in a hybrid FSO/dual-hop FSO–RF configuration, a primary FSO backhaul is supported by a dual-hop FSO–RF link for improved reliability, as shown in Fig. 1.6. Additionally, hybrid systems can be structured with two parallel dual-hop configurations such as dual-hop RF–FSO/dual-hop FSO–RF systems, as depicted in Fig. 1.7.

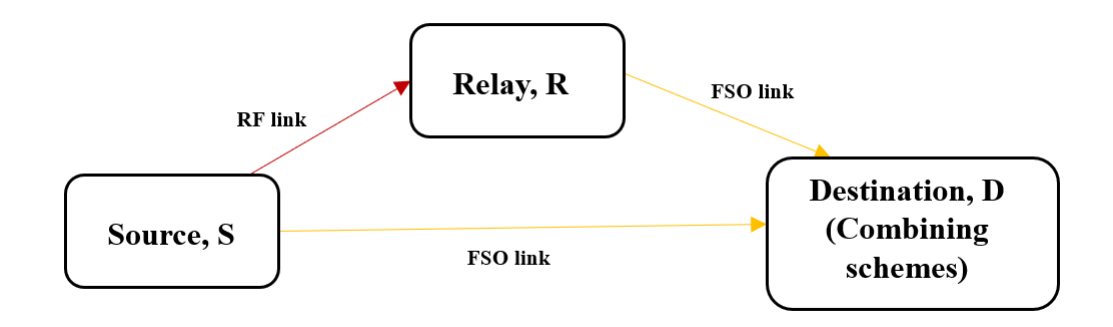


Figure 1.6: Relay-assisted hybrid FSO/dual-hop RF-FSO system.

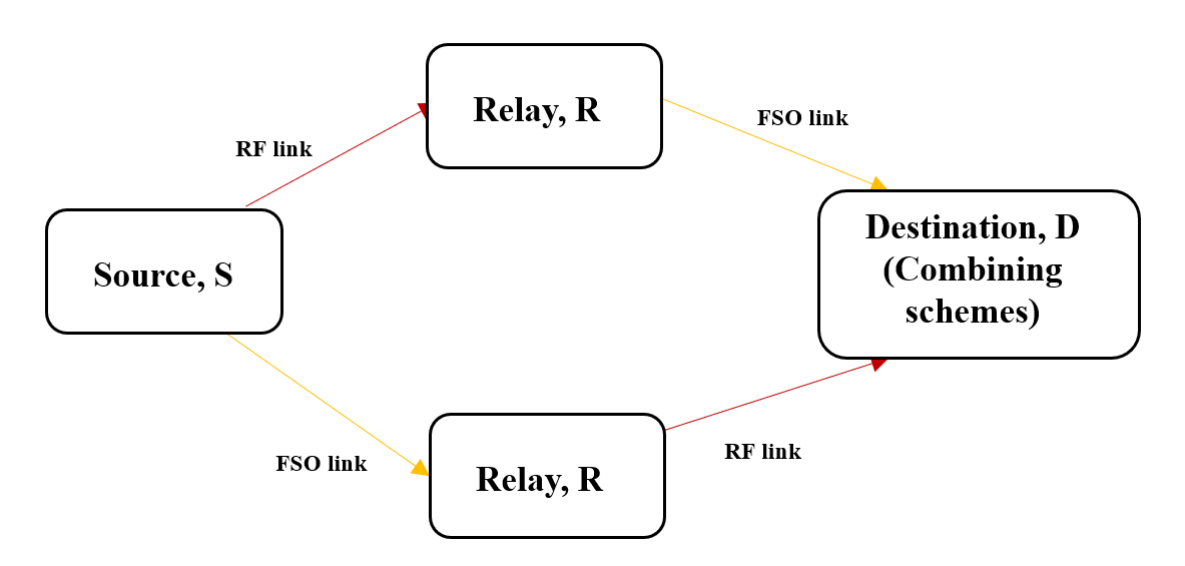


Figure 1.7: Relay-assisted hybrid dual-hop RF-FSO/dual-hop FSO-RF system.

## 1.4.3 Multiuser Diversity

With the exponential growth in mobile users and bandwidth-hungry applications, the existing RF spectrum has become increasingly overcrowded. Despite advancements in cellular infrastructure, mobile network operators continue to face challenges in delivering seamless and high-capacity services. Instead of solely relying on acquiring additional bandwidth, a more practical and sustainable solution is to optimize the utilization of the available spectrum. Scheduling is responsible for allocating resource among users by determining when and which user should transmit or receive, thereby significantly influencing bandwidth utilization efficiency. Various scheduling schemes are explored in the literature such as Round Robin Scheduling (RRS), Greedy Scheduling (GS), Proportional Fainess Scheduling (PFS), and Cumulative Distribution function based Scheduling (CDFS).

• Round Robin Scheduling (RRS): In the RRS, each user is selected in a predefined cyclic order regardless of the channel conditions. The user index for trasnmission at the nth time slot is given as [49]

$$m^* = (n \bmod M) + 1 \tag{1.17}$$

• Greedy Scheduling (GS): According to the greedy scheduling, mth user is selected based on the best instantaneous SNR for transmission. Hence, the mathematical expression for selecting the mth best user can be given as [50]:

$$m^* = \underset{m \in 1, 2, \dots, M}{\arg \max} (\Gamma_m)$$
 (1.18)

where,  $\Gamma_m$  is the instantaneous SNR of mth user.

• Proportional Fairness based Scheduling (PFS)

In the PFS scheme, mth user is chosen based on the maximum value of normalized SNR for the RF link. Therefore, mth user selection is expressed mathematically as [51]:

$$m^* = \arg \max_{m \in 1, 2, \dots, M} \left( \frac{\Gamma_m}{\bar{\Gamma}_m} \right). \tag{1.19}$$

where,  $\bar{\Gamma}_{\rm m} = \mathbb{E}(\Gamma_m)$ .

• Cumulative Distribution function based Scheduling (CDFS): The CDF-based scheduling system schedules the mth user based on the maximum CDF value for the RF link with channel access ratio (CAR), denoted as  $v_m$ . Therefore, mathematical expression for selecting the mth user is as follows:

$$m^* = \underset{m \in 1, 2 \dots M}{\arg \max} \left( F_{\Gamma_m}(x) \right)^{\frac{1}{\upsilon_m}}. \tag{1.20}$$

where, large value of  $\upsilon_m$  signifies that the mth user will be scheduled more as compared to the other users for data transmission and  $\sum_{m=1}^{M} \upsilon_m = 1$ . Specifically, ensuring that  $\upsilon_m = \frac{1}{M}$  to maintain fairness in channel access for all users.

## 1.4.4 Different Diversity Schemes

Receiver diversity is among the most effective methods for countering the negative impact of fading in wireless communication systems. The core principle of diversity lies in providing the receiver with multiple independently faded replicas of the transmitted signal. Such schemes are hybrid FSO/RF systems, Multiple-Input Multiple-Output (MIMO) systems and aperture averaging etc.

 Hybrid FSO/RF systems in which same data is sent over both the FSO and RF links. As these links are subject to independent fading characteristics owing to their distinct propagation media and significantly improves the system's resilience and reliability. To harness this diversity effectively, various combining strategies are employed at the receiver, including SC, MRC, EGC, and Adaptive Combining, each offering different trade-offs in terms of complexity and performance.

• Selection Combining: SC is basic diversity technique, where the receiver monitor all M branches and selects the one with the maximum instantaneous SNR, denoted by  $\Gamma_i$ , where  $(i \in \{1, 2, ..M\})$ . This method requires minimal processing complexity and performs well when at least one branch consistently offers a strong signal.

$$\Gamma_{SC} = \max(\Gamma_1, \Gamma_2, \dots, \Gamma_M) \tag{1.21}$$

• MRC: MRC is an optimal diversity combining technique that maximize the output SNR. This scheme involves co-phasing the signals from all M branches and combining them after weighting each by its corresponding SNR. This ensures that stronger signals contribute more to the final output, while weaker ones have a reduced impact. The total output SNR is the sum of the individual SNRs across all branches, offering the best possible performance among linear combining schemes.

$$\Gamma_{\text{MRC}} = \sum_{i=1}^{M} \Gamma_i \tag{1.22}$$

• EGC: EGC is a diversity combining technique where all received signals are co-phased and combined with equal weights, regardless of their individual SNRs. Unlike MRC, EGC does not require amplitude information of the channel, only the phase needs to be estimated. While EGC is less complex than MRC, it still achieves performance close to MRC, making it a practical choice for systems where reduced computational complexity is desired. The output SNR of EGC for M branches is given by:

$$\Gamma_{\text{EGC}} = \frac{\left(\sum_{i=1}^{M} \sqrt{\Gamma_i}\right)^2}{M} \tag{1.23}$$

• GSC: GSC combines the benefits of SC and MRC by selecting a best L out of M available branches based on their instantaneous SNR values and then coherently combining them using MRC. This approach provides a balance between performance and complexity. By utilizing only the strongest branches, GSC achieves near-optimal performance with reduced hardware and computational requirements compared to full MRC. These combining strategies play a vital role in enhancing the reliability, especially under conditions of channel fading and dynamic environmental variations.

$$\Gamma_{\text{GSC}} = \sum_{i=1}^{L} \Gamma_{(n)} \tag{1.24}$$

- where,  $\Gamma_{(n)}$  denotes the nth largest SNR among the M available diversity branches  $(i.e.\Gamma_{(1)} \geq \Gamma_{(2)} \geq ... \geq \Gamma_{(M)})$ .
- Adaptive combining: In this approach, the system primarily uses the FSO link for data transmission as long as its instantaneous SNR stays above a certain threshold. If the SNR drops below this level, the RF link is turned on to maintain a stable connection. During this period, data is sent over both the FSO and RF links simultaneously, with the FSO link's data rate adjusted to match the RF link, allowing for efficient signal combination. The receiver uses MRC to merge the signals from both paths, improving overall reliability. Once the FSO link's SNR recovers and crosses the threshold again, the system reverts to FSO-only transmission, turning off the RF link to save power and spectrum.
- 2. MIMO Systems: MIMO systems mitigate multipath fading by ensuring that signals reach the receiver through multiple independent paths. MIMO technique is one strategy in which multiple transmit and receive antennas are installed to support multiple transmissions of the same signal. But, the total cost of implementing the MIMO system increases because of the requirement of additional antennas.
- 3. **Aperture averaging:** It is an effective method for reducing the fading effect by employing a larger receiving. The larger aperture helps smooth out the rapid intensity variation caused by turbulence, resulting in lower scintillation compared to small or point receiver. This method acts as a form of receiver diversity in FSO communication systems. It becomes effective when the receiver aperture exceeds the fading correlation length, defined as  $\sqrt{\lambda L}$ , where  $\lambda$  is the optical wavelength and L is the link distance. This technique has been extensively studied in the literature [52,53].

## 1.5 Research Motivation

User scheduling schemes for MU dual-hop RF-FSO systems have garnered significant research interest in current and future wireless networks. These schemes aim to efficiently allocate wireless resources to cater to the diverse needs and conditions of all users. Their primary object tive is to decide who should send and receive data and at what time, which affects the efficiency of bandwidth utilities. An effective scheduling scheme should leverage multiuser diversity to achieve substantial system performance while addressing the challenge of ensuring equitable service (fairness). In the region, where users experience lower average SNR, accessing channel resources becomes problematic, particularly in the presence of users enjoying comparatively higher average SNR levels. Consequently, the system allocates resources to users with weaker channels to ensure their requirements are satisfied. However, such allocations do not contribute favorably to achieving optimum system performance. This situation introduces a conflict be tween the objectives of meeting individual user channel access and optimizing overall system. performance.

## 1.6 Thesis Organization

This thesis is organized into eight chapters. The summary of the work presented in each chapter is briefly outlined as follows:

- Chapter 1 Introduction: This chapter provides an overview of wireless communication systems, outlines the key challenges they face, discusses various mitigation techniques, and presents the motivation of the research.
- Chapter 2: Literature Review This chapter explores existing research contributions related to FSO systems, dual-hop RF-FSO systems, and hybrid FSO/RF architectures. It also identifies key research gaps that form the basis of this thesis and outlines its primary objectives.
- Chapter 3: FSO System This chapter investigates the performance of FSO systems over IGG-distributed channels. Novel mathematical expressions for the PDF and CDF of the received SNR under IM/DD detection are derived. A comparative analysis of IGG,  $\mathcal{F}$ , and IGGG distributions is conducted to assess their fitting accuracy to empirical data. Furthermore, unified analytical expressions for outage probability (OP) and average bit error rate (ABER) are developed for digital modulation schemes, along with their asymptotic forms at high SNR. An upper bound for OP is also provided.
- Chapter 4: Multiuser Dual-hop RF-FSO System with Perfect CSI This chapter examines a multiuser dual-hop RF-FSO system employing the CDF based scheduling scheme in the presence of i.n.i.d. co-channel interference (CCI). A unified OP expression is derived. System performance is further optimized through power allocation among users and the relay under a total power constraint, and by determining the optimal channel access ratios (CAR) for users.
- Chapter 5: Multiuser Dual-hop RF-FSO System with Imperfect CSI This chapter builds upon Chapter 4 by incorporating channel estimation errors in both RF and FSO links. OP expressions under imperfect CSI are derived, and performance is enhanced through optimized power allocation and CAR under total power constraints.
- Chapter 6: Dual-hop Multiuser RF-Hybrid FSO/RF Relaying System —
   This chapter addresses the OP analysis of a dual-hop multiuser RF-hybrid FSO/RF system with CDF based scheduling scheme under i.n.i.d. CCI. Optimal power allocation and CAR values are determined to minimize OP while satisfying power constraints.
- Chapter 7: Design of MIMO-FSO and WDM-FSO Systems This chapter focuses on the practical design and simulation of MIMO-FSO and WDM-FSO systems using OptiSystem software, utilizing real-time weather data from Leh, Ladakh. BER, quality factor, and eye diagrams are presented to evaluate system performance.

• Chapter 8: Conclusion and Future Scope — This final chapter summarizes the key findings of the research and outlines potential directions for future work in the field.

# Chapter 2

# **Literature Survey**

This chapter explored the research contributions on FSO systems, dual-hop RF-FSO systems, and hybrid FSO/RF architectures. It also identifies key research gaps and outlines the primary objectives.

## 2.1 Literature Survey on FSO communication System

Accurately modeling the atmospheric turbulence is curcial to predict and analyze the performance of FSO system. In the literature, various statistical models have been utilized to characterize the variations in optical signals, including LN distribution [7], NE distribution [27], and IG distribution [8]. Performance metrics have been analysed using LN model assuming IM/DD with OOK in [54] and in [55] respectively. The OP of FSO systems with multiple transmit/receive apertures has been further evaluated in [56]. Authors have derived analytical expressions for the ABER under IG turbulence-induced fading. These results are applicable to IM/DD systems with Q-ary PPM and HD systems using differential phase shift keying (DPSK), offering a simplified alternative to the LN model [8]. OP and ABER for digital sub-carrier intensity modulated (SIM) have been evaluated for FSO system in atmospheric turbulence using NE distribution [57]. Further, OP, outage capacity, average capacity and ABER for OOK with IM/DD have been evaluated in [27]. These distributions are called single-family distributions. However, these distributions are not suitable for all atmospheric turbulence conditions. For example, LN distribution and IG distribution describe turbulence-induced fading under only a weak turbulence regime, whereas NE distribution is used for an extreme turbulence regime. In order to address the limitations of single-family distributions, double-family distributions have been proposed such as Log Normal Rician distribution [14], I-K distribution [58], Gamma-Gamma (GG) distribution [9], [10],  $\alpha - \mu$  distribution [11], Double Generalized Gamma distribution (DGG) [15], [59], Exponentiated Weibull (EW) distribution [13], Double Weibull distribution [12], Malaga ( $\mathcal{M}$ ) distribution [16], Fischer-Snedecor ( $\mathcal{F}$ ) distribution [17], Inverted GG- Gamma (IGGG) distribution [18] and Inverse Gaussian Gamma (IGG) distribution [19]. The I-K distribution, an extension of the K distribution, is suitable for both weak and strong turbulence conditions [58], while GG distribution is more suitable for strong turbulence conditions [10]. The  $\alpha - \mu$  distribution is a generalized distribution that includes fundamental distributions like Rayleigh, Rician, Nakagami, and K distributions as special cases for specific values of fading parameters [11]. DGG distribution effectively models turbulence conditions across a wide range—from weak to strong—but this accuracy is accompanied by increased computational complexity [15]. EW distribution is effective under diverse atmospheric conditions, especially where GG and LN distributions fails to accurately model the irradiance fluctuation due to the impact of aperture averaging [13]. The Double Weibull distribution provides superior accuracy compared to the GG distribution from moderate to strong turbulence conditions [12]. The  $\mathcal M$  distribution functions as a generalized statistical model that encompasses both LN and GG distributions as particular instances, thereby providing greater flexibility in modeling a wide range of turbulence conditions [16].  $\mathcal F$  distribution provide a more tractable model using elementary functions compared to other models. however, it often fails to accurately fit experimental data across all turbulence regimes [17].

Table 2.1: Literature survey on FSO communication system

Ref	Author's Name/Year	System Model	Key Contribution
[60]	O. S. Badarneh et al., 2023	IGGG turbulence channel under IM/DD detection scheme in the presence of pointing error	OP, ABER, EC, Diversity Order
[61]	Y. M. Shishter et al., 2023	IGIGG and IGIGGG fading channels used	Proposed IGIGG and IGIGGG distributions and derived PDF, CDF, MGF
[18]	Y. M. Shishter et al., 2022	IGGG fading channel with aperture averaging	Proposed IGGG distribution and derived PDF, CDF
[17]	K. P. Peppas et al., 2020	${\mathcal F}$ fading channel under IM/DD and HD detection schemes	Proposed $\mathcal F$ distribution and derived PDF, CDF, OP, ABER, Diversity Order
[62]	A. A. Ibrahim et al., 2020	${\mathcal M}$ fading channel under channel estimation error	OP, ABER, Diversity Order
[19]	M. Cheng et al, 2018	IGG fading channel with aperture averaging	Proposed IGG distribution and derived PDF, CDF, OP
[16]	I. S. Ansari et al., 2015	${\mathcal M}$ fading channel using IM/DD and HD detection schemes accounts for pointing errors	OP, ABER, EC, Diversity Order
[15]	M. A. Kashani et al., 2015	DGG fading channel with IM/DD detection scheme	OP, ABER, Diversity Order
[13]	B. Porras et al.,2013	Exponentiated Weibull fading model under aperture averaging	ABER, Diversity Order
[63]	N. D. Chatzidiamantis et. al, 2010	Double Weibull fading model under IM/DD detection scheme	OP, ABER, Diversity Order

The IGGG distribution was introduced in [18] and combines the Inverse Gamma and Gamma distributions to characterize large-scale fluctuations, while Gamma distribution is employed to characterize small-scale irradiance fluctuations. Further, two novel fading distributions: Inverse Gamma/Inverse Gamma/Gamma (IGIGG) distribution and Inverse Gamma/Inverse Gamma/Gamma/Gamma (IGIGGG) distribution are introduced in [61]. In the IGIGG distribution, large-scale fluctuations are represented as the product of two inverse Gamma distributions, while small-scale irradiance fluctuations are modelled by Gamma distribution. On the other hand, large-scale fluctua-

tions are modelled as the product of two Inverse Gamma and Gamma distributions, and small-scale irradiance fluctuation by Gamma distribution in IGIGGG distribution. OP, and ABER have been evaluated using IGGG distribution with pointing errors in [60]. The IGG distribution, first introduced in [19], models atmospheric turbulence by representing small-scale irradiance fluctuations with a Gamma distribution and large-scale irradiance fluctuations with an IG distribution. The PDF and cumulative distribution function (CDF) in terms of fade threshold have been obtained. The resulting PDF was shown to agree very well with the experimental data. However, IGG is mathematically intractable and the CDF was obtained as an infinite series. Further, for long-distance transmission, system performance deteriorates due to fading effects. Studies have been conducted on aperture averaging to enhance performance of the systems [64]. Aperture averaging mitigates the effects of atmospheric turbulence by using a photodetector with a larger aperture, allowing it to collect a broader segment of the optical beam and smooth out signal fluctuations in [65]. Various modulation schemes have been studied, including OOK [66], [67], M-ary Phase Shift Keying (MPSK) [68], [69], Differential Phase Shift Keying (DPSK) [70], Coherent Binary Frequency Shift Keying (CBFSK), and Polarization Shift Keying (PolSK) [71]. A literature review of single-hop FSO channel models and their corresponding contributions is summarized in Table 2.1.

The literature survey on single-hop FSO communication systems indicates that the IGG model provides the best alignment with experimental data, especially under low irradiance conditions as compared to  $\mathcal F$  distribution and IGGG distribution, as evidenced by a lower mean squared error (MSE  $_{\rm IGG} < {\rm MSE}_{\mathcal F}, {\rm MSE}_{\rm IGGG}$ ). Despite its accuracy, IGG model suffers from mathematical intractability, with its CDF expressed as an infinite series, limiting its practical analytical use. Additionally, the impact of modulation techniques, and different detection schemes on FSO system under IGG distribution has not been investigated. In contrast, the  $\mathcal F$  distribution is less precise but offers a simpler mathematical expression using elementary functions, making it more analytically convenient. This highlights a critical trade-off between model accuracy and tractability that remains under-explored in current literature.

# 2.2 Literature Survey on MU Dual-hop RF-FSO system with Perfect CSI

The rapid proliferation of mobile devices on internet connectivity for both personal and professional use necessitate robust communication frameworks that can handle multiple users simultaneously. This demand is further amplified by the rise of applications requiring high bandwidth, such as video conferencing, online gaming, and cloud computing. Consequently, there is a pressing need for systems that can efficiently manage multiple simultaneous connections while maintaining high data rates and low latency. To effectively serve a large number of users, future wireless networks must deliver reliable and efficient communication services. The challenge intensifies as the demand for high-speed data and uninterrupted connectivity continues to grow. In this regard, multiuser dual-hop relaying systems offer a promising solution. Many researchers have analysed the performance of such system employing various user scheduling schemes

such as absolute SNR, normalized SNR, proportional fairness scheduling (PFS) [72], greedy scheduling (GS) [51], highest SNR based scheduling [73], [74], best channel selection [75], generalized order user scheduling [76], and opportunistic scheduling [77], [78], [79], [80], and [81], [82].

The authors examined the EC for the dual-hop FSO-RF system by employing transmit beamforming based on channel state information and utilizing proportional fairness scheduling (PFS) in [72]. The relay assisted MU TWR assisted FSO system with different scheduling schemes such as GS, PFS and selective multiuser diversity scheduling have been studied in [51]. The selection of the user with maximum SNR has been considered for relay assisted dual-hop RF-RF system considering i.n.i.d CCI in [73] and for dual-hop RF-FSO system in [74], where RF link is modeled using NE distribution and FSO link is characterized by GG distribution. The authors in [75] have derived OP, ABER and EC for MU dual-hop RF-FSO AF relaying systems using best channel condition where the RF channel is subjected to  $\eta - \mu$  fading and assumed  $\mathcal{M}$ distribution for FSO link. Authors examined the performance of MU dual-hop RF-FSO system employing opportunistic user scheduling scheme with a multiple antenna where Nakagami-m has been assumed for RF link while FSO link undergoes GG distributed fading in [77] and the impact of CCI was further incorporated in [83]. Additionally, similar work was extended by considering Rayleigh/Gamma-Gamma fading channels [78]. In [80], authors analysed the performance of MU dual-hop FSO-RF system utilizing opportunistic user scheduling and considered  $\mathcal{M}$ -distributed fading for the FSO link and shadowed  $\kappa - \mu$  fading for the RF link and considered  $\alpha - \mu/GG$  fading models for the same scheduling scheme in [82].

OP and ABER analyses for MU RF-FSO system in the presence of CCI have been conducted based on channel statistics [81], where RF links is modeled by Nakagami-m fading and the FSO link is characterized by  $\alpha-\mu$  distribution. Using same scheduling scheme, performance have been investigated for MU dual-hop system in [79], where RF links experience Nakagami-m fading and FSO link is modeled using DGG distribution. However, imperfect channel estimation hinders the selection of the best user in opportunistic scheduling scheme. To address this issue, generalized order based scheduling scheme has been explored for MU dual-hop RF-FSO in [76] and transmit antenna selection based system has been analyzed in [84]. These studies have accounted perfect CSI at the relay in dual-hop systems as shown in Table. 2.2.

From Table 2.2, it is evident that the performance of a MU dual-hop RF-FSO system has not been analyzed by using  $\mathcal{F}$  distribution for the FSO channel. Moreover, fairness-based scheduling scheme with perfect channel estimates remains unexplored in the presence of CCI.

Table 2.2: Literature Survey for Dual-hop System with Perfect Channel Estimation and Scheduling Schemes

Ref	Author's Name/Year	Dual-hop System	First hop	Second hop	Scheduling Scheme	CCI	Key Contribution
[82]	A. Goel et al., 2020	RF/FSO	$\alpha - \mu$	Gamma-Gamma	Opportunistic Scheduling	×	OP,ABER
[72]	H. Kong et al., 2020	FSO/RF	Gamma-Gamma	Rayleigh	PFS	×	EC
[79]	Tonk et al., 2020	RF/FSO	Nakagami-m	Double Generalized Gamma	Opportunistic Scheduling	✓	OP, ABER
[80]	I. Trigui et al.,2019	FSO/RF	$\mathcal{M}$	shadowed $\kappa - \mu$	Opportunistic Scheduling		OP, ABER, Diversity Order, Power Alloca- tion
[84]	K. O. Odeyemi et al., 2019	RF/FSO	Nakagami-m	Exponential Weibull	Generalized order user scheduling	×	OP, ABER
[74]	M. A. Amirabadi, 2019	RF-FSO	Negative Exponential	Gamma-Gamma	Highest SNR based Scheduling	×	OP, ABER
[81]	A. Upadhya et al., 2019	RF/FSO	Nakagami-m	$\alpha$ - $\mu$	Opportunistic Scheduling		OP, ABER
[78]	A. H. A. El- Malek et al., 2017	RF/FSO	Rayleigh	Gamma-Gamma	Opportunistic Scheduling		OP, Diversity Order, Power Allocation
[83]	A. H. A. El- Malek et al., 2017	RF/FSO	Nakagami-m	Gamma-Gamma	Opportunistic Scheduling		OP, Diversity Order, Power Allocation
[75]	L. Yang et al., 2017	RF/FSO	$\eta - \mu$	$\mathcal{M}$	Best channel selection	×	OP, ABER, EC, Diversity Order
[73]	A. K. Mandpura et al., 2016	RF/RF	Rayleigh	Rayleigh	High SNR based Scheduling		OP, Diversity Order
[51]	P. Puri et al., 2016	FSO/FSO	$\mathcal{M}$	$\mathcal{M}$	Absolute SNR, Nor- malized SNR, Selec- tive MU diversity	×	OP, ABER
[77]	A. H. A. El- Malek et al., 2016	RF/FSO	Nakagami-m	Gamma-Gamma	Opportunistic Scheduling	×	OP, ABER, EC, Diversity Order, Power Allocation
[76]	A. M. Salhab, 2015	RF/FSO	Rayleigh	Gamma-Gamma	Generalized order user scheduling	×	OP, ABER, EC, Diversity Order

# 2.3 Literature Survey on MU Dual-hop RF-FSO system with Imperfect CSI

Imperfect Channel State Information (CSI) in wireless communication occurs when the transmitter and receiver has outdated knowledge of the channel conditions. CSI plays a vital role in optimizing signal transmission, ensuring efficient use of bandwidth, and mitigating interference. However, in real-world scenarios, acquiring perfect CSI is challenging due to factors such as feedback delay, estimation errors, user mobility, and hardware limitations. As a result, most real-world systems rely on estimated CSI obtained via feedback mechanisms. Therefore, it becomes critical to account for the impact of channel estimation errors on system performance [85]. Some studies have extensively explored the effects of channel estimation errors on dual-hop RF/FSO communication systems [76,86–96] as shown in the Table 2.3. In [86], the performance of a dual-hop FSO-hybrid FSO/RF system was analyzed within a satellite–air–ground integrated network (SAGIN) framework, taking into account the presence of eavesdroppers on both FSO and RF links, interference on the RF link, and imperfect CSI on the FSO link. Secrecy performance of a non-orthogonal multiple access (NOMA)-based dual-hop system was analyzed, taking into account imperfect CSI at both links in [87].

Similarly, [88] examined the performance of dual-hop RF-FSO system in terms of OP, ABER and EC, also accounting for imperfect CSI on both links. The authors of [90] analyzed the secrecy OP of a single-input-multiple- output(SIMO) dual hop RF-FSO system with imperfect CSI at both links in the presence of eavesdropper where multiple antennas were deployed at both the relay and the eavesdropper, and MRC was used to improve the system performance. This work was further extended to a multiple-inputmultiple- output (MIMO) scenrio in [89] by incorporating various transmit antenna selection (TAS) schemes. The authors analyzed the performance of a dual-hop RF-FSO system employing a partial relay antenna selection scheme in the presence of interference and imperfect CSI at RF link, where Rayleigh fading was assumed for the RF and Double-Weibull fading for the FSO link in [92], while in [91], Nakagami-m fading and DGG fading were considered for the RF and FSO links respectively. The performance of a dual-hop RF-FSO system with imperfect CSI at the relay was analysed in [76], considering a Rayleigh faded RF link and an FSO link by GG distribution. This work was further extended in [93] by modeling the RF link by Nakagami-m fading and FSO link with GG turbulence. Authors investigated the performance metrics of a MU dual-hop RF-FSO system with generalized order scheduling, considering imperfect channel for the RF link in [77]. The RF link was modeled by Rayleigh fading, while FSO link experienced GG fading with pointing error. The same system model was also considered using opportunistic user-based scheduling, along with power allocation optimization to enhance the system performance [77]. In [96], the authors investigated the performance of a MU dual-hop RF-RF system with opportunistic user-based scheduling, considering imperfect channel for the RF links.

Table 2.3: Literature Survey for Dual-hop System with Imperfect Channel Estimation and Scheduling Schemes

Ref	Author's Name	Dual-hop	First-hop	Second-hop	Scheduling Schemes	CCI	Channel Estimation at First-hop	Channel Estimation at Second- hop	Key Contribution	
[86]	X. Li et al., 2025	FSO/hybrid FSO-RF	Gamma- Gamma	Shadowed Rician and Nakagami-m	×	✓	✓	✓	SOP, ST, SPSC	
[87]	Y. Zhuang et al., 2022	FSO/RF	Rayleigh	Gamma-Gamma	-	×	✓	✓	SOP	
[88]	Z. Zhang et al., 2022	RF/FSO	α-μ	М	-	×	✓	✓	PDF, CDF, OP, ABER, EC, Diver- sity Order	
[89]	H. Lei et al., 2020	RF/FSO	Nakagami-m	$\mathcal{M}$	Transmit An- tenna Selection	×	✓	✓	PDF, CDF, EST, Diversity Order	
[90]	H. Lei et al. 2018	RF/FSO	Rayleigh	Gamma-Gamma	-	×	✓	✓	OP	
[91]	E. Balti et al., 2018	RF/FSO	Nakagami-m	Double General- ized Gamma	Partial Relay Se- lection	✓	✓	×	OP, ABER, EC	
[92]	E. Balti et al., 2017	RF/FSO	Rayleigh	Double-Weibull	Partial Relay Se- lection	×	✓	×	OP, EC, Upper Bound	
[93]	M. Petkovic et al, 2017	RF/FSO	Nakagami-m	Gamma-Gamma	-	×	✓	×	OP	
[94]	A. M. Salhab et al., 2016	RF/FSO	Rayleigh	Gamma-Gamma	Opportunistic Scheduling	×	✓	×	OP, ABER, Diversity Order, Power Allocation	
[95]	G. T. Djordjevic et al., 2015	RF/FSO	Rayleigh	Gamma-Gamma	Gamma - × ✓		×	OP, ABER, Trans- mitter Beam Waist		
[76]	A. M. Salhab, 2015	RF/FSO	Rayleigh	Gamma-Gamma	Generalized order User Scheduling	×	✓	×	OP, ABER, EC, Diversity Order	
[96]	Y. Gu et al., 2013	RF/RF	Rayleigh	Rayleigh	Opportunistic Scheduling	✓	✓	✓	OP, ABER, Diversity Order	

Table 2.3 highlights that the performance analysis of a MU dual-hop RF-FSO system remains unexplored when employing  $\mathcal{F}$  distribution to model the FSO channel. Moreover, fairness-based scheduling scheme under the influence of imperfect channel estimation, and CCI has not yet been addressed in the existing literature.

# 2.4 Literature Survey on hybrid FSO/RF Communication System

Hybrid FSO/RF technology holds significant promise as it can greatly improve the availability and reliability of communication compared to standalone links. It offers high data rates and improved resilience to varying weather conditions. By combining the strengths of both FSO and RF technologies, this hybrid approach enables the links to compensate for each other's limitations, ensuring efficient and robust data transmission even under highly variable channel conditions. These hybrid systems are available in single-hop system [97–104], dual-hop system [105–110]. Single-hop systems are favored for short range communications where data transmission takes place through two parallel FSO and RF links, either simultaneously or via a switching mechanism. Different combining schemes are performed at the receiver such as SC, MRC, EGC and Adaptive combining. To increase coverage areas, dual-hop systems have been deployed and various relaying techniques, such as AF and DF are employed.

For instance, authors of [97] deduced the mathematical expression for OP, ABER for multi-hop parallel hybrid FSO/RF system incorporating SC scheme. [103] has been performed the outage analysis for hybrid FSO/RF system using adaptive combining without considering pointing error. This work was later extended in [98], where pointing error was incorporated and the ABER was also derived. In [99], the performance of hybrid FSO/RF system was analyzed for SC scheme, where RF link follows  $\eta - \mu$ distribution and FSO link employs the  $\mathcal{M}$  with the consideration of pointing error. The OP, ABER and EC of the hybrid system with GG fading for FSO and Rayleigh fading for RF were evaluated with hard-switching scheme in [100]. In [101], performance has been evaluated using the SC for the hybrid system. In [102], the hard-switching scheme is incorporated to analyse the performance, where the RF link experiences Rician fading and employs 16-quadrature amplitude modulation (QAM), while the FSO link is modeled using the GG distribution with pointing error effects. In [104], authors derived closed-form expressions for the ABER and the EC of the hybrid FSO/RF system employing hard switching. They studied the performance of the FSO link under weak atmospheric conditions using of M-PSK modulation and considered two hybrid configurations: single-threshold and dual-threshold switching schemes. In [105], a new channel selection policy is proposed for hybrid FSO/RF space-air-ground integrated networks. This policy dynamically enhances system performance, and an OP analysis is conducted to evaluate its effectiveness. The performance of DF based dual hop RF-hybrid RF/FSO system empoying SC was analysed in [106]. The authors in [107] analyzed the performance of a SAGIN-based dual-hop FSO-hybrid FSO/RF system in the presence of an eavesdropper on the FSO link, employing a hard-switching scheme. The analysis of a dual-hop hybrid system using SC has been presented in [108], where the RF link is modeled by Shadowed-Rician distribution and the FSO link using the GG distribution. An optimal power allocation expression was also derived to enhance system performance. The performance of dual-hop RF-hybrid FSO/RF system with AF based protocol, considering SC has been done in [110], where the FSO link using a GG distribution and the RF link with Rayleigh fading. Furthermore, [109] investigated the performance of similar systems with DF based protocol, modeling the FSO link using the  $\mathcal M$  distribution and the RF link by Rayleigh fading considering both SC and MRC schemes. A concise summary of existing research on hybrid FSO/RF systems is presented in Table 2.4.

Table 2.4: Literature survey for Hybrid FSO/RF Communication System

Ref	Author's Name,	System Model		RF link	FSO link	Diversity	Key Contribution	
	Year	First Hop	Second Hop					
[105]	P. S. Bithas et al., 2024	, FSO Hybrid FSO/RF		Shadowing Double- scattering	Gamma-Gamma with pointing error	lower signaling overhead channel SC	OP	
[106]	H. Joshi et al., 2023	RF Hybrid FSO/RF		Nakagami-m	$\mathcal{M}$ with pointing error	SC	OP, MGF, ABER, EC	
[97]	Y. Wu et al., 2023	Hyb	rid FSO/RF	Nakagami-m	$\mathcal{M}$ with pointing error	SC	OP, ABER	
[107]	V. Bankey et al., 2022	FSO	Hybrid FSO-RF	Gamma-Gamma	Shadowed-Rician	Hard-Switching	SOP	
[108]	R. Deka et al., 2022	Hybrid FSO/RF	Hybrid FSO/RF	Shadowed-Rician	Gamma-Gamma	SC	OP, ABER, Power Allocation	
[109]	D. R. Pattanayak et al., 2020	RF	Hybrid FSO/RF	Rayleigh	$\mathcal{M}$ with pointing error	SC/MRC	OP	
[98]	M. Siddharth et al., 2020	Hybrid FSO/RF		Nakagami-m	Gamma-Gamma with pointing error	Adaptive Com- bining with MRC	OP, ABER	
[110]	M. Torabi et al., 2019	RF Hybrid FSO/RF		Rayleigh	Gamma-Gamma with pointing error	SC	OP, ABER, EC	
[99]	K. O. Odeyemi et al., 2019	Hyb	rid FSO/RF	$\eta - \mu$	$\mathcal{M}$ with pointing error	SC	OP, ABER	
[100]	H. Khalid et al., 2019	Hyb	rid FSO/RF	Rayleigh	Gamma-Gamma	Hard-Switching	OP, ABER, EC	
[101]	W. M. R. Shakir, 2018	Hyb	rid FSO/RF	Rayleigh	Gamma-Gamma	SC	OP, ABER	
[102]	A. Touati et al., 2016	Hybrid FSO/RF		Rician	Gamma-Gamma with pointing error	Hard-Switching	OP, ABER	
[103]	T. Rakia et al., 2015	Hybrid FSO/RF		Nakagami-m	Gamma-Gamma	Adaptive Com- bining with MRC	OP	
[104]	M. Usman et al., 2014	Hybrid FSO/RF		Nakagami-m	Log-normal	Single FSO threshold and dual FSO thresh- old	OP, ABER, EC	

Previous studies have explored various diversity combining techniques, such as SC and MRC, at the receiver to enhance system performance. Further improvements can be achieved by incorporating MU transmission at the source and modeling the FSO channel using the  $\mathcal F$  distribution. However, the performance analysis of dual-hop MU RF-hybrid FSO/RF systems using SC at the receiver, integrated with a fairness-based scheduling strategy under the influence of CCI, remains largely unexplored in the literature.

### 2.5 Research Gaps

Based on the literature review discussed in the preceding sections, the identified research gaps are summarized as follows:

- 1. While the IGG,  $\mathcal{F}$ , and IGGG distributions have been introduced in the literature to model atmospheric turbulence in FSO systems, the performance analysis of FSO systems under IGG-distributed turbulence remains unexplored. Additionally, the effect of modulation techniques, and detection schemes on system performance under IGG distribution has not been investigated.
- 2. To improve the performance of dual-hop RF-FSO system, multiuser diversity has been studied in literature. However, the performance of MU dual-hop RF-FSO system with fairness based user scheduling scheme and perfect channel estimation in the presence of CCI has not been studied.
- 3. The performance of MU dual-hop RF-FSO system with fairness based user scheduling scheme in the presence of imperfect channel estimation, and CCI has not been studied.
- 4. In literature, diversity combining (such as SC and MRC) at the receiver had been studied to enhance the performance of hybrid FSO/RF system. The system performance can be further enhanced by exploiting multiuser diversity at the source. The performance of MU dual-hop RF-Hybrid FSO/RF systems with SC combining at the receiver using fairness based user scheduling scheme in the presence of CCI has not been studied.

### 2.6 Objectives and Scope of the Work

Therefore, to address these research gaps, we have formulated the following research objectives:

- **Objective 1:** To design and analyse the performance of improved free space optical communication system using different modulation and detection techniques.
- **Objective 2:** To design and analyse the performance of dual-hop RF-FSO relay system for large coverage area.
- **Objective 3:** To design and analyse the performance of hybrid RF/FSO system for worst weather conditions.
- **Objective 4:** To compare the performance of proposed system with existing system.

This research focuses on the modeling, simulation, and analysis of FSO systems, MU dual-hop RF-FSO systems, and dual-hop MU RF-hybrid FSO/RF systems under diverse channel conditions. It considers various modulation and detection techniques, realistic channel conditions, and aims to enhance system reliability, coverage, and data rate. The study also includes performance comparison with existing systems to demonstrate the advantages of the proposed approach.

## Chapter 3

# Performance Analysis of FSO System Over Inverse Gaussian Gamma Turbulence Channel

In this chapter, the performance of a FSO communication system is studied. The significant contributions of this chapter are as follows:

- FSO system over IGG distributed channel is considered and novel mathematical expressions for PDF and CDF of the received SNR are derived to describe the statistical behaviour of the received SNR under IM/DD detection scheme.
- A comparison of IGG distribution with  $\mathcal{F}$  distribution and IGGG distribution is performed to demonstrate an accurate fit to the experiment data.
- New unified analytical expressions for the OP and ABER for MPSK, OOK, CBFSK, and DPSK digital modulation schemes are derived based on its PDF and CDF.
- For gaining further insights, asymptotic expressions are obtained for OP, and ABER in the high SNR region. Also, the upper bound on OP is obtained.
- Monte Carlo simulation is carried out to verify the analytical expressions.

### 3.1 System Model and Statistical Characteristics

Consider a system illustrated in Fig. 3.1, where a source node (S) communicates with a destination node (D) over an FSO channel using IM/DD detection scheme. The received signal, *y* is expressed as:

$$y = \eta h_{\text{IGG}} x + n, \tag{3.1}$$

where,  $\eta$  denotes photodetector responsivity, x is the transmitted signal from S and has an average power of one Watt, n is the zero mean additive white gaussian noise (AWGN) and is distributed as  $\mathcal{N}(0,\sigma_{\text{AWGN}}^2)$ . Further, the FSO channel fading coefficient  $h_{\text{IGG}}$  follows an IGG distribution which results from both large-scale effects denoted as  $h_L$  and small-scale effects denoted as  $h_S$ .



Figure 3.1: System model of the considered communication system.

The fading coefficient can be expressed as:  $h_{\rm IGG}=h_Lh_S$ . Further,  $h_L$  is modelled by IG distribution as defined in [8] and  $h_S$  is modelled by Gamma distribution defined in [111]. The PDFs for  $h_L$  and  $h_S$  are as follows:

$$f_{h_L}(h_L) = \sqrt{\frac{\alpha}{2\pi h_L^3}} e^{\alpha} e^{-\frac{\alpha}{2}\left(h_L + \frac{1}{h_L}\right)}, \tag{3.2a} \label{eq:fhl}$$

$$f_{h_S}(h_S) = \frac{\beta^{\beta} h_S^{\beta - 1}}{\Gamma \beta} e^{-\beta h_S}, \tag{3.2b}$$

where, the gamma function is denoted by  $\Gamma(.)$ , and  $\alpha$  and  $\beta$  represent the severity of fading associated with large-scale and small-scale turbulent eddies, respectively. The expression for  $\alpha$  and  $\beta$  is given by as [19]:

$$\alpha = \frac{1}{e^{\sigma_{lnL}^2} - 1}.\tag{3.3a}$$

$$\beta = \frac{1}{e^{\sigma_{lnS}^2} - 1}.\tag{3.3b}$$

where,  $\sigma_{lnL}^2$  and  $\sigma_{lnS}^2$  denotes the log-irradiance variances [17]. The PDF of  $h_{IGG}$  is derived from (3.2a), and (3.2b) as follows:

$$f_{\rm IGG}(h_{\rm IGG}) = \sqrt{\frac{2\alpha}{\pi}} \frac{\beta^{\beta} h_{IGG}^{\beta-1} e^{\alpha}}{\Gamma \beta} \left(1 + \frac{2\beta h_{\rm IGG}}{\alpha}\right)^{-\frac{\beta}{2} - \frac{1}{4}} K_{\beta + \frac{1}{2}} \left(\alpha \sqrt{1 + \frac{2\beta h_{\rm IGG}}{\alpha}}\right), h_{\rm IGG} \ge 0 \quad (3.4)$$

where,  $K_v(.)$  refers to modified Bessel function of the second kind of order v. The received instantaneous SNR,  $\gamma$  and average SNR,  $\bar{\gamma}$  for the considered system employing IM/DD detection scheme is expressed as  $\gamma = \frac{(\eta h_{\rm IGGG})^2}{\sigma_{\rm AWGN}^2}$  and  $\bar{\gamma} = \frac{\eta^2 E^2 |h_{\rm IGGG}|}{\sigma_{\rm AWGN}^2}$ .

The  $n^{th}$  moment of  $h_{IGG}$ ,  $\mu_n(h_{IGG})$  is obtained by using (3.4) and integral identity given in [112] as:

$$\mu_n(h_{\rm IGG}) = E|h^n_{\rm IGG}| = \frac{\Gamma\left(n+\beta\right)e^\alpha}{\beta^n\Gamma\left(\beta\right)} \sqrt{\frac{2\alpha}{\pi}} K_{\frac{1}{2}-n}(\alpha). \tag{3.5}$$

By employing variable substitution in (3.4), the PDF of IGG in terms of received instantaneous SNR is calculated as:

$$f_{\gamma}(\gamma) = \sqrt{\frac{\alpha}{2\pi}} \frac{\beta^{\beta} e^{\alpha} \gamma^{\frac{\beta}{2} - 1}}{\bar{\gamma}^{\frac{\beta}{2}}} \left( 1 + \frac{2\beta}{\alpha} \sqrt{\frac{\gamma}{\bar{\gamma}}} \right)^{-\frac{\beta}{2} - \frac{1}{4}} K_{\beta + \frac{1}{2}} \left( \alpha \sqrt{1 + \frac{2\beta}{\alpha} \sqrt{\frac{\gamma}{\bar{\gamma}}}} \right). \quad (3.6)$$

To derive the CDF of IGG in terms of received instantaneous SNR,  $F_{\gamma}(\gamma)$ , the series expansion of  $K_v(.)$  as given in [113, Eq.(03.04.06.0030.01)] is utilized in (3.6). Through a sequence of algebraic manipulations, the expression can be reformulated as follows:

$$\begin{split} F_{\gamma}(\gamma) &= \int_{0}^{\gamma} f_{\gamma}(\gamma) d\gamma = \sqrt{\frac{2\alpha}{\pi}} \frac{\beta^{\beta} e^{\alpha}}{\bar{\gamma}^{\frac{\beta}{2}} \Xi^{\beta} \Gamma \beta} \left( \frac{\pi}{2 \sin(\pi \Lambda)} \right) \\ &\sum_{p=0}^{\infty} \left\{ A_{11} \int_{0}^{\Xi \sqrt{\gamma}} \frac{\varrho^{\beta-1}}{(1+\varrho)^{\frac{\beta}{2}+\frac{1}{4}-p+\frac{\Lambda}{2}}} d\varrho - A_{22} \int_{0}^{\Xi \sqrt{\gamma}} \frac{\varrho^{\beta-1}}{(1+\varrho)^{\frac{\beta}{2}+\frac{1}{4}-p-\frac{\Lambda}{2}}} d\varrho \right\}, \quad (3.7) \end{split}$$

where,  $\Xi=\frac{2\beta}{\alpha\sqrt{\gamma}},\ \varrho=\Xi\sqrt{\gamma},\ A_{11}=\frac{(\frac{\alpha}{2})^{2p-\Lambda}}{\Gamma(p-\Lambda+1)p!}$  and  $A_{22}=\frac{(\frac{\alpha}{2})^{2p+\Lambda}}{\Gamma(p+\Lambda+1)p!}$ . Also, the value of parameter  $\beta$  is required to satisfy  $\Lambda=(\beta+\frac{1}{2})\notin\mathbb{Z}$ . When  $(\beta+\frac{1}{2})\in\mathbb{Z}$ , a very small value,  $\delta$  is added to  $\beta$  to satisfy the condition  $(\beta+\frac{1}{2})\notin\mathbb{Z}$  [114]. With the aid of integral identities as [112, Eq.(3.194.1)] and [113, Eq. (07.23.26.0004.01)], we can obtain (3.7) in a closed-form as:

$$F_{\gamma}(\gamma) = \sqrt{\frac{2\alpha}{\pi}} \frac{\beta^{\beta} e^{\alpha}}{\bar{\gamma}^{\frac{\beta}{2}} \Gamma \beta} \left( \frac{\pi}{2 \sin(\pi \Lambda)} \right) \sum_{p=0}^{\infty} \left\{ \left( \frac{(\frac{\alpha}{2})^{2p-\Lambda}}{\Gamma(p-\Lambda+1)p!} \right) \frac{\gamma^{\frac{\beta}{2}}}{\Gamma(\frac{\beta}{2} + \frac{1}{4} - p + \frac{\Lambda}{2})} \right.$$

$$G_{2,2}^{1,2} \left( \frac{2\beta}{\alpha} \sqrt{\frac{\gamma}{\bar{\gamma}}} \Big|^{\frac{3}{4} - \frac{\beta}{2} + p - \frac{\Lambda}{2}, 1 - \beta} \right) - \left( \frac{(\frac{\alpha}{2})^{2p+\Lambda}}{\Gamma(p+\Lambda+1)p!} \right) \frac{\gamma^{\frac{\beta}{2}}}{\Gamma(\frac{\beta}{2} + \frac{1}{4} - p - \frac{\Lambda}{2})}$$

$$G_{2,2}^{1,2} \left( \frac{2\beta}{\alpha} \sqrt{\frac{\gamma}{\bar{\gamma}}} \Big|^{\frac{3}{4} - \frac{\beta}{2} + p + \frac{\Lambda}{2}, 1 - \beta} \right) \right\}. \quad (3.8)$$

### 3.2 Amount of Fading

One of the unified performance measures is AOF that quantifies the severity of fading. The  $n^{th}$  order AOF is defined in [16]:

$$AOF_{IGG}^{n} = \frac{\mu_{n}(h_{IGG})}{\left(\mu_{n-1}(h_{IGG})\right)^{2}} - 1.$$
 (3.9)

By substituting n = 2 in (3.5) and using these values in (3.9), the second- order AOF<sub>IGG</sub>, called scintillation index is written as:

$$AOF_{IGG} = \left(1 + \frac{1}{\alpha}\right) \left(1 + \frac{1}{\beta}\right) - 1. \tag{3.10}$$

Scintillation index is primarily caused by the variation in the refractive index of the atmosphere due to turbulence. As light travels through the atmosphere, it experiences random changes in the intensity leading to scintillation. High scintillation index values indicate significant signal fading, where received optical power fluctuation rapidly.

# 3.3 Comparison with Previous Models and Experimental Data

We perform a comparison between the PDF of IGG distribution as defined in (3.4) and  $\mathcal{F}$  distribution in [17], as well as IGGG distribution in [18]. This comparison is conducted to assess the accuracy of these models using experimental data taken from [115] under moderate to strong turbulent atmospheric conditions.

The PDF of  $h_{\mathcal{F}}$  for  $\mathcal{F}$  distribution is given as [17, Eq. (6)]

$$f(h_{\mathcal{F}}) = \frac{a^a (b-1)^b h_{\mathcal{F}}^{a-1}}{\beta(a,b) \left(ah_{\mathcal{F}} + (b-1)\right)^{a+b}}.$$
 (3.11)

where,  $a = \frac{1}{e^{\sigma_{lnS-1}^2}}$ ;  $b = \frac{1}{e^{\sigma_{lnL-1}^2}} + 2$ .

$$AOF_{\mathcal{F}} = \left(1 + \frac{1}{a}\right) \left(1 + \frac{1}{b-2}\right) - 1.$$
 (3.12)

The PDF of  $h_{\rm IGGG}$  for IGGG distribution is given as [18, Eq. (31)]:

$$\begin{split} f(h_{\mathrm{IGGG}}) &= \left(\frac{\sigma\mu}{\psi-1}\right)^{\sigma} \frac{\Gamma(\sigma+\psi)\Gamma(\mu+\psi)}{\Gamma\sigma\Gamma\mu\Gamma\psi} h_{IGGG}^{\sigma-1} \, U(\sigma+\psi; 1+\sigma-\mu; \frac{\sigma\mu}{\psi-1} h_{\mathrm{IGGG}}), \\ & h_{\mathrm{IGGG}} \geq 0 \quad (3.13) \end{split}$$

where,  $\mu = \frac{1}{e^{\sigma_{lnS-1}^2}}$ ,  $\sigma = \frac{1}{e^{0.5\sigma_{lnL-1}^2}}$ ,  $\psi = \sigma + 2$ .

$$AOF_{IGGG} = \left(1 + \frac{1}{\sigma}\right) \left(1 + \frac{1}{\psi - 2}\right) \left(1 + \frac{1}{\mu}\right) - 1. \tag{3.14}$$

$$MSE = \frac{1}{N} \sum_{i=1}^{N} \left( f(h_{\text{exp}}) - f(h_{\text{IGG}/\mathcal{F}/\text{IGGG}}) \right)^{2}. \tag{3.15}$$

The small-scale and large-scale fading parameters for IGG,  $\mathcal{F}$ , and IGGG distributions are computed based on experimental data [115] and tabulated in Table. 3.1. The PDFs for the three models are plotted along with the experimental data in Fig. 3.2 and Fig.

3.3 for a wide range values of D,  $C_n^2$ ,  $l_0$ . The mean squared error (MSE) is computed to quantify the deviation between the experimental data and PDF of the three models, as shown in Table 3.1. It is found that  $MSE_{IGG}$  is less than  $MSE_{\mathcal{F}}$  and  $MSE_{IGGG}$ . This suggests that IGG model closely aligns with the experimental data and offers a superior fit, particularly when dealing with low irradiance values as compared to  $\mathcal{F}$  distribution and IGGG distribution.

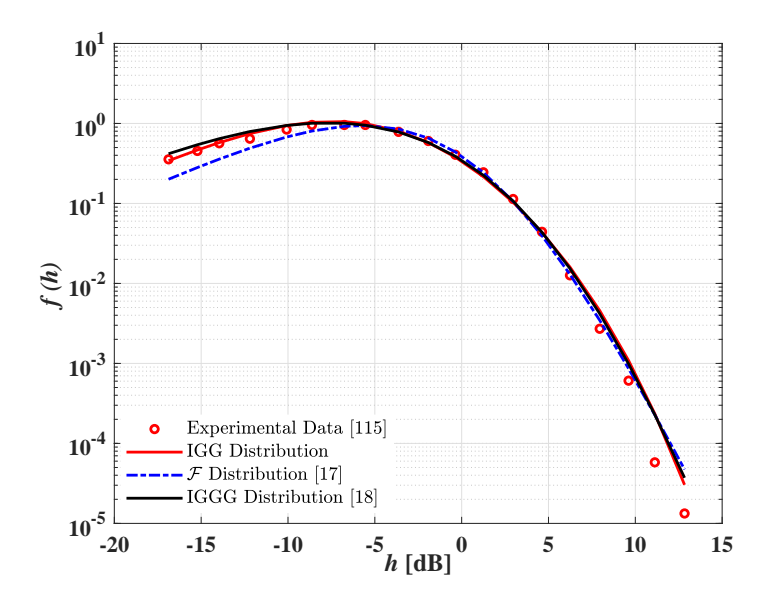


Figure 3.2: Comparison between IGG distribution,  $\mathcal{F}$  distribution, and IGGG distribution in the context of experimental data provided in [115, Figure 19].

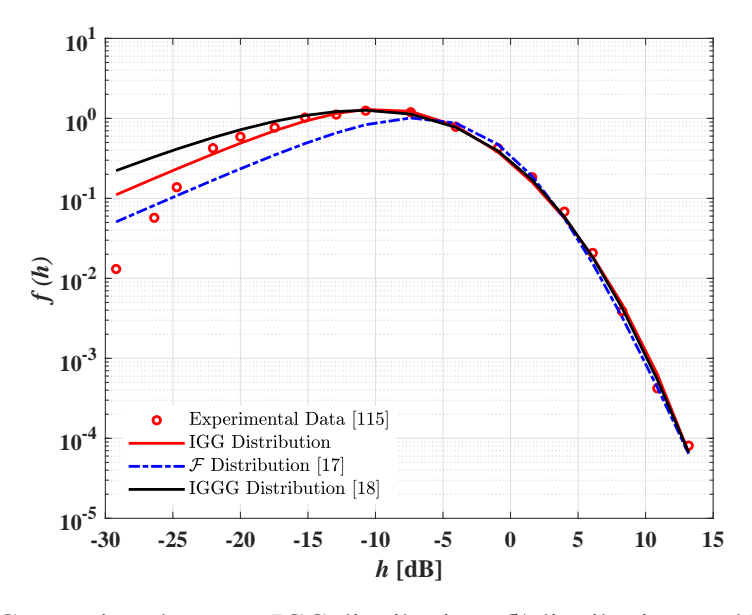


Figure 3.3: Comparison between IGG distribution,  $\mathcal{F}$  distribution, and IGGG distribution in the context of experimental data provided in [ [115, Figure 21].

Table 3.1: Comparison with Previous Models and Experimental Data

Cases	Experimental Data with wavelength, $\lambda = 532$ nm, Transmission range, L = 980m, outer scale turbulence, $L_0 = 0.8$ m [115]			IGG		F [17]		IGGG [18]		MSE <sub>IGG</sub>	$MSE_{\mathcal{F}}$	MSE <sub>IGGG</sub>
	D(mm)	$C_n^2$	$l_0$ (mm)	α	β	a	b	σ	$\mu$			
Case1	1.5	$5 \times 10^{-14}$	5.69	1.36	1.99	1.99	3.36	3.15	1.99	0.0022	0.0095	0.0030
Case2	4	$9 \times 10^{-14}$	6.02	0.88	1.74	1.74	2.88	2.14	1.74	0.0037	0.0570	0.0145

### 3.4 Performance Metrics

We evaluate the performance metrics, including, OP, and ABER of the FSO communication system under IGG fading in this section. These expressions enable us to evaluate the system performance under various channel conditions.

### 3.4.1 Exact and Asymptotic Outage Probability

The probability that instantaneous SNR  $(\gamma)$  at the receiver's input drops below a specific SNR threshold,  $\gamma_{th}$  is called outage probability denoted by  $P_{\text{out}}(\gamma_{th})$  and mathematically expressed as [16]:

$$P_{\text{out}}(\gamma_{th}) = P_r(\gamma \le \gamma_{th}) = F_{\gamma}(\gamma_{th}). \tag{3.16}$$

From (3.8),  $P_{\text{out}}(\gamma_{th})$  is expressed in closed form by replacing the value of the  $\gamma$  with  $\gamma_{th}$  and expressed as:

$$\begin{split} P_{\text{out}}(\gamma_{th}) &= \sqrt{\frac{2\alpha}{\pi}} \frac{\beta^{\beta} e^{\alpha}}{\bar{\gamma}^{\frac{\beta}{2}} \Gamma \beta} \left( \frac{\pi}{2 \sin(\pi \Lambda)} \right) \sum_{p=0}^{\infty} \Biggl\{ \left( \frac{(\frac{\alpha}{2})^{2p-\Lambda}}{\Gamma(p-\Lambda+1)p!} \right) \\ &\times G_{2,2}^{1,2} \left( \frac{2\beta}{\alpha} \sqrt{\frac{\gamma_{th}}{\bar{\gamma}}} \left| \frac{3}{4} - \frac{\beta}{2} + p - \frac{\Lambda}{2}, 1 - \beta \right. \right) \frac{\gamma_{th}^{\frac{\beta}{2}}}{\Gamma(\frac{\beta}{2} + \frac{1}{4} - p + \frac{\Lambda}{2})} - \left( \frac{(\frac{\alpha}{2})^{2p+\Lambda}}{\Gamma(p+\Lambda+1)p!} \right) \\ &\times \frac{\gamma_{th}^{\frac{\beta}{2}}}{\Gamma(\frac{\beta}{2} + \frac{1}{4} - p - \frac{\Lambda}{2})} G_{2,2}^{1,2} \left( \frac{2\beta}{\alpha} \sqrt{\frac{\gamma_{th}}{\bar{\gamma}}} \left| \frac{3}{4} - \frac{\beta}{2} + p + \frac{\Lambda}{2}, 1 - \beta \right. \right) \Biggr\}. \quad (3.17) \end{split}$$

Further, (3.17) can be simplified for  $\bar{\gamma}$  which is in the denominator by using [113, Eq. (07.34.17.0011.01)] as follows:

$$\begin{split} P_{\mathrm{out}}(\gamma_{th}) &= \sqrt{\frac{2\alpha}{\pi}} \frac{e^{\alpha}}{\Gamma\beta} \left( \frac{\pi}{2\sin(\pi\Lambda)} \right) \sum_{p=0}^{\infty} \left\{ \left( \frac{(\frac{\alpha}{2})^{\beta+2p-\Lambda}}{\Gamma(p-\Lambda+1)p!} \right) \frac{1}{\Gamma(\frac{\beta}{2} + \frac{1}{4} - p + \frac{\Lambda}{2})} \right. \\ & \left. G_{2,2}^{1,2} \left( \frac{2\beta}{\alpha} \sqrt{\frac{\gamma_{th}}{\bar{\gamma}}} \middle| \frac{3}{4} + \frac{\beta}{2} + p - \frac{\Lambda}{2}, 1 \right) - \left( \frac{(\frac{\alpha}{2})^{\beta+2p+\Lambda}}{\Gamma(p+\Lambda+1)p!} \right) \frac{1}{\Gamma(\frac{\beta}{2} + \frac{1}{4} - p - \frac{\Lambda}{2})} \right. \\ & \times G_{2,2}^{1,2} \left( \frac{2\beta}{\alpha} \sqrt{\frac{\gamma_{th}}{\bar{\gamma}}} \middle| \frac{3}{4} + \frac{\beta}{2} + p + \frac{\Lambda}{2}, 1 \right) \right\}. \end{split} \tag{3.18}$$

To obtain insights the system performance at high SNR i.e.  $\bar{\gamma} \to \infty$ , we expand the Meijer-G function in (3.18) using [113, Eq. (07.34.06.0040.01)]. By doing so, an asymptotic expression of OP is obtained as:

$$\begin{split} P_{\text{out}}^{\infty}(\gamma_{th}) &= \sqrt{\frac{2\alpha}{\pi}} \frac{e^{\alpha}}{\Gamma(1+\beta)} \left(\frac{\pi}{2\sin(\pi\Lambda)}\right) \left(\beta\sqrt{\frac{\gamma_{th}}{\bar{\gamma}}}\right)^{\beta} \\ &\times \sum_{p=0}^{\infty} \left(\frac{(\frac{\alpha}{2})^{2p-\Lambda}}{\Gamma(p-\Lambda+1)p!} - \frac{(\frac{\alpha}{2})^{2p+\Lambda}}{\Gamma(p+\Lambda+1)p!}\right). \end{split} \tag{3.19}$$

The asymptotic OP expression can be rewritten in terms of the diversity order,  $G_d$  i.e.,  $P_{\text{out}}^{\infty} \propto \bar{\gamma}^{-G_d}$ , where  $G_d = \frac{\beta}{2}$ . Therefore, the diversity order relies on the severity of fading, which is a small-scale turbulent eddy parameter,  $\beta$ .

### 3.4.2 Upper Bound on Outage Probability

Using the approximation  $K_v(x) \sim \frac{1}{2}\Gamma(v)\left(\frac{x}{2}\right)^{-v}$ , [116, Eq. (1.4)] in (3.8) and using integral identities [112, Eq.(3.194.1)] and [113, Eq. (07.23.26.0004.01)], upper bound of the  $F_{\gamma}(\gamma)$  is obtained as:

$$F_{\gamma}^{U}(\gamma) \sim \frac{e^{\alpha}}{\sqrt{\pi} \Gamma \beta} \left(\frac{2\beta}{\alpha}\right)^{\beta} \left(\frac{\gamma}{\bar{\gamma}}\right)^{\frac{\beta}{2}} G_{2,2}^{1,2} \left(\frac{2\beta}{\alpha} \sqrt{\frac{\gamma}{\bar{\gamma}}} \middle|_{0,-\beta}^{\frac{1}{2} - \beta, 1 - \beta}\right). \tag{3.20}$$

### 3.4.3 Exact and Asymptotic Average Bit Error Probability

The ABER is another crucial parameter to evaluate the system's reliability. The different modulation schemes and their respective ABER are discussed below.

#### **Digital Binary modulations**

ABER of the proposed system with digital binary modulation schemes is given as [117]:

$$\bar{P}_{be} = \frac{g^f}{2\Gamma f} \int_0^\infty \gamma^{f-1} e^{-g\gamma} F_{\gamma}(\gamma) d\gamma, \qquad (3.21)$$

where, f and g are the parameters that depend on the type of modulation schemes [118]. We substitute the expression (3.8) in (3.21), and use the identity [113, Eq. (07.34.21.0088.01)] to integrate (3.21). Further after some mathematical manipulations, the closed form expression of ABER for digital binary modulation schemes is given by:

$$\begin{split} \bar{P}_{be} &= \frac{1}{8\Gamma f} \sqrt{\frac{2\alpha}{\pi}} \frac{\beta^{\beta} e^{\alpha}}{\Gamma(\beta)\bar{\gamma}^{\frac{\beta}{2}}} \left(\frac{1}{\sin(\pi\Lambda)}\right) \sum_{p=0}^{\infty} \left\{ \left(\frac{(\frac{\alpha}{2})^{2p-\Lambda}}{\Gamma(p-\Lambda+1)p!}\right) \frac{2^{\left(\frac{\beta}{2} - \frac{3}{4} - p + \frac{\Lambda}{2}\right)} g^{-\frac{\beta}{2}}}{\Gamma(\frac{\beta}{2} + \frac{1}{4} - p + \frac{\Lambda}{2})} \right. \\ G_{5,4}^{2,5} \left(\frac{(\frac{2\beta}{\alpha})^{2}}{g\bar{\gamma}} \middle| \mathfrak{R}_{2}\right) - \left(\frac{(\frac{\alpha}{2})^{2p+\Lambda}}{\Gamma(p+\Lambda+1)p!}\right) \frac{2^{\left(\frac{\beta}{2} - \frac{3}{4} - p - \frac{\Lambda}{2}\right)} g^{-\frac{\beta}{2}}}{\Gamma(\frac{\beta}{2} + \frac{1}{4} - p - \frac{\Lambda}{2})} G_{5,4}^{2,5} \left(\frac{(\frac{2\beta}{\alpha})^{2}}{g\bar{\gamma}} \middle| \mathfrak{R}_{3}\right) \right\}, \end{split}$$
(3.22)

$$\begin{split} \text{where, } \mathfrak{R}_1 &= \left[1 - \left(\frac{\beta}{2} + f\right), \frac{\left(\frac{3}{4} - \frac{\beta}{2} + p - \frac{\Lambda}{2}\right)}{2}, \frac{\left(\frac{7}{4} - \frac{\beta}{2} + p - \frac{\Lambda}{2}\right)}{2}, \frac{(1-\beta)}{2}, \frac{(2-\beta)}{2}\right]; \\ \mathfrak{R}_2 &= \left[0, \frac{1}{2}, -\frac{\beta}{2}, \frac{1-\beta}{2}\right]; \mathfrak{R}_3 = \left[1 - \left(\frac{\beta}{2} + f\right), \frac{\left(\frac{3}{4} - \frac{\beta}{2} + p + \frac{\Lambda}{2}\right)}{2}, \frac{\left(\frac{7}{4} - \frac{\beta}{2} + p + \frac{\Lambda}{2}\right)}{2}, \frac{(1-\beta)}{2}, \frac{(2-\beta)}{2}\right]. \end{split}$$

Similar to the asymptotic OP expression, the asymptotic ABER expression is obtained by using the expressions [113, Eqs. (07.34.17.0011.01),(07.34.06.0040.01)] in (3.22) as follows:

$$\begin{split} \bar{P}_{be}^{\infty} &= \frac{1}{8\Gamma f} \sqrt{\frac{2\alpha}{\pi}} \frac{e^{\alpha}}{\Gamma(\beta) \sin(\pi\Lambda)} \sum_{p=0}^{\infty} \left\{ \left( \frac{(\frac{\alpha}{2})^{\beta+2p-\Lambda}}{\Gamma(p-\Lambda+1)p!} \right) \frac{2^{\left(\frac{\beta}{2}-\frac{3}{4}-p+\frac{\Lambda}{2}\right)}}{\Gamma(\frac{\beta}{2}+\frac{1}{4}-p+\frac{\Lambda}{2})} I_{1} \right. \\ & \left. - \left( \frac{(\frac{\alpha}{2})^{\beta+2p+\Lambda}}{\Gamma(p+\Lambda+1)p!} \right) \frac{2^{\left(\frac{\beta}{2}-\frac{3}{4}-p-\frac{\Lambda}{2}\right)}}{\Gamma(\frac{\beta}{2}+\frac{1}{4}-p-\frac{\Lambda}{2})} I_{2} \right\}, \quad (3.23) \end{split}$$

$$\begin{split} &\text{where, } I_1 = \sum_{j=1}^2 \left\{ \frac{\prod_{i=1}^2 \Gamma(\Re_{5,i} - \Re_{5,j}) \prod_{i=1}^5 \Gamma(1 - \Re_{4,i} + \Re_{5,j})}{\prod_{i=3}^4 \Gamma(1 - \Re_{5,i} + \Re_{5,j})} \left( \frac{\left(\frac{2\beta}{\alpha}\right)^2}{g\bar{\gamma}} \right)^{\Re_{5,j}} \right\}; \\ &I_2 = \sum_{j=1}^2 \left\{ \frac{\prod_{i=1}^2 \Gamma(\Re_{5,i} - \Re_{5,j}) \prod_{i=1}^5 \Gamma(1 - \Re_{6,i} + \Re_{5,j})}{\prod_{i=3}^4 \Gamma(1 - \Re_{5,i} + \Re_{5,j})} \left( \frac{\left(\frac{2\beta}{\alpha}\right)^2}{g\bar{\gamma}} \right)^{\Re_{5,j}} \right\}; \\ &\Re_4 = \left[ 1 - f, \frac{\left(\frac{3}{4} + \frac{\beta}{2} + p - \frac{\Lambda}{2}\right)}{2}, \frac{\left(\frac{7}{4} + \frac{\beta}{2} + p - \frac{\Lambda}{2}\right)}{2}, \frac{1}{2}, 1 \right]; \Re_5 = \left[ \frac{\beta}{2}, \frac{1 + \beta}{2}, 0, \frac{1}{2} \right]; \\ &\Re_6 = \left[ 1 - f, \frac{\left(\frac{3}{4} + \frac{\beta}{2} + p + \frac{\Lambda}{2}\right)}{2}, \frac{\left(\frac{7}{4} + \frac{\beta}{2} + p + \frac{\Lambda}{2}\right)}{2}, \frac{1}{2}, 1 \right]. \end{split}$$

### MPSK modulation

The ABER of the proposed system under M-ary PSK modulation schemes is given by [119]:

$$\bar{P}_{be,\text{MPSK}} = \frac{A}{2} \int_0^\infty erfc(B\sqrt{\gamma}) f_{\gamma}(\gamma) d\gamma, \qquad (3.24)$$

where, A takes a value of 1 when M = 2, and 2 for M > 2.  $B = \sin(\pi/M)$  for all values of M, where M is the modulation order. On the substitution of (3.6) into (3.24),

and applying series expansion of the  $K_v(.)$  given in [113, Eq. (03.04.06.0030.01)] and using integral identities [112, Eqs. (8.4.14.2), (8.4.2.5)] in (3.24), the  $\bar{P}_{be,\text{MPSK}}$ becomes:

$$\begin{split} \bar{P}_{be,\text{MPSK}} &= \frac{A}{2} \sqrt{\frac{\alpha}{2}} \frac{\beta^{\beta} e^{\alpha}}{\Gamma(\beta) \bar{\gamma}^{\frac{\beta}{2}}} \left( \frac{1}{2 \sin(\pi \Lambda)} \right) \sum_{p=0}^{\infty} \left\{ \frac{A_{11}}{\Gamma\left(\frac{\beta}{2} + \frac{1}{4} - p + \frac{\Lambda}{2}\right)} \right. \\ & \int_{0}^{\infty} \gamma^{\frac{\beta}{2} - 1} G_{1,2}^{2,0} \left( \gamma B^{2} \bigg|_{\mathfrak{R}_{8}}^{\mathfrak{R}_{7}} \right) G_{1,1}^{1,1} \left( \Xi \sqrt{\gamma} \bigg|_{\mathfrak{R}_{8}}^{\mathfrak{R}_{9}} \right) d\gamma - \frac{A_{22}}{\Gamma\left(\frac{\beta}{2} + \frac{1}{4} - p - \frac{\Lambda}{2}\right)} \\ & \int_{0}^{\infty} \gamma^{\frac{\beta}{2} - 1} G_{1,2}^{2,0} \left( \gamma B^{2} \bigg|_{\mathfrak{R}_{8}}^{\mathfrak{R}_{7}} \right) G_{1,1}^{1,1} \left( \Xi \sqrt{\gamma} \bigg|_{\mathfrak{R}_{10}}^{\mathfrak{R}_{11}} \right) d\gamma \right\}, \quad (3.25) \end{split}$$
 where,  $\mathfrak{R}_{7} = \left[ 1 \right]; \mathfrak{R}_{8} = \left[ 0, \frac{1}{2} \right]; \mathfrak{R}_{9} = \left[ \left( \frac{3}{4} - \frac{\beta}{2} + p - \frac{\Lambda}{2} \right) \right]; \mathfrak{R}_{10} = \left[ 0 \right];$  
$$\mathfrak{R}_{11} = \left[ \left( \frac{3}{4} - \frac{\beta}{2} + p + \frac{\Lambda}{2} \right) \right].$$

With the aid of [113, Eq. (07.34.21.0013.01)] to (3.25) and performing some algebraic operations,  $P_{be,MPSK}$  expression is obtained in the closed-form as follows:

$$\begin{split} P_{be,\text{MPSK}} &= \frac{A}{8\pi B^{\beta}} \sqrt{\frac{\alpha}{2}} \frac{\beta^{\beta} e^{\alpha}}{\Gamma(\beta) \bar{\gamma}^{\frac{\beta}{2}}} \left( \frac{1}{\sin(\pi\Lambda)} \right) \sum_{p=0}^{\infty} \left\{ \left( \frac{(\frac{\alpha}{2})^{2p-\Lambda}}{\Gamma(p-\Lambda+1)p!} \right) \right. \\ &\times \frac{2^{\left(\frac{\beta}{2} + \frac{1}{4} - p + \frac{\Lambda}{2}\right)}}{\Gamma\left(\frac{\beta}{2} + \frac{1}{4} - p + \frac{\Lambda}{2}\right)} G_{4,3}^{2,4} \left( \left( \frac{2\beta}{\alpha B \sqrt{\bar{\gamma}}} \right)^{2} \middle| \mathfrak{R}_{12} \right) - \left( \frac{(\frac{\alpha}{2})^{2p+\Lambda}}{\Gamma(p+\Lambda+1)p!} \right) \\ &\times \frac{2^{\left(\frac{\beta}{2} + \frac{1}{4} - p - \frac{\Lambda}{2}\right)}}{\Gamma\left(\frac{\beta}{2} + \frac{1}{4} - p - \frac{\Lambda}{2}\right)} G_{4,3}^{2,4} \left( \left( \frac{2\beta}{\alpha B \sqrt{\bar{\gamma}}} \right)^{2} \middle| \mathfrak{R}_{13} \right) \right\}, \quad (3.26) \end{split}$$
 where,  $\mathfrak{R}_{12} = \left[ \frac{\left(\frac{3-\beta}{4} + p - \frac{\Lambda}{2}\right)}{2}, \frac{\left(\frac{7-\beta}{2} + p - \frac{\Lambda}{2}\right)}{2}, 1 - \frac{\beta}{2}, \frac{\left(1-\beta\right)}{2} \right]; \, \mathfrak{R}_{13} = \left[ 0, \frac{1}{2}, -\frac{\beta}{2} \right]; \end{split}$ 

$$\begin{split} \text{where, } \mathfrak{R}_{12} &= \left\lfloor \frac{\left(\frac{3}{4} - \frac{\beta}{2} + p - \frac{\Lambda}{2}\right)}{2}, \frac{\left(\frac{7}{4} - \frac{\beta}{2} + p - \frac{\Lambda}{2}\right)}{2}, 1 - \frac{\beta}{2}, \frac{(1 - \beta)}{2} \right\rfloor; \\ \mathfrak{R}_{14} &= \left\lfloor \frac{\left(\frac{3}{4} - \frac{\beta}{2} + p + \frac{\Lambda}{2}\right)}{2}, \frac{\left(\frac{7}{4} - \frac{\beta}{2} + p + \frac{\Lambda}{2}\right)}{2}, 1 - \frac{\beta}{2}, \frac{(1 - \beta)}{2} \right\rfloor. \end{split}$$

The asymptotic ABER for MPSK modulation can be obtained from (3.26) by using [113, Eqs. (07.34.17.0011.01),(07.34.06.0040.01)] for  $\bar{\gamma} \to \infty$  as:

$$\begin{split} \bar{P}_{be,\text{MPSK}}^{\infty} &= \frac{A}{8\pi} \left(\frac{\alpha}{2}\right)^{\beta + \frac{1}{2}} \frac{e^{\alpha}}{\Gamma(\beta) \sin(\pi\Lambda)} \sum_{p=0}^{\infty} \Bigg\{ \left(\frac{(\frac{\alpha}{2})^{2p-\Lambda}}{\Gamma(p-\Lambda+1)p!}\right) \\ &\times \frac{2^{\left(\frac{\beta}{2} + \frac{1}{4} - p + \frac{\Lambda}{2}\right)}}{\Gamma(\frac{\beta}{2} + \frac{1}{4} - p + \frac{\Lambda}{2})} I_3 - \left(\frac{(\frac{\alpha}{2})^{2p+\Lambda}}{\Gamma(p+\Lambda+1)p!}\right) \frac{2^{\left(\frac{\beta}{2} + \frac{1}{4} - p - \frac{\Lambda}{2}\right)}}{\Gamma(\frac{\beta}{2} + \frac{1}{4} - p - \frac{\Lambda}{2})} I_4 \Bigg\}, \quad (3.27) \end{split}$$
 where, 
$$I_3 = \sum_{j=1}^2 \Bigg\{ \frac{\prod_{i=1}^2 \Gamma(\Re_{16,i} - \Re_{16,j}) \prod_{i=1}^4 \Gamma(1 - \Re_{15,i} + \Re_{16,j})}{\prod_{i=3}^3 \Gamma(1 - \Re_{16,i} + \Re_{16,j})} \left(\frac{2\beta}{\alpha B\sqrt{\tilde{\gamma}}}\right)^{2\Re_{16,j}} \Bigg\};$$

$$\begin{split} I_4 &= \sum_{j=1}^2 \left\{ \frac{\prod_{\substack{i=1\\i\neq j}}^2 \Gamma(\Re_{16,i} - \Re_{16,j}) \prod_{\substack{i=1\\i\neq j}}^4 \Gamma(1-\Re_{17,i} + \Re_{16,j})}{\prod_{\substack{i=3\\i\neq j}}^3 \Gamma(1-\Re_{16,i} + \Re_{16,j})} \Big(\frac{2\beta}{\alpha B \sqrt{\bar{\gamma}}}\Big)^{2\Re_{16,j}} \right\}; \\ \Re_{15} &= \left[ \frac{\left(\frac{3}{4} + \frac{\beta}{2} + p - \frac{\Lambda}{2}\right)}{2}, \frac{\left(\frac{7}{4} + \frac{\beta}{2} + p - \frac{\Lambda}{2}\right)}{2}, 1, \frac{1}{2} \right]; \\ \Re_{16} &= \left[ \frac{\beta}{2}, \frac{1+\beta}{2}, 0 \right]; \Re_{17} = \left[ \frac{\left(\frac{3}{4} + \frac{\beta}{2} + p + \frac{\Lambda}{2}\right)}{2}, \frac{\left(\frac{7}{4} + \frac{\beta}{2} + p + \frac{\Lambda}{2}\right)}{2}, 1, \frac{1}{2} \right]. \end{split}$$

### 3.5 Results and Discussion

In this section, we discuss the numerical and simulation findings for the FSO communication system over IGG distribution under different environmental turbulence conditions. The system parameters are considered based on the literature [64], [120]. For analysis, transmission range  $L=3.5{\rm km}$ , optical wavelength  $\lambda=1550{\rm nm}$  are considered by taking receiver aperture diameter  $D=10{\rm mm}$ , the outer scale of turbulence  $L_0=0.8{\rm m}$  and inner scale of turbulence  $l_0=5.98{\rm mm}$ . The fading parameters,  $\alpha$  and  $\beta$  are calculated using (3.3a), (3.3b) and with the refractive index  $C_n^2$  and Rytov variance  $\sigma_n^2$ . where,  $\sigma_n^2=0.5C_n^2k^{\frac{7}{6}}L^{\frac{11}{6}}$ , and  $k=2\pi/\lambda$ . Specifically,  $\sigma_n^2<1,\sigma_n^2\approx 1$  and  $\sigma_n^2>1$  corresponds to the weak, moderate, and strong turbulence conditions respectively. The refraction index structure parameter,  $C_n^2=9\times 10^{-15}{\rm m}^{-2/3}$ ,  $2\times 10^{-14}{\rm m}^{-2/3}$  and  $8\times 10^{-14}{\rm m}^{-2/3}$  is assumed for weak, moderate, and strong atmospheric turbulence respectively which results  $\sigma_n^2=0.7241$ ,  $(\alpha,\beta)=(3.1833,2.9021)$ ,  $\sigma_n^2=1.6092$ ,  $(\alpha,\beta)=(1.9363,1.8276)$  and  $\sigma_n^2=6.4369$ ,  $(\alpha,\beta)=(1.5297,1.4262)$  respectively. Furthermore, Monte-Carlo simulations provide a perfect match with exact analytic results which validates the derived expression and the accuracy of the computation of the Meijer-G function. Note that number of iterations is taken as  $10^6$  for Monte-Carlo Simulation. Moreover, the agreement between asymptotic and exact analytic expressions offers valuable insights into the system's performance.

Table 3.2: Truncation Accuracy of Summation Limits for OP and ABER

Expression	Truncation		Chosen		
	limits	$\bar{\gamma} = 0 \text{ dB}$	$\bar{\gamma}$ = 10 dB	$\bar{\gamma}$ = 15 dB	limits
	p = 8	0.922179	0.154843	$5.081306 \times 10^{-2}$	
$P_{\mathrm{out}}(\gamma_{th})$	p = 10	0.641037	0.154349	$5.077285 \times 10^{-2}$	
	p = 14	0.638926	0.154348	$5.077277 \times 10^{-2}$	
	p = 15	0.638926	0.154348	$5.077277 \times 10^{-2}$	
					p = 15
	p = 10	0.172298	$3.558596 \times 10^{-2}$	$1.199607 \times 10^{-2}$	
$\bar{P}_{be}$	p = 12	0.163211	$3.558478 \times 10^{-2}$	$1.199603 \times 10^{-2}$	
	p = 14	0.163145	$3.558478 \times 10^{-2}$	$1.199603 \times 10^{-2}$	
	p = 15	0.163144	$3.558478 \times 10^{-2}$	$1.199603 \times 10^{-2}$	

Table 3.2 shows the truncation precision for the computed OP and ABER vaules and lists the maximum number of series terms considered, as ashown in the sixth column. The Table 3.2 reveals that extending the summation beyond 15 terms yields minimal improvement in the performance metrics.

For comparing these distributions, small-scale turbulent eddies are fixed for IGG,  $\mathcal{F}$  and IGGG distributions, i.e.  $\beta=\alpha=\mu$ . However, large-scale turbulent eddies are varied for these three distributions for a particular atmospheric turbulence condition, as shown in Table 3.1. Using the fixed values of large-scale turbulent eddies for different distributions for a particular atmospheric turbulence condition, the AOF is the same for these considered distributions as shown in Fig. 3.4.

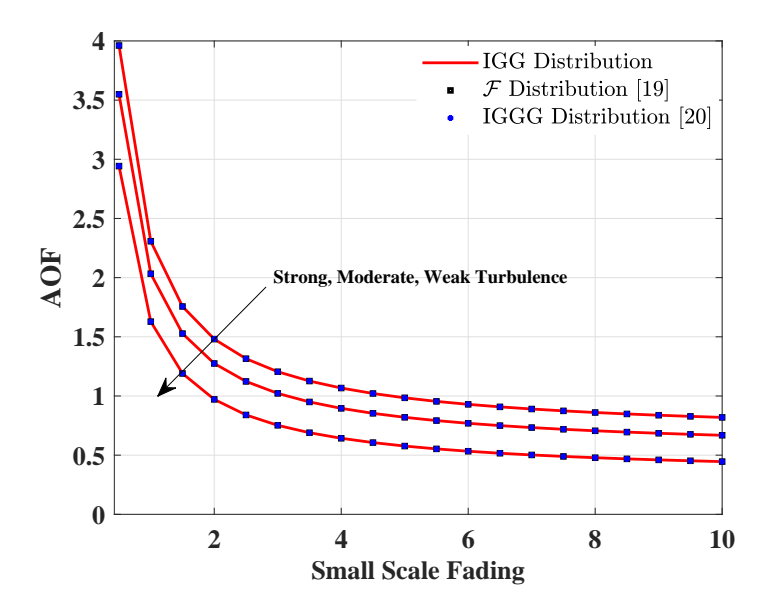


Figure 3.4: AOF of IGG,  $\mathcal{F}$ , and IGGG distributions under different atmospheric turbulence conditions.

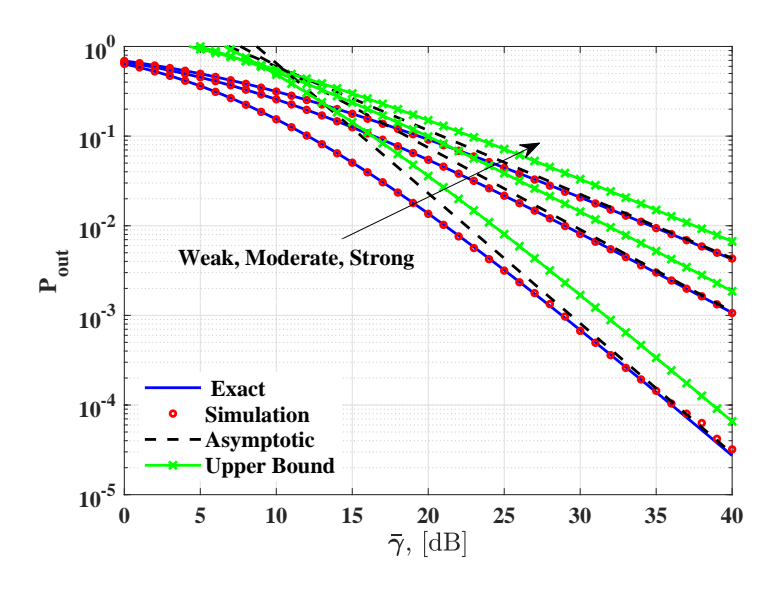


Figure 3.5: OP for different atmospheric turbulence conditions with  $\gamma_{th}$  = 0 dB and D = 10mm.

Fig. 3.5, Fig. 3.6, and Fig. 3.7 exhibit the results of exact OP, asymptotic OP, upper bound on OP, and simulated OP for the received average SNR,  $\bar{\gamma}$  with IM/DD detection scheme. Fig. 3.5 depicts the analysis of OP under different atmospheric turbulence

conditions for  $\gamma_{th}$  = 0 dB and D = 10mm. The results suggest that OP performance is more favourable under weak turbulence circumstances than other turbulence settings. When  $\bar{\gamma}$  is set to 30dB, OP values are  $6.72 \times 10^{-4}, 8.09 \times 10^{-3}$  and  $2.09 \times 10^{-2}$  for weak, moderate, and strong turbulence conditions respectively. The effect of threshold  $\gamma_{th}$  on OP is depicted in Fig. 3.6 under strong turbulence conditions. The findings show a substantial loss in performance when the  $\gamma_{th}$  increases from -5dB to 5dB. For instance, at  $\bar{\gamma}$  = 30dB, OP values are  $9.40 \times 10^{-3}$  for  $\gamma_{th}$  = -5dB,  $2.09 \times 10^{-2}$  for  $\gamma_{th}$  = 0 dB, and  $4.42 \times 10^{-2}$  for 5dB.

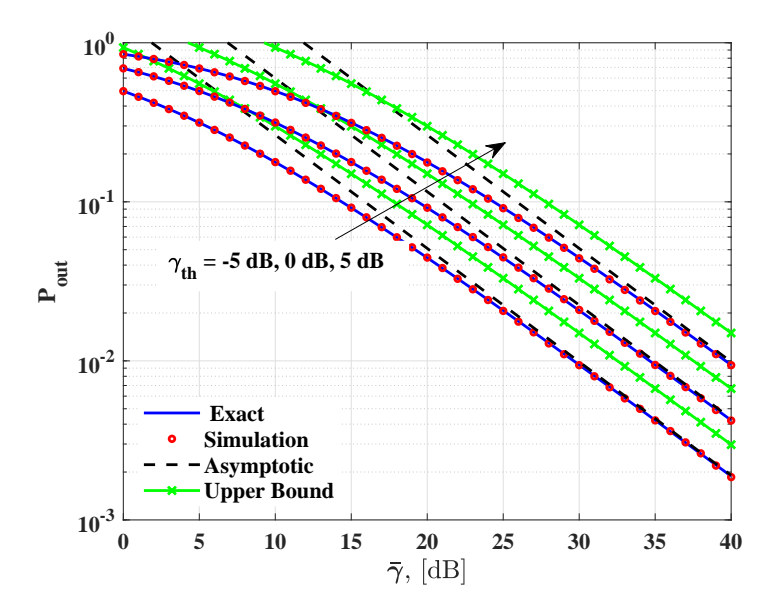


Figure 3.6: OP for different thresholds,  $\gamma_{th}$  under strong turbulence conditions.

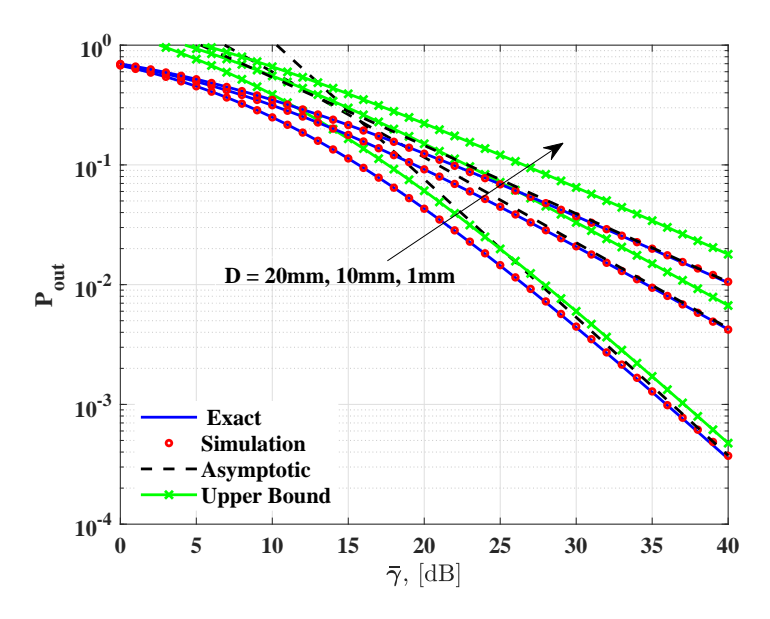


Figure 3.7: OP for different aperture, D under strong turbulence conditions with  $\gamma_{th}$  = 0 dB.

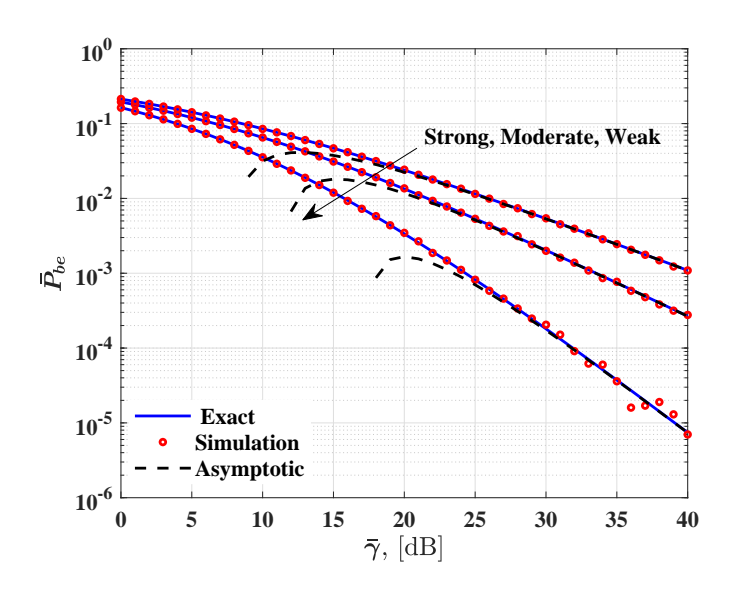


Figure 3.8: ABER for different atmospheric turbulence conditions with BPSK modulation and D = 10mm.

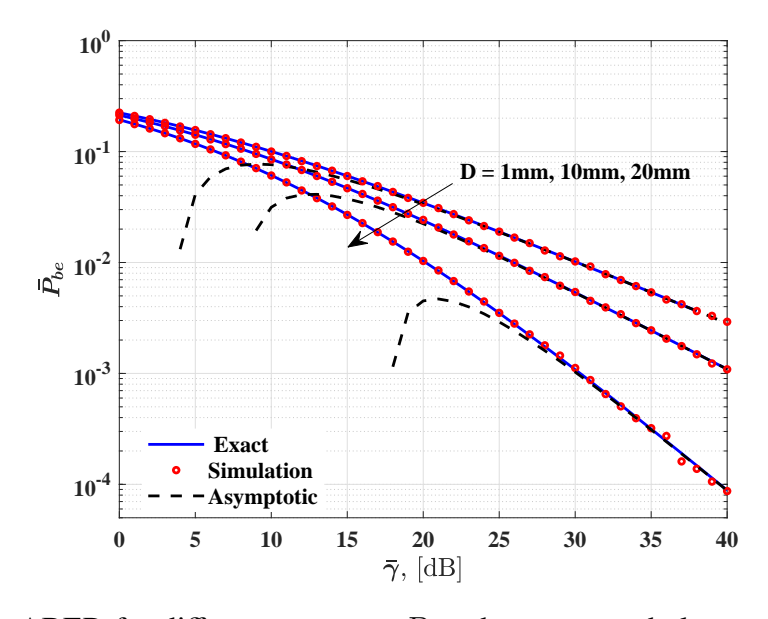


Figure 3.9: ABER for different aperture, D under strong turbulence conditions with BPSK modulation.

In Fig. 3.7, OP is analysed for different aperture, D under strong atmospheric turbulence conditions with  $\gamma_{th}=0$  dB. Considering,  $(\alpha,\beta)=(1.5262,1.1392)$  for D=1mm,  $(\alpha,\beta)=(1.5297,1.4262)$  for D=10mm, and  $(\alpha,\beta)=(1.5402,2.3064)$  for D=20mm. It is evident that at  $\bar{\gamma}=30$ dB, OP values are  $4.47\times10^{-3}$  for D=20mm,  $2.09\times10^{-2}$  for D=10mm, and  $3.73\times10^{-2}$  for D=1mm. The ABER performance is evaluated using exact, asymptotic, and simulated results and is presented in Fig. 3.8 to Fig. 3.11. These figures depict ABER performance for the received average SNR,  $\bar{\gamma}$  with IM/DD detection scheme. Several modulation schemes including BPSK, DPSK, CBFSK, OOK, and MPSK are employed to evaluate the ABER performance. In Fig. 3.8, ABER is for strong, moderate, and weak turbulence with the BPSK modulation scheme, and D

= 10mm is depicted. For instance, at  $\bar{\gamma}$  = 30dB ,  $\bar{P}_{be}$  is  $1.81 \times 10^{-4}, 2 \times 10^{-3}$  and  $5.42 \times 10^{-3}$  corresponding to the weak, moderate, and strong turbulence conditions respectively.

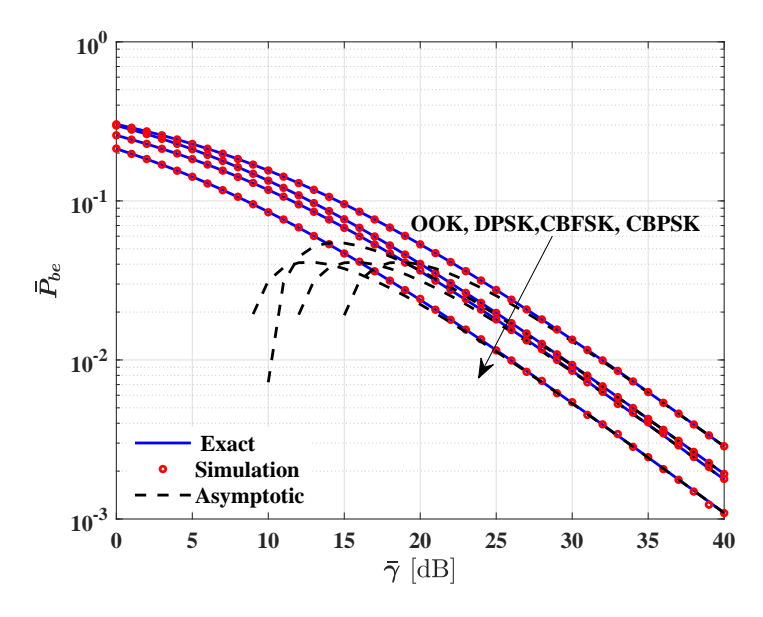


Figure 3.10: ABER for various modulation schemes under strong turbulence conditions with D = 10mm.

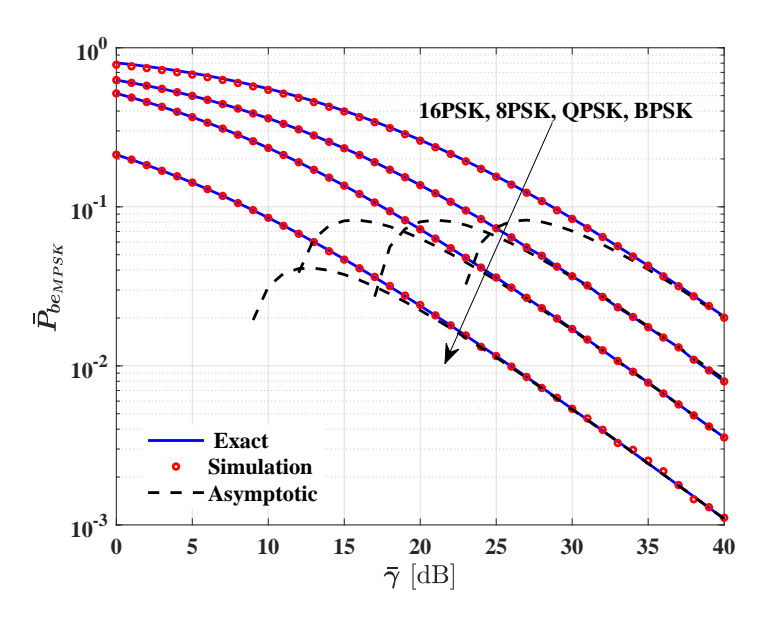


Figure 3.11: ABER for MPSK modulation schemes under strong turbulence conditions with D = 10mm.

Fig. 3.9 shows ABER for different aperture D under strong turbulence conditions with BPSK modulation. The values of  $(\alpha,\beta)=(1.5262,\ 1.1392),\ (1.5297,\ 1.4262)$  and  $(1.5402,\ 2.3064)$  are corresponding to D=1mm, 10mm, and 20mm respectively. When  $\bar{\gamma}$  is set at 30dB,  $\bar{P}_{be}$  is  $1.12\times 10^{-3}$  for D=20mm,  $5.42\times 10^{-3}$  for D=10mm, and  $1.02\times 10^{-2}$  for D=1mm. Fig. 3.10 depicts the impact of modulation schemes

on ABER under strong turbulence conditions with D = 10mm. The results suggest that BPSK modulation works better than other modulation schemes. Specifically, at  $\bar{\gamma}=30\text{dB},\ \bar{P}_{be}$  is  $5.42\times10^{-3}$  for BPSK,  $8.55\times10^{-3}$  for CBFSK,  $9.30\times10^{-3}$  for DPSK, and  $1.34\times10^{-2}$  for OOK modulation. Fig. 3.11 presents ABER for MPSK modulation schemes under strong turbulence situations with D = 10mm. It is observed that BPSK outperforms QPSK, 8PSK, and 16PSK. For instance, at  $\bar{\gamma}=30\text{dB},\ \bar{P}_{be,\text{MPSK}}$  is  $5.42\times10^{-3}, 1.70\times10^{-2}, 3.66\times10^{-2}, \text{and } 8.39\times10^{-2}$  for BPSK, QPSK, 8PSK, and 16PSK, respectively. It is noteworthy that ABER exhibits significant variation among different M-ary binary modulation schemes.

## Chapter 4

# Performance Analysis of Multiuser Dual-hop RF-FSO Systems with Perfect CSI

This chapter presents a performance analysis of a MU dual-hop RF-FSO relaying system with perfect CSI for uplink transmission. The system employs a user scheduling scheme and accounts for the impact of CCI at the relay node. The RF and FSO links are modeled by Rayleigh fading and  $\mathcal F$  distribution, respectively.

The key contributions of this chapter are summarized as follows:

- A unified closed-form expression for the OP is derived for the MU dual-hop RF-FSO DF relaying system,. The analysis incorporates CDF-based scheduling scheme, accounts for i.n.i.d CCI and considers the variations in power and fading channel gain across users and the relay.
- An asymptotic OP expression is obtained in the high SINR regime to provise insights such as diversity order.
- An optimal power allocation is formulated for the users and relay to minimize the OP while satisfying a total power constraint.
- The optimal channel access ratios for the users are determined to further enhance the system performance.

## 4.1 System and Channel Model

### 4.1.1 System Model

Consider a MU dual-hop RF-FSO relay based system for uplink transmission, taking into account CCI. The system comprises M users communicating with the destination node D via a relay node R while contending with interference from N RF interferers at relay R as depicted in Fig. 4.1.

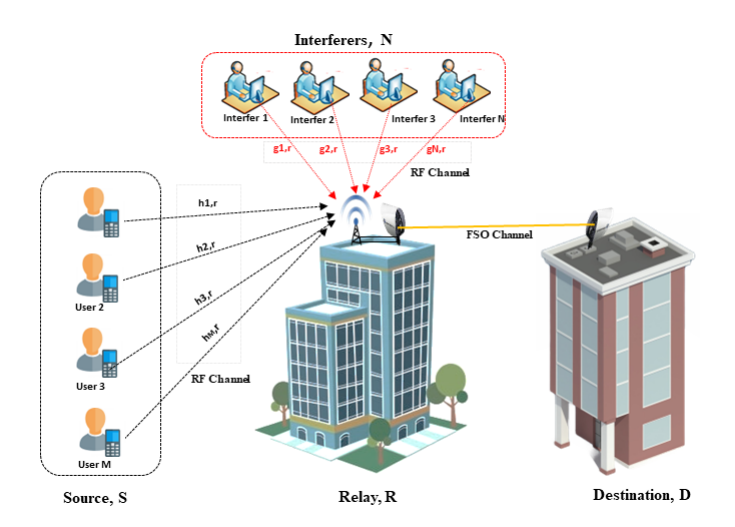


Figure 4.1: System model of MU relay system with i.n.i.d CCI.

In the two hop transmission process, the mth user scheduled for data transmission sends a unit energy symbol,  $x_{m,r}$  (m=1,2...,M) to the relay R in the RF hop. The received signal, denoted as  $y_{m,r}$  at relay R from mth user in the vicinity of CCI is expressed as:

$$y_{m,r} = \sqrt{P_s} h_{m,r} x_{m,r} + \sum_{n=1}^{N} \sqrt{P_{I_{n,r}}} g_{I_{n,r}} x_{I_{n,r}} + n_r, \tag{4.1}$$

where,  $P_s$  represents available transmit power at user, RF channel fading coefficients between mth user and R, denoted as  $h_{m,r}$ , follow a Rayleigh distribution with mean 0 and variance  $\Omega_{m,r}$  denoted as  $h_{m,r} \sim CN(0,\Omega_{m,r})$ ,  $x_{m,r}$  is the transmitted data of mth user with  $\mathbb{E}(|x_{m,r}|^2)=1$ ,  $P_{I_{n,r}}$  is transmit power of nth interferer, channel fading coefficient between nth interferer and R is denoted by  $g_{I_{n,r}} \sim CN(0,\Omega_{I_{n,r}})$ ,  $x_{I_{n,r}}$  is the transmitted data of nth interferer with  $\mathbb{E}(|x_{I_{n,r}}|^2)=1$ , and  $n_r \sim CN(0,\sigma^2)$ . The instantaneous signal-to-interference-noise ratio (SINR), denoted as  $\Gamma_{m,r}$  for the RF hop can be written as:

$$\begin{split} \Gamma_{m,r} &= \frac{P_s |h_{m,r}|^2}{\sum_{n=1}^N P_{I_{n,r}} |g_{I_{n,r}}|^2 + \sigma^2}, \\ &\triangleq \frac{X_m}{Z+1}, \end{split} \tag{4.2}$$

where, 
$$X_m=\gamma_s|h_{m,r}|^2$$
,  $Z=\sum_{n=1}^N\gamma_{I_{n,r}}|g_{I_{n,r}}|^2$ ,  $\gamma_s\triangleq\frac{P_s}{\sigma^2}$ ,  $\gamma_{I_{n,r}}\triangleq\frac{P_{I_{n,r}}}{\sigma^2}$ .

In the FSO hop, DF protocol is employed at R to decodes the received signal. After decoding, R re-encodes the signal for subsequent transmissions, converting the electrical signals to optical signals for transmission over FSO channel which is susceptible to atmospheric turbulence. Afterwards, photodetector detects optical signal at the receiver and converts it back into an electrical form.

The received signal,  $y_{r,d}$  at D is written as:

$$y_{r,d} = \eta \sqrt{P_r} I_{r,d} x_{r,d} + n_d,$$
 (4.3)

 $P_r$  represents transmit power of relay,  $I_{r,d}$  represents turbulence induced light intensity modeled by  $\mathcal F$  Distribution,  $x_{r,d}$  is transmitted signal from R with  $\mathbb E(|x_{r,d}|^2)=1$  and  $n_d \sim CN(0, \sigma^2)$  [121].

The instantaneous SNR, denoted as  $\Gamma_{r,d}$  for the FSO link is expressed as:

$$\Gamma_{r,d} = \gamma_r |I_{r,d}|^2, \tag{4.4}$$

where,  $\gamma_r \triangleq \frac{\eta^2 P_r}{\sigma^2}$ . The average SNR for the FSO link is expressed as:

$$\bar{\Gamma}_{r,d} = \gamma_r(\mathbb{E}|I_{r,d}|)^2. \tag{4.5}$$

The equivalent end-to-end instantaneous SINR, denoted as  $\Gamma_{e2e}$  for DF based relaying system with user scheduling scheme is expressed as:

$$\Gamma_{e2e} = \min(\Gamma_{m^*,r}, \Gamma_{r,d}^r) \tag{4.6}$$

where,  $m^*$  is the scheduled user which is different for various user scheduling schemes.

#### 4.1.2 **Channel Model**

The PDF and CDF of Rayleigh distribution fading channel for user and relay link are expressed as follows:

$$f_{X_m}(x) \; \triangleq \frac{1}{\gamma_s \Omega_{m,r}} e^{\frac{-x}{\gamma_s \Omega_{m,r}}}, F_{X_m}(x) \; \triangleq 1 - e^{\frac{-x}{\gamma_s \Omega_{m,r}}}$$

The PDF of Z which is sum of N independent exponential random variable is given by [122, Eq. (39)]:

$$f_Z(z) = \frac{1}{\Gamma N} \left( \frac{1}{\gamma_{I_{n,r}} \Omega_{I_{n,r}}} \right)^N z^{N-1} e^{\frac{-z}{\gamma_{I_{n,r}} \Omega_{I_{n,r}}}}$$

The CDF of Rayleigh distribution fading channel for the RF hop is provided in [123]

$$F_{\Gamma_{m,r}}(x) = 1 - \frac{e^{\frac{-x}{\gamma_s \Omega_{m,r}}}}{\prod_{n=1}^{N} \left(1 + \frac{\gamma_{I_{n,r}} \Omega_{I_{n,r}}}{\gamma_s \Omega_{m,r}} x\right)}.$$
 (4.7)

The PDF of  $\mathcal{F}$  distribution fading channel for FSO hop is given as [17, Eq. (20)]

$$f_{\Gamma_{r,d}}(x) = \frac{a^a (b-1)^b \gamma_r^{\ b/2} \ x^{\frac{a}{2}-1}}{2\beta(a,b) (a\sqrt{x} + (b-1)\sqrt{\gamma_r})^{a+b}}, \tag{4.8}$$

where, a and b are the fading parameters for small and large scales, respectively. The CDF of  $\mathcal{F}$  distribution fading channel for FSO hop can be calculated from (4.8) using the identities [112, Eq. (3.194.1)] and [113, Eq. (07.23.26.0004.01)] as follows:

$$F_{\Gamma_{r,d}}(x) = \left(\frac{a}{b-1}\right)^a \frac{1}{\Gamma a \; \Gamma b} \left(\frac{x}{\gamma_r}\right)^{a/2} G_{2,2}^{1,2} \left(\frac{a}{(b-1)} \sqrt{\frac{x}{\gamma_r}} \middle| 1 - a - b, 1 - a \right). \tag{4.9}$$

The complementary CDF of the  $\Gamma_{r,d}$  is obtained by using the identities [112, Eq.  $(3.194.2^6)$ ] and [113, Eqs. (07.23.26.0004.01), (07.34.16.0002.01)] as follows:

$$F_{\Gamma_{r,d}}^{C}(x) = \left(\frac{b-1}{a}\right)^{b} \frac{1}{\Gamma a \Gamma b} \left(\frac{\gamma_{r}}{x}\right)^{b/2} G_{2,2}^{2,1} \left(\frac{a}{(b-1)} \sqrt{\frac{x}{\gamma_{r}}} \begin{vmatrix} 1, 1+b \\ a+b, b \end{vmatrix}\right). \tag{4.10}$$

The mathematical expression for selecting the mth user using greedy-based scheduling scheme is as follows:

$$m^* = \underset{m \in 1, 2, \dots, M}{\arg \max} \left( \frac{X_m}{Z+1} \right). \tag{4.11}$$

The mathematical expression for selecting the mth user using PFS-based scheduling scheme is as follows:

$$m^* = \arg\max_{m \in 1, 2 \dots M} \left(\frac{\Gamma_{m,r}}{\bar{\Gamma}_{m,r}}\right). \tag{4.12}$$

where,  $\bar{\Gamma}_{\text{m,r}} = \mathbb{E}(\Gamma_{m,r})$ .

The mathematical expression for selecting the mth user using CDF-based scheduling scheme is as follows:

$$m^* = \underset{m \in 1, 2, \dots, M}{\arg \max} \left( F_{\Gamma_{m,r}}(x) \right)^{\frac{1}{v_m}}.$$
 (4.13)

### 4.2 Performance Metrics

### 4.2.1 Outage Probability

It is the probability that instantaneous end-to-end SINR,  $\Gamma_{e2e}$  is less than an acceptable threshold,  $\gamma_{th}$  and it is defined as:

$$\begin{split} P^S_{\Gamma_{e2e}}(\gamma_{th}) &= \Pr(\Gamma_{e2e} < \gamma_{th}) = \Pr\Big(\min(\Gamma_{m^*,r},\Gamma^r_{r,d}) < \gamma_{th}\Big), \\ &= F^S_{\Gamma_{m^*,r}}(\gamma_{th}) + F_{\Gamma_{r,d}}(\gamma_{th}) - F^S_{\Gamma_{m^*,r}}(\gamma_{th})F_{\Gamma_{r,d}}(\gamma_{th}). \end{split} \tag{4.14}$$

where,  $\gamma_{th}=2^{2\rho}-1,~\rho$  denotes the target rate,  $S\in(\text{GS},\text{PFS},\text{CDFS})$  refers to Greedy Scheduling, Proportional Fairness Scheduling and Cumulative Distribution Function based Scheduling respectively and  $F^S_{\Gamma_{m^*,r}}$  denotes the CDF of first hop for scheduling schemes.

Further, (4.14) can be simplified as:

$$P_{\Gamma_{e^{2}e}}^{S}(\gamma_{th}) = F_{\Gamma_{m^*}}^{S}(\gamma_{th}) F_{\Gamma_{r,d}}^{C}(\gamma_{th}) + F_{\Gamma_{r,d}}(\gamma_{th}). \tag{4.15}$$

#### **OP of Greedy Scheduling**

The CDF of the RF link with CCI using greedy scheduling (4.11) is given as:

$$\begin{split} \mathbf{F}_{\Gamma_{\mathbf{m}*,\mathbf{r}}}^{\mathrm{GS}}(\gamma_{th}) &= & \mathrm{Pr}\Bigg(\max_{m\in 1,2...M}(\Gamma_{m,r}) \leq \gamma_{th}\Bigg), \\ &= & \prod_{m=1}^{M}F_{\Gamma_{m,r}}(\gamma_{th}). \end{split} \tag{4.16}$$

By using (4.7), (4.9), (4.10) and (4.16) into (4.15), the unified closed-form expression for OP with GS can be obtained as:

$$\begin{split} P_{\Gamma_{e2e}}^{\text{GS}}(\gamma_{th}) &= \prod_{m=1}^{M} \left( 1 - \frac{e^{\frac{-\gamma_{th}}{\gamma_{s}\Omega_{m,r}}}}{\prod_{n=1}^{N} \left( 1 + \frac{\gamma_{I_{n,r}}\Omega_{I_{n,r}}\gamma_{th}}{\gamma_{s}\Omega_{m,r}} \right)} \right) \left( \frac{b-1}{a} \right)^{b} \frac{1}{\Gamma a \, \Gamma b} \left( \frac{\gamma_{r}}{\gamma_{th}} \right)^{b/2} \\ &\times \mathbf{G}_{2,2}^{2,1} \left( \frac{a}{(b-1)} \sqrt{\frac{\gamma_{th}}{\gamma_{r}}} \middle| 1, 1+b \atop a+b, b \right) + \left( \frac{a}{b-1} \right)^{a} \frac{1}{\Gamma a \Gamma b} \left( \frac{\gamma_{th}}{\gamma_{r}} \right)^{a/2} \\ &\times G_{2,2}^{1,2} \left( \frac{a}{(b-1)} \sqrt{\frac{\gamma_{th}}{\gamma_{r}}} \middle| 1-a-b, 1-a \atop 0, -a \right). \end{split} \tag{4.17}$$

#### **OP of Proportional Fairness Scheduling Scheme**

$$\mathbf{F}_{\Gamma_{\mathrm{m*r}}}^{\mathrm{PFS}}(\gamma_{th}) = \mathrm{Pr} \left( \max_{m \in 1, 2 .... M} \left( \frac{\Gamma_{\mathrm{m,r}}}{\overline{\Gamma}_{\mathrm{m,r}}} \right) \ \bigcap \ \Gamma_{m,r} < \gamma_{th} \right). \tag{4.18}$$

After some mathematical manipulations, (4.18) is obtained in (4.19) as follows:

$$\mathbf{F}_{\Gamma_{\mathrm{m*,r}}}^{\mathrm{PFS}}(\gamma_{th}) = \frac{1}{M} \sum_{m=1}^{M} \left( F_{\Gamma_{m,r}}(\gamma_{th}) \right)^{M}. \tag{4.19}$$

The closed-form expression for OP using PFS based system is calculated as:

$$\begin{split} \mathbf{P}_{\Gamma_{e2e}}^{\mathrm{PFS}}(\gamma_{th}) &= \frac{1}{M} \sum_{m=1}^{M} \left( 1 - \frac{e^{\frac{-\gamma_{th}}{\gamma_{s}\Omega_{m,r}}}}{\prod_{n=1}^{N} \left( 1 + \frac{\gamma_{I_{n,r}}\Omega_{I_{n,r}}\gamma_{th}}{\gamma_{s}\Omega_{m,r}} \right)} \right)^{M} \left( \frac{b-1}{a} \right)^{b} \frac{1}{\Gamma a \, \Gamma b} \\ &\times \left( \frac{\gamma_{r}}{\gamma_{th}} \right)^{b/2} G_{2,2}^{2,1} \left( \frac{a}{(b-1)} \sqrt{\frac{\gamma_{th}}{\gamma_{r}}} \begin{vmatrix} 1, 1+b \\ a+b, b \end{pmatrix} + \left( \frac{a}{b-1} \right)^{a} \frac{1}{\Gamma a \Gamma b} \left( \frac{\gamma_{th}}{\gamma_{r}} \right)^{a/2} \\ &\times G_{2,2}^{1,2} \left( \frac{a}{(b-1)} \sqrt{\frac{\gamma_{th}}{\gamma_{r}}} \begin{vmatrix} 1-a-b, 1-a \\ 0, -a \end{pmatrix} \right). \end{split} \tag{4.20}$$

### OP of CDF Scheduling

The CDF of the user-relay RF link with i.n.i.d interferers for CDF based scheduling can be expressed using (4.13) as follows:

$$\mathsf{F}^{\mathsf{CDFS}}_{\Gamma_{\mathsf{m*r}}}(\gamma_{th}) = \mathsf{Pr}\left(\max_{m \in 1,2...M} \left(F_{\Gamma_{m,r}}(x)\right)^{\frac{1}{\upsilon_m}} \ \bigcap \Gamma_{m,r} < \gamma_{th}\right). \tag{4.21}$$

The final expression for CDF of the RF link with CDF based scheduling is obtained in (4.22) as follows:

$$F_{\Gamma_{m*,r}}^{\text{CDFS}}(\gamma_{th}) = \sum_{m=1}^{M} v_m \left( 1 - \frac{e^{\frac{-\gamma_{th}}{\gamma_s \Omega_{m,r}}}}{\prod_{n=1}^{N} \left( 1 + \frac{\gamma_{I_{n,r}} \Omega_{I_{n,r}} \gamma_{th}}{\gamma_s \Omega_{m,r}} \right)} \right)^{\frac{1}{v_m}}.$$
 (4.22)

The derivation of (4.22) is given in Appendix I. Substituting (4.7), (4.9), (4.10) and (4.22) into (4.15), the closed-form expression for exact OP with CDF based scheduling is obtained as:

$$\begin{split} P_{\Gamma_{e2e}}^{\text{CDFS}}(\gamma_{\text{th}}) &= \sum_{m=1}^{M} \upsilon_{m} \left( 1 - \frac{e^{\frac{-\gamma_{th}}{\gamma_{s}\Omega_{m,r}}}}{\prod_{n=1}^{N} \left( 1 + \frac{\gamma_{I_{n,r}}\Omega_{I_{n,r}}\gamma_{th}}{\gamma_{s}\Omega_{m,r}} \right)} \right)^{\frac{1}{\upsilon_{m}}} \left( \frac{b-1}{a} \right)^{b} \frac{1}{\Gamma a \, \Gamma b} \\ &\times \left( \frac{\gamma_{r}}{\gamma_{th}} \right)^{b/2} G_{2,2}^{2,1} \left( \frac{a}{(b-1)} \sqrt{\frac{\gamma_{\text{th}}}{\gamma_{r}}} \begin{vmatrix} 1, 1+b \\ a+b, b \end{pmatrix} + \left( \frac{a}{b-1} \right)^{a} \frac{1}{\Gamma a \Gamma b} \left( \frac{\gamma_{\text{th}}}{\gamma_{r}} \right)^{a/2} \\ &\times G_{2,2}^{1,2} \left( \frac{a}{(b-1)} \sqrt{\frac{\gamma_{\text{th}}}{\gamma_{r}}} \begin{vmatrix} 1-a-b, 1-a \\ 0, -a \end{pmatrix} \right). \end{split} \tag{4.23}$$

OP is expressed as a function of  $\gamma_t$  to assess the system's performance with variation in the total available power  $P_t$  within the network. Here, we denote the total power  $P_t = P_s + P_r$ , where  $\gamma_t = \frac{P_t}{\sigma^2}$ . Additionally, we assume  $\gamma_s = \beta \gamma_t, \gamma_r = (1-\beta)\gamma_t, \gamma_{I_{n,r}} = \gamma_t/\zeta_{I_{n,r}}$ , where  $\beta$  represents the fraction of total power given to user and relay, and  $\zeta_{I_{n,r}}$  denotes the fraction of total power allocated to interferers.

### 4.2.2 Asymptotic Outage Performance

The closed form expressions for OP with different scheduling techniques provide limited insights. Hence, for a deeper insight into the influence of different parameters on system performance, OP expression provided in (4.15) at high SNR, i.e.,  $\gamma_t$  approaches infinity, can be written as follows:

$$P_{\Gamma_{e2e}}^{\infty,S}(\gamma_{th}) \simeq F_{\Gamma_{m*,r}}^{\infty}(\gamma_{th}) + F_{\Gamma_{r,d}}^{\infty}(\gamma_{th}). \tag{4.24}$$

At high value of SNR, terms involving  $1/\gamma_t$  become negligible and can be ignored i.e.

$$e^{\frac{-\gamma_{th}}{\gamma_s\Omega_{m,r}}}=1,\;\left(1+\frac{\gamma_{I_{n,r}}\Omega_{I_{n,r}}\gamma_{th}}{\gamma_s\Omega_{m,r}}\right)^{-1}\approx e^{(-\frac{\gamma_{I_{n,r}}\Omega_{I_{n,r}}\gamma_{th}}{\gamma_s\Omega_{m,r}})}\;\text{when}\;\frac{\gamma_{I_{n,r}}\Omega_{I_{n,r}}\gamma_{th}}{\gamma_s\Omega_{m,r}}<<1,$$

the CDF expression of RF link given in (4.7) becomes

$$F_{\Gamma_{m,r}}^{\infty}(\gamma_{th}) \simeq \left(1 - e^{-\left(\frac{\gamma_{th}}{\gamma_s\Omega_{m,r}}\right)\sum_{n=1}^{N}\gamma_{I_{n,r}}\Omega_{I_{n,r}}\right)},$$

$$\simeq \left(\frac{\gamma_{th}}{\gamma_s\Omega_{m,r}}\right)\sum_{n=1}^{N}\gamma_{I_{n,r}}\Omega_{I_{n,r}}.$$
(4.25)

The CDF for FSO link is derived at high SNR by utilizing the expressions [113, Eqs. (07.34.16.0001.01), (07.34.06.0006.01)] in (4.9) as follows:

$$F_{\Gamma_{r,d}}^{\infty}(\gamma_{th}) \simeq \frac{\Gamma(a+b)}{\Gamma(a+1)\Gamma b} \left(\frac{a}{(b-1)} \sqrt{\frac{\gamma_{th}}{\gamma_r}}\right)^{a}. \tag{4.26}$$

Furthermore, the diversity order can be evaluated using  $P^{\infty,S}_{\Gamma_{e2e}}=(G_c\gamma_t)^{-G_d}$  where,  $G_c$  and  $G_d$  represent the coding gain and diversity order respectively. Substituting (4.25) and (4.26) in (4.24) and utilizing (4.16) for greedy scheduling, the asymptotic OP can be calculated as follows:

$$P_{\Gamma_{e2e}}^{\infty,\mathrm{GS}}(\gamma_{th}) \simeq \prod_{m=1}^{M} \left[ \left( \frac{\gamma_{th}}{\gamma_{s}\Omega_{m,r}} \right) \sum_{n=1}^{N} \gamma_{I_{n,r}} \Omega_{I_{n,r}} \right] + \frac{\Gamma(a+b)}{\Gamma(a+1)\Gamma b} \left( \frac{a}{(b-1)} \sqrt{\frac{\gamma_{th}}{\gamma_{r}}} \right)^{a}. \tag{4.27}$$

The diversity order for greedy scheduling,  $G_d = \min\{0, a/2\} = 0$  is obtained. By substituting (4.25) and (4.26) into (4.24) using (4.19) for PFS based scheme, we obtain the unified asymptotic outage probability expression as follows:

$$\begin{split} P_{\Gamma_{e2e}}^{\infty,\mathrm{PFS}}(\gamma_{th}) &\simeq \frac{1}{M} \sum_{m=1}^{M} \left[ \left( \frac{\gamma_{th}}{\gamma_s \Omega_{m,r}} \right) \sum_{n=1}^{N} \gamma_{I_{n,r}} \Omega_{I_{n,r}} \right]^M \\ &+ \frac{\Gamma(a+b)}{\Gamma(a+1)\Gamma b} \left( \frac{a}{(b-1)} \sqrt{\frac{\gamma_{\mathrm{th}}}{\gamma_c}} \right)^a. \quad (4.28) \end{split}$$

Diversity order reflected from (4.28) is  $G_d = \min\{0, a/2\} = 0$ . Substituting (4.25) and (4.26) in (4.24) and using (4.22) for cumulative distribution function based scheduling, the asymptotic OP is obtained as follows:

$$\begin{split} P_{\Gamma_{e2e}}^{\infty,\text{CDFS}}(\gamma_{th}) &\simeq \sum_{m=1}^{M} \upsilon_{m} \left[ \left( \frac{\gamma_{th}}{\gamma_{s}\Omega_{m,r}} \right) \sum_{n=1}^{N} \gamma_{I_{n,r}} \Omega_{I_{n,r}} \right]^{\frac{1}{\upsilon_{m}}} \\ &+ \frac{\Gamma(a+b)}{\Gamma(a+1)\Gamma b} \left( \frac{a}{(b-1)} \sqrt{\frac{\gamma_{\text{th}}}{\gamma_{r}}} \right)^{a}. \end{split} \tag{4.29}$$

Therefore, the diversity order for CDFS is  $G_d=\min[0,a/2]=0$  due to the relationship between  $\ \gamma_{I_{n,r}}=\gamma_t/\zeta_{I_{n,r}}$  and  $\gamma_s=\beta\gamma_t.$ 

## 4.3 Optimum Performance Analysis

### 4.3.1 Optimal Power Allocation

To optimize power allocation for the user and relay while minimizing OP in the context of CDF-based scheduling (4.29), the objective function can be represented by the following expression:

$$\begin{array}{lcl} (P_s^*,P_r^*) &=& \displaystyle \mathop{\arg\min}_{(P_s,P_r)} P_{\Gamma_{e2e}}^{\infty,\text{CDFS}}(\gamma_{th}), \\ && \mathrm{subject\ to}\ P_s = \beta P_t, P_r = (1-\beta)P_t \end{array} \tag{4.30}$$

To give equal fairness to all the users, we assume  $v=v_1=v_2.....=v_M$  with  $\sum_{m=1}^M v_m=1$  and substituting  $P_s=\beta P_t, P_r=(1-\beta)P_t$  in (4.29). We obtain:

$$\begin{split} P_{\Gamma_{e2e}}^{\infty,\text{CDFS}}(\gamma_{th}) &\simeq \upsilon \left(\frac{\gamma_{th}}{P_t} \sum_{n=1}^{N} \gamma_{I_{n,r}} \Omega_{I_{n,r}} \right)^{\frac{1}{\upsilon}} \left(\frac{1}{\Omega_{1,r}^{\frac{1}{\upsilon}}} + \frac{1}{\Omega_{2,r}^{\frac{1}{\upsilon}}} ..... \frac{1}{\Omega_{M,r}^{\frac{1}{\upsilon}}} \right) \left(\frac{1}{\beta}\right)^{1/\upsilon} \\ &+ \frac{\Gamma(a+b)}{\Gamma(a+1)\Gamma b} \left(\frac{a}{(b-1)} \sqrt{\frac{\gamma_{th}}{P_t}}\right)^a \left(\frac{1}{(1-\beta)}\right)^{a/2} (4.31) \end{split}$$

To determine the optimal value of  $\beta$ , we set the first derivative of the above expression with respect to  $\beta$  to zero, which gives the optimal  $\beta$  expression as follows:

$$\frac{\partial P_{\Gamma_{e2e}}^{\infty,\text{CDFS}}(\gamma_{th})}{\partial \beta} \simeq -\left(\frac{\gamma_{th}}{P_t} \sum_{n=1}^{N} \gamma_{I_{n,r}} \Omega_{I_{n,r}}\right)^{\frac{1}{v}} \left(\frac{1}{\Omega_{1,r}^{\frac{1}{v}}} + \frac{1}{\Omega_{2,r}^{\frac{1}{v}}} \dots \frac{1}{\Omega_{M,r}^{\frac{1}{v}}}\right) \left(\frac{1}{\beta^*}\right)^{\frac{1}{v}+1} + \frac{\Gamma(a+b)}{2\Gamma a\Gamma b} \left(\frac{a}{(b-1)} \sqrt{\frac{\gamma_{th}}{P_t}}\right)^a \left(\frac{1}{1-\beta^*}\right)^{\frac{a}{2}+1} = 0.$$
(4.32)

Solving for  $\beta^*$ , we get:

$$\beta^* \simeq \frac{\left(\frac{\gamma_{th}}{P_t} \sum_{n=1}^N \gamma_{I_{n,r}} \Omega_{I_{n,r}}\right)^{\frac{1}{1+\upsilon}}}{\left[\frac{\Gamma(a+b)}{2\Gamma a \Gamma b} \left(\frac{a}{(b-1)} \sqrt{\frac{\gamma_{th}}{P_t}}\right)^a\right]^{\frac{\upsilon}{\upsilon+1}}} \left(1-\beta^*\right)^{\frac{\frac{a}{2}+1}{\frac{1}{\upsilon}+1}} \left(\frac{1}{\Omega_{1,r}^{\frac{1}{\upsilon}}} + \frac{1}{\Omega_{2,r}^{\frac{1}{\upsilon}}} ..... \frac{1}{\Omega_{M,r}^{\frac{1}{\upsilon}}}\right)^{\frac{\upsilon}{\upsilon+1}}.$$

Finding a closed-form equation for the optimal power allocation coefficient might be challenging. Standard iterative root-finding procedures, such as Bisection's or Newton's, can be used to find a numerical solution. In a special case where  $v = \frac{2}{a}$ , the optimal power allocation coefficient is obtained as follows:

$$\beta^* \simeq \frac{1}{\left(1 + \frac{\left(\frac{\Gamma(a+b)}{2\Gamma a \Gamma b} \left(\frac{a}{(b-1)} \sqrt{\frac{\gamma_{th}}{P_t}}\right)^a\right)^{\frac{\upsilon}{\upsilon+1}}}{\left(\frac{\gamma_{th}}{P_t} \sum_{n=1}^N \gamma_{I_{n,r}} \Omega_{I_{n,r}}\right)^{\frac{1}{1+\upsilon}} \left(\frac{1}{\Omega_{I,r}^{\frac{1}{\upsilon}}} + \frac{1}{\Omega_{U,r}^{\frac{1}{\upsilon}}} \cdots \frac{1}{\Omega_{M,r}^{\frac{1}{\upsilon}}}\right)^{\frac{\upsilon}{\upsilon+1}}}\right)}.$$
(4.33)

### 4.3.2 Optimal CAR Allocation

To optimize the CAR so as to minimize the OP for CDF based scheduling (4.29), the objective function can be formulated as follows:

$$\begin{array}{lcl} (\upsilon_{1}^{*}, \upsilon_{2}^{*}, .., \upsilon_{M}^{*}) & = & \underset{(\upsilon_{1}, \upsilon_{2}, ..., \upsilon_{M})}{\arg\min} P_{\Gamma_{e2e}}^{\infty, \text{CDF-SINRS}}(\gamma_{th}), \\ & & \text{subject to } \sum_{m=1}^{M} \upsilon_{m} = 1. \end{array} \tag{4.34}$$

To solve the above objective function, we employ the method of Lagrange multipliers to derive the optimal user CAR as follows:

$$\begin{split} F_{\Gamma_{e2e}}^{\infty,\text{CDFS}}(\upsilon_1,\upsilon_2,..,\upsilon_M,\lambda) &= \sum_{m=1}^M \upsilon_m \left[ \left( \frac{\gamma_{th}}{\gamma_s \Omega_{m,r}} \right) \sum_{n=1}^N \gamma_{I_{n,r}} \Omega_{I_{n,r}} \right]^{\frac{1}{\upsilon_m}} \\ &+ \frac{\Gamma(a+b)}{\Gamma(a+1)\Gamma b} \left( \frac{a}{(b-1)} \sqrt{\frac{\gamma_{\text{th}}}{\gamma_r}} \right)^a + \lambda \Big( \sum_{m=1}^M \upsilon_m - 1 \Big). \end{split} \tag{4.35}$$

Differentiating (4.35) with respect to with respect to  $v_m$ , setting the derivative to zero, and simplifying yields:

$$\upsilon_{m}^{*} = \frac{\ln\left(\frac{\gamma_{th}}{\gamma_{s}\Omega_{m,r}}\sum_{n=1}^{N}\gamma_{I_{n,r}}\Omega_{I_{n,r}}\right)}{1 + W\left(\lambda\left(\left(\frac{\gamma_{th}}{\gamma_{s}\Omega_{m,r}}\sum_{n=1}^{N}\gamma_{I_{n,r}}\Omega_{I_{n,r}}\right)^{\frac{-1}{\ln\left(\frac{\gamma_{th}}{\gamma_{s}\Omega_{m,r}}\sum_{n=1}^{N}\gamma_{I_{n,r}}\Omega_{I_{n,r}}\right)}\right)\right)}. \tag{4.36}$$

The above expression involves the Lambert W function, denoted as W(.) [124]. The derivation of (4.36) is presented in Appendix II. By substituting the power series expansion of W(z), as given in [113, Eq. (01.31.06.0002.01)], into (4.36). This yields the following closed-form expression for  $v_m^*$  as:

$$v_m^* = \frac{\ln\left(\frac{\gamma_{th}}{\gamma_s\Omega_{m,r}}\sum_{n=1}^N\gamma_{I_{n,r}}\Omega_{I_{n,r}}\right)}{1 + \sum_{k=1}^\infty \frac{(-k)^{k-1}}{k!}\lambda^k \left(\frac{\gamma_{th}}{\gamma_s\Omega_{m,r}}\sum_{n=1}^N\gamma_{I_{n,r}}\Omega_{I_{n,r}}\right)^{\frac{-k}{\ln\left(\frac{\gamma_{th}}{\gamma_s\Omega_{m,r}}\sum_{n=1}^N\gamma_{I_{n,r}}\Omega_{I_{n,r}}\right)}}. \tag{4.37}$$

Now, to calculate the value of  $\lambda$ , all the individual CAR are summed and equated to unity, resulting in the following expression:

$$\frac{\ln\left(\frac{\gamma_{th}}{\gamma_s\Omega_{1,r}}\sum_{n=1}^{N}\gamma_{I_{n,r}}\Omega_{I_{n,r}}\right)}{1+\sum_{k=1}^{\infty}\frac{(-k)^{k-1}}{k!}\lambda^k\left(\frac{\gamma_{th}}{\gamma_s\Omega_{1,r}}\sum_{n=1}^{N}\gamma_{I_{n,r}}\Omega_{I_{n,r}}\right)^{\frac{-k}{\ln\left(\frac{\gamma_{th}}{\gamma_s\Omega_{1,r}}\sum_{n=1}^{N}\gamma_{I_{n,r}}\Omega_{I_{n,r}}\right)}}{1+\sum_{k=1}^{\infty}\frac{(-k)^{k-1}}{k!}\lambda^k\left(\frac{\gamma_{th}}{\gamma_s\Omega_{2,r}}\sum_{n=1}^{N}\gamma_{I_{n,r}}\Omega_{I_{n,r}}\right)^{\frac{-k}{\ln\left(\frac{\gamma_{th}}{\gamma_s\Omega_{2,r}}\sum_{n=1}^{N}\gamma_{I_{n,r}}\Omega_{I_{n,r}}\right)}}{1+\sum_{k=1}^{\infty}\frac{(-k)^{k-1}}{k!}\lambda^k\left(\frac{\gamma_{th}}{\gamma_s\Omega_{M,r}}\sum_{n=1}^{N}\gamma_{I_{n,r}}\Omega_{I_{n,r}}\right)^{\frac{-k}{\ln\left(\frac{\gamma_{th}}{\gamma_s\Omega_{M,r}}\sum_{n=1}^{N}\gamma_{I_{n,r}}\Omega_{I_{n,r}}\right)}}-1=0.$$

$$1+\sum_{k=1}^{\infty}\frac{(-k)^{k-1}}{k!}\lambda^k\left(\frac{\gamma_{th}}{\gamma_s\Omega_{M,r}}\sum_{n=1}^{N}\gamma_{I_{n,r}}\Omega_{I_{n,r}}\right)^{\frac{-k}{\ln\left(\frac{\gamma_{th}}{\gamma_s\Omega_{M,r}}\sum_{n=1}^{N}\gamma_{I_{n,r}}\Omega_{I_{n,r}}\right)}}}-1=0.$$

$$(4.38)$$

Finding a closed-form solution for  $\lambda$  is difficult. The value of  $\lambda$  can be obtained using numerical methods.

### 4.4 Simulation Results

This section presents the accuracy of analytical and asymptotic expressions for considered system assuming three users at the source, a single relay and one destination. For RF link, we suppose that three users are at (0,0), (0.2,0.5), (0.5,0.1), while the relay is at (1,0) and the three interferers are at (0,2.1), (1.1,2) and (2.2,-1). The channel variance  $\Omega_{(.)} = \mu d_{i,j}$ , and  $d_{i,j} = (\bar{d}_{i,j}/d_0)^{-\epsilon}$ , where,  $d_{i,j}$  is the normalized distance between node i and node j, where  $\bar{d}_{i,j}$  is the actual euclidean distance between them,  $d_0$  is the reference distance,  $\mu$  is the propagation constant and  $\epsilon$  is the path loss exponent [125]. Further,  $\Omega_{(.)}$  is calculated by considering  $d_0 = 1$ ,  $\mu = 1$  and  $\epsilon = 3$ . For the FSO link, fading parameters (a,b) = (4.5916,7.0941), (a,b) = (2.3378,4.5323), and (a,b) = (1.4321,3.4948) are taken for weak, moderate, and strong turbulent environments respectively [64].

Fig. 4.2, Fig. 4.3 and Fig. 4.4 depict the OP with GS, PFS and CDFS based systems for different interferers power, under strong turbulence condition with  $\beta=0.5$ . It can be noted that the outage performance degrades with an increase in interferers power. The analytic expression for OP derived for GS (4.17), PFS (4.20) and CDFS (4.23) are closely match with the simulation results. Further at high values of  $\gamma_t$ , OP saturates implying that the diversity gain, denoted as  $G_d=$  is 0.

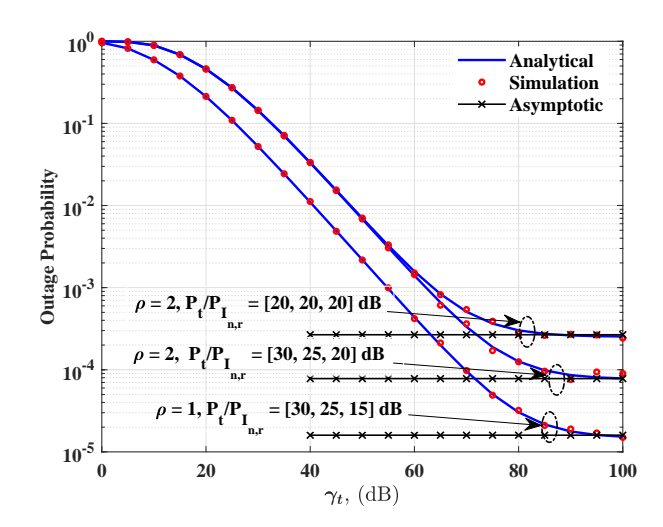


Figure 4.2: OP versus  $\gamma_t$  over i.n.i.d CCI and data rates considering GS based system under strong turbulence condition fixed  $\beta = 0.5$ .

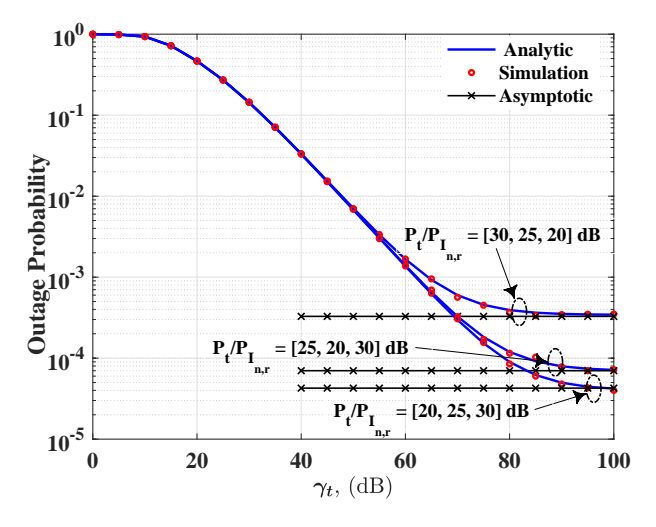


Figure 4.3: OP versus  $\gamma_t$  over i.n.i.d CCI considering PFS based system under strong turbulence condition for  $\rho = 2$ ,  $\beta = 0.5$ .

Fig. 4.5 shows the OP of considered systems versus  $\gamma_t$  for various turbulence conditions at fixed interferers power with  $\rho=1,\ \beta=0.5$  and  $\upsilon_m=[0.6,0.3,0.1]$ . The result shows that system performance deteriorates as the turbulence increases. Also, there are error floors at the high SNRs which implies OP cannot improve further with increase in  $\gamma_t$ . Fig. 4.6 indicates the effect of power allocation at both the user and relay nodes on the OP, as evaluated using (4.33), under moderate turbulence conditions. The results are shown for different data rates and interferer power levels, assuming  $\upsilon_m=[1/3,1/3,1/3]$ . The optimal power allocation coefficient, as derived in (4.33) minimizes the OP across a broad range of interference power and data rates. Fig. 4.7 presents the OP performance of system comparing equal and optimized power allocation with  $\upsilon_m=[1/3,1/3,1/3]$  in moderate turbulence conditions. The power allocation coefficient are calculated from (4.33) which is  $(\beta,\beta^*)=(0.5,0.8562)$  for  $\rho=1$ 

 $2, P_t/P_{I_{n,r}}$  = [30, 25, 20] dB,  $(\beta, \beta^*)$  = (0.5, 0.7133) for  $\rho$  = 2,  $P_t/P_{I_{n,r}}$  = [25, 25, 25] dB, and  $(\beta, \beta^*)$  = (0.5, 0.7507) for  $\rho$  = 1,  $P_t/P_{I_{n,r}}$  = [20, 20, 20] dB. It is evident that optimizing the power allocation to both the user and the relay significantly enhances the OP performance.

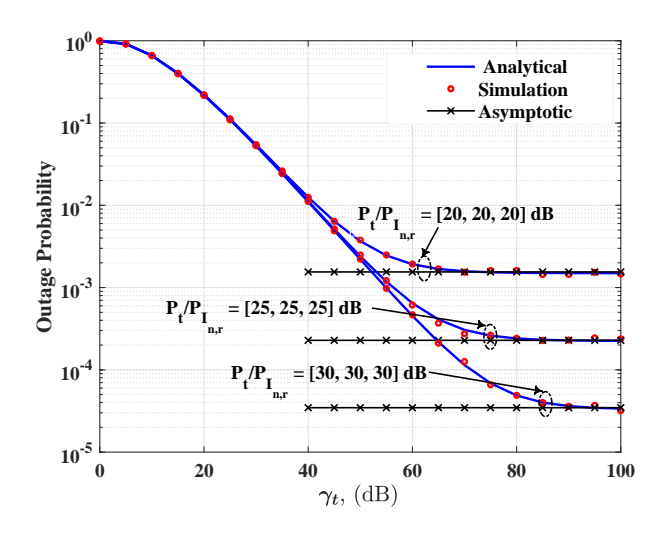


Figure 4.4: OP versus  $\gamma_t$  over i.n.i.d CCI considering CDFS based system under strong turbulence condition fixed at  $\rho=1,\,\beta=0.5$  and  $\upsilon_m=[0.6,0.3,0.1].$ 

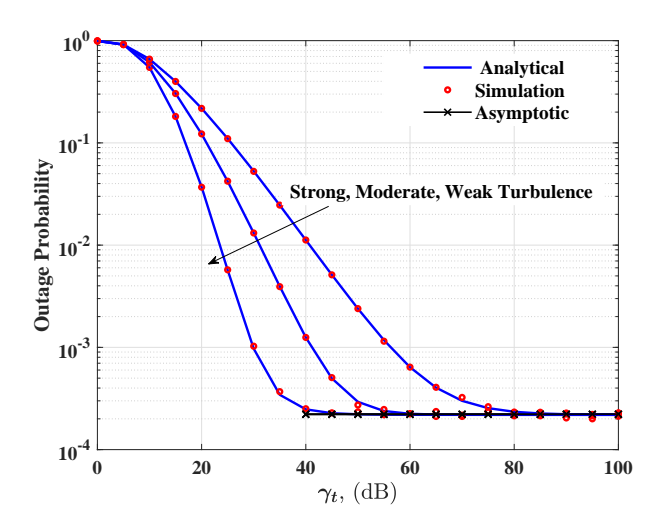


Figure 4.5: OP versus  $\gamma_t$  under different turbulence conditions considering CDFS based system fixed at  $P_t/P_{I_{n,r}}$  = [20, 25, 30] (dB),  $\rho$  = 1,  $\beta$  = 0.5 and  $\upsilon_m$  = [0.6, 0.3, 0.1].

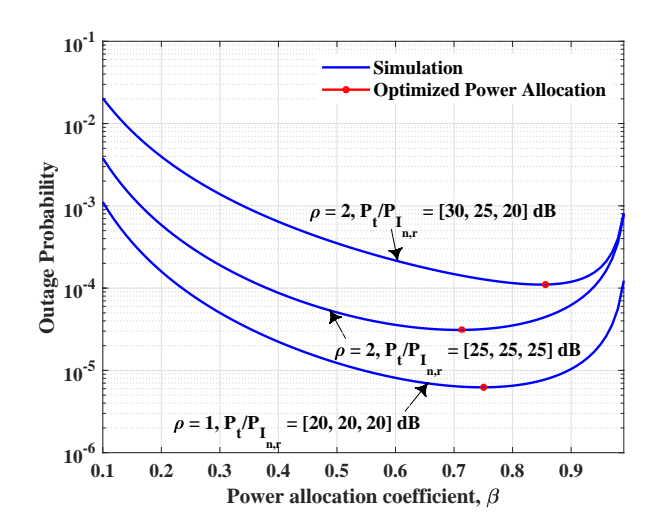


Figure 4.6: OP versus power allocation coefficient considering CDFS based system under moderate turbulence condition fixed at  $v_m = [1/3, 1/3, 1/3]$ .

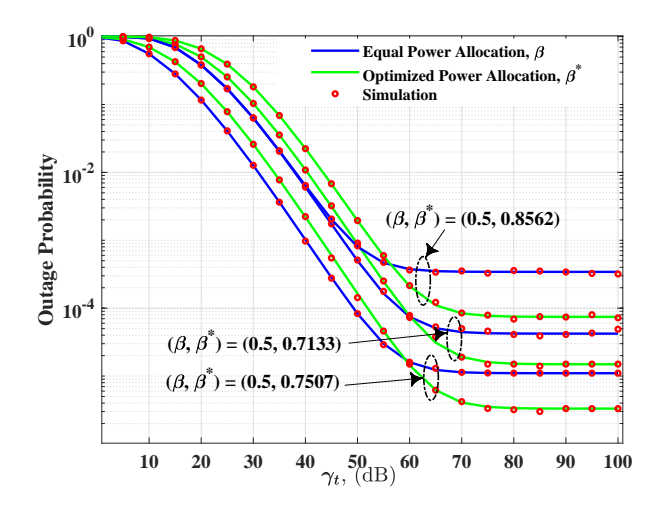


Figure 4.7: OP versus  $\gamma_t$  over equal power and optimized power allocation, considering CDFS based system under moderate turbulence condition fixed at  $\upsilon_m = [1/3, 1/3, 1/3]$ .

Fig. 4.8 reveals the OP of considered system versus  $\gamma_t$  for greedy scheduling (4.17) and with equal and optimized CARs to the users for CDF based scheduling using (4.37) with  $v_m = [1/3, 1/3, 1/3]$  and  $\beta = 0.5$  under moderate turbulence conditions. The figure demonstrates that optimizing the CAR significantly enhances the OP performance, closely approaching the results obtained through greedy scheduling. Fig. 4.9 depicts the comparison of CAR among three users under following user scheduling schemes; GS, CDFS with equal CAR and CDFS with unequal CAR. In the GS scheme, user 3 receives a significantly higher CAR (approximately 0.75), indicating that this user dominates the channel access. This is because GS prioritizes the user with the best instantaneous channel conditions and user 3 is located closer to the relay at position (0.5,

0.1). In contrast, CDFS with equal fairness assigns equal CAR values (around 0.33) to all users, ensuring a uniform and fair distribution of channel access regardless of instantaneous channel conditions. GS scheme provides better outage performance at the cost of fairness. When fairness is strictly enforced, as in equal CAR in CDFS scheme, outage performance deteriorates because users with weaker channels receive the same access as those with stronger ones. To address this trade-off, the CDFS scheme with optimized CAR offers a practical balance by assigning a higher CAR to user 1, who is farther from the relay and thus more vulnerable to poor channel conditions, improving the overall system performance.

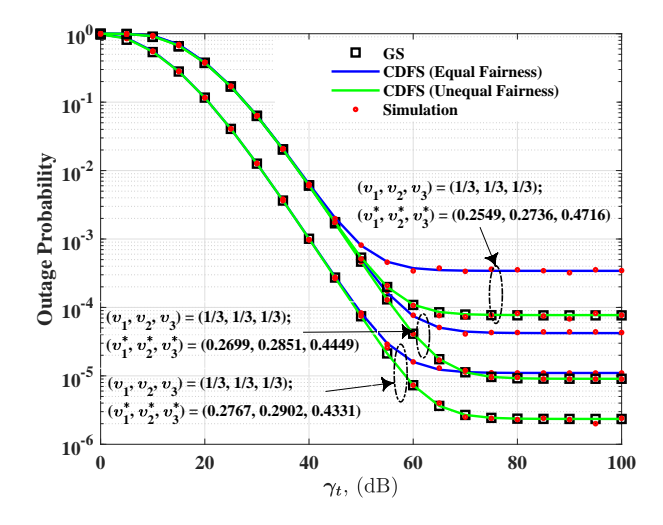


Figure 4.8: OP versus  $\gamma_t$  over equal channel access ratio and optimized channel access ratios for both GS and CDFS based systems under moderate turbulence condition fixed at  $\beta=0.5$ .

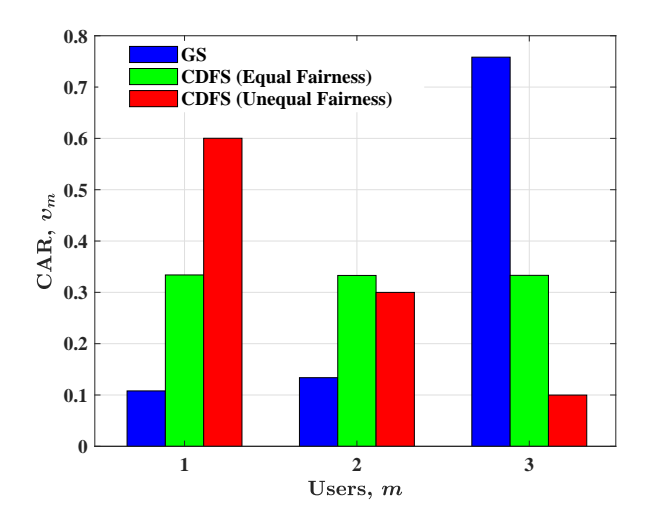


Figure 4.9: Comparison of channel access ratio,  $v_m$  for different scheduling schemes.

# Chapter 5

# Performance Analysis of Multiuser Dual-hop RF-FSO Systems with Imperfect CSI

This chapter presents a performance analysis of a MU dual-hop RF-FSO relaying system for uplink transmission under imperfect CSI. The system employs a user scheduling scheme and considers the impact of co-channel interference (CCI) at the relay node. The RF and FSO links are modeled using Rayleigh fading and Fisher Snedecor,  $\mathcal{F}$  distribution, respectively.

The key contributions of this chapter are as follows:

- A MU dual-hop RF/FSO relaying system affected by CCI at the relay is investigated. The user-relay (RF) link undergoes Rayleigh fading, and the relay-destination (FSO) link experiences turbulence, modeled by the F distribution. A CDF-based scheduling scheme is employed at the relay, and a closed-form expression for the OP is derived considering imperfect CSI on both links.
- An asymptotic expression for the OP is derived in the high SNR regime, enabling the analysis of the impact of channel estimation errors on system performance.
- Power allocation under total power constraint is performed to enhance the overall system performance.
- The optimal CAR is performed, and the resulting improvements in system performance are demonstrated.

# **5.1** System and Channel Model

Consider MU dual-hop RF-FSO system as depicted in Fig. 5.1, where M mobile users (denoted as  $m_1, m_2, ..., m_M$ ) transmit data from S to destination D through R operating in the presence of N co-channel interference, and noise. The relay employs cumulative distribution function scheduling scheme to select the user for transmission [126].

We assume that both users and interferers experience the flat Rayleigh fading channels where  $h_{m,r}$  and  $g_{I_{n,r}}$  denote the channel gain for the mth user and nth interferer respectively.

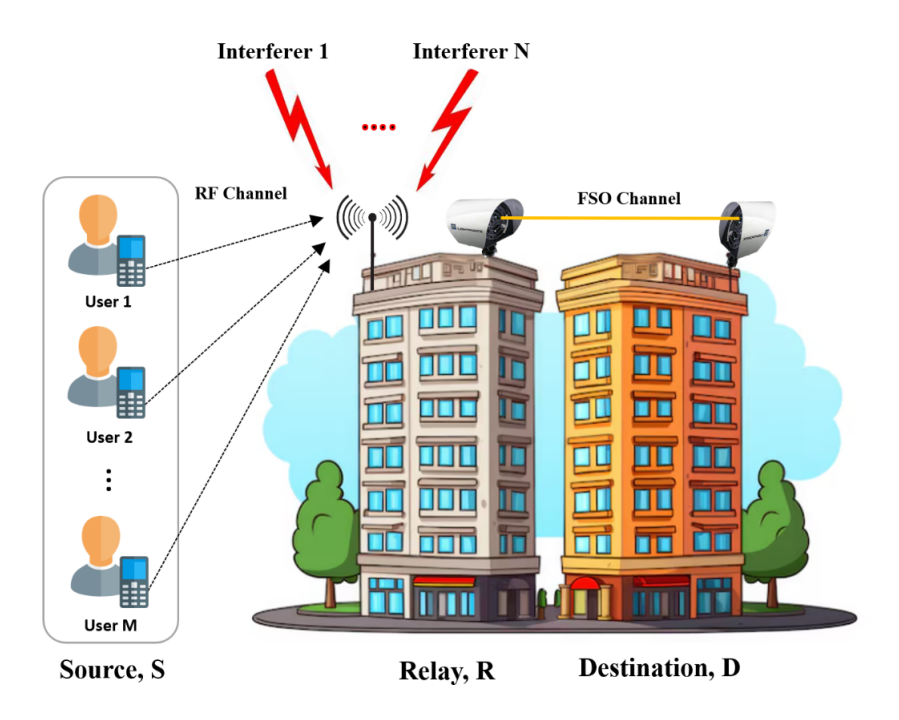


Figure 5.1: System model of a MU dual-hop RF-FSO system in the presence of interferers under channel imperfection.

The received signal at the relay,  $y_{m,r}$  can be expressed as:

$$y_{\text{m,r}} = \sqrt{P_s} h_{\text{m,r}} x_{\text{m,r}} + \sum_{n=1}^{N} \sqrt{P_{I_{n,r}}} g_{I_{n,r}} x_{I_{n,r}} + n_r,$$
 (5.1)

where,  $P_s$  and  $P_{I_{n,r}}$  are the available transmit power of the user and nth interferer respectively,  $x_{\rm m,r}$  is the transmitted symbols of the mth user with  $\mathbb{E}(|x_{\rm m,r}|^2)=1$  and  $x_{I_{n,r}}$  is the symbol transmitting by nth interferer with  $\mathbb{E}(|x_{I_{n,r}}|^2)=1$  and  $n_r\sim C\mathcal{N}(0,\sigma^2)$ . The channel gain for source-relay (S-R) link is distributed as  $h_{\rm m,r}\sim C\mathcal{N}(0,\Omega_{\rm m,r})$ , while the channel gain for the interferer-relay (I-R) link is distributed as  $g_{I_{n,r}}\sim C\mathcal{N}(0,\Omega_{I_{n,r}})$ .

The imperfect channel gain for the S-R link, denoted as  $\hat{h}_{m,r}$ , is provided in [85]:

$$h_{\rm m,r} = \zeta_{\rm SR} \hat{\mathbf{h}}_{\rm m,r} + \sqrt{1 - \zeta_{\rm SR}^2} \epsilon_{\rm SR},\tag{5.2}$$

where,  $\epsilon_{\rm SR}$  is a complex Gaussian RV,  $\sigma_{\epsilon_{\rm SR}}^2$  denoted as  $\epsilon_{\rm SR} \sim C \mathcal{N}(0, \sigma_{\epsilon_{\rm SR}}^2)$ ,  $\zeta_{\rm SR}$  is the correlation coefficient of the channel gain, with values ranging from  $0 \leq \zeta_{\rm SR} \leq 1$ . A higher  $\zeta_{\rm SR}$  value indicates a lower estimation error for the CSI and when  $\zeta_{\rm SR} \rightarrow 1$ , it implies an error-free estimation.

The instantaneous SINR for an imperfect RF channel in the presence of CCI is given by:

$$\begin{split} \hat{\Gamma}_{\text{m,r}} &= \frac{P_s \zeta_{\text{SR}}^2 |\hat{h}_{m,r}|^2}{\sum_{n=1}^N P_{I_{n,r}} |g_{I_{n,r}}|^2 + P_s (1 - \zeta_{\text{SR}}^2) \sigma_{\epsilon_{\text{SR}}}^2 + \sigma^2}, \\ &\triangleq \frac{\hat{X}_m}{\hat{Z} + 1}, \end{split} \tag{5.3}$$

where, 
$$\hat{X}_m = \hat{\gamma}_s |\hat{h}_{m,r}|^2$$
,  $\hat{Z} = \sum_{n=1}^N \hat{\gamma}_{I_{n,r}} |g_{I_{n,r}}|^2$ ,  $\gamma_s \triangleq \frac{P_s}{\sigma^2}$ ,  $\gamma_{I_{n,r}} \triangleq \frac{P_{I_{n,r}}}{\sigma^2}$ ,  $\hat{\gamma}_s = \frac{\gamma_s \zeta_{\rm SR}^2}{\gamma_s (1 - \zeta_{\rm SR}^2) \sigma_{\epsilon_{\rm SR}}^2 + 1}$  and  $\hat{\gamma}_{I_{n,r}} = \frac{\gamma_{I_{n,r}}}{\gamma_s (1 - \zeta_{\rm SR}^2) \sigma_{\epsilon_{\rm SR}}^2 + 1}$ .

The PDF of  $|\hat{h}_{m,r}|^2$  for mth user and relay link is expressed as follows:

$$f_{|\hat{h}_{m,r}|^2}(x) = \frac{1}{\mathbb{E}(|\hat{h}_{m,r}|^2)} e^{-\frac{x}{\mathbb{E}(|\hat{h}_{m,r}|^2)}}. \tag{5.4}$$

The PDF and CDF of  $\hat{X}_m$  for the mth user and relay link are expressed as:

$$f_{\hat{X}_m}(x) \quad \triangleq \quad \frac{1}{\hat{\gamma}_{\mathrm{s}}\hat{\Omega}_{\mathrm{m,r}}} \exp\left(\frac{-x}{\hat{\gamma}_{\mathrm{s}}\hat{\Omega}_{\mathrm{m,r}}}\right), F_{\hat{X}_m}(x) \quad \triangleq \quad 1 \, - \, \exp\left(\frac{-x}{\hat{\gamma}_{\mathrm{s}}\hat{\Omega}_{\mathrm{m,r}}}\right). \quad (5.5)$$

where,  $\hat{\Omega}_{\text{m,r}} = \mathbb{E}(|\hat{h}_{m,r}|^2).$ 

The PDF of  $\hat{Z}$  which is sum of N independent exponential RV is given by [122, Eq. (39)]:

$$f_{\hat{Z}}(z) = \frac{1}{\Gamma N} \left( \frac{1}{\hat{\gamma}_{I_{n,r}} \Omega_{I_{n,r}}} \right)^N z^{N-1} e^{-\frac{z}{\hat{\gamma}_{I_{n,r}} \Omega_{I_{n,r}}}}. \tag{5.6}$$

The PDF of  $\epsilon_{SR}$  is written as:

$$f_{\epsilon_{\rm SR}}(\epsilon_{\rm SR}) = \frac{1}{\sqrt{2\pi}\sigma_{\epsilon_{\rm SR}}} e^{-\frac{\epsilon_{\rm SR}^2}{2\sigma_{\epsilon_{\rm SR}}^2}}.$$
 (5.7)

The CDF of  $\hat{\Gamma}_{m,r}$  under imperfect RF channel in the presence of CCI is provided by [123]:

$$F_{\hat{\Gamma}_{\text{m,r}}}(x) = 1 - \frac{\exp\left(\frac{-x}{\hat{\gamma}_{s}\hat{\Omega}_{\text{m,r}}}\right)}{\prod_{n=1}^{N} \left(1 + \frac{\hat{\gamma}_{I_{n,r}}\Omega_{I_{n,r}}}{\hat{\gamma}_{s}\hat{\Omega}_{\text{m,r}}}x\right)}.$$
 (5.8)

At  $\zeta_{\rm SR} \to 1$ , the CDF of SINR for a perfect RF channel in presence of CCI, denoted as  $\Gamma_{m,r}$  becomes:

$$F_{\Gamma_{m,r}}(x) = 1 - \frac{\exp\left(\frac{-x}{\hat{\gamma}_{s}\hat{\Omega}_{\text{m,r}}}\right)}{\prod_{n=1}^{N} \left(1 + \frac{\gamma_{\text{l,n,r}}\Omega_{\text{l,n,r}}}{\gamma_{s}\Omega_{m,r}}x\right)}.$$
(5.9)

where, 
$$\Gamma_{m,r} = \frac{P_s |h_{m,r}|^2}{\sum_{n=1}^N P_{I_{n,r}} |g_{I_{n,r}}|^2 + \sigma^2}$$
.

In the DF protocol, R decodes and re-encodes the signal, converts it to optical signal for FSO transmission, and at destination D, a photo-detector converts back to electrical form, yielding received signal,  $y_{r,d}$  as follows as:

$$y_{r,d} = \eta \sqrt{P_r} \hat{I}_{r,d} x_{r,d} + n_d, \tag{5.10}$$

where,  $P_r$  represents transmit power of R,  $\hat{I}_{r,d}$  is the imperfect FSO channel which is modeled by  $\mathcal{F}$  distribution, accounting for turbulence effects,  $x_{r,d}$  is transmitted signal from R with  $\mathbb{E}(|x_{r,d}|^2)=1$  and  $n_d\sim CN(0,\sigma^2)$ .

The instantaneous SNR,  $\hat{\Gamma}_{r,d}$  for the imperfect FSO channel can be expressed as:

$$\hat{\Gamma}_{r,d} = \gamma_r |\hat{I}_{r,d}|^2, \bar{\hat{\Gamma}}_{r,d} = \gamma_r \mathbb{E}|\hat{I}_{r,d}|^2, \tag{5.11}$$

where,  $\gamma_r \triangleq \frac{\eta^2 P_r}{\sigma^2}$ ,  $\hat{\hat{\Gamma}}_{\rm r,d}$  represents the average SNR of the FSO link.

The PDF of  $\hat{\Gamma}_{r,d}$  under imperfect  $\mathcal{F}$  turbulence channel is provided by [127]:

$$f_{\hat{\Gamma}_{\text{r,d}}}(x) = \begin{cases} \frac{2^{a+b-3}}{\pi\sqrt{2\pi}\Gamma(a)\Gamma(b)} e^{\left(\frac{-x}{2\sigma_{\text{RD}}^2(1-\zeta_{\text{RD}}^2)\gamma_r}\right)} \sum_{k=0}^{\infty} \frac{2^{\frac{k}{2}}\phi(k)x^{\frac{k-1}{2}}}{k!\left(\gamma_r\sigma_{\epsilon_{\text{RD}}}^2(1-\zeta_{\text{RD}}^2)\right)^{\frac{k+1}{2}}}, & x > 0\\ 1 - \chi(k), & x = 0 \end{cases}$$
(5.12)

where, 
$$\phi(k) = G_{2,3}^{3,2} \left( \frac{\zeta_{\text{RD}}^2(b-1)^2}{2a^2\sigma_{\epsilon_{\text{RD}}}^2(1-\zeta_{\text{RD}}^2)} \bigg| \frac{1-a}{2}, \frac{2-a}{2} \right)$$
, and  $\chi(k) = \frac{2^{a+b-3}}{\pi\sqrt{\pi}\Gamma(a)\Gamma(b)} \sum_{k=0}^{\infty} \frac{2^k\phi(k)}{k!}$ 

 $\Gamma(\frac{k+1}{2})$ , a and b are the fading parameters,  $\epsilon_{\text{RD}} \sim C\mathcal{N}(0, \sigma_{\epsilon_{\text{RD}}}^2)$  is the Gaussian RV over the FSO channel, and  $\zeta_{\text{RD}}$  denotes the correlation coefficient.

The CDF of  $\hat{\Gamma}_{r,d}$  under imperfect  $\mathcal{F}$  turbulence channel is given by [127]:

$$F_{\hat{\Gamma}_{\text{r,d}}}(x) = \begin{cases} \frac{2^{a+b-3}}{\pi\sqrt{\pi}\Gamma(a)\Gamma(b)} \sum_{k=0}^{\infty} \frac{2^{k}\phi(k)}{k!} G_{1,2}^{1,1} \left( \frac{x}{2\sigma_{\epsilon_{\text{RD}}}^{2}}(1-\zeta_{\text{RD}}^{2})\gamma_{r}} \middle| \frac{1}{2}, 0 \right), & x > 0 \\ 1 - \chi(k), & x = 0 \end{cases}$$
(5.13)

At  $\zeta_{\rm RD} \to 1$ , the CDF of  $\Gamma_{r,d}$  for the perfect FSO channel is given by [17]:

$$F_{\Gamma_{r,d}}(x) = \left(\frac{a}{b-1}\right)^a \frac{1}{\Gamma a \Gamma b} \left(\frac{x}{\gamma_r}\right)^{a/2} G_{2,2}^{1,2} \left(\frac{a}{(b-1)} \sqrt{\frac{x}{\gamma_r}} \middle| 1 - a - b, 1 - a \right). \tag{5.14}$$

where,  $\Gamma_{r,d}=\gamma_r{|I_{r,d}|}^2$  and  $I_{r,d}$  is the perfect  $\mathcal F$  turbulence channel.

The equivalent end-to-end instantaneous SNR for imperfect channel at both hops, denoted as  $\hat{\Gamma}_{e2e}$  with user scheduling schemes by employing DF based relaying is expressed as:

 $\hat{\Gamma}_{e2e} = \min(\hat{\Gamma}_{m*,r}, \hat{\Gamma}_{r,d}), \tag{5.15}$ 

where,  $m^*$  is the scheduled user which is selected by user scheduling schemes.

The mathematical expression for selecting the mth best user according to GS scheme can be given as:

$$m^* = \underset{m \in 1, 2, \dots, M}{\arg \max} \left( \frac{\hat{X}_m}{\hat{Z} + 1} \right).$$
 (5.16)

The mathematical expression for selecting the mth user according to CDF based scheme is as follows:

$$m^* = \underset{m \in 1, 2, \dots, M}{\arg \max} \left( F_{\hat{\Gamma}_{m,r}}(x) \right)^{\frac{1}{\upsilon_m}}.$$
 (5.17)

# 5.2 Outage Probability

It is the probability that the instantaneous end-to-end SNR,  $\hat{\Gamma}_{e2e}$  is less than an acceptable threshold,  $\gamma_{th}$  and it is defined as:

$$\begin{split} P^S_{\hat{\Gamma}_{e2e}}(\gamma_{th}) &= \Pr(\hat{\Gamma}_{e2e} < \gamma_{th}), \\ &= \Pr\Big(\min(\hat{\Gamma}_{m*,r}, \hat{\Gamma}_{r,d}) < \gamma_{th}\Big), \\ &= F^S_{\hat{\Gamma}_{m*,r}}(\gamma_{th}) + F_{\hat{\Gamma}_{r,d}}(\gamma_{th}) - F^S_{\hat{\Gamma}_{m*,r}}(\gamma_{th}) F_{\hat{\Gamma}_{r,d}}(\gamma_{th}). \end{split} \tag{5.18}$$

where,  $\gamma_{th}=2^{2\rho}-1,~\rho$  denotes the target rate,  $S\in(\text{GS},\text{CDFS})$  refers to greedy based scheduling, and cumulative distribution function based scheduling respectively and  $F_{\hat{\Gamma}_{m^*,r}}^{\text{S}}$  denotes the CDF of the RF hop for different scheduling schemes.

Further, (5.18) can be simplified as:

$$P_{\hat{\Gamma}_{c,d}}^{S}(\gamma_{th}) = F_{\hat{\Gamma}_{m*r}}^{S}(\gamma_{th}) F_{\hat{\Gamma}_{rd}}^{C}(\gamma_{th}) + F_{\hat{\Gamma}_{rd}}(\gamma_{th}). \tag{5.19}$$

where,  $F_{\hat{\Gamma}_{r,d}}^{C}$  represents the complementary CDF of the FSO link.

The complementary CDF under imperfect  $\mathcal{F}$  turbulence channel is obtained by using the identities [112, Eq. (3.381.3<sup>8</sup>)] and [128, Eq. (8.4.16.2)] as follows:

$$\mathbf{F}_{\hat{\Gamma}_{\mathrm{r,d}}}^{\mathbf{C}}(x) = \frac{2^{a+b-3}}{\pi\sqrt{\pi}\Gamma(a)\Gamma(b)} \sum_{k=0}^{\infty} \frac{2^k\phi(k)}{k!} G_{1,2}^{2,0}\left(\frac{x}{2\sigma_{\epsilon_{\mathrm{ND}}}^2(1-\zeta_{\mathrm{RD}}^2)\gamma_r}\bigg| \begin{matrix} 1\\ 0, \frac{k+1}{2} \end{matrix}\right). \tag{5.20}$$

Further, complementary CDF under perfect  $\mathcal{F}$  turbulence channel is obtained by using the identities [112, Eq. (3.194.2<sup>6</sup>)] and [113, Eqs. (07.23.26.0004.01), (07.34.16.0002.01)] as follows:

$$F_{\Gamma_{r,d}}^{C}(x) = \left(\frac{b-1}{a}\right)^{b} \frac{1}{\Gamma a \Gamma b} \left(\frac{\gamma_{r}}{x}\right)^{b/2} G_{2,2}^{2,1} \left(\frac{a}{(b-1)} \sqrt{\frac{x}{\gamma_{r}}} \middle| 1, 1+b \right). \tag{5.21}$$

#### **OP for Greedy Scheduling**

The CDF of the RF hop in the presence of CCI using GS scheme in (5.16) is written as:

$$F_{\hat{\Gamma}_{m*,r}}^{GS}(\gamma_{th}) = \prod_{m=1}^{M} F_{\hat{\Gamma}_{m,r}}(\gamma_{th}). \tag{5.22}$$

By substituting (5.8) using (5.22), (5.13), and (5.20) into (5.19), we can derive the unified analytical expression of OP with GS under imperfect CSI at both hops as follows:

$$\begin{split} P_{\hat{\Gamma}_{\text{e2e,NoCSI}}}^{\text{GS}}(\gamma_{th}) &= 1 - \chi(k) + \prod_{m=1}^{M} \left( 1 - \frac{e^{\frac{-\gamma_{th}}{\hat{\gamma}_{\text{s}}\hat{\Omega}_{\text{m,r}}}}}{\prod_{n=1}^{N} \left( 1 + \frac{\hat{\gamma}_{I_{\text{n,r}}}\Omega_{I_{\text{n,r}}}}{\hat{\gamma}_{\text{s}}\hat{\Omega}_{\text{m,r}}} \gamma_{th} \right) \right) \frac{2^{a+b-3}}{\pi \sqrt{\pi}\Gamma(a)\Gamma(b)} \\ &\times \sum_{k=0}^{\infty} \frac{2^{k}\phi(k)}{k!} G_{1,2}^{2,0} \left( \frac{\gamma_{th}}{2\sigma_{\epsilon_{\text{RD}}}^{2}(1 - \zeta_{\text{RD}}^{2})\gamma_{r}} \bigg| 0, \frac{1}{k+1} \right) + \frac{2^{a+b-3}}{\pi \sqrt{\pi}\Gamma(a)\Gamma(b)} \sum_{k=0}^{\infty} \frac{2^{k}\phi(k)}{k!} \\ &\times G_{1,2}^{1,1} \left( \frac{\gamma_{th}}{2\sigma_{\epsilon_{\text{RD}}}^{2}(1 - \zeta_{\text{RD}}^{2})\gamma_{r}} \bigg| \frac{1}{k+1}, 0 \right). \quad (5.23) \end{split}$$

#### **OP for CDF Scheduling**

The CDF of RF hop using CDF based scheduling scheme in (5.17) in the presence of CCI is written as:

$$\mathbf{F}_{\hat{\Gamma}_{\mathrm{m*,r}}}^{\mathrm{CDFS}}(\gamma_{th}) = \Pr\Biggl(\max_{m \in 1,2,...M} \Bigl(\mathbf{F}_{\hat{\Gamma}_{\mathrm{m,r}}}(x)\Bigr)^{\frac{1}{\upsilon_m}} \ \bigcap \hat{\Gamma}_{\mathrm{m,r}} < \gamma_{th}\Biggr). \tag{5.24}$$

The final expression of CDF for RF hop with CDF based scheduling is obtained in (5.25) as follows:

$$F_{\hat{\Gamma}_{m*,r}}^{\text{CDFS}}(\gamma_{th}) = \sum_{m=1}^{M} v_{m} \left( 1 - \frac{e^{\frac{-\gamma_{th}}{\hat{\gamma}_{s}\hat{\Omega}_{m,r}}}}{\prod_{n=1}^{N} \left( 1 + \frac{\hat{\gamma}_{I_{n,r}}\Omega_{I_{n,r}}}{\hat{\gamma}_{s}\hat{\Omega}_{m,r}} \gamma_{th} \right)} \right)^{\frac{1}{v_{m}}}.$$
 (5.25)

The derivation of (5.25) is given in Appendix III.

By substituting (5.25), (5.13), and (5.20) into (5.19), the closed-form expression of OP with CDF based scheduling under imperfect CSI at both hops is obtained as follows:

$$\begin{split} P_{\hat{\Gamma}_{\text{e2e, NoCSI}}}^{\text{CDFS}}(\gamma_{th}) &= 1 - \chi(k) + \sum_{m=1}^{M} \upsilon_{m} \left( 1 - \frac{e^{\frac{-\gamma_{th}}{\hat{\gamma}_{\text{s}}\hat{\Omega}_{\text{m,r}}}}}{\prod_{n=1}^{N} \left( 1 + \frac{\hat{\gamma}_{\text{I}_{\text{n,r}}}\Omega_{\text{I}_{\text{n,r}}}}{\hat{\gamma}_{\text{s}}\hat{\Omega}_{\text{m,r}}} \gamma_{th} \right)} \right)^{\frac{1}{\upsilon_{m}}} \\ &\times \frac{2^{a+b-3}}{\pi \sqrt{\pi} \Gamma(a) \Gamma(b)} \sum_{k=0}^{\infty} \frac{2^{k} \phi(k)}{k!} G_{1,2}^{2,0} \left( \frac{\gamma_{th}}{2\sigma_{\epsilon_{\text{RD}}}^{2}} (1 - \zeta_{\text{RD}}^{2}) \gamma_{r} \middle| 0, \frac{k+1}{2} \right) + \frac{2^{a+b-3}}{\pi \sqrt{\pi} \Gamma(a) \Gamma(b)} \\ &\times \sum_{k=0}^{\infty} \frac{2^{k} \phi(k)}{k!} G_{1,2}^{1,1} \left( \frac{\gamma_{th}}{2\sigma_{\epsilon_{\text{RD}}}^{2}} (1 - \zeta_{\text{RD}}^{2}) \gamma_{r} \middle| \frac{1}{2}, 0 \right). \end{split} (5.26)$$

OP is expressed as a function of  $\gamma_t$  to assess the system's performance with variation in the total available power  $P_t$  within the network. Here, we denote the total power  $P_t = P_s + P_r$ , where  $\gamma_t = \frac{P_t}{\sigma^2}$ . Additionally, we assume  $\gamma_s = \beta \gamma_t, \gamma_r = (1-\beta)\gamma_t, \gamma_{I_{n,r}} = \gamma_t/\zeta_{I_{n,r}}$ , where  $\beta$  represents the fraction of total power allocated to the user and relay, while  $\zeta_{I_{n,r}}$  is the fraction of total power given to interferers.

#### **Asymptotic Outage Performance**

The closed form expressions for OP with different scheduling schemes provide limited insights. Hence, to get a deeper insight at high SNR, i.e.,  $\gamma_t$  approaches infinity, the OP expression provided in (5.18) becomes as:

$$P_{\hat{\Gamma}_{c,2}}^{\infty,S}(\gamma_{th}) \simeq F_{\hat{\Gamma}_{m+r}}^{\infty}(\gamma_{th}) + F_{\hat{\Gamma}_{r,d}}^{\infty}(\gamma_{th}) - F_{\hat{\Gamma}_{m+r}}^{\infty}(\gamma_{th}) F_{\hat{\Gamma}_{r,d}}^{\infty}(\gamma_{th}). \tag{5.27}$$

At high value of SNR, terms involving  $1/\gamma_t$  become negligible and can be ignored i.e.  $e^{\frac{-\gamma_{\rm th}}{\hat{\gamma}_{\rm s}\hat{\Omega}_{\rm m,r}}}=e^{\frac{-\gamma_{th}(1-\zeta_{\rm sR}^2)\sigma_{\xi_{\rm SR}}^2}{\zeta_{\rm sR}^2\hat{\Omega}_{\rm m,r}}}$  and  $\prod_{n=1}^N\left(1+\frac{\hat{\gamma}_{\rm l_{n,r}}\Omega_{\rm l_{n,r}}}{\hat{\gamma}_{\rm s}\hat{\Omega}_{\rm m,r}}\gamma_{th}\right)^{-1}\approx e^{\frac{-\sum_{n=1}^N\gamma_{l_{n,r}}\Omega_{\rm l_{n,r}}}{\gamma_{\rm s}\zeta_{\rm sR}^2\hat{\Omega}_{\rm m,r}}\gamma_{th}}$ . Further, apply series expansion of exponential function as given in [112, Eq. (1.211.1)], the asymptotic CDF expression for RF hop under imperfect RF channel given in (5.8) becomes:

$$\begin{split} F_{\hat{\Gamma}_{\text{m,r}}}^{\infty}(\gamma_{th}) &\simeq \left(\frac{(1-\zeta_{\text{SR}}^2)\sigma_{\epsilon_{\text{SR}}}^2}{\zeta_{\text{SR}}^2\hat{\Omega}_{\text{m,r}}} + \frac{\sum_{n=1}^N \gamma_{I_{\text{n,r}}}\Omega_{I_{n,r}}}{\gamma_s\zeta_{\text{SR}}^2\hat{\Omega}_{\text{m,r}}}\right) \gamma_{th} \\ &- \frac{\gamma_{th}^2}{2} \left(\frac{(1-\zeta_{\text{SR}}^2)\sigma_{\epsilon_{\text{SR}}}^2}{\zeta_{\text{SR}}^2\hat{\Omega}_{\text{m,r}}} + \frac{\sum_{n=1}^N \gamma_{I_{n,r}}\Omega_{I_{n,r}}}{\gamma_s\zeta_{\text{SR}}^2\hat{\Omega}_{\text{m,r}}}\right)^2. \end{split} (5.28)$$

At  $\zeta_{\text{SR}} \to 1$ , the asymptotic expression of the CDF for the RF hop is obtained by using (5.9) as follows:

$$F_{\Gamma_{\rm m,r}}^{\infty}(\gamma_{th}) \simeq \frac{\gamma_{\rm th}}{\gamma_{\rm s}\Omega_{\rm m,r}} \sum_{n=1}^{N} \gamma_{I_{n,r}} \Omega_{I_{n,r}}. \tag{5.29}$$

The asymptotic of the CDF expression for FSO hop under imperfect  $\mathcal{F}$  turbulence channel is found by utilizing the expressions [113, Eq. (07.34.06.0006.01)] in (5.13) as follows:

$$F_{\hat{\Gamma}_{r,d}}^{\infty}(\gamma_{th}) \simeq 1 - \chi(k) + \frac{2^{a+b-2}}{\pi\sqrt{\pi}\Gamma(a)\Gamma(b)} \sum_{k=0}^{\infty} \frac{2^{k}\phi(k)}{(k+1)!} \left(\frac{\gamma_{th}}{2\sigma_{\epsilon_{RD}}^{2}(1-\zeta_{RD}^{2})\gamma_{r}}\right)^{\frac{k+1}{2}}.$$
(5.30)

At  $\zeta_{RD} \to 1$ , the asymptotic expression of the CDF for FSO hop is found by utilizing the expressions [113, Eqs. (07.34.16.0001.01), (07.34.06.0006.01)] in (5.14) as follows:

$$F_{\Gamma_{r,d}}^{\infty}(\gamma_{th}) \simeq \frac{\Gamma(a+b)}{\Gamma(a+1)\Gamma b} \left(\frac{a}{(b-1)} \sqrt{\frac{\gamma_{th}}{\gamma_r}}\right)^a.$$
 (5.31)

Using (5.25), (5.28), and (5.30) in (5.27) under imperfect CSI at both links and performed some algebraic manipulations to obtain the asymptotic expression for CDF based scheduling as follows:

Case 1: Imperfect RF and Imperfect FSO links  $(0 < (\zeta_{SR}, \zeta_{RD}) < 1)$ 

$$\begin{split} \mathbf{P}_{\hat{\Gamma}_{\text{e2e, NoCSI}}}^{\infty,\text{CDFS}}(\gamma_{th}) &\simeq 1 - \chi(k) + \frac{2^{a+b-2}}{\pi\sqrt{\pi}\Gamma(a)\Gamma(b)} \sum_{k=0}^{\infty} \frac{2^{k}\phi(k)}{(k+1)!} \left(\frac{\gamma_{th}}{2\sigma_{\epsilon_{\text{RD}}}^{2}(1-\zeta_{\text{RD}}^{2})\gamma_{r}}\right)^{\frac{k+1}{2}} + \sum_{m=1}^{M} \\ &\times v_{m} \left\{ \left(\frac{(1-\zeta_{\text{SR}}^{2})\sigma_{\epsilon_{\text{SR}}}^{2}}{\zeta_{\text{SR}}^{2}\hat{\Omega}_{\text{m,r}}} + \frac{\sum_{n=1}^{N}\gamma_{I_{\text{n,r}}}\Omega_{I_{n,r}}}{\gamma_{s}\zeta_{\text{SR}}^{2}\hat{\Omega}_{\text{m,r}}}\right) \gamma_{th} - \frac{\gamma_{th}^{2}}{2} \left(\frac{(1-\zeta_{\text{SR}}^{2})\sigma_{\epsilon_{\text{SR}}}^{2}}{\zeta_{\text{SR}}^{2}\hat{\Omega}_{\text{m,r}}} + \frac{\sum_{n=1}^{N}\gamma_{I_{n,r}}\Omega_{I_{n,r}}}{\gamma_{s}\zeta_{\text{SR}}^{2}\hat{\Omega}_{\text{m,r}}}\right)^{2} \right\}^{\frac{1}{\nu_{m}}} \\ &\times \left(\chi(k) - \frac{2^{a+b-2}}{\pi\sqrt{\pi}\Gamma(a)\Gamma(b)} \sum_{k=0}^{\infty} \frac{2^{k}\phi(k)}{(k+1)!} \left(\frac{\gamma_{th}}{2\sigma_{\epsilon_{\text{RD}}}^{2}(1-\zeta_{\text{RD}}^{2})\gamma_{r}}\right)^{\frac{k+1}{2}}\right). \end{split} \tag{5.32}$$

Furthermore, diversity order can be evaluated using  $P_{\hat{\Gamma}_{e2e}}^{\infty,S}=(G_c\gamma_t)^{-G_d}$ . Therefore, diversity order for CDFS is  $G_d=0$ .

Case2: Perfect RF and Imperfect FSO links ( $\zeta_{\rm SR} \to 1; 0 < \zeta_{\rm RD} < 1$ ) At  $\zeta_{\rm SR} \to 1$ , the asymptotic OP expression is obtained under imperfect CSI at FSO channel for CDF based scheduling by substituting (5.29) using (5.25) and (5.30) in (5.27) as follows:

$$\begin{split} \mathbf{P}_{\hat{\Gamma}_{\text{e2e, Perfect RF}}}^{\infty, \text{CDFS}}(\gamma_{th}) &\simeq 1 - \chi(k) + \frac{2^{a+b-2}}{\pi\sqrt{\pi}\Gamma(a)\Gamma(b)} \sum_{k=0}^{\infty} \frac{2^k \phi(k)}{(k+1)!} \left( \frac{\gamma_{th}}{2\sigma_{\epsilon_{\text{RD}}}^2(1-\zeta_{\text{RD}}^2)\gamma_r} \right)^{\frac{k+1}{2}} + \\ & \left( \chi(k) - \frac{2^{a+b-2}}{\pi\sqrt{\pi}\Gamma(a)\Gamma(b)} \sum_{k=0}^{\infty} \frac{2^k \phi(k)}{(k+1)!} \left( \frac{\gamma_{th}}{2\sigma_{\epsilon_{\text{RD}}}^2(1-\zeta_{\text{RD}}^2)\gamma_r} \right)^{\frac{k+1}{2}} \right) \\ & \times \sum_{m=1}^{M} \upsilon_m \left( \sum_{n=1}^{N} \frac{\Omega_{\mathbf{I}_{\mathbf{n},\mathbf{r}}} \gamma_{\mathbf{I}_{\mathbf{n},\mathbf{r}}} \gamma_{\mathbf{th}}}{\Omega_{\mathbf{m},\mathbf{r}} \gamma_{\mathbf{s}}} \right)^{\frac{1}{\upsilon_m}}. \quad (5.33) \end{split}$$

Case3: Imperfect RF and Perfect FSO links  $(0 < \zeta_{SR} < 1; \zeta_{RD} \to 1)$ At  $\zeta_{RD} \to 1$ , the asymptotic OP expression is obtained under imperfect CSI at RF channel for CDF based scheduling by substituting (5.28) using (5.25) and (5.31) in (5.27) as follows:

$$\begin{split} &P_{\hat{\Gamma}_{\text{e2e, Perfect FSO}}}^{\infty, \text{CDFS}}(\gamma_{th}) \simeq \sum_{m=1}^{M} \upsilon_{m} \bigg\{ \bigg( \frac{(1-\zeta^{2})\sigma_{\epsilon}^{2}}{\zeta^{2}\hat{\Omega}_{\text{m,r}}} + \frac{\sum_{n=1}^{N} \gamma_{I_{n,r}} \Omega_{I_{n,r}}}{\gamma_{s} \zeta^{2}\hat{\Omega}_{\text{m,r}}} \bigg) \gamma_{th} \\ &- \frac{\gamma_{th}^{2}}{2} \left( \frac{(1-\zeta^{2})\sigma_{\epsilon}^{2}}{\zeta^{2}\hat{\Omega}_{\text{m,r}}} + \frac{\sum_{n=1}^{N} \gamma_{I_{n,r}} \Omega_{I_{n,r}}}{\gamma_{s} \zeta^{2}\hat{\Omega}_{\text{m,r}}} \bigg)^{2} \right\}^{\frac{1}{\upsilon_{m}}} + \frac{\Gamma(a+b)}{\Gamma(a+1)\Gamma b} \left( \frac{a}{(b-1)} \sqrt{\frac{\gamma_{th}}{\gamma_{r}}} \right)^{a}. \end{split} \tag{5.34}$$

# 5.3 Optimum Performance Analysis

# 5.3.1 Optimal Power Allocation

To optimize power allocation for both the user and relay while minimizing OP in the context of CDF-based scheduling given in (5.32), the objective function can be represented by the following expression:

$$\begin{array}{ll} (P_s^*,P_r^*) &=& \displaystyle \mathop{\arg\min}_{(\mathrm{P}_s,P_r)} P_{\hat{\Gamma}_{\mathrm{e2e,NoCSI}}}^{\infty,\mathrm{CDFS}}(\gamma_{th}), \\ & & \mathrm{subject\ to}\ P_s = \beta P_t, P_r = (1-\beta) P_t \end{array}$$

To give equal fairness to all the users, we assume  $v_1 = v_2 \dots = v_M$  with  $\sum_{m=1}^M v_m = 1$  and substituting  $P_s = \beta P_t$ ,  $P_r = (1 - \beta)P_t$  in (5.32), we obtain:

$$\begin{split} & P_{\hat{\Gamma}_{e2e,\text{NoCSI}}}^{\infty,\text{CDFS}}(\gamma_{th}) \!\!\simeq\!\! 1 \!\!-\!\! \chi(k) \!+\! \tfrac{2^{a+b-2}}{\pi\sqrt{\pi}\Gamma(a)\Gamma(b)} \sum_{k=0}^{\infty} \! \tfrac{2^k\phi(k)}{(k\!+\!1)!} \left( \frac{\gamma_{th}}{2\sigma_{\epsilon_{\text{RD}}}^2(1\!-\!\zeta_{\text{RD}}^2)(1\!-\!\beta)P_t} \right)^{\frac{k+1}{2}} + \\ & \sum_{m=1}^{M} \! v_m \! \left\{ \left( \frac{(1\!-\!\zeta_{\text{SR}}^2)\sigma_{\epsilon_{\text{SR}}}^2}{\zeta_{\text{SR}}^2\hat{\Omega}_{\text{m,r}}} \! +\! \frac{\sum_{n=1}^{N} \! \gamma_{I_{n,r}} \! \Omega_{I_{n,r}}}{\beta P_t \zeta_{\text{SR}}^2\hat{\Omega}_{\text{m,r}}} \right) \! \gamma_{th} \! -\! \frac{\gamma_{th}^2}{2} \left( \frac{(1\!-\!\zeta_{\text{SR}}^2)\sigma_{\epsilon_{\text{SR}}}^2}{\zeta_{\text{SR}}^2\hat{\Omega}_{\text{m,r}}} \! +\! \frac{\sum_{n=1}^{N} \! \gamma_{I_{\text{n,r}}} \! \Omega_{I_{\text{n,r}}}}{\beta P_t \zeta_{\text{SR}}^2\hat{\Omega}_{\text{m,r}}} \right)^2 \right\}^{\frac{1}{\upsilon_m}} \\ & \times \left( \chi(k) \! -\! \frac{2^{a+b-2}}{\pi\sqrt{\pi}\Gamma(a)\Gamma(b)} \sum_{k=0}^{\infty} \! \frac{2^k\phi(k)}{(k\!+\!1)!} \left( \frac{\gamma_{th}}{2\sigma_{\epsilon_{\text{RD}}}^2(1\!-\!\zeta_{\text{RD}}^2)(1\!-\!\beta)P_t} \right)^{\frac{k\!+\!1}{2}} \right). \end{split} \tag{5.36}$$

Here  $\frac{\partial^2 P_{\hat{\Gamma}_{\text{e2e,NoCSI}}}^{\infty,\text{CDFS}}(\gamma_{th})}{\partial \beta^2} > 0$  for  $\beta \in (0,1)$ , indicating that the objective function is strictly convex. To determine the optimal value of  $\beta$ , we equate the first derivative of the above

expression with respect to  $\beta$  to zero, which is expressed as follows:

$$\frac{\partial P_{\hat{\Gamma}_{c2c,\text{NoCSI}}}^{\infty,\text{CDFS}}(\gamma_{th})}{\partial \beta} \simeq \frac{2^{a+b-3}}{\pi \sqrt{\pi} \Gamma(a) \Gamma(b)} \sum_{k=0}^{\infty} \frac{2^{k} \phi(k)}{k!} \left( \frac{\gamma_{th}}{2\sigma_{\epsilon_{\text{RD}}}^{2}(1-\zeta_{\text{RD}}^{2})P_{t}} \right)^{\frac{k+1}{2}} \left( \frac{1}{1-\beta^{*}} \right)^{\frac{k+3}{2}} + \\ \sum_{m=1}^{M} \Lambda_{m,r}^{\frac{1}{\upsilon_{m}}-1} \left\{ -\frac{\sum_{n=1}^{N} \gamma_{I_{\text{n,r}}} \Omega_{I_{\text{n,r}}}}{\beta^{*2} P_{t} \zeta_{\text{SR}}^{2} \hat{\Omega}_{\text{m,r}}} \gamma_{th} + \frac{1}{\beta^{*3}} \left( \frac{\sum_{n=1}^{N} \gamma_{I_{\text{n,r}}} \Omega_{I_{\text{n,r}}}}{P_{t} \zeta_{\text{SR}}^{2} \hat{\Omega}_{\text{m,r}}} \gamma_{th} \right)^{2} + \left( \frac{(1-\zeta_{\text{SR}}^{2})\sigma_{\epsilon_{\text{SR}}}^{2}}{\zeta_{\text{SR}}^{2} \hat{\Omega}_{\text{m,r}}} \right) \\ \left( \frac{\sum_{n=1}^{N} \gamma_{I_{\text{n,r}}} \Omega_{I_{\text{n,r}}}}{\beta^{*2} P_{t} \zeta_{\text{SR}}^{2} \hat{\Omega}_{\text{m,r}}} \gamma_{th}^{2} \right) \right\} \left( \chi(k) - \frac{2^{a+b-2}}{\pi \sqrt{\pi} \Gamma(a) \Gamma(b)} \sum_{k=0}^{\infty} \frac{2^{k} \phi(k)}{(k+1)!} \left( \frac{\gamma_{th}}{2\sigma_{\epsilon_{\text{RD}}}^{2}(1-\zeta_{\text{RD}}^{2})(1-\beta^{*})P_{t}} \right)^{\frac{k+1}{2}} \right) - \\ \sum_{m=1}^{M} \upsilon_{m} \Lambda_{m,r}^{\frac{1}{\upsilon_{m}}} \frac{2^{a+b-3}}{\pi \sqrt{\pi} \Gamma(a) \Gamma(b)} \sum_{k=0}^{\infty} \frac{2^{k} \phi(k)}{k!} \left( \frac{\gamma_{th}}{2\sigma_{\epsilon_{\text{RD}}}^{2}(1-\zeta_{\text{RD}}^{2})P_{t}} \right)^{\frac{k+3}{2}} = 0. \quad (5.37)$$

$$\text{where, } \Lambda_{m,r} = \left( \frac{(1 - \zeta_{\text{SR}}^2) \sigma_{\epsilon_{\text{SR}}}^2}{\zeta_{\text{SR}}^2 \hat{\Omega}_{\text{m,r}}} + \frac{\sum_{n=1}^N \gamma_{I_{\text{n,r}}} \Omega_{I_{\text{n,r}}}}{\beta^* P_t \zeta_{\text{SR}}^2 \hat{\Omega}_{\text{m,r}}} \right) \gamma_{th} - \frac{\gamma_{th}^2}{2} \left( \frac{(1 - \zeta_{\text{SR}}^2) \sigma_{\epsilon_{\text{SR}}}^2}{\zeta_{\text{SR}}^2 \hat{\Omega}_{\text{m,r}}} + \frac{\sum_{n=1}^N \gamma_{I_{\text{n,r}}} \Omega_{I_{\text{n,r}}}}{\beta^* P_t \zeta_{\text{SR}}^2 \hat{\Omega}_{\text{m,r}}} \right)^2.$$

Obtaining the closed-form equation for the optimal power allocation coefficient,  $\beta^*$  is challenging and standard iterative root-finding methods, include Bisection's or Newton's can be used to find a numerical solution. The time complexity of the bisection algorithm in a given interval (u,v) and precision of  $\epsilon$  is  $\mathcal{O}(\log w)$ , where  $w=\lfloor \frac{v-u}{\epsilon} \rfloor$ .

# 5.3.2 Optimal CAR Allocation

To optimize the CAR so as to minimize the OP for CDF based scheduling (5.34), the objective function can be formulated as follows:

$$\begin{array}{ll} (\upsilon_1^*, \upsilon_2^*, .., \upsilon_M^*) & = & \underset{(\upsilon_1, \upsilon_2, .., \upsilon_M)}{\arg\min} \mathrm{P}_{\hat{\Gamma}_{\mathrm{e2e, Perfect FSO}}}^{\infty, \mathrm{CDFS}}(\gamma_{th}), \\ & & \text{subject to } \sum_{m=1}^M \upsilon_m = 1. \end{array} \tag{5.38}$$

To solve the above objective function, the Lagrangian multipliers method is used to determine the optimal CAR for the users as follows:

$$\begin{split} \mathbf{F}_{\hat{\Gamma}_{\text{e2e, Perfect FSO}}}^{\infty, \text{CDFS}}(\upsilon_1, \upsilon_2, ..., \upsilon_M, \lambda) &= \sum_{m=1}^M \upsilon_m \left(\Lambda_{m,r}\right)^{\frac{1}{\upsilon_m}} + \frac{\Gamma(a+b)}{\Gamma(a+1)\Gamma b} \left(\frac{a}{(b-1)} \sqrt{\frac{\gamma_{\text{th}}}{\gamma_r}}\right)^a \\ &+ \lambda \Big(\sum_{m=1}^M \upsilon_m - 1\Big). \quad (5.39) \end{split}$$

By utilizing the condition  $\frac{\partial^2 P_{\hat{\Gamma}_{\text{e2e, Perfect FSO}}}^{\infty, \text{CDFS}}(\gamma_{th})}{\partial v_m^2} > 0$  for  $\sum_{m=1}^M v_m = 1$ , it indicates that the objective function is strictly convex.

To determine the optimized value of  $v_m^*$ , the first derivative of (5.39) with respect to  $v_m$  is taken, set to zero, and algebraic manipulations are performed, leading to the following expression:

$$v_m^* = \frac{\ln\left(\Lambda_{m,r}\right)}{1 + W\left(\lambda\left(\left(\Lambda_{m,r}\right)^{\frac{-1}{\ln(\Lambda_{m,r})}}\right)\right)}.$$
 (5.40)

The above expression involves the Lambert W function, denoted as W(.) [124]. The proof of (5.40) is provided in Appendix IV. Further, utilizing the power series,  $W(z) = \sum_{k=1}^{\infty} \frac{(-k)^{k-1}}{k!} z^k$ , [113, Eq. (01.31.06.0002.01)] in (5.40), the closed-form expression for  $v_m^*$  is obtained as:

$$v_m^* = \frac{\ln\left(\Lambda_{m,r}\right)}{1 + \sum_{k=1}^{\infty} \frac{\left(-k\right)^{k-1}}{k!} \lambda^k \Lambda_{m,r}^{\frac{-k}{\ln(\Lambda_{m,r})}}}.$$
(5.41)

Now, to calculate the value of  $\lambda$ , summing of all the individual CAR and equating to unity. We obtain the following:

$$\begin{split} \frac{\ln\left(\Lambda_{1,r}\right)}{1 + \sum_{k=1}^{\infty} \frac{(-k)^{k-1}}{k!} \lambda^{k} \left(\Lambda_{1,r}\right)^{\frac{-k}{\ln(\Lambda_{1,r})}}} + \frac{\ln\left(\Lambda_{2,r}\right)}{1 + \sum_{k=1}^{\infty} \frac{(-k)^{k-1}}{k!} \lambda^{k} \left(\Lambda_{2,r}\right)^{\frac{-k}{\ln(\Lambda_{2,r})}}} + \dots \\ + \frac{\ln\left(\Lambda_{M,r}\right)}{1 + \sum_{k=1}^{\infty} \frac{(-k)^{k-1}}{k!} \lambda^{k} \left(\Lambda_{M,r}\right)^{\frac{-k}{\ln(\Lambda_{M,r})}}} - 1 = 0. \quad (5.42) \end{split}$$

Finding a closed-form solution for  $\lambda$  is difficult. The value of  $\lambda$  can be obtained by using bisection method.

# 5.4 Simulation Results

This section presents the accuracy of derived expressions for the considered system assuming three users, a single relay and one destination. For RF hop, we assume that the three users are at (0,0), (0.2,0.5), (0.5,0.1), while the relay is at (1,0) and the three interferers are at (0,2.1), (1.1,2) and (2.2,-1). The channel variance  $\Omega_{(.)} = \mu d_{i,j}$ , and  $d_{i,j} = (\bar{d}_{i,j}/d_0)^{-\xi}$ , where,  $d_{i,j}$  is the normalized distance between node i and node j, where  $\bar{d}_{i,j}$  is the actual Euclidean distance between them,  $d_0$  is the reference distance,  $\mu$  is the propagation constant and  $\xi$  is the path loss exponent [129]. Further,  $\Omega_{(.)}$  is calculated by considering  $d_0 = 1$ ,  $\mu = 1$  and  $\xi = 3$ . Assume  $\sigma_{\epsilon_{\rm SR}}^2 = \sigma_{\epsilon_{\rm RD}}^2 = \sigma_{\epsilon}^2$ . For the FSO hop, fading parameters (a,b)=(4.5916,7.0941), (a,b)=(2.3378,4.5323), and (a,b)=(1.4321,3.4948) are taken for weak, moderate, and strong turbulent environments respectively [64]. In the analytical expressions, the infinite summation terms can be truncated to those listed in the Table 5.1 to maintain the truncation precision. From Table 5.1, k = 185 terms have been used to obtain the results over a wide range of different parameters and increasing the values beyond k = 185 does not have sig-

nificant influence on performance metrics. Furthermore, the Monte-Carlo simulations align perfectly with the exact analytic results, thereby validating the derived expressions. It is important to note that the number of iterations for Monte-Carlo Simulation is set to  $10^6$ .

Table 5.1: Truncation accuracy of summation limit

Parameter	Truncation	Weak	Moderate	Strong		
	limits	Turbulence	Turbulence	Turbulence		
			$\zeta_{\rm SR} = 0.98, \zeta_{\rm RD} = 0.8$ $\zeta_{\rm SR} = 0.98, \zeta_{\rm RD} = 0.75$ $\zeta_{\rm SR} = 0.98, \zeta_{\rm RD} = 0.7$			
	k = 5	0.368117320691043	0.395919867076866	0.416711052916665	0.390702966957236	0.372602152102296
	k = 15	0.165434189035159	0.230716197787088	0.278433232071588	0.270743541164186	0.269518967101799
	k = 35	0.107637442481876	0.164999463531357	0.214200531048431	0.220356471052884	0.229998875053582
	k = 55	0.097854261832061	0.147913016042985	0.194180379986248	0.205655030604734	0.219113864752622
Outage Probability,	k = 85	0.094108131703812	0.138708634493340	0.181725520696739	0.196853613241084	0.212805652926906
$\gamma_t = 60 \text{ dB}$	k = 105	0.093265573914793	0.135935469135757	0.174700720688415	0.193942306837203	0.210764852685186
	k = 125	0.092831364619627	0.134232420288688	0.174700720688415	0.192046470274892	0.209451370304017
	k = 155	0.092501507445056	0.132685657474007	0.171966277897934	0.190215652474322	0.208196685073172
	k = 185	0.092407225722412	0.132170450313579	0.170996529214856	0.189573019982106	0.207759980792310

Fig. 5.2 and Fig. 5.3 illustrate the OP of the CDFS based system for various  $\zeta_{\rm SR}$  and  $\zeta_{\rm RD}$  under strong turbulence condition. From these figures, it is evident that imperfect CSI significantly impacts OP performance. Higher values of  $\zeta_{\rm SR}$  and  $\zeta_{\rm RD}$  contribute to improved OP performance, as a larger correlation coefficient indicates a more accurate estimation. Notable, the influence of  $\zeta_{\rm RD}$  on the OP performance is more pronounced than that of  $\zeta_{\rm SR}$ . Further, analytic expression for OP of CDFS based system in (5.26) accurately matches with the simulation results. Moreover, at high values of  $\gamma_t$ , OP saturates at approximately 1- $\chi(k)$  indicating a diversity order of  $G_d=0$ . This saturation occurs because it is independent of  $\gamma_t$  which implies OP cannot improve further with increase of  $\gamma_t$ .

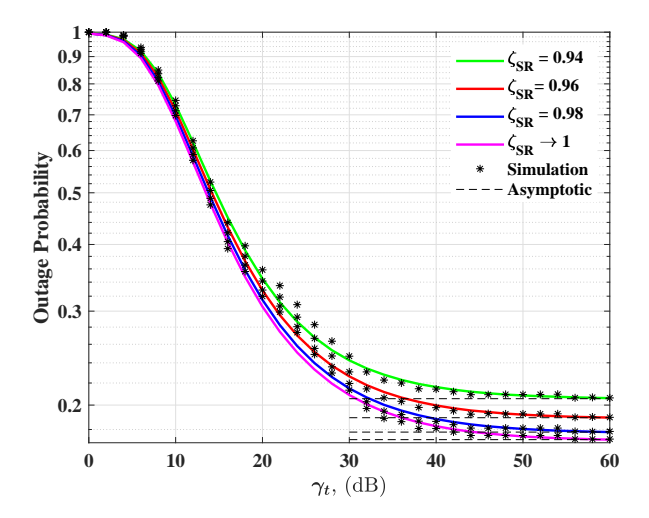


Figure 5.2: OP versus  $\gamma_t$  over different values of  $\zeta_{\rm SR}$  considering CDFS based system fixed at  $P_t/P_{I_{n,r}}$  = [20, 25, 30] (dB) under strong turbulence condition fixed at  $\rho=1$ ,  $\zeta_{\rm RD}=0.8$ ,  $\sigma_\epsilon^2=0.5$ ,  $\beta=0.5$ , and  $\upsilon_m=[0.6,0.3,0.1]$ .

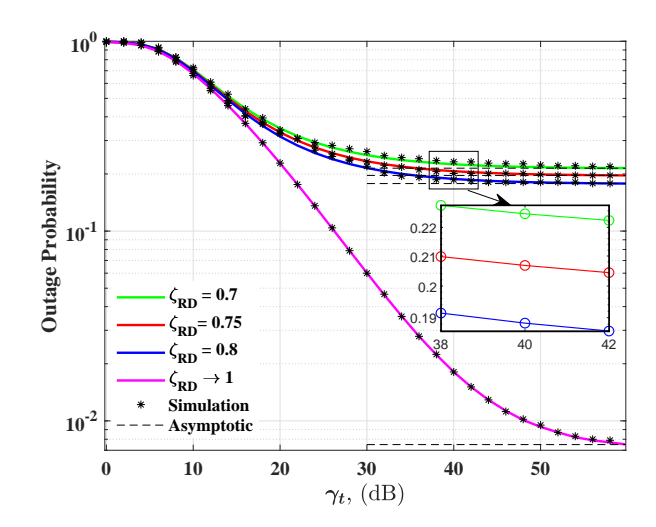


Figure 5.3: OP versus  $\gamma_t$  over different values of  $\zeta_{\rm RD}$  considering CDFS based system fixed at  $P_t/P_{I_{n,r}}$  = [20, 25, 30] (dB) under strong turbulence condition fixed at  $\rho=1$ ,  $\zeta_{\rm RF}=0.98,\,\sigma_\epsilon^2=0.5,\,\beta=0.5,\,$  and  $\upsilon_m=[0.6,0.3,0.1].$ 

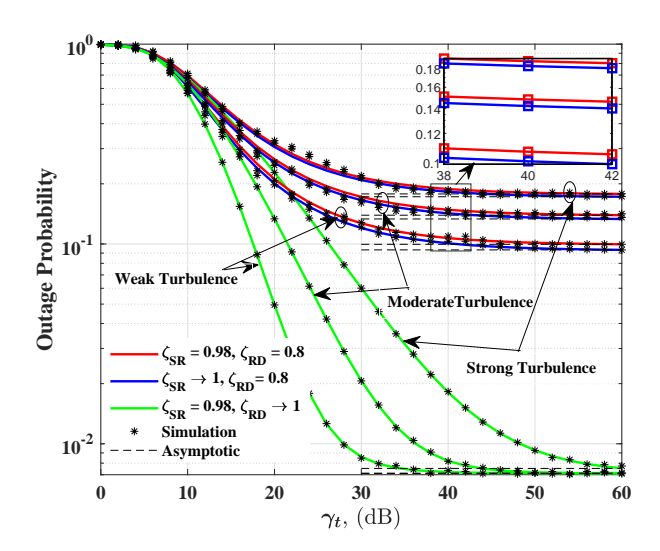


Figure 5.4: OP versus  $\gamma_t$  under different turbulence conditions considering CDFS based system fixed at  $P_t/P_{I_{n,r}}$  = [20, 25, 30] (dB),  $\rho=1$ ,  $\sigma_\epsilon^2=0.5$ ,  $\beta=0.5$  and  $\upsilon_m=[0.6,0.3,0.1]$ .

In Fig. 5.4, impact of turbulence can be observed on the OP of the considered system. In the figure we have considered three scenarios: Imperfect RF link only ( $\zeta_{RD} \rightarrow 1$ ), Imperfect FSO link only ( $\zeta_{SR} \rightarrow 1$ ), and Imperfect RF & FSO link. From the figure it can be observed that the asymptotic outage performance with imperfect RF & FSO link and imperfect FSO link only, is almost similar over a wide range of turbulence conditions. Further, the asymptotic expression of the outage performance in (5.32) and (5.33) differ by a constant factor term. Thus imperfection in the channel estimation of FSO link severely affects the outage performance. It implies that the system performance is limited by the imperfect FSO link. Further, comparing the performance of imperfect RF only, it is observed that the RF link dominates the system performance when FSO

link is perfect. In Fig. 5.5, the impact of power allocation at user and relay on the OP can be observed under moderate turbulence conditions for varying values of data rates and interferers power. The optimal power allocation coefficient,  $\beta^*$  is obtained using (5.37), that minimizes the outage probability over a wide range of interference power and data rates. In the figure we have considered three scenarios: Imperfect RF link only ( $\zeta_{RD} \rightarrow 1$ ), Imperfect FSO link only ( $\zeta_{SR} \rightarrow 1$ ), and Imperfect both links. As shown in figure, the outage performance decreases and then increases as the power allocation coefficient,  $\beta$  varies in the range (0,1), indicating that there is an optimum value of power allocation coefficient, which is obtained by solving (5.37). The optimal power allocation coefficient,  $\beta^*$  obtained using (5.37) minimizes the outage probability across a broad range of interference power and data rates.

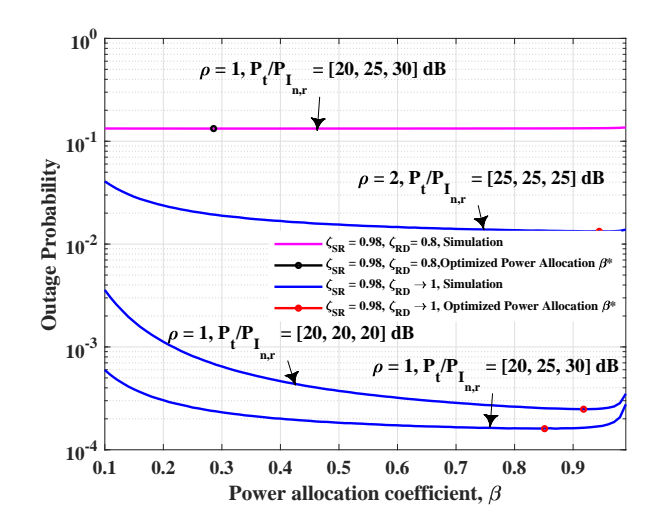


Figure 5.5: OP versus power allocation coefficient considering CDFS based system under moderate turbulence condition fixed at  $\sigma_{\epsilon}^2=0.5$  and  $\upsilon_m=[1/3,1/3,1/3]$ .

Fig. 5.6 illustrates the OP for both equal and optimized power allocation under moderate turbulence conditions for the following three scenarios: Imperfect RF link only ( $\zeta_{RD} \to 1$ ), Imperfect FSO link only ( $\zeta_{SR} \to 1$ ), and imperfect RF & FSO link. The power allocation coefficient are calculated using (5.37) which is ( $\beta, \beta^*$ ) = (0.5, 0.8513) for  $\rho$  = 1,  $P_t/P_{I_{n,r}}$  = [20, 25, 30] dB, ( $\beta, \beta^*$ ) = (0.5, 0.9179) for  $\rho$  = 1,  $P_t/P_{I_{n,r}}$  = [20, 20, 20] dB, ( $\beta, \beta^*$ ) = (0.5, 0.9446) for  $\rho$  = 2,  $P_t/P_{I_{n,r}}$  = [25, 25, 25] dB, and ( $\beta, \beta^*$ ) = (0.5, 0.9615) for  $\rho$  = 2,  $P_t/P_{I_{n,r}}$  = [30, 25, 20] dB. This optimization results in a significant enhancement in the OP performance with improvement 0.6843 dB for ( $\beta, \beta^*$ ) = (0.5, 0.8513), 1.9714 dB for ( $\beta, \beta^*$ ) = (0.5, 0.9179), 0.6787 dB for ( $\beta, \beta^*$ ) = (0.5, 0.9446), and 1.2310 dB for ( $\beta, \beta^*$ ) = (0.5, 0.9615). From the figure it can be observed that there is improvement in the outage performance with power allocation with imperfect RF link only.

In Fig. 5.7, the CDF based scheduling with equal CAR and optimized CAR derived using (5.41) under moderate turbulence conditions are considered for the following three scenarios: Imperfect RF link only ( $\zeta_{RD} \rightarrow 1$ ), Imperfect FSO link only ( $\zeta_{SR} \rightarrow 1$ ), and perfect RF & FSO link. The outage performance with optimum CAR values is compared with the performance obtained using greedy scheduling. It can be seen that

optimizing the CAR substantially enhances OP performance, closely approaching that of greedy scheduling.

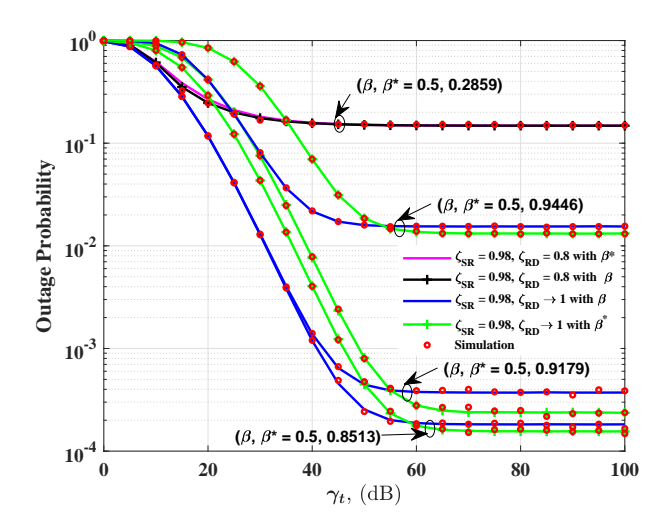


Figure 5.6: OP versus  $\gamma_t$  over equal power and optimized power allocation, considering CDFS based system under moderate turbulence condition fixed at  $\sigma^2_\epsilon=0.5$  and  $\upsilon_m=[1/3,1/3,1/3]$ .

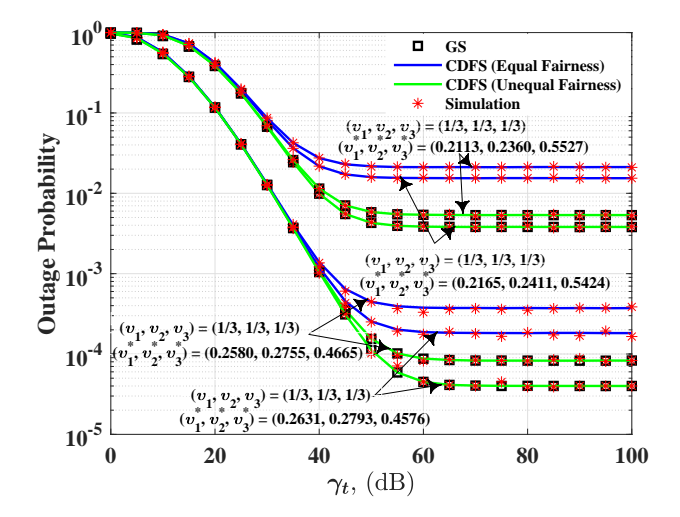


Figure 5.7: OP versus  $\gamma_t$  with equal and optimized channel access ratio for both GS and CDFS based systems under moderate turbulence condition fixed at  $\sigma_\epsilon^2=0.5$  and  $\beta=0.5$ .

# Chapter 6

# Performance Analysis of Dual-hop Multiuser RF-hybrid FSO/RF System

This chapter presents a comprehensive performance analysis of a MU dual-hop RF-hybrid FSO/RF communication system, where the first hop utilizes an RF link employing CDF-based user scheduling scheme. In the second hop, hybrid parallel FSO and RF links are employed, with SC implemented at the destination to enhance link reliability. The key contributions of this chapter are summarized as follows:

- Closed-form expressions for OP and ABER are derived for the proposed system. The RF links are modeled using Nakagami-m fading, while the FSO links are characterized by the  $\mathcal{F}$  distribution with the inclusion of pointing errors. The analysis also incorporates the effects of i.n.i.d CCI and employs CDF-based user selection.
- An asymptotic expression for OP in the high SNR regime is derived to determine the diversity order of the system, offering deeper insights into its performance under ideal conditions.
- Optimal power allocation strategies for both users and relays are formulated under a total power constraint, based on the asymptotic OP expression, to enhance system performance.
- The optimal values of the CAR for users are derived to further improve overall performance, particularly in scenarios with resource-sharing constraints.

# **6.1** System and Channel Model

In Fig. 6.1, a source node (S) with M users transmits data to a destination node (D) via a relay node (R), while contending with interference from N RF interferers at relay. The first-hop consists of an RF system between source and relay, and the second-hop employs a hybrid FSO/RF system from relay to destination.

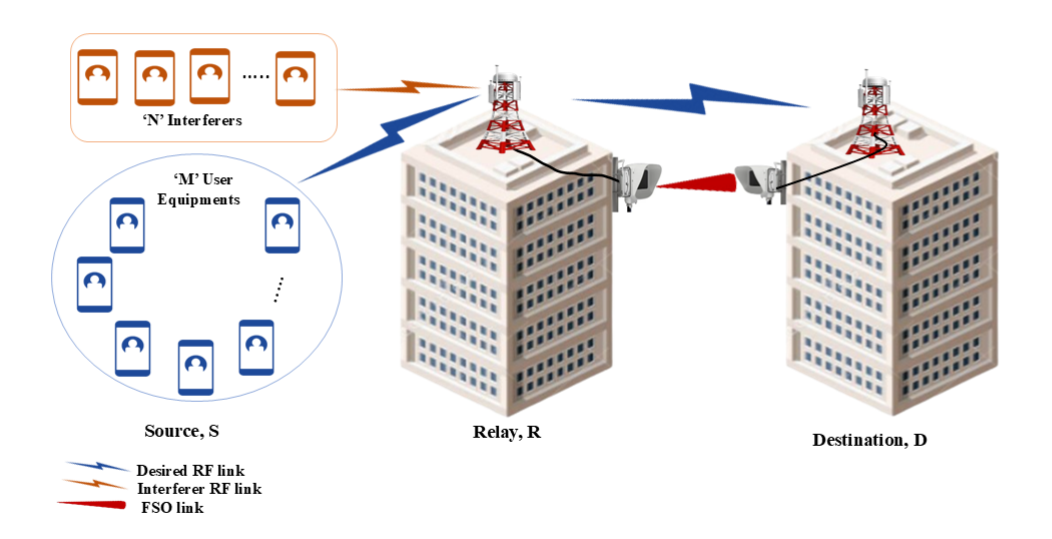


Figure 6.1: Dual-hop MU RF and hybrid FSO/RF system with i.n.i.d CCI.

#### RF system (First-hop)

In the first-hop, mth user at the source transmits the RF signal,  $x_{m,r} (m=1,2...,M)$  to the relay through S-R link. The received signal at the relay, denoted by  $y_{m,r}$  in the presence of CCI is written as:

$$y_{m,r}^{\rm SR} = \sqrt{P_s} h_{m,r} x_{m,r} + \sum_{n=1}^{N} \sqrt{P_{\rm I}} g_{I_{n,r}} x_{I_{n,r}} + n_r^{\rm SR}, \tag{6.1}$$

where,  $P_s$  and  $P_{\rm I}$  are the transmit power of the RF signal at the source and interferer respectively,  $x_{m,r}$  and  $x_{I_{n,r}}$  are the transmitted information of the mth user and nth interferer with unit energy respectively. The channel gain for S-R link and interferer-relay (I-R) link are modeled by Nakagami-m distributions with parameters  $(m_{m,r},\Omega_{m,r})$  for S-R link and  $(m_{I_{n,r}},\Omega_{I_{n,r}})$  for I-R link and  $n_r^{\rm SR} \sim C\mathcal{N}(0,\sigma^2)$ .

The instantaneous signal-to-interference-noise ratio denoted as  $\Gamma^{SR}_{m,r}$  for the S-R link can be written as:

$$\Gamma_{\text{m,r}}^{\text{SR}} = \frac{P_s |h_{m,r}|^2}{\sum_{n=1}^{N} P_{\text{I}} |g_{I_{n,r}}|^2 + \sigma^2},$$

$$\triangleq \frac{X_m}{Z+1},$$
(6.2)

where,  $X_m=\gamma_s|h_{m,r}|^2$ ,  $Z=\sum_{n=1}^N\gamma_I|g_{I_{n,r}}|^2$ ,  $\gamma_s\triangleq\frac{P_s}{\sigma^2}$ ,  $\gamma_I\triangleq\frac{P_1}{\sigma^2}$ .

#### Hybrid FSO/RF system (Second-hop)

The relay employs both FSO and RF transmitters to forward the decoded signal to destination. After demodulation and decoding, the signal is transmitted simultaneously over parallel FSO and RF links. The received signals at destination through R-D FSO and R-D RF links respectively can be expressed as:

$$y_{\rm r,d}^{\rm FSO} = \sqrt{\eta P_r^{\rm FSO}} I_{\rm r,d} x_{\rm r,d} + n_d^{\rm FSO}, \ y_{\rm r,d}^{\rm RF} = \sqrt{P_r^{\rm RF}} h_{\rm r,d} x_{\rm r,d} + n_d^{\rm RF},$$
 (6.3)

 $P_r^{\mathrm{FSO}}$  and  $P_r^{\mathrm{RF}}$  are the transmit power of FSO signal and RF signal at relay,  $x_{\mathrm{r,d}}$  is the transmitted symbol at relay with unit energy. The channel gain,  $I_{\rm r,d}=I_aI_p$  where  $I_a$ is the atmospheric turbulence modeled by  $\mathcal{F}$  distribution and  $I_p$  is the pointing error.  $h_{\rm r,d}$  follows Nakagami-*m* distribution for R-D RF link with parameters  $(m_{\rm r,d},\Omega_{\rm r,d})$ , and assuming  $n_d^{\rm FSO}=n_d^{\rm RF}\sim CN(0,\sigma^2)$ . The instantaneous SNR,  $\Gamma_{\rm r,d}^{\rm FSO}$  for the R-D FSO link and  $\Gamma_{\rm r,d}^{\rm RF}$  for R-D RF link can be

written as:

$$\Gamma_{\rm r,d}^{\rm FSO} = \gamma_r^{\rm FSO} |I_{\rm r,d}|^2, \Gamma_{\rm r,d}^{\rm RF} = \gamma_r^{\rm RF} |h_{\rm r,d}|^2,$$
(6.4)

where,  $\gamma_r^{\rm FSO} \triangleq \frac{\eta P_r^{\rm FSO}}{\sigma^2}$ ,  $\gamma_r^{\rm RF} \triangleq \frac{P_r^{\rm RF}}{\sigma^2}$ . Based on the SC scheme, the instantaneous SNR of the hybrid system at the destination is defined as:

$$\Gamma_{\text{hybrid}}^{\text{RD}} = \max(\Gamma_{\text{r,d}}^{\text{FSO}}, \Gamma_{\text{r,d}}^{\text{RF}}) \tag{6.5}$$

Further, equivalent end-to-end instantaneous SNR, denoted as  $\Gamma_{e2e}$  for DF based relaying system with user scheduling scheme is expressed as:

$$\Gamma_{e2e} = \min(\Gamma_{\text{m*,r}}^{\text{SR}}, \Gamma_{\text{hybrid}}^{\text{RD}}) \tag{6.6}$$

where,  $m^*$  is the scheduled user.

#### 6.1.1 **Channel Model**

#### RF system (First-hop)

The PDF and CDF of the Nakagami-m distribution for integer values of  $m_{\rm m,r}$  for the S-R link are given in [130]:

$$\begin{split} f_{X_m}(x) &= \frac{m_{\rm m,r}^{m_{\rm m,r}} x^{m_{\rm m,r}-1}}{\Gamma(m_{\rm m,r})(\gamma_{\rm s}\Omega_{\rm m,r})^{m_{\rm m,r}}} {\rm exp}\bigg(-\frac{m_{\rm m,r}}{\gamma_{\rm s}\Omega_{\rm m,r}}x\bigg). \\ F_{X_m}(x) &= 1 - \frac{\Gamma(m_{\rm m,r},\frac{m_{\rm m,r}}{\gamma_{\rm s}\Omega_{\rm m,r}}x)}{\Gamma(m_{\rm m,r})}. \end{split} \tag{6.7}$$

According to [131], the approximate PDF of Z can be expressed using the PDF of a single Gamma distributed RV:

$$f_Z(z) = \frac{m_{\rm I}^{m_{\rm I}} z^{m_{\rm I}-1}}{\Gamma(m_{\rm I})(\gamma_{\rm I}\Omega_{\rm I})^{m_{\rm I}}} {\rm exp} \bigg( -\frac{m_{\rm I}}{\gamma_{\rm I}\Omega_{\rm I}} z \bigg), \tag{6.8} \label{eq:fZ}$$

$$\begin{split} &\text{where, } \Omega_{\mathrm{I}} = \sum_{n=1}^{N} \Omega_{I_{n,r}}, m_{\mathrm{I}} = \frac{\Omega_{\mathrm{I}}^{2}}{E(\phi^{2}) - \Omega_{\mathrm{I}}^{2}}, E(\phi^{j}) = \sum_{j_{1}=0}^{j} \sum_{j_{2}=0}^{j_{1}} \sum_{j_{3}=0}^{j_{2}} \dots \sum_{j_{N-1}=0}^{j_{N-2}} \binom{j}{j_{1}} \binom{j_{1}}{j_{2}} \dots \binom{j_{N-2}}{j_{N-1}} \\ &\times E[|g_{I_{1,r}}|^{2(j-j_{1})}] E[|g_{I_{2,r}}|^{2(j_{1}-j_{2})}] \dots E[|g_{I_{N,r}}|^{2(j_{N-1})}], \\ &E[|g_{I_{n,r}}|^{j}] = \frac{\Gamma(m_{I_{n,r}} + \frac{j}{2})}{\Gamma m_{I_{n,r}}} \left(\frac{\Omega_{I_{n,r}}}{m_{I_{n,r}}}\right)^{\frac{j}{2}}. \end{split}$$

The CDF of  $\Gamma^{\rm SR}_{\rm m,r}$  under i.n.i.d CCI with fixed power can be calculated by substituting (6.7) and (6.8) into  $\int_0^\infty F_{X_m}(y(z+1))f_Z(z)dz$  after using [112, Eq. (8.352.2)], and performing the integration using [112, Eq. (3.351.3)], the CDF can be obtained as:

$$\begin{split} F_{\Gamma^{\text{SR}}_{\text{m,r}}}(y) &= 1 - \sum_{l=0}^{m_{\text{m,r}}-1} \sum_{k=0}^{l} \binom{l}{k} \frac{\Gamma(k+m_{\text{I}})}{l! \Gamma(m_{\text{I}})} \left(\frac{\gamma_{\text{I}} \Omega_{\text{I}}}{m_{\text{I}}}\right)^{k} \left(\frac{m_{\text{m,r}}}{\gamma_{\text{s}} \Omega_{\text{m,r}}} y\right)^{l} e^{-\frac{m_{\text{m,r}}}{\gamma_{\text{s}} \Omega_{\text{m,r}}} y} \\ &\times \frac{1}{\left(1 + \frac{m_{\text{m,r}} \gamma_{\text{I}} \Omega_{\text{I}}}{m_{\text{I}} \gamma_{\text{s}} \Omega_{\text{m,r}}} y\right)^{k+m_{\text{I}}}}. \end{split} \tag{6.9}$$

#### Hybrid FSO/RF system (Second-hop)

The PDF and CDF of  $\mathcal{F}$  distribution and incorporating the effect of pointing error for the R-D FSO link are provided in [64]:

$$\begin{split} f_{\Gamma^{\text{FSO}}_{\text{r,d}}}(x) &= \frac{\omega^2 x^{-1}}{2\Gamma(a)\Gamma(b)} G_{2,2}^{2,1} \left( \frac{a\omega^2}{(b-1)(1+\omega^2)} \sqrt{\frac{x}{\bar{\gamma}_{\text{r,d}}^{\text{FSO}}}} \right|^{1-b,\,1+\omega^2} a, \omega^2 \right), \\ F_{\Gamma^{\text{FSO}}_{\text{r,d}}}(x) &= \frac{\omega^2}{\Gamma(a)\Gamma(b)} G_{3,3}^{2,2} \left( \frac{a\omega^2}{(b-1)(1+\omega^2)} \sqrt{\frac{x}{\bar{\gamma}_{\text{r,d}}^{\text{FSO}}}} \right|^{1-b,\,1,\,1+\omega^2} a, \omega^2, 0 \right), \end{split} \tag{6.10}$$

where,  $\bar{\gamma}_{\mathrm{r,d}}^{\mathrm{FSO}} = \gamma_r^{\mathrm{FSO}} \mathbb{E}^2 |I_{\mathrm{r,d}}|$ , nth moment denoted by  $\mathbb{E}[|I_{\mathrm{r,d}}|^n] = \left(\frac{(b-1)A_0}{a}\right)^n \frac{\omega^2 \Gamma(a+n) \Gamma(b-n)}{(\omega^2+n) \Gamma(a) \Gamma(b)}$ ,  $\omega = \omega_{z_{eq}}/2\sigma_s$ , where  $A_0$  represents the fraction of collected optical power,  $\omega_{z_{eq}}$  denotes the equivalent beam radius at the receiver,  $\sigma_s$  is the standard deviation of pointing error displacement at the receiver. The parameters a and b correspond to the fading coefficients associated with small-scale and larg-scale turbulent eddies respectively. When  $\omega \to \infty$ , effect of pointing error becomes negligible.

The PDF of the Nakagami-*m* distribution for the R-D RF link is given in [130]:

$$\begin{split} f_{\Gamma_{\rm r,d}^{\rm RF}}(x) &= \frac{m_{\rm r,d}^{m_{\rm r,d}} x^{m_{\rm r,d}-1}}{\Gamma(m_{\rm r,d}) (\gamma_r^{\rm RF} \Omega_{\rm r,d})^{m_{\rm m,r}}} {\rm exp} \bigg( -\frac{m_{\rm r,d}}{\gamma_r^{\rm RF} \Omega_{\rm r,d}} x \bigg). \\ F_{\Gamma_{r,d}^{\rm RF}}(x) &= 1 - \frac{\Gamma(m_{\rm r,d}, \frac{m_{\rm r,d}}{\gamma_r^{\rm RF} \Omega_{\rm r,d}} x)}{\Gamma(m_{\rm r,d})}. \end{split} \tag{6.11}$$

The CDF of hybrid FSO/RF system, denoted as  $F_{\Gamma^{\rm RD}_{\rm hybrid}}(x)$  for SC scheme can be written as:

$$F_{\Gamma_{\text{hybrid}}^{\text{RD}}}(x) = F_{\Gamma_{\text{r,d}}^{\text{FSO}}}(x)F_{\Gamma_{\text{r,d}}^{\text{RF}}}(x). \tag{6.12}$$

The mathematical expression for selecting the mth best user for GS-based scheme can be given as:

$$m^* = \underset{m \in 1, 2, \dots, M}{\arg \max} \left( \frac{X_m}{Z+1} \right). \tag{6.13}$$

The mathematical expression for selecting the mth user for CDFS-based scheme is as follows:

$$m^* = \underset{m \in 1, 2, \dots, M}{\arg \max} \left( F_{\Gamma_{m,r}^{SR}}(x) \right)^{\frac{1}{v_m}}. \tag{6.14}$$

# **6.2** Performance Metrics

This section presents the analytical derivations of OP, and ABER for the considered system employing a CDF-based scheduling scheme.

# 6.2.1 Outage Probability

A communication system experiences an outage when the instantaneous SNR,  $\Gamma_{e2e}$  falls below the acceptable threshold,  $\gamma_{\rm th}$ . It is defined as:

$$\begin{split} P_{\Gamma_{e2e}}(\gamma_{\text{th}}) &= \Pr(\Gamma_{e2e} < \gamma_{\text{th}}) &= \Pr\Big(\min(\Gamma_{m^*,r}^{\text{SR}}, \Gamma_{\text{hybrid}}^{\text{RD}}) < \gamma_{\text{th}}\Big), \\ &= F_{\Gamma_{m^*,r}^{\text{SR}}}(\gamma_{\text{th}}) + F_{\Gamma_{\text{hybrid}}^{\text{RD}}}(\gamma_{\text{th}}) - F_{\Gamma_{m^*,r}^{\text{SR}}}(\gamma_{\text{th}}) F_{\Gamma_{\text{hybrid}}^{\text{RD}}}(\gamma_{\text{th}}). \end{split} \tag{6.15}$$

where,  $\gamma_{th}=2^{2\rho}-1,~\rho$  denotes the target rate.  $F_{\Gamma^{\rm SR}_{m^*,r}}(\gamma_{\rm th})$  denotes the CDF of the first-hop and  $F_{\Gamma^{\rm RD}_{\rm hybrid}}(\gamma_{\rm th})$  represents the CDF of the second-hop.

For the CDF-based scheduling scheme, the CDF of first-hop can be expressed using (6.14) as:

$$F_{\Gamma_{m^*,r}^{\text{CDFS}}}^{\text{CDFS}}(\gamma_{th}) = \Pr\Bigg( \Big(F_{\Gamma_{\text{m,r}}^{\text{SR}}}(x)\Big)^{\frac{1}{\upsilon_k}} < \Big(F_{\Gamma_{\text{m,r}}^{\text{SR}}}(x)\Big)^{\frac{1}{\upsilon_m}} \forall \ k\epsilon 1, 2...M \bigcap_{k \neq m} \Gamma_{\text{m,r}}^{\text{SR}} < \gamma_{th} \Bigg). \tag{6.16}$$

The closed-form expression of OP employing CDF-based scheduling scheme is obtained as:

$$\begin{split} P_{\Gamma_{e2e}}^{\text{CDFS}}(\gamma_{th}) &= \sum_{m=1}^{M} \upsilon_{m} \bigg(1 - \sum_{l=0}^{m_{\text{m,r}}-1} \sum_{k=0}^{l} \binom{l}{k} \frac{\Gamma(k+m_{\text{I}})}{l! \Gamma(m_{\text{I}})} \bigg(\frac{\gamma_{\text{I}} \Omega_{\text{I}}}{m_{\text{I}}}\bigg)^{k} \bigg(\frac{m_{\text{m,r}}}{\gamma_{s} \Omega_{\text{m,r}}} \gamma_{th}\bigg)^{l} \\ &\times e^{-\frac{m_{\text{m,r}}}{\gamma_{s} \Omega_{\text{m,r}}} \gamma_{th}} \frac{1}{\bigg(1 + \frac{m_{\text{m,r}} \gamma_{\text{I}} \Omega_{\text{I}}}{m_{\text{I}} \gamma_{s} \Omega_{\text{m,r}}} \gamma_{th}\bigg)^{k+m_{\text{I}}}\bigg)^{\frac{1}{\upsilon_{m}}} \bigg\{1 - \frac{\omega^{2}}{\Gamma(a) \Gamma(b)} \\ &\times G_{3,3}^{2,2} \left(\frac{a\omega^{2}}{(b-1)(1+\omega^{2})} \sqrt{\frac{\gamma_{th}}{\bar{\gamma}_{\text{r,d}}^{\text{FSO}}}} \bigg|^{1-b,1,1+\omega^{2}} \right) \bigg(1 - \frac{\Gamma(m_{\text{r,d}}, \frac{m_{\text{r,d}}}{\gamma_{\text{r}}^{\text{RF}}\Omega_{\text{r,d}}} x)}{\Gamma(m_{\text{r,d}})}\bigg)\bigg\} + \\ &\frac{\omega^{2}}{\Gamma(a)\Gamma(b)} \bigg(1 - \frac{\Gamma(m_{\text{r,d}}, \frac{m_{\text{r,d}}}{\gamma_{\text{r}}^{\text{RF}}\Omega_{\text{r,d}}} x)}{\Gamma(m_{\text{r,d}})}\bigg)G_{3,3}^{2,2} \left(\frac{a\omega^{2}}{(b-1)(1+\omega^{2})} \sqrt{\frac{\gamma_{th}}{\bar{\gamma}_{\text{r,d}}^{\text{FSO}}}} \bigg|^{1-b,1,1+\omega^{2}} \right). \end{split} \tag{6.17}$$

The proof of (6.17) is presented in Appendix V.

OP is employed to assess the system's performance and expressed as a function of  $\gamma_t$ , where  $\gamma_t = \frac{P_t}{\sigma^2}$ . Total power  $P_t = P_s + P_r$ , assuming  $\gamma_s = \beta \gamma_t$ ,  $\gamma_r^{\rm FSO} = \gamma_r^{\rm RF} = \gamma_r = (1-\beta)\gamma_t$ . Let  $\beta$  denotes the fraction of total power allocated to the user and relay.

# **6.2.2** Asymptotic Outage Probability

The closed-form OP expression employing CDF-based scheduling scheme offers restricted insight into parameter influence on performance. Therefore, to gain a deeper understanding of how different parameters affect system performance, the OP expression provided in (6.15) at high SNR, i.e.,  $\gamma_t$  approaches infinity, can be simplified as follows:

$$P^{\infty}_{\Gamma_{e2e}}(\gamma_{\rm th}) \simeq F^{\infty}_{\Gamma^{\rm SR}_{m*,r}}(\gamma_{\rm th}) + F^{\infty}_{\Gamma^{\rm RD}_{\rm hybrid}}(\gamma_{\rm th}), \tag{6.18}$$
 where,  $F^{\infty}_{\Gamma^{\rm RD}_{\rm hybrid}}(\gamma_{\rm th}) \simeq F^{\infty}_{\Gamma^{\rm FSO}_{\rm r,d}}(\gamma_{\rm th}) F^{\infty}_{\Gamma^{\rm RF}_{\rm r,d}}(\gamma_{\rm th}).$ 

#### RF system (First-hop)

At high value of SNR,  $\gamma_t \to \infty$ ,  $\frac{\Gamma(m_{\rm m,r},\frac{m_{\rm m,r}}{\beta\gamma_t\Omega_{\rm m,r}}x)}{\Gamma(m_{\rm m,r})} \simeq 1 - \frac{\left(\frac{m_{\rm m,r}}{\beta\gamma_t\Omega_{\rm m,r}}x\right)^{m_{\rm m,r}}}{\Gamma(m_{\rm m,r}+1)}$  in (6.7) and substitute into  $\int_0^\infty F_{X_m}(y(z+1))f_Z(z)dz$ . With the utilization of [112, Eq. (3.351.3)], the asymptotic CDF expression for the first-hop becomes:

$$F_{\Gamma_{\rm m,r}}^{\infty}(x) \simeq \frac{1}{\Gamma m_{\rm I} \Gamma(m_{\rm m,r}+1)} \left(\frac{m_{\rm m,r}x}{\beta \gamma_t \Omega_{\rm m,r}}\right)^{m_{\rm m,r}} \sum_{k=0}^{m_{\rm m,r}} {m_{\rm m,r} \choose k} \Gamma(k+m_{\rm I}) \left(\frac{\gamma_{\rm I}\Omega_{\rm I}}{m_{\rm I}}\right)^k. \tag{6.19}$$

#### **Hybrid FSO/RF system (Second-hop)**

By utilizing the expression [113, Eq (07.34.06.0006.01)] in (6.10), the asymptotic CDF expression for the second-hop FSO link can be written as:

$$\begin{split} F^{\infty}_{\Gamma^{\mathrm{FSO}}_{\mathrm{r,d}}}(x) &\simeq \frac{\omega^2}{\Gamma(a)\Gamma(b)} \sum_{j=1}^2 \Bigg\{ \frac{\prod_{\substack{i=1\\i\neq j}}^2 \Gamma(\Re_{2i}-\Re_{2j}) \prod_{\substack{i=1\\i\neq j}}^2 \Gamma(1-\Re_{1i}+\Re_{2j})}{\Gamma(\Re_{13}-\Re_{2j})\Gamma(1-\Re_{23}+\Re_{2j})} \\ &\qquad \times \Bigg( \frac{a\omega^2}{(b-1)(1+\omega^2)} \sqrt{\frac{x}{\bar{\gamma}^{\mathrm{FSO}}_{\mathrm{r,d}}}} \Bigg)^{\Re_{2j}} \Bigg\}, \quad (6.20) \end{split}$$

where,  $\mathfrak{R}_1=[\mathfrak{R}_{11},\mathfrak{R}_{12},\mathfrak{R}_{13}]=[1-b,1,1+\omega^2]; \mathfrak{R}_2=[\mathfrak{R}_{21},\mathfrak{R}_{22},\mathfrak{R}_{23}]=[a,\omega^2,0].$  With the aid of identity,  $\frac{\Gamma(m_{\mathrm{r,d}},\frac{m_{\mathrm{r,d}}}{(1-\beta)\gamma_t\Omega_{\mathrm{r,d}}}x)}{\Gamma(m_{\mathrm{r,d}})}\simeq 1-\frac{\left(\frac{m_{\mathrm{r,d}}}{(1-\beta)\gamma_t\Omega_{\mathrm{r,d}}}x\right)^{m_{\mathrm{r,d}}}}{\Gamma(m_{\mathrm{r,d}}+1)}$  in (6.11), the asymptotic CDF expression for the second-hop RF link can be calculated as follows:

$$F_{\Gamma_{\mathrm{r,d}}^{\mathrm{RF}}}^{\infty}(x) \simeq \frac{1}{\Gamma(m_{\mathrm{r,d}}+1)} \left(\frac{m_{\mathrm{r,d}}}{(1-\beta)\gamma_{t}\Omega_{\mathrm{r,d}}}x\right)^{m_{\mathrm{r,d}}}$$
(6.21)

To calculate the asymptotic OP expression for CDF-based scheduling scheme, substitute (6.19), (6.20) and (6.21) into (6.18), the asymptotic expression can be expressed as:

$$\begin{split} F_{\Gamma_{e2e}}^{\infty,\text{CDFS}}(\gamma_{th}) &\simeq \sum_{m=1}^{M} \upsilon_{m} \bigg\{ \frac{1}{\Gamma m_{\text{I}} \, \Gamma(m_{\text{m,r}}+1)} \bigg( \frac{m_{\text{m,r}} \gamma_{th}}{\beta \gamma_{t} \Omega_{\text{m,r}}} \bigg)^{m_{\text{m,r}}} \sum_{k=0}^{m_{\text{m,r}}} \bigg( \frac{m_{\text{m,r}}}{k} \bigg) \Gamma(k+m_{\text{I}}) \\ &\times \bigg( \frac{\gamma_{\text{I}} \Omega_{\text{I}}}{m_{\text{I}}} \bigg)^{k} \bigg\}^{\frac{1}{\upsilon_{m}}} + \frac{\omega^{2}}{\Gamma(a)\Gamma(b)} \frac{1}{\Gamma(m_{\text{r,d}}+1)} \bigg( \frac{m_{\text{r,d}}}{(1-\beta)\gamma_{t} \Omega_{\text{r,d}}} \gamma_{th} \bigg)^{m_{\text{r,d}}} \\ &\times \sum_{j=1}^{2} \bigg\{ \frac{\prod_{\substack{i=1\\i\neq j}}^{2} \Gamma(\mathfrak{R}_{2i}-\mathfrak{R}_{2j}) \prod_{\substack{i=1\\i\neq j}}^{2} \Gamma(1-\mathfrak{R}_{1i}+\mathfrak{R}_{2j})}{\Gamma(\mathfrak{R}_{13}-\mathfrak{R}_{2j})\Gamma(1-\mathfrak{R}_{23}+\mathfrak{R}_{2j})} \bigg( \frac{a\omega^{2}}{(b-1)(1+\omega^{2})} \sqrt{\frac{\gamma_{th}}{\bar{\gamma}_{\text{r,d}}^{\text{FSO}}}} \bigg)^{\mathfrak{R}_{2j}} \bigg\}. \end{split}$$

The diversity order,  $G_d$  is defined as  $-\lim_{\gamma_t \to \infty} \frac{\log(F_{\Gamma_{e2e}}(\gamma_t))}{\log(\gamma_t)}$  which represents the slope of the curve. From (6.22), it is evident that this system model attains a  $G_d = \min\left(\min(\frac{m_{1r}}{v_1},\frac{m_{2r}}{v_2}..\frac{m_{Mr}}{v_M}),\min(\frac{a}{2},\frac{\omega^2}{2}) + m_{r,d}\right)$  for  $P_I = 0$  dB. When  $m_{m,r} = m_{r,d} = m_s, v_1 = v_2... = v_M = v$ , diversity order simplifies to  $G_d = \min\left(m_s M,\min(\frac{a}{2},\frac{\omega^2}{2}) + m_s\right)$ , even for varying interferer power levels. This assumption does not alter the system asymptotic behavior.

When  $\Omega_{I_{1,r}}=\Omega_{I_{2,r}}...=\Omega_{I_{N,r}}=\Omega$  and  $m_{I_{1,r}}=m_{I_{2,r}}...=m_{I_{N,r}}=m,m_{\rm I}$  becomes equal to  $Nm,\,\Omega_{\rm I}=N\Omega.$  From (6.22), the asymptotic OP expression for CDF based scheduling becomes:

$$\begin{split} F_{\Gamma_{e2e}}^{\infty,\text{CDFS}}(\gamma_{th}) &\simeq \sum_{m=1}^{M} \upsilon_{m} \bigg\{ \frac{1}{\Gamma(Nm)} \frac{1}{\Gamma(m_{\text{m,r}}+1)} \bigg( \frac{m_{\text{m,r}} \gamma_{th}}{\beta \gamma_{t} \Omega_{\text{m,r}}} \bigg)^{m_{\text{m,r}}} \sum_{k=0}^{m_{\text{m,r}}} \bigg( \frac{m_{\text{m,r}}}{k} \bigg) \Gamma(k+Nm) \\ &\times \bigg( \frac{\gamma_{\text{I}} \Omega}{m} \bigg)^{k} \bigg\}^{\frac{1}{\upsilon_{m}}} + \frac{\omega^{2}}{\Gamma(a)\Gamma(b)} \frac{1}{\Gamma(m_{\text{r,d}}+1)} \bigg( \frac{m_{\text{r,d}}}{(1-\beta)\gamma_{t} \Omega_{\text{r,d}}} \gamma_{th} \bigg)^{m_{\text{r,d}}} \\ &\times \sum_{j=1}^{2} \bigg\{ \frac{\prod_{\substack{i=1\\i\neq j}}^{2} \Gamma(\Re_{2i} - \Re_{2j}) \prod_{\substack{i=1\\i\neq j}}^{2} \Gamma(1-\Re_{1i} + \Re_{2j})}{\Gamma(\Re_{13} - \Re_{2j})\Gamma(1-\Re_{23} + \Re_{2j})} \times \bigg( \frac{a\omega^{2}}{(b-1)(1+\omega^{2})} \sqrt{\frac{\gamma_{th}}{\bar{\gamma}_{\text{r,d}}^{\text{FSO}}}} \bigg)^{\Re_{2j}} \bigg\}. \end{split} \tag{6.23}$$

## **6.2.3** Average Bit Error Rate

The ABER of the system with digital binary modulation schemes is given as [117]:

$$\begin{split} \bar{P}_{be} &= \underbrace{\frac{g^f}{2\Gamma(f)} \int_0^\infty \gamma^{f-1} e^{-g\gamma} F_{\Gamma^{\text{SR}}_{m^*,r}}(\gamma)}_{\bar{P}_{be_1}} + \underbrace{\frac{g^f}{2\Gamma(f)} \int_0^\infty \gamma^{f-1} e^{-g\gamma} F_{\Gamma^{\text{RD}}_{\text{hybrid}}}(\gamma)}_{\bar{P}_{be_2}} \\ &- \underbrace{\frac{g^f}{2\Gamma(f)} \int_0^\infty \gamma^{f-1} e^{-g\gamma} F_{\Gamma^{\text{SR}}_{m^*,r}}(\gamma) F_{\Gamma^{\text{FSO}}_{\text{r,d}}}(\gamma) \, d\gamma}_{\bar{P}_{be_3}} \\ &+ \underbrace{\frac{g^f}{2\Gamma(f)} \int_0^\infty \gamma^{f-1} e^{-g\gamma} F_{\Gamma^{\text{SR}}_{m^*,r}}(\gamma) F_{\Gamma^{\text{FSO}}_{\text{r,d}}}(\gamma) \frac{\Gamma\left(m_{\text{r,d}}, \frac{m_{\text{r,d}}}{\gamma^{\text{RF}}_r \Omega_{\text{r,d}}} \gamma\right)}{\Gamma(m_{\text{r,d}})} \, d\gamma}_{\bar{P}_{be_4}} \end{split} \tag{6.24}$$

where, f and g are the parameters that depend on chosen modulation scheme. Using multinomial expansion, (V.2) becomes:

$$F_{\Gamma_{m^*,r}^{SR}}(\gamma) = \sum_{m=1}^{M} \upsilon_m \left( 1 + \sum_{l=0}^{m_{m,r}-1} \sum_{k=0}^{l} C_{m,l,k} A_{m,l,k}(\gamma) \right)^{\frac{1}{\upsilon_m}}$$

$$= \sum_{m=1}^{M} \upsilon_m \left( \sum_{\substack{i_0 + \sum\limits_{l=0}^{m_{m,r}-1} \sum\limits_{l=0}^{l} i_{lk} = \frac{1}{\upsilon_m}} \frac{\left(\frac{1}{\upsilon_m}\right)!}{\sum_{l=0}^{m_{m,r}-1} \prod\limits_{l=0}^{l} i_{lk}!} \prod_{l=0}^{m_{m,r}-1} \prod\limits_{k=0}^{l} \left( C_{m,l,k} A_{m,l,k}(\gamma) \right)^{i_{lk}} \right).$$

$$(6.25)$$

$$\begin{split} \text{where, } A_{m,l,k}(\gamma) &= \gamma^l e^{-\frac{m_{\text{m,r}}}{\gamma_s \Omega_{\text{m,r}}} \gamma} \frac{1}{\left(1 + \frac{m_{\text{m,r}} \gamma_l \Omega_l}{m_l \gamma_s \Omega_{\text{m,r}}} \gamma\right)^{k + m_l}}, \\ C_{m,l,k} &= -\binom{l}{k} \frac{\Gamma(k + m_l)}{l! \Gamma(m_l)} \left(\frac{\gamma_l \Omega_l}{m_l}\right)^k \left(\frac{m_{\text{m,r}}}{\gamma_s \Omega_{\text{m,r}}}\right)^l. \end{split}$$

By substituting (6.25) into (6.24) and with the aid of identity [132, Eq. (2.3.6.9)], the term  $\bar{P}_{be_1}$  is obtained as:

$$\begin{split} \bar{P}_{be_{1}} &= \frac{g^{f}}{2\Gamma(f)} \sum_{m=1}^{M} \upsilon_{m} \left( \sum_{i_{0} + \sum\limits_{l=0}^{m_{m,r}-1} \sum\limits_{k=0}^{l} i_{lk} = \frac{1}{\upsilon_{m}}} \frac{\left(\frac{1}{\upsilon_{m}}\right)!}{i_{0}!} \prod_{l=0}^{m_{m,r}-1} \prod_{l=0}^{l} i_{lk}! \right. \\ &\times C_{m,l,k}^{i_{lk}} \frac{\Gamma(f + li_{lk})}{\left(\frac{m_{\text{m,r}} \gamma_{\text{l}} \Omega_{\text{l}}}{m_{\text{l}} \gamma_{s} \Omega_{\text{m,r}}}\right)^{f + li_{lk}}} \Psi\left(f + li_{lk}, f + li_{lk} + 1 - (k + m_{\text{I}})i_{lk}; \frac{(g + \frac{m_{\text{m,r}} i_{lk}}{\gamma_{s} \Omega_{\text{m,r}}})}{\frac{m_{\text{m,r}} \gamma_{\text{l}} \Omega_{\text{l}}}{m_{\text{l}} \gamma_{s} \Omega_{\text{m,r}}}}\right) \right). \end{split}$$

$$(6.26)$$

where,  $\Psi$  denotes the Tricomi confluent hypergeometric function. Further, substitute (V.3) in (6.24) and with the utilization of identities [112, Eq. (8.352.2)] and [113, Eq. (07.34.21.0088.01)], the term  $\bar{P}_{be_2}$  is obtained as:

$$\begin{split} \bar{P}_{be_2} &= \frac{2^{a+b-2}\omega^2}{4\pi\Gamma(f)\Gamma(a)\Gamma(b)} \\ &\times G_{7,6}^{4,5} \left( \frac{a^2\omega^4}{g(b-1)^2(1+\omega^2)^2\bar{\gamma}_{\mathrm{r,d}}^{\mathrm{FSO}}} \middle| 1 - f, \frac{1-b}{2}, \frac{2-b}{2}, \frac{1}{2}, 1, \frac{1+\omega^2}{2}, \frac{2+\omega^2}{2} \right) \\ &- \frac{2^{a+b-2}g^f\omega^2}{4\pi\Gamma(f)\Gamma(a)\Gamma(b)} \sum_{z=0}^{m_{r,d}-1} \frac{1}{z!} \left( \frac{m_{r,d}}{\gamma_r^{\mathrm{RF}}\Omega_{r,d}} \right)^z \left( g + \frac{m_{r,d}}{\gamma_r^{\mathrm{RF}}\Omega_{r,d}} \right)^{-(f+z)} \\ &\times G_{7,6}^{4,5} \left( \frac{a^2\omega^4}{\left(g + \frac{m_{r,d}}{\gamma_r^{\mathrm{RF}}\Omega_{r,d}}\right)(b-1)^2(1+\omega^2)^2\bar{\gamma}_{\mathrm{r,d}}^{\mathrm{FSO}}} \middle| 1 - (f+z), \frac{1-b}{2}, \frac{2-b}{2}, \frac{1}{2}, 1, \frac{1+\omega^2}{2}, \frac{2+\omega^2}{2} \right) \right. \end{split} \tag{6.27}$$

By substituting (6.25) and (V.3) into the integral expression for  $\bar{P}_{be_3}$  and applying the identity as given by [128, Eq. (8.4.2.5)], followed by the expansion of the MeijerG-function as given in [113, Eq. 07.34.02.0001.01], the integral is evaluated using [112, Eq. (3.381.4)]. Finally, by expressing the equation in terms of bivariate Fox H-function as defined in [133, Eq. (1.1)], the closed-form expression for term  $\bar{P}_{be_3}$  is derived as follows:

$$\bar{P}_{be_{3}} = \frac{g^{f}\omega^{2}}{2\Gamma(f)\Gamma(a)\Gamma(b)} \sum_{m=1}^{M} v_{m} \sum_{\substack{i_{0} + \sum\limits_{l=0}^{m_{m,r}-1} \sum\limits_{l=0}^{l} i_{lk} = \frac{1}{v_{m}}}} \frac{\left(\frac{1}{v_{m}}\right)!}{i_{0}!} \prod_{l=0}^{m_{m,r}-1} \prod\limits_{k=0}^{l} i_{lk}!} \sum_{l=0}^{m_{m,r}-1} \sum_{k=0}^{l} i_{lk}! \sum_{l=0}^{l} \frac{C_{m,l,k}^{i_{lk}}}{\xi_{1_{m,r}}^{f+li_{lk}+1}\Gamma\left[(k+m_{\text{I}}) i_{lk}\right]} H_{1,0:1,1;3,3}^{0,1:1,1;2,2} \left(\frac{\frac{m_{m,r}\gamma_{\text{I}}\Omega_{\text{I}}}{m_{\text{I}}\gamma_{s}} \bigcap_{m,r}\xi_{1_{m,r}}}{\frac{a\omega^{2}}{(b-1)(1+\omega^{2})\sqrt{\bar{\gamma}_{r,d}^{\text{FSO}}}\xi_{1_{m,r}}}} \right| p_{1} : p_{2}; p_{3} - : p_{4}; p_{5}$$

$$(6.28)$$

where, 
$$p_1 = \left\{ (-f - li_{lk}); 1, \frac{1}{2} \right\}, p_2 = \left\{ (1 - (k + m_{\rm I})i_{lk}, 1) \right\}, \\ p_3 = \left\{ (1 - b, 1), (1, 1), (1 + \omega^2) \right\}, p_4 = (0, 1), p_5 = \left\{ (a, 1), (\omega^2, 1), (0, 1) \right\}, \\ \xi_{1m,r} = (g + \frac{m_{\rm m.r}}{\gamma_s \Omega_{\rm m.r}} i_{lk}).$$

Similar to  $\bar{P}_{be_3}$ , the term  $\bar{P}_{be_4}$  is derived by substituting (6.25) and (V.3) into (6.24) and apply the identities [128, Eq. (8.4.2.5)], [112, Eq.(3.381.4)] and [133, Eq. (1.1)], the closed-form expression for  $\bar{P}_{be_4}$  is obtained as:

$$\begin{split} \bar{P}_{be_4} = & \frac{g^f \omega^2}{2\Gamma(f)\Gamma(a)\Gamma(b)} \sum_{m=1}^{M} v_m \sum_{z=0}^{m_{r,d}-1} \frac{1}{z!} \left( \frac{m_{r,d}}{\gamma_r^{\text{RF}}\Omega_{r,d}} \right)^z \\ \times & \sum_{i_0 + \sum\limits_{l=0}^{m_{m,r}-1} \sum\limits_{k=0}^{l} i_{lk} = \frac{1}{v_m}} \frac{\left(\frac{1}{v_m}\right)!}{i_0!} \prod_{l=0}^{m_{m,r}-1} \prod\limits_{k=0}^{l} i_{lk}!} \sum_{l=0}^{m_{m,r}-1} \sum_{k=0}^{l} \frac{C_{m,l,k}^{i_{lk}}}{\xi_{2_{m,r}}^{f+z+li_{lk}+1}\Gamma[(k+m_{\text{I}})i_{lk}]} \\ \times & H_{1,0:1,1;3,3}^{0,1:1,1;2,2} \left( \frac{m_{m,r}\gamma_{\text{I}}\Omega_{\text{I}}}{m_{\text{I}}\gamma_s\Omega_{m,r}\xi_{2_{m,r}}} \right| p_6:p_2:p_3 \\ -:p_4:p_5 \right). \quad (6.29) \end{split}$$

where,  $p_6 = \{(-f-z-li_{lk}); 1, \frac{1}{2}\}, \xi_{2m,r} = (g + \frac{m_{\rm r,d}}{\gamma_r^{\rm RF}\Omega_{r,d}} + \frac{m_{\rm m,r}}{\gamma_s\Omega_{\rm m,r}}i_{lk}).$  By substituting (6.26), (6.27), (6.28), and (6.29) into (6.24), the closed-form expression for ABER is obtained.

# 6.3 Optimum Performance Analysis

This section presents an optimal performance analysis by determining the best CAR values and efficiently allocating transmit power between the source and relay.

## **6.3.1** Optimal CAR Assignments

To minimize the OP of the considered system by optimizing the CAR value, the objective function can be formulated as follows:

$$(v_1^*, v_2^*, .., v_M^*) = \underset{(v_1, v_2, ..., v_M)}{\arg \min} P_{\Gamma_{e2e}}^{\infty, \text{CDFS}}(\gamma_{th}),$$

$$\text{subject to } \sum_{m=1}^M v_m = 1.$$

$$(6.30)$$

To solve the above objective function, the Lagrangian multipliers method is employed to determine the optimal CAR for the users as follows:

$$F_{\Gamma_{e2e}}^{\infty,\text{CDFS}}(\upsilon_{1},\upsilon_{2},..,\upsilon_{M},\lambda) = \sum_{m=1}^{M} \upsilon_{m} \left(Z_{\text{m,r}}\right)^{\frac{1}{\upsilon_{m}}} + Z_{\text{r,d}} + \lambda \left(\sum_{m=1}^{M} \upsilon_{m} - 1\right). \quad (6.31)$$

where, 
$$Z_{\rm m,r} = \frac{1}{\Gamma m_{\rm I}} \frac{1}{\Gamma(m_{\rm m,r}+1)} \left(\frac{m_{\rm m,r}\gamma_{th}}{\beta\gamma_t\Omega_{\rm m,r}}\right)^{m_{\rm m,r}} \sum_{k=0}^{m_{\rm m,r}} {m_{\rm m,r} \choose k} \Gamma(k+m_{\rm I}) \left(\frac{\gamma_{\rm I}\Omega_{\rm I}}{m_{\rm I}}\right)^k, \text{ and }$$
 
$$Z_{\rm r,d} = \frac{\omega^2}{\Gamma(a)\Gamma(b)} \frac{1}{\Gamma(m_{\rm r,d}+1)} \left(\frac{m_{\rm r,d}}{(1-\beta)\gamma_t\Omega_{\rm r,d}}\gamma_{th}\right)^{m_{\rm r,d}} \sum_{m_{\rm r,d}} {m_{\rm r,d} \choose k} \Gamma(k+m_{\rm I}) \left(\frac{\gamma_{\rm I}\Omega_{\rm I}}{m_{\rm I}}\right)^k, \text{ and }$$
 
$$\sum_{j=1}^2 \left\{ \frac{\prod_{i=1}^2 \Gamma(\Re_{2i}-\Re_{2j}) \prod_{i=1}^2 \Gamma(1-\Re_{1i}+\Re_{2j})}{\Gamma(\Re_{13}-\Re_{2j})\Gamma(1-\Re_{23}+\Re_{2j})} \left(\frac{a\omega^2}{(b-1)(1+\omega^2)} \sqrt{\frac{\gamma_{th}}{\bar{\gamma}_{\rm r,d}^{\rm FSO}}}\right)^{\Re_{2j}} \right\}.$$

The Hessian Matrix for  $F^{\infty, \text{CDFS}}_{\Gamma_{e2e}}(v_1, v_2, .., v_M)$  is given by

$$\nabla^{2}F(v_{1},v_{2},..,v_{M}) = \begin{bmatrix} \frac{(\ln Z_{1,r})^{2}Z_{1,r}^{\frac{1}{v_{1}}}}{v_{1}^{3}} & 0 & \dots & 0\\ 0 & \frac{(\ln Z_{2,r})^{2}Z_{2,r}^{\frac{1}{v_{2}}}}{v_{2}^{3}} & \dots & 0\\ \vdots & \vdots & \ddots & \vdots\\ 0 & 0 & \dots & \frac{(\ln Z_{\mathrm{M,r}})^{2}Z_{\mathrm{M,r}}^{\frac{1}{w_{M}}}}{v_{M}^{3}} \end{bmatrix}$$
(6.32)

All the diagonal entries of the Hessian matrix are positive and the function  $F^{\infty, \text{CDFS}}_{\Gamma_{e2e}}(\upsilon_1, \upsilon_2, ..., \upsilon_M)$  is strictly convex. To get the optimized value of  $\upsilon_m^*$  the first derivative of (6.31) is taken with respect to each  $\upsilon_m$  and  $\lambda$  and resulting expressions are equated to zero. After performing some algebraic manipulations and solving the resulting equations, a closed-form solution for the optimal CAR at the mth user is presented below:

$$v_m^* = \frac{\ln(Z_{m,r})}{1 + W\left(\lambda(Z_{m,r})^{\frac{-1}{\ln(Z_{m,r})}}\right)},$$
(6.33)

where, W(.) denotes the Lambert W function [124]. The proof of (6.33) is given in Appendix VI.

Further, by applying the power series expansion of W(z), as given in [113, Eq. (01.31.06.0002.01)], a closed-form expression for  $v_m^*$  is derived from (6.33):

$$v_m^* = \frac{\ln(Z_{m,r})}{1 + \sum_{k=1}^{\infty} \frac{(-k)^{k-1}}{k!} \lambda^k (Z_{m,r})^{\frac{-k}{\ln(Z_{m,r})}}}.$$
(6.34)

To calculate the value of  $\lambda$ , we sum all the individual CAR values and set the result equal to unity, leading to the following equation:

$$\begin{split} \frac{\ln\left(Z_{1,r}\right)}{1+\sum_{k=1}^{\infty}\frac{(-k)^{k-1}}{k!}\lambda^{k}(Z_{1,r})^{\frac{-k}{\ln(Z_{1,r})}}} + \frac{\ln\left(Z_{2,r}\right)}{1+\sum_{k=1}^{\infty}\frac{(-k)^{k-1}}{k!}\lambda^{k}(Z_{2,r})^{\frac{-k}{\ln(Z_{2,r})}}} + \\ \dots + \frac{\ln\left(Z_{\mathrm{M,r}}\right)}{1+\sum_{k=1}^{\infty}\frac{(-k)^{k-1}}{k!}\lambda^{k}(Z_{\mathrm{M,r}})^{\frac{-k}{\ln(Z_{\mathrm{M,r}})}}} - 1 = 0. \quad (6.35) \end{split}$$

Finding a closed-form solution for  $\lambda$  is difficult. The value of  $\lambda$  can be obtained by using numerical methods.

## **6.3.2** Optimum Power Allocation

When  $m_{\rm m,r}=1, m_{\rm r,d}=1, m=1$ , Nakagami-m distribution converts into Rayleigh distribution for i.i.d interferers and (6.23) is written as:

$$\begin{split} F_{\Gamma_{e2e}}^{\infty,\text{CDFS}}(\gamma_{th}) &\simeq \sum_{m=1}^{M} \upsilon_{m} \bigg\{ \frac{\gamma_{th}}{\beta \gamma_{t} \Omega_{\text{m,r}}} + \frac{\gamma_{\text{I}} N \Omega}{\beta \gamma_{t} \Omega_{\text{m,r}}} \gamma_{th} \bigg\}^{\frac{1}{\upsilon_{m}}} + \frac{\gamma_{th}}{(1-\beta) \gamma_{t} \Omega_{\text{r,d}}} \frac{\omega^{2}}{\Gamma(a) \Gamma(b)} \\ &\times \sum_{j=1}^{2} \bigg\{ \frac{\prod_{\substack{i=1\\i\neq j}}^{2} \Gamma(\mathfrak{R}_{2i} - \mathfrak{R}_{2j}) \prod_{\substack{i=1\\i\neq j}}^{2} \Gamma(1-\mathfrak{R}_{1i} + \mathfrak{R}_{2j})}{\Gamma(\mathfrak{R}_{13} - \mathfrak{R}_{2j}) \Gamma(1-\mathfrak{R}_{23} + \mathfrak{R}_{2j})} \bigg( \frac{a\omega^{2}}{(b-1)(1+\omega^{2})} \sqrt{\frac{\gamma_{th}}{\bar{\gamma}_{\text{r,d}}^{\text{FSO}}}} \bigg)^{\mathfrak{R}_{2j}} \bigg\} \end{split}$$

To optimize the power allocation between source and relay while minimizing the OP of the considered system, we can mathematically express the objective function as follows:

$$\begin{array}{lcl} (P_s^*,P_r^*) & = & \displaystyle \operatorname*{arg\;min}_{(P_s,P_r)} P_{\Gamma_{e2e}}^{\infty,\mathrm{CDFS}}(\gamma_{th}), \\ & & \mathrm{subject\;to}\; P_s = \beta P_t, P_r = (1-\beta)P_t. \end{array} \tag{6.37}$$

To give equal fairness to all the users, we assume  $v=v_1=v_2.....=v_M$  with  $\sum_{m=1}^M v_m=1$  and substituting  $P_s=\beta P_t$ ,  $P_r^{\rm FSO}=(1-\beta)P_t$  and  $P_r^{\rm RF}=(1-\beta)P_t$  in (6.36) assuming  $\sigma^2=1$ .

After some mathematical manipulations, we can obtained as follows:

$$\begin{split} P_{\Gamma_{e2e}}^{\infty,\text{CDFS}}(\gamma_{th}) &\simeq \upsilon \left(\frac{\gamma_{th}}{P_t}(1+\gamma_I N\Omega)\right)^{\frac{1}{\upsilon}} \left(\frac{1}{\Omega_{1,r}^{\frac{1}{\upsilon}}} + \frac{1}{\Omega_{2,r}^{\frac{1}{\upsilon}}} ..... \frac{1}{\Omega_{M,r}^{\frac{1}{\upsilon}}}\right) \left(\frac{1}{\beta}\right)^{1/\upsilon} + \\ &\left(\frac{\gamma_{th}}{P_t \Omega_{r,d}}\right) \left\{\frac{\omega^2 \Gamma(a+b) I^a}{(\omega^2 - a) \Gamma(1+a) \Gamma(b)} \left(\frac{1}{1-\beta}\right)^{\frac{a}{2}+1} + \frac{\Gamma(a-\omega^2) \Gamma(b+\omega^2) I^{\omega^2}}{\Gamma(a) \Gamma(b)} \right. \\ & \times \left(\frac{1}{1-\beta}\right)^{\frac{\omega^2}{2}+1} \right\}. \quad (6.38) \end{split}$$

where, 
$$I = \frac{a}{(b-1)A_0} \sqrt{\frac{\gamma_{th}}{P_t}}$$
.

To determine the optimal value of  $\beta$ , the first derivative of the above expression with respect to  $\beta$  is taken and set to zero, which yields:

$$\frac{\partial P_{\Gamma_{e2e}}^{\infty, \text{CDFS}}(\gamma_{th})}{\partial \beta} \simeq -\mathcal{C}_1 \left(\frac{1}{\beta^*}\right)^{\frac{1}{\upsilon}+1} + \mathcal{C}_2 \left(\frac{1}{1-\beta^*}\right)^{\frac{a}{2}+2} + \mathcal{C}_3 \left(\frac{1}{1-\beta^*}\right)^{\frac{\omega^2}{2}+2} = 0. \tag{6.39}$$

where, 
$$\mathcal{C}_1 = \left(\frac{\gamma_{th}}{P_t}(1+\gamma_I N\Omega)\right)^{\frac{1}{v}}\left(\frac{1}{\Omega_{1,r}^{\frac{1}{v}}} + \frac{1}{\Omega_{2,r}^{\frac{1}{v}}}.....\frac{1}{\Omega_{M,r}^{\frac{1}{v}}}\right),$$
 
$$\mathcal{C}_2 = \left(\frac{\gamma_{th}}{P_t\Omega_{\mathrm{r,d}}}\right)\frac{\omega^2\Gamma(a+b)I^a}{(\omega^2-a)\Gamma(1+a)\Gamma(b)}\left(\frac{a}{2}+1\right), \text{and } \mathcal{C}_3 = \left(\frac{\gamma_{th}}{P_t\Omega_{\mathrm{r,d}}}\right)\frac{\Gamma(a-\omega^2)\Gamma(b+\omega^2)I^{\omega^2}}{\Gamma(a)\Gamma(b)}\left(\frac{\omega^2}{2}+1\right).$$
 Solving for  $\beta^*$ , we get:

$$\beta^* \simeq \begin{cases} \left(\frac{\mathcal{C}_1}{\mathcal{C}_2}\right)^{\frac{1}{\overline{v}+1}} (1-\beta^*)^{\frac{\frac{a}{2}+2}{\overline{v}+1}}, & \omega^2/2 > a/2\\ \left(\frac{\mathcal{C}_1}{\mathcal{C}_3}\right)^{\frac{1}{\overline{v}+1}} (1-\beta^*)^{\frac{\frac{a}{2}+2}{\overline{v}+1}}, & \omega^2/2 < a/2. \end{cases}$$
(6.40)

Obtaining a closed-form equation for the optimal power allocation coefficient might be challenging. Therefore, standard iterative root-finding methods such as Bisection or Newton-Raphson algorithm can be used to find a numerical solution.

## **6.4** Simulation Results

This section evaluates the derived expressions for the system and validates them using Monte Carlo simulations. We consider three users at the source, three interferers at the relay, a single relay with two transmitter and one destination with two receiver. For the RF links, we assume the locations of all nodes as follows: three users are positioned at (0,0), (0.2,0.5), (0.5,0.1); three interferers are located at (0,2.1), (1.1,2) and (2.2,-1); relay is at (1,0); and destination is at (4.5,0). The channel variance  $\Omega_{(.)}$  is defined as  $\mu d_{i,j}$ , where  $d_{i,j}=(\bar{d}_{i,j}/d_0)^{-\epsilon}$  [129]. For our calculations,  $\Omega_{(.)}$  is calculated with  $d_0=1$  for the RF link and  $d_0=4.5$  for the FSO link, with  $\mu=1$  and  $\epsilon=3$ . For the FSO link,  $A_0=0.8, (a,b)$  are set to (4.5916,7.0941), (2.3378,4.5323), and (1.4321,3.23)

, 3.4948) for weak, moderate, and strong turbulent environments respectively as given by [64]. In the first-hop, fading parameters for three users are  $\left\{m_{\rm m,r}\right\}_{m=1}^3=\{2,3,3\}$ , for three interferers  $\left\{m_{I_{n,r}}\right\}_{n=1}^3=\{1.5,2,2.5\}$ , and  $\left\{m_{\rm r,d}\right\}=\{2\}$  for the second-hop. Monte Carlo simulations were carried out with  $10^6$  iterations.

Fig. 6.2 depicts the OP versus  $\gamma_t$  under varying threshold SNR in strong turbulence conditions. The figure show that as  $\gamma_t$  increases, the outage probability decreases. Additionally, with the increase of  $\gamma_{th}$ , OP performance decreases. Moreover, the Monte Carlo simulation results showed an excellent agreement with the analytical expressions, thereby validating the accuracy of the derived formulations.

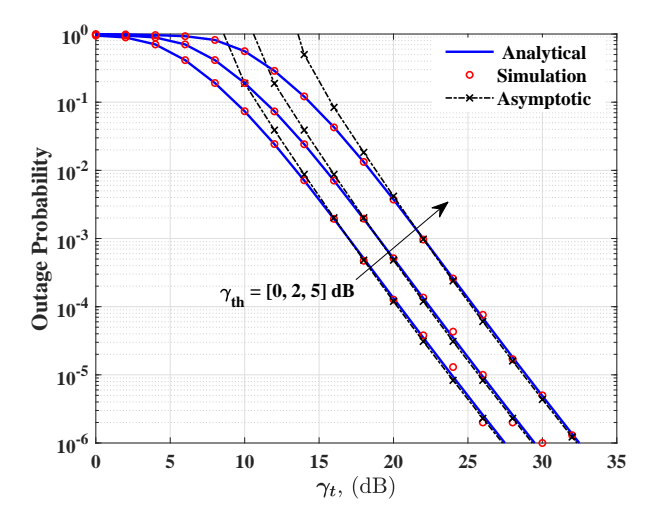


Figure 6.2: OP versus  $\gamma_t$  over i.n.i.d CCI considering CDFS based system under strong turbulence condition fixed at  $P_I$  = 5 dB,  $\beta=0.5$ ,  $\omega=1.33$  and  $v_m=[0.6,0.3,0.1]$ .

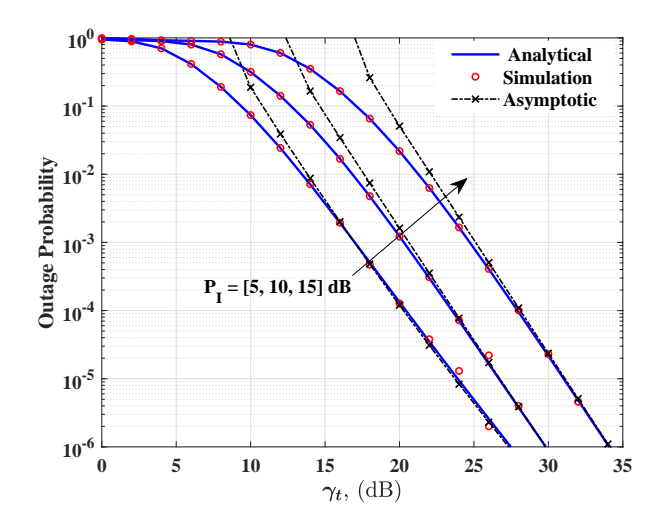


Figure 6.3: OP versus  $\gamma_t$  over i.n.i.d CCI considering CDFS based system under strong turbulence conditions fixed at  $\gamma_{th}$  = 0 dB,  $\beta$  = 0.5,  $\omega$  = 1.33 and  $\upsilon_m$  = [0.6, 0.3, 0.1].

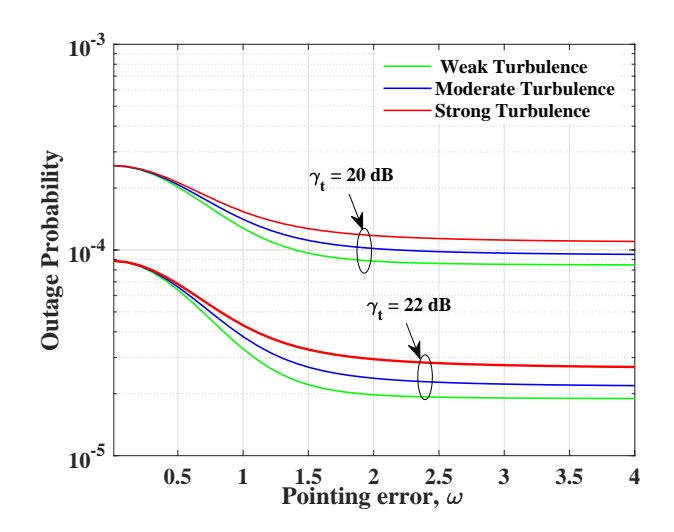


Figure 6.4: OP versus  $\omega$  over i.n.i.d CCI considering CDFS based system under different turbulence conditions fixed at  $\gamma_{th}$  = 0 dB,  $P_I$  = 5 dB,  $\beta$  = 0.5, and  $\upsilon_m$  = [0.6, 0.3, 0.1].

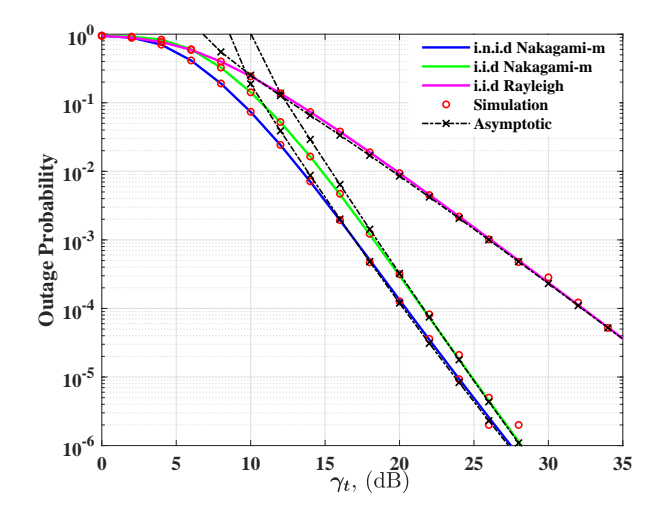


Figure 6.5: OP versus  $\gamma_t$  under strong turbulence conditions fixed at  $\gamma_{th}=0$  dB,  $P_I=5$  dB,  $\beta=0.5$ ,  $\omega=1.33$  and  $v_m=[0.6,0.3,0.1]$ . We have set,  $m_{1,r}=2,m_{2,r}=3,m_{3,r}=3,m_{\rm r,d}=2,m_I=6.23027, \Omega_I=0.4664$  for i.n.i.d Nakagami-m fading,  $m_{1,r}=2,m_{2,r}=3,m_{3,r}=3,m_{\rm r,d}=2,m=2.5, \Omega=0.2624$  for i.i.d Nakagami-m fading and  $m_{1,r}=m_{2,r}=m_{3,r}=m_{\rm r,d}=m=1, \Omega=0.2624$  for i.i.d Rayleigh fading

Fig. 6.3 depicts the OP versus  $\gamma_t$  for varying interferer power,  $P_{\rm I}$ . It is evident that increased the interferer power leads to degraded system performance. Fig. 6.4 shows the influence of pointing error on the outage probability. An increase in  $\omega$ , reduces the effect of pointing error, thereby improving system performance. It also confirms that stronger turbulence conditions degrade performance more significantly. The OP performance for different fading parameters is depicted in Fig. 6.5. As the values of m increases, the OP decreases because the effect of fading on the wireless signal is less with higher value of m.

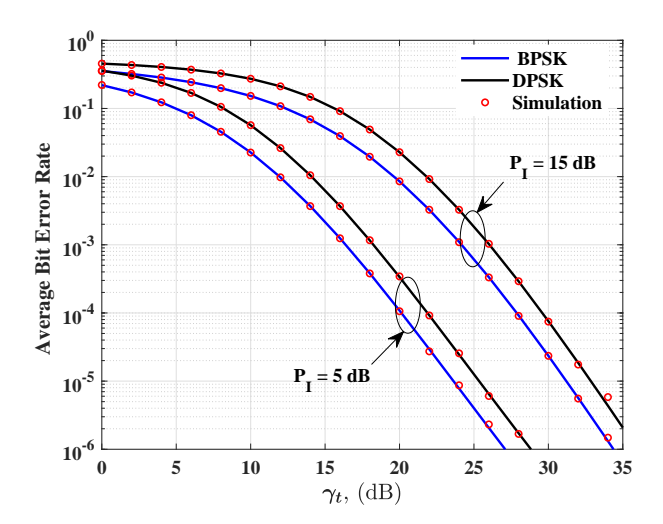


Figure 6.6: ABER versus  $\gamma_t$  for different modulations under strong turbulence conditions fixed at  $\beta=0.5,\,\omega=1.33$  and  $\upsilon_m=[0.6,0.3,0.1].$ 

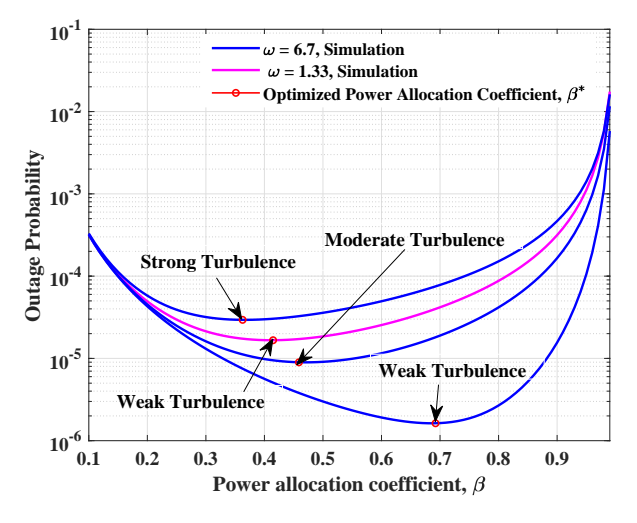


Figure 6.7: OP versus power allocation coefficient considering CDFS based system under different turbulence conditions and pointing errors at  $\gamma_{th}$  = 0 dB,  $P_I$  = 10 dB, and  $\upsilon_m = [1/3, 1/3, 1/3]$ .

Fig. 6.6 illustrates the ABER performance of BPSK and DPSK modulations under varying interference power. It is evident that BPSK outperforms DPSK demonstrating lower bit error rates across all interference conditions. The variation of the outage performance with respect to the power allocation coefficient,  $\beta$  is shown in Fig. 6.7. The optimum value of  $\beta$  is obtained using (6.40). The aim is to obtain the value of  $\beta$  that minimizes the outage probability in the presence of fading, co-channel interference, turbulence, and pointing errors. The optimal power allocation coefficients obtained are  $\beta^* = 0.4148$  for  $\omega = 1.33$  under weak turbulence conditions, and  $\beta^* = 0.6923$ ,  $\beta^* = 0.4589$  and  $\beta^* = 0.3627$  for  $\omega = 6.7$  under weak, moderate and strong turbulence conditions respectively. From the figure, it can be inferred that the optimum value of  $\beta$  obtained using (6.40) coincides with the simulation value.

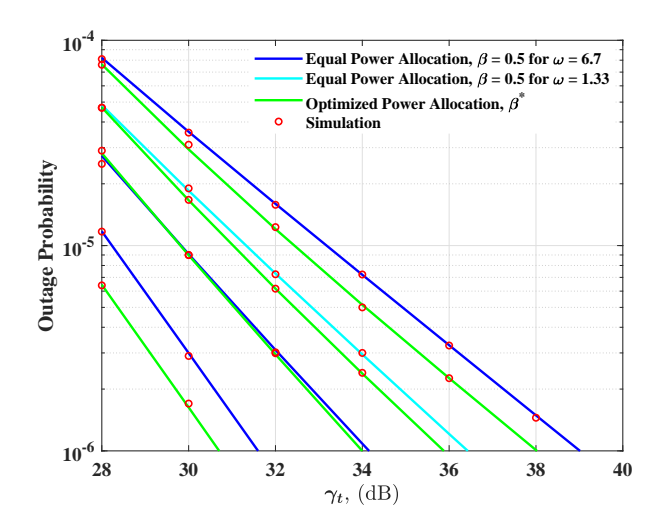


Figure 6.8: OP versus  $\gamma_t$  over equal power and optimized power allocation considering CDFS based system under different turbulence conditions and pointing errors at  $\gamma_{th}$  = 0 dB,  $P_I$  = 10 dB, and  $v_m$  = [1/3, 1/3, 1/3].

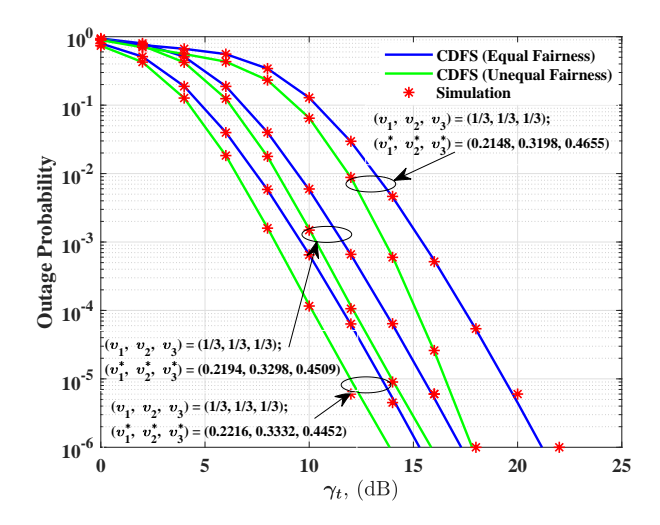


Figure 6.9: OP versus  $\gamma_t$  over equal channel access ratio and optimized channel access ratios for CDFS based systems under strong turbulence condition fixed at  $\beta=0.5,\,\omega=1.33$ . We have set,  $m_{1,r}=2, m_{2,r}=3, m_{3,r}=3, m_{\rm r,d}=5, m_I=6.23027, \Omega_I=0.4664$  for i.n.i.d Nakagami-m fading.

In Fig. 6.8, we demonstrate that utilizing the optimized value  $\beta^*$ , results to a significant enhancement in OP performance. We plot the OP versus  $\gamma_t$  for the CDFS-based system under turbulence conditions and pointing error, considering both equal and optimized power allocation for  $\gamma_{th}=0$  dB,  $P_I=10$  dB, and  $\upsilon_m=[1/3,1/3,1/3]$ . We observe an improvement of 0.6 dB for  $\beta^*=0.4148$  under weak turbulence, 1 dB for  $\beta^*=0.6923$ , 0.2 dB for  $\beta^*=0.4589$  and 1 dB for  $\beta^*=0.3627$  under weak, moderate and strong turbulence conditions respectively.

Fig. 6.9 illustrates the OP of considered system versus  $\gamma_t$  for a CDFS-based scheme with both equal and optimized CAR. For the case of equal CAR,  $v_m = [1/3, 1/3, 1/3]$ 

and  $\beta=0.5$  under strong turbulence conditions. The figure demonstrates that optimizing the CAR results in a substantial improvement in OP performance. The improvement is 1.5 dB for  $\upsilon_m=[0.2216,0.3332,0.4452]$  fixed at  $\gamma_{th}$  = 0 dB,  $P_I$  = 0 dB, 1.5 dB for  $\upsilon_m=[0.2194,0.3298,0.4509]$  fixed at  $\gamma_{th}$  = 2 dB,  $P_I$  = 0 dB, 2.7 dB for  $\upsilon_m=[0.2148,0.3198,0.4655]$  fixed at  $\gamma_{th}$  = 0 dB,  $P_I$  = 10 dB at OP =  $10^{-5}$ .

# **Chapter 7**

# MIMO-FSO and WDM-FSO Communication Systems

To mitigate the detrimental effects of atmospheric turbulence in free-space optical (FSO) communication, advanced techniques such as Multiple-Input Multiple-Output (MIMO) FSO and Wavelength Division Multiplexing (WDM) FSO systems have been proposed. The MIMO technique enhances system reliability by reducing signal attenuation and improving bit error rate (BER) performance under turbulent conditions.

However, when multiple wavelength signals are transmitted through a single FSO channel, issues such as beam dispersion, beam wandering, and wavefront distortion arise. To address these challenges, WDM-FSO systems employing multiple beams are utilized, which help maintain signal integrity and improve overall system performance. The key contributions of this chapter are summarized as follows:

• The performance of both MIMO-FSO and WDM-FSO systems is evaluated using real-time meteorological data from Leh, Ladakh (India) as shown in Table 7.1. This region, known for its harsh weather and high susceptibility to natural disasters, demands robust communication solutions. FSO technology serves as a reliable medium to ensure continuous connectivity in such environments.

# 7.1 System Model

MIMO-FSO and wavelength division multiplexing (WDM)-FSO communication systems are presented in and Fig. 7.1 and Fig. 7.2. The transmitter consists of user-defined bit sequences (UDBS) with non -return to zero (NRZ) line coding, CW laser source of power 10 mW at wavelength 1550 nm, Mach-Zehnder modulator (MZM), and optical amplifier like Erbium-doped Fiber Amplifier (EDFA). User-defined NRZ bit sequence of length 1024 bits having to vary data rate from 1 Gbps to 5 Gbps is modulated by a laser source with the help of MZM. Further, the modulated optical signal is amplified with the help of EDFA and separated by the same signal by using an optical splitter. Then it is transmitted through the multiple beams of FSO channels. All the transmitted signals are united by using an optical combiner and received by Avalanche photodiode (APD).

Then, it is filtered by a low-pass Bessel filter and analyzed by a BER analyzer as shown in Fig. 7.1.

WDM-FSO system has two optical signals having wavelengths 1550 nm and 1550.8 nm with an adjacent channel spacing of 0.8 nm and multiplexed by the multiplexer. After separate both signals, they are transmitted through the multiple beams of FSO channels. Then the receivers receive all the transmitted signals and combine these signals by using the combining technique. Further, it is routed to a demultiplexer that is tuned to a particular wavelength as shown in Fig. 7.2. Simulated parameters are used for both the proposed systems as shown in Table. 7.2.

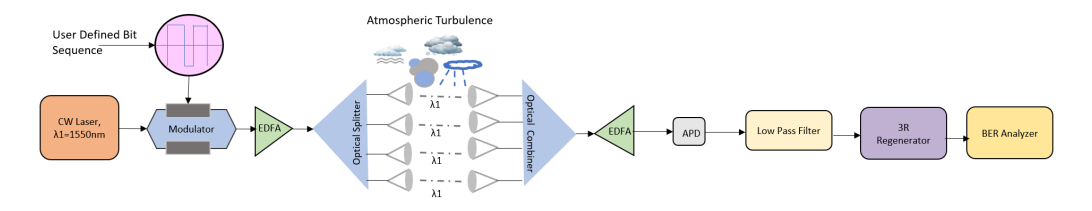


Figure 7.1: Proposed MIMO-FSO communication system.

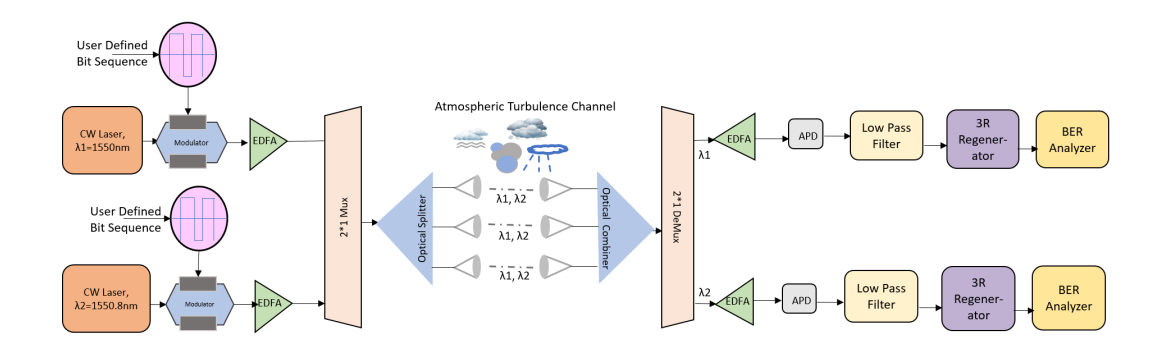


Figure 7.2: Proposed WDM-FSO communication system.

Table 7.1: Real-Time data for Leh, Ladakh for the year 2020 [	134	J
---	-----	---

Month	Visibility (km)	Precipitation (mm/h)	Dry Snow (mm/h)	Avg. Wind Speed (m/s)
Jan	8.3	0.17	0.16	3.53
Feb	9.0	0.41	0.36	3.36
Mar	8.3	0.33	0.31	2.97
Apr	8.9	0.49	0.45	2.61
May	8.8	0.38	0.32	2.33
Jun	7.4	0.31	0.19	1.94
Jul	7.4	0.22	0.10	1.61
Aug	8.2	0.25	0.10	1.64
Sep	9.1	0.28	0.16	2.17
Oct	9.5	0.29	0.27	2.83
Nov	8.5	0.23	0.22	3.31
Dec	8.6	0.14	0.12	3.47

Most FSO communication systems are developed so far all over the world in which data transmitted wirelessly using a laser source can be corrupted when it propagates through atmospheric turbulence. Atmospheric turbulence depends on weather conditions and

Table 7.2: Parameters Values for Proposed Systems

Parameters	Values
Operating wavelength	1550 nm
Data rate	1 Gbps – 5 Gbps
Sequence length	1024 bits
Samples per bit	64
Laser power	10 mW
Channel length, $R$	1  km - 5  km
EDFA gain	20 dB
Attenuation (due to rain, fog, and smog)	5.86 dB/km
Transmitter aperture diameter, $D_t$	25 mm
Receiver aperture diameter, $D_r$	80 mm
Transmitter and Receiver loss	1 dB
Beam divergence, $\phi$	2 mrad
Transmitter and Receiver loss	1 dB

geographical location. Here we have analyzed the MIMO FSO system and WDM FSO system in Leh, Ladakh location in which rain, fog, dry snow, scintillation loss, geometric loss, and Rytov variance are considered over Gamma-Gamma distribution. These are the major atmospheric elements that attenuate the laser power. Most FSO communication systems are developed so far all over the world in which data transmitted wirelessly using a laser source can be corrupted when it propagates through atmospheric turbulence. Atmospheric turbulence depends on weather conditions and geographical location. Here we have analyzed the MIMO FSO system and WDM FSO system in Leh, Ladakh location in which rain, fog, dry snow, scintillation loss, geometric loss, and Rytov variance are considered over Gamma-Gamma distribution. These are the major atmospheric elements that attenuate the laser power. Then total attenuation  $\alpha_{Total}$  and geometric loss  $L_{\rm geo\_loss}$  (dB) are calculated by using (7.1) and (7.2) respectively. For rain attenuation,  $\alpha_{rain}$ , fog attenuation,  $\alpha_{fog}$  and dry snowfall,  $\alpha_{drv \, snow}$  are evaluated by using (7.3), (7.4), and (7.5) respectively, where P (mm/h) is the precipitation in (7.3). Further, to calculate the fog attenuation as in (7.4), the most widely used Kim model is implemented in our simulation to get the value of p, dynamic visibility, V (km), and wavelength  $\lambda$  (nm). Additionally, S, snow rate (mm/h),  $a = 5.42 \times 10^{-5} + 5.4958776$ and b = 1.38 in (7.5).

$$\alpha_{\text{Total}} (dB/km) = \alpha_{\text{rain}} + \alpha_{\text{fog}} + \alpha_{\text{dry snow}}$$
 (7.1)

$$L_{\rm geo\_loss} ({\rm dB}) = -20\log\frac{D_r}{D_t + \phi R} \tag{7.2}$$

$$\alpha_{\text{rain}} (dB/km) = 1.076 P^{0.67}$$
 (7.3)

$$\alpha_{\rm fog}~({\rm dB/km}) = \frac{3.91}{V} \left(\frac{\lambda}{550~{\rm nm}}\right)^{-p} \eqno(7.4)$$

$$\alpha_{\rm drv\,snow}\,({\rm dB/km}) = a\,S^b \tag{7.5}$$

The PDF of Gamma-Gamma distribution which is used to characterize the amplitude fluctuations in the atmospheric conditions [135] as given as:

$$P(I) = \frac{2(\alpha\beta)^{(\alpha+\beta)/2}}{\Gamma(\alpha)\Gamma(\beta)} I^{(\alpha+\beta)/2-1} K_{\alpha-\beta} (2\sqrt{\alpha\beta} I)$$
 (7.6)

where,  $\alpha=\exp\Bigl(\frac{0.49\,\sigma^2}{(1+1.11\,\sigma^{12/5})^{5/6}}\Bigr)-1, \beta=\exp\Bigl(\frac{0.51\,\sigma^2}{(1+0.69\,\sigma^{12/5})^{5/6}}\Bigr)-1,$  are small and large scale eddies,  $K_{\nu}(\cdot)$  is the modified Bessel function of the second kind,  $\Gamma(\cdot)$  the Gamma function, and Rytov variance  $\sigma^2=1.23\,C_n^2\,k^{7/6}\,R^{11/6}$  for a plane wave, with  $k=2\pi/\lambda$ , channel length R (m), and  $C_n^2$  is

$$C_n^2 = 0.00594 \, (v/27)^2 \, (10^{-5}h)^{10} \, e^{-h/1000} + 2.7 \times 10^{-16} \, e^{-h/1500} + 1.7 \times 10^{-14} \, e^{-h/100}, \tag{7.7}$$

where average wind speed v (m/s) of Leh Ladakh at altitude h=3524, m according to the Hufnagel-Valley Model [136].

Scintillation Loss = 
$$\sqrt{92.68 \left(\frac{2\pi \times 10^9}{\lambda}\right)^{7/6} C_n^2 R^{11/6}}$$
 (7.8)

Then rainfall attenuation, fog attenuation, dry snow attenuation, total attenuation, Refractive index structure parameters,  $C_n^2$  are calculated by using from (7.1) to (7.7) as shown in Table 7.3. The values of  $L_{\rm geo\,loss}$ ,  $\sigma^2$  and scintillation loss are given in Table 7.4.

Table 7.3: Measured rainfall attenuation, fog attenuation, dry snow attenuation, total attenuation, and refractive index structure parameter,  $C_n^2$  for Leh, Ladakh during the year 2020

Month	$lpha_{ m rain}$	$\alpha_{ m fog}$	$\alpha_{ m dry\;snow}$	$lpha_{ ext{Total}}$	Average Attenuation (dB/km)	Average $C_n^2$
January	1.44	0.53	1.88	3.85		
February	2.56	0.49	5.77	8.82		
March	2.22	0.53	4.67	7.42		
April	2.91	0.50	8.03	11.44		
May	2.45	0.50	4.97	7.93		
June	2.15	0.60	2.47	5.22	5.86	$2.58 \times 10^{-17}$
July	1.72	0.60	0.98	3.29		
August	1.82	0.54	0.97	3.34		
September	1.99	0.49	1.94	4.42		
October	2.02	0.46	3.88	6.37		
November	1.74	0.52	2.88	5.14		
December	1.23	0.51	1.34	3.09		

Table 7.4: Measured parameters such as geometric loss ( $L_{\rm geo\,loss}$ ), Rytov variance ( $\sigma^2$ ), and scintillation loss with varying channel length R

<b>Channel Length</b> ,	$L_{\rm geo\ loss}\ ({ m dB})$	$\sigma^2$ (Rytov Variance)	<b>Scintillation Loss</b>
$R\left(\mathbf{km}\right)$			
1	-28.066701	0.0005136662	0.1966
2	-34.033518	0.0018304983	0.3712
3	-37.537341	0.0038494911	0.5383
4	-40.027101	0.0065231545	0.7007
5	-41.959888	0.0098203287	0.8598

#### 7.2 Results and Discussion

We have analyzed the performance of our proposed MIMO FSO and WDM FSO system under the atmospheric turbulence of the outdoor environment to get information about the reliability of the system. Due to turbulence, signal power received by the APD receiver is decreased due to the atmospheric turbulence channel parameters like rain, fog, smog, and scintillation effect. We have carried out our simulation on Optisystem 18.

#### Case 1. Proposed MIMO FSO system

Firstly, in our proposed MIMO-FSO system, we have considered 4 number of FSO channels between transmitter and receiver. In this, only one user transmitted the same information through multiple FSO channels by varying the channel length from 3 km to 4 km for a constant data rate of 5 Gbps as in Fig. 7.3 and also change the data rates from 1 Gbps to 5 Gbps at constant channel length of 4 km as in Fig. 7.4. We have seen that BER decreases as we increase the number of FSO channels, and the corresponding Quality Factor also improved with the same as shown in Fig. 7.5. Error-free transmission is possible for a 4 MIMO-FSO communication system up to a channel length of 3.5 km compared to others as given in Fig. 7.3. It concludes that increase the data rate from 1 Gbps to 5Gbps, system performance degraded as presented in Fig. 7.4. According to ITU-U (G-series, supplement 39), the design of an optical communication system is considered to accept a maximum value of BER i.e.,  $10^{-12}$ , and Q-factor to be greater than and equal to 7. Hence, our proposed system cannot transmit any data after 5 km. So, our 4 MIMO-FSO system is used to transmit the data with a data rate of 3Gb/s up to a channel length of 5km.

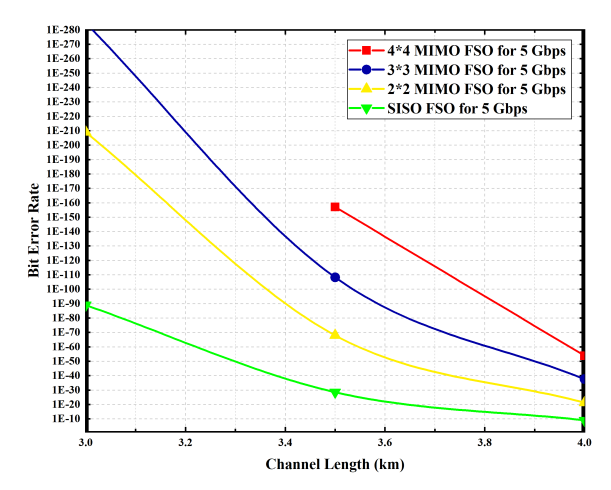


Figure 7.3: Bit error rate versus channel length.

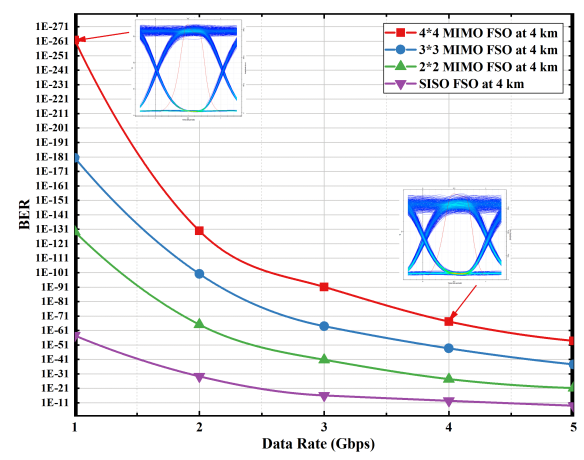
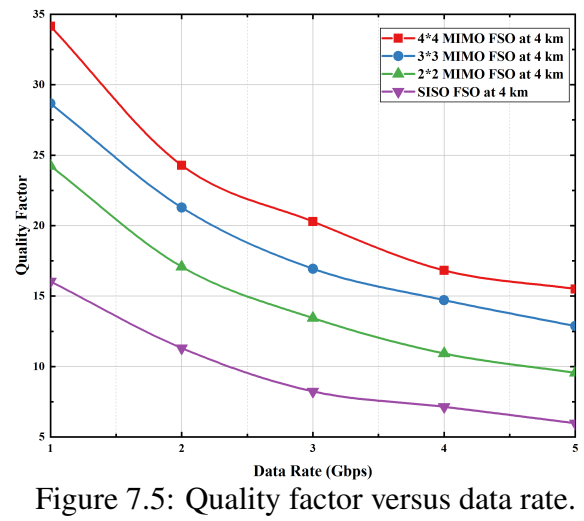


Figure 7.4: Bit error rate versus data rate.



#### Case 2. Proposed hybrid WDM FSO system

In WDM-FSO System, two different users are transmitted their data over multiple FSO channels instead of one user in the case of the MIMO-FSO system. Here we have considered a maximum of 3 numbers of FSO channels in it. We know, BER will increase as the channel length and data rate are increased. But we can enhance the system performance by increasing the number of beams between transmitters and receivers as shown in Fig. 7.6.

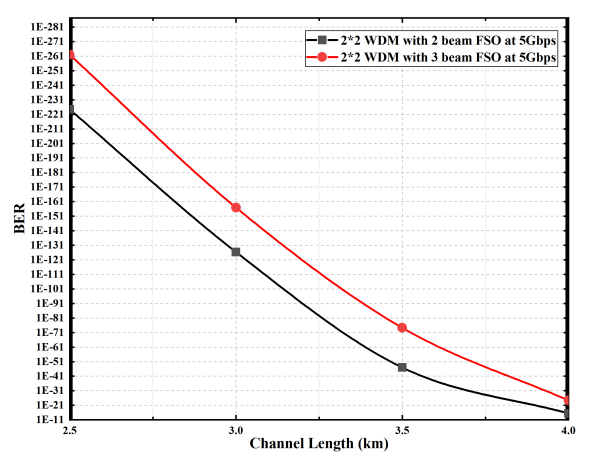


Figure 7.6: Bit error rate versus channel length at a data rate of 5Gb/s.

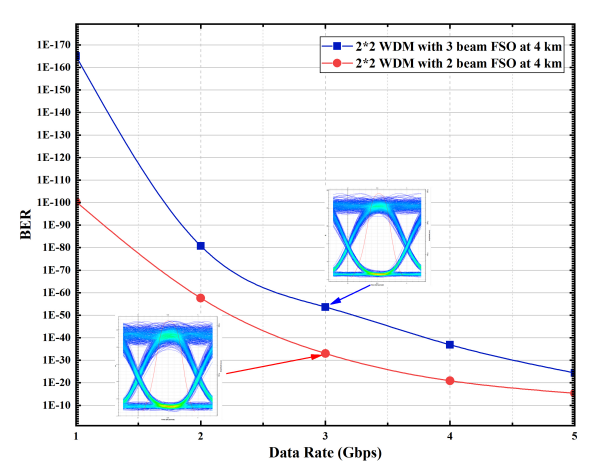


Figure 7.7: Bit error rate versus data rate at channel length of 4km.

Fig. 7.7 reveals that the WDM-FSO system with 2 beams is much vulnerable to atmospheric conditions as compared to the 3 beams WDM-FSO system. BER has been recorded  $9.48 \times 10^{-34}$  and  $2.20 \times 10^{-54}$  for 2 beams and 3 beams at channel length of 4 km for 3 Gbps respectively and also has a higher quality factor in case for 3 beams as compared to two beams as shown in Fig. 7.8. The performance of MIMO-FSO and WDM-FSO systems is associated in terms of BER vs transmitted power by taking channel length of 3 km at a data rate of 5 Gbps as shown in Fig. 7.9. It shows that double the number of beams in MIMO-FSO, BER is decreased from  $1.64 \times 10^{-41}$  to  $7.69 \times 10^{-92}$  by assuming a channel length of 4 km at a data rate of 3 Gbps. Thus, higher the multiple beams in MIMO-FSO gives more improvement in the system. Similarly, if

one more beam is added to the WDM-FSO system, BER decreased from  $9.48\times10^{-34}$  to  $2.20\times10^{-54}$ .

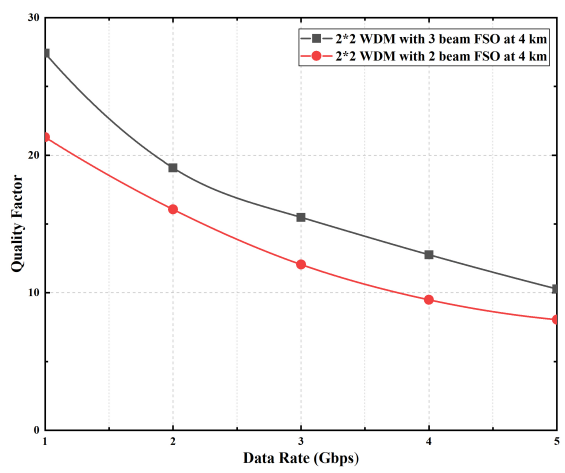


Figure 7.8: Quality factor versus data rate at channel length of 4km.

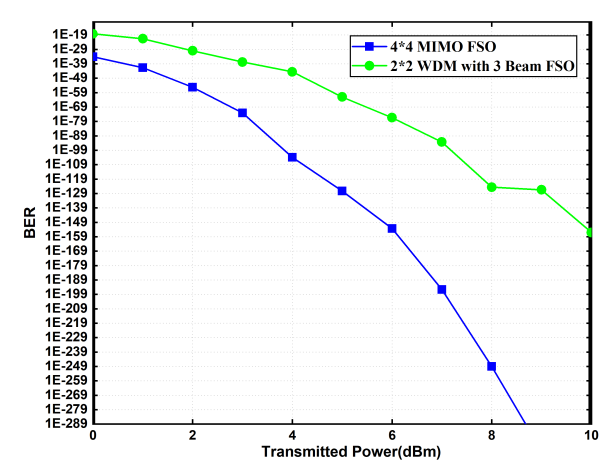


Figure 7.9: BER versus transmitted power at channel length of 3km

#### Comparison between MIMO FSO and WDM FSO system

Performance of MIMO FSO and WDM FSO systems is associated in terms of BER vs transmitted power by taking channel length of 3 km at a data rate of 5 Gbps as shown in Fig. 7.9. Comparison between both systems is presented in Table. 7.5. It shows that double the number of beams in MIMO FSO, BER is decreased from  $1.64 \times 10^{-41}$  to  $7.69 \times 10^{-92}$  by assuming a channel length of 4 km at a data rate of 3 Gbps. Thus, higher the multiple beams in MIMO FSO gives more improvement in the system. Similarly, if one more beam is added to the WDM FSO system, BER decreased from  $9.48 \times 10^{-34}$  to  $2.20 \times 10^{-54}$ .

Table 7.5: BER of MIMO FSO and WDM FSO communication systems

Sy	ystems	2×2 MIMO FSO	3×3 MIMO FSO	4×4 MIMO FSO	2×2 WDM FSO (2 beams)	2×2 WDM FSO (3 beams)
	BER	$1.64 \times 10^{-41}$	$1.01 \times 10^{-64}$	$7.69 \times 10^{-92}$	$9.48 \times 10^{-34}$	$2.20 \times 10^{-54}$

## **Chapter 8**

# Conclusion, Future Scope and Social Impact

#### 8.1 Conclusion

This chapter presented the performance of FSO system under atmospheric turbulence modeled by the IGG distribution for IM/DD scheme. New analytical expressions for OP and ABER were obtained under various atmospheric conditions. The accuracy of these expressions was verified with Monte-Carlo simulations. It was observed that severe atmospheric turbulence significantly impairs OP and ABER performance. BPSK modulation consistently yielded better ABER results compared to other binary modulation formats. Further, asymptotic results for the OP and ABER were derived and some useful insights were obtained. The analysis demonstrated that the diversity order was directly affected by  $\beta/2$ . This implies that a higher value of  $\beta$  contributes to a higher diversity order which in turn, enhances the system performance. This improvement can be particularly advantageous in addressing the detrimental impact of fading, making the FSO system more robust and effective, especially in challenging communication environments.

We have also analysed the performance of MU dual-hop RF-FSO system employing GS, PFS, and CDFS based schemes, considering i.n.i.d CCI under perfect channel estimation at both RF and FSO links. Analytical and asymptotic expressions for the OP were formulated assuming Rayleigh/ $\mathcal{F}$  fading models. Further, power allocation was formulated to improve system performance. Moreover, optimizing channel access ratios for users was conducted to enhance outage performance.

The performance of the MU dual-hop RF-FSO relaying system was analytically evaluated under imperfect channel estimation in both transmission links. The RF links was modeled with Rayleigh fading, while FSO link was characterized by the  $\mathcal{F}$  distribution. CDFS scheme was used to control channel access ratios and ensure fairness. Further, an analytical and asymptotic closed-form expression for OP was derived considering i.n.i.d CCI to the relay with non-identical power and non-identical RF channel gain among users and relay. Optimal power allocation and channel access ratios expressions were derived to minimize the system OP. In our study, the lowest outage performance was observed with an imperfect RF link, while the outage performance for the imper-

fect RF-imperfect FSO links and only imperfect FSO link cases was nearly similar. Moreover, it is concluded that optimal power allocation can greatly improve system performance across a wide range of interference power levels and data rates under only imperfect RF link. A substantial performance improvement with CDFS-based system and with power allocation was demonstrated as compared to a GS scheme.

Next, the performance of a dual-hop MU RF and hybrid FSO/RF system was analyzed by taking into account i.n.i.d CCI and pointing errors. The RF links exhibited Nakagami-m fading, while FSO links was subjected to Fisher Snedecor,  $\mathcal{F}$  distribution under the effect of pointing error. The relay selects the users according to the CDF based scheduling scheme and then forwards the data via hybrid FSO/RF links. To enhance system performance, we formulated expressions for optimal power allocation to user and relay, as well as optimized CAR.

Finally, the performance of MIMO FSO and hybrid WDM FSO systems have been proposed for Leh, Ladakh under worst weather conditions by considering the rain, fog, dry snow, scintillation loss, geometric losses, and Rytov variance over Gamma-Gamma distribution. All-weather data is collected for the year 2020 for analysis. The result shows that  $4\times4$  MIMO FSO system perform better as compared to other FSO system. It can transmit the information successfully up to 5 km at data rate of 3Gbps for  $4\times4$  MIMO FSO during worst atmospheric conditions for Leh Ladakh. On the other hand, the multiple beams WDM FSO system also enhances the system link availability up to 5 km at a data rate of 1 Gbps for 3 beams WDM FSO.

## 8.2 Future Scope

Several challenging problems outlined in Chapter 1 have been addressed in this thesis. However, there remain noteworthy research issues that warrant further investigation. Some potential directions for future work include the following:

- The current multiuser dual-hop RF-FSO communication system presented in this
  thesis employs a single antenna at both the source and relay. This work can be
  extended by incorporating multiple antennas at the source and relay to exploit of
  spatial diversity, thereby enhancing system capacity and reliability. The performance analysis of a MIMO-based MU dual-hop RF-FSO system can be explored
  for future study.
- Given that perfect CSI is rarely achievable in practical scenarios, future work may extend the performance analysis of MIMO multiuser dual-hop RF-FSO systems by accounting for channel estimation errors.
- Considering correlated fading channels in the performance analysis of MIMO multiuser dual-hop RF-FSO systems can provide meaningful insights into system degradation and constitutes a promising area for future investigation.
- Furthermore, a multi-user multi-relay communication system can be employed to take the benefits of multi-user diversity and improve overall system performance.

Therefore, incorporating MIMO with practical considerations like channel estimation errors and correlated fading into the current system provides a more realistic performance assessment and serves as a stepping stone toward the development of advanced hybrid communication architectures for future 6G and IoT networks.

## 8.3 Social Impact

This thesis work has significant social relevance and practical implications, particularly in scenarios where conventional communication infrastructures are unavailable, damaged, or difficult to deploy.

- Rapid Communication Restoration in Disaster-Hit Areas: During natural
  disasters such as earthquakes, floods, or cyclones, terrestrial and optical fiber
  networks often fail, leading to major communication breakdowns. The solutions
  proposed in this work can be quickly deployed to establish emergency communication links without physical cables. Their flexibility and cost-effectiveness
  enable rapid setup of temporary networks for coordinating rescue operations, resource distribution, and timely information dissemination.
- Last-Mile Connectivity in Remote and Hilly Regions: In mountainous or remote areas, extending fiber or wired networks is technically challenging and economically infeasible. This thesis provides approaches that can be easily implemented to bridge last-mile connectivity gaps. These methods ensure reliable, high-capacity communication, enabling access to education, telemedicine, egovernance, and internet services in underserved regions.
- Urban Communication and Network Scalability: In dense urban environments, multiple user devices require high-capacity links to relay aggregated traffic to central nodes. The techniques developed in this thesis support scalable, resilient, and high-throughput connectivity, ensuring reliable performance even where conventional infrastructure is limited.

Overall, this thesis work contributes to building a resilient, inclusive, and high-capacity communication ecosystem, ensuring connectivity even in the most difficult terrains and during critical situations.

## References

- [1] Cisco. (2020) Cisco annual internet report (2018–2023). [Online]. Available: https://www.cisco.com/c/en/us/solutions/collateral/executive-perspectives/annual-internet-report/white-paper-c11-741490.pdf
- [2] M. A. Khalighi and M. Uysal, "Survey on free space optical communication: A communication theory perspective," *IEEE Communications Surveys & Tutorials*, vol. 16, no. 4, pp. 2231–2258, 2014.
- [3] Z. Ghassemlooy, S. Arnon, M. Uysal, Z. Xu, and J. Cheng, "Emerging optical wireless communications-advances and challenges," *IEEE Journal on Selected Areas in Communications*, vol. 33, no. 9, pp. 1738–1749, 2015.
- [4] M. Z. Chowdhury, M. T. Hossan, A. Islam, and Y. M. Jang, "A comparative survey of optical wireless technologies: Architectures and applications," *IEEE Access*, vol. 6, pp. 9819–9840, 2018.
- [5] M. Elamassie and M. Uysal, "Free space optical communication: An enabling backhaul technology for 6G non-terrestrial networks," in *Photonics*, vol. 10, no. 11. MDPI, 2023, p. 1210.
- [6] R. Rani and G. Kaur, "Design and analysis of MIMO FSO system and WDM FSO system for Leh (ladakh), India under worst weather conditions," in 2021 7th International Conference on Signal Processing and Communication (ICSC). IEEE, 2021, pp. 31–36.
- [7] D. T. Wayne, R. L. Phillips, L. C. Andrews, T. Leclerc, P. Sauer, and J. Stryjewski, "Comparing the Log-Normal and Gamma-Gamma model to experimental probability density functions of aperture averaging data," in *Free-Space Laser Communications X*, vol. 7814. SPIE, 2010, pp. 163–175.
- [8] N. D. Chatzidiamantis, H. G. Sandalidis, G. K. Karagiannidis, and M. Matthaiou, "Inverse Gaussian modeling of turbulence-induced fading in free-space optical systems," *Journal of Lightwave Technology*, vol. 29, no. 10, pp. 1590–1596, 2011.
- [9] H. Khanna, M. Aggarwal, and S. Ahuja, "Performance analysis of a variable-gain amplify-and-forward relayed mixed RF-FSO system," *International Journal of Communication Systems*, vol. 31, no. 1, p. e3400, 2018.

- [10] A. Kumar and P. Garg, "Physical layer security for dual-hop FSO/RF system using generalized  $\Gamma\Gamma/\eta$   $\mu$  fading channels," *International Journal of Communication Systems*, vol. 31, no. 3, p. e3468, 2018.
- [11] P. Jain, N. Jayanthi, M. Lakshmanan, A. Saxena, and A. Jain, "Outage probability and Average Capacity analysis over α-μ distribution in free space optical communication system," in 2019 international conference on vision towards emerging trends in communication and networking (ViTECoN). IEEE, 2019, pp. 1–4.
- [12] N. D. Chatzidiamantis, H. G. Sandalidis, G. K. Karagiannidis, S. A. Kotsopoulos, and M. Matthaiou, "New results on turbulence modeling for free-space optical systems," in *2010 17th International Conference on Telecommunications*. IEEE, 2010, pp. 487–492.
- [13] R. Barrios Porras, "Exponentiated Weibull fading channel model in free-space optical communications under atmospheric turbulence," 2013.
- [14] J. H. Churnside and S. F. Clifford, "Log-normal Rician probability-density function of optical scintillations in the turbulent atmosphere," *Journal of the Optical Society of America A*, vol. 4, no. 10, pp. 1923–1930, 1987.
- [15] M. A. Kashani, M. Uysal, and M. Kavehrad, "A novel statistical channel model for turbulence-induced fading in free-space optical systems," *Journal of Lightwave Technology*, vol. 33, no. 11, pp. 2303–2312, 2015.
- [16] I. S. Ansari, F. Yilmaz, and M.-S. Alouini, "Performance analysis of free-space optical links over Malaga ( $\mathcal{M}$ ) turbulence channels with pointing errors," *IEEE Transactions on Wireless Communications*, vol. 15, no. 1, pp. 91–102, 2015.
- [17] K. P. Peppas, G. C. Alexandropoulos, E. D. Xenos, and A. Maras, "The Fischer–Snedecor  $\mathcal{F}$  distribution model for turbulence-induced fading in free-space optical systems," *Journal of Lightwave Technology*, vol. 38, no. 6, pp. 1286–1295, 2020.
- [18] Y. M. Shishter, R. Young, and F. H. Ali, "Irradiance probability density function for turbulence induced fading in free space optics," *Journal of the Optical Society of America A*, vol. 39, no. 7, pp. 1267–1274, 2022.
- [19] M. Cheng, Y. Guo, J. Li, X. Zheng, and L. Guo, "Inverse Gaussian Gamma distribution model for turbulence-induced fading in free-space optical communication," *Applied Optics*, vol. 57, no. 12, pp. 3031–3037, 2018.
- [20] A. A. Farid and S. Hranilovic, "Outage capacity optimization for free-space optical links with pointing errors," *Journal of Lightwave technology*, vol. 25, no. 7, pp. 1702–1710, 2007.
- [21] F. Yang, J. Cheng, and T. A. Tsiftsis, "Free-space optical communication with nonzero boresight pointing errors," *IEEE Transactions on Communications*, vol. 62, no. 2, pp. 713–725, 2014.

- [22] B. Sklar, "Rayleigh fading channels in mobile digital communication systems. i. characterization," *IEEE Communications magazine*, vol. 35, no. 7, pp. 90–100, 2002.
- [23] A. Abdi, C. Tepedelenlioglu, M. Kaveh, and G. Giannakis, "On the estimation of the k parameter for the rice fading distribution," *IEEE Communications letters*, vol. 5, no. 3, pp. 92–94, 2002.
- [24] M. K. Simon and M.-S. Alouini, *Digital communication over fading channels*. John Wiley & Sons, 2004.
- [25] M. D. Yacoub, "The  $\kappa$ - $\mu$  distribution and the  $\eta$ - $\mu$  distribution," *IEEE Antennas and Propagation Magazine*, vol. 49, no. 1, pp. 68–81, 2007.
- [26] K. Kiasaleh, "Performance of apd-based, ppm free-space optical communication systems in atmospheric turbulence," *IEEE transactions on communications*, vol. 53, no. 9, pp. 1455–1461, 2005.
- [27] H. Nistazakis, V. Assimakopoulos, and G. Tombras, "Performance estimation of free space optical links over negative exponential atmospheric turbulence channels," *Optik*, vol. 122, no. 24, pp. 2191–2194, 2011.
- [28] M. Uysal and J. Li, "Ber performance of coded free-space optical links over strong turbulence channels," in 2004 IEEE 59th Vehicular Technology Conference. VTC 2004-Spring (IEEE Cat. No. 04CH37514), vol. 1. IEEE, 2004, pp. 352–356.
- [29] W. Gappmair and M. Flohberger, "Error performance of coded fso links in turbulent atmosphere modeled by gamma-gamma distributions," *IEEE transactions on wireless communications*, vol. 8, no. 5, pp. 2209–2213, 2009.
- [30] A. Jurado-Navas, J. M. Garrido-Balsells, J. F. Paris, A. Puerta-Notario, and J. Awrejcewicz, "A unifying statistical model for atmospheric optical scintillation," *Numerical simulations of physical and engineering processes*, vol. 181, no. 8, pp. 181–205, 2011.
- [31] H.-B. Jeon, S.-M. Kim, H.-J. Moon, D.-H. Kwon, J.-W. Lee, J.-M. Chung, S.-K. Han, C.-B. Chae, and M.-S. Alouini, "Free-space optical communications for 6G wireless networks: Challenges, opportunities, and prototype validation," *IEEE Communications Magazine*, vol. 61, no. 4, pp. 116–121, 2023.
- [32] A. Celik, I. Romdhane, G. Kaddoum, and A. M. Eltawil, "A top-down survey on optical wireless communications for the internet of things," *IEEE Communications Surveys & Tutorials*, 2022.
- [33] E. Lee, J. Park, D. Han, and G. Yoon, "Performance analysis of the asymmetric dual-hop relay transmission with mixed RF/FSO links," *IEEE Photonics Technology Letters*, vol. 23, no. 21, pp. 1642–1644, 2011.

- [34] K. T. Hemachandra and N. C. Beaulieu, "Outage analysis of opportunistic scheduling in dual-hop multiuser relay networks in the presence of interference," *IEEE Transactions on Communications*, vol. 61, no. 5, pp. 1786–1796, 2013.
- [35] I. S. Ansari, F. Yilmaz, and M.-S. Alouini, "Impact of pointing errors on the performance of mixed RF/FSO dual-hop transmission systems," *IEEE Wireless Communications Letters*, vol. 2, no. 3, pp. 351–354, 2013.
- [36] S. Anees and M. R. Bhatnagar, "Performance of an amplify-and-forward dual-hop asymmetric RF–FSO communication system," *Journal of Optical Communications and Networking*, vol. 7, no. 2, pp. 124–135, 2015.
- [37] L. Han, X. Liu, Y. Wang, and B. Li, "Performance analysis of mixed Rayleigh and  $\mathcal{F}$  distribution RF-FSO cooperative systems with AF relaying," *Electronics*, vol. 11, no. 15, p. 2299, 2022.
- [38] D. R. Pattanayak, S. Rai, V. K. Dwivedi, and G. Singh, "A statistical channel model for a decode-and-forward based dual hop mixed RF/FSO relay network," *Optical and Quantum Electronics*, vol. 50, pp. 1–17, 2018.
- [39] V. Palliyembil, J. Vellakudiyan, and P. Muthuchidambaranathan, "Performance analysis of RF-FSO communication systems over the Málaga distribution channel with pointing error," *Optik*, vol. 247, p. 167891, 2021.
- [40] I. Avram, N. Aerts, H. Bruneel, and M. Moeneclaey, "Quantize and forward cooperative communication: Channel parameter estimation," *IEEE Transactions on Wireless Communications*, vol. 11, no. 3, pp. 1167–1179, 2012.
- [41] K. Kumar and D. K. Borah, "Quantize and encode relaying through FSO and hybrid FSO/RF links," *IEEE Transactions on Vehicular Technology*, vol. 64, no. 6, pp. 2361–2374, 2014.
- [42] J. Ding, X. Xie, L. Tan, J. Ma, and D. Kang, "Dual-hop RF/FSO systems over  $\kappa$ - $\mu$  shadowed and Fisher-Snedecor  $\mathcal{F}$ ," *Journal of Lightwave Technology*.
- [43] M. A. Amirabadi and V. T. Vakili, "A novel hybrid FSO/RF communication system with receive diversity," *Optik*, vol. 184, pp. 293–298, 2019.
- [44] W. Zhang, S. Hranilovic, and C. Shi, "Soft-switching hybrid fso/rf links using short-length raptor codes: Design and implementation," *IEEE Journal on Selected Areas in Communications*, vol. 27, no. 9, pp. 1698–1708, December 2009.
- [45] I. S. Ansari, M.-S. Alouini, and F. Yilmaz, "On the performance of hybrid RF and RF/FSO fixed gain dual-hop transmission systems," in 2013 Saudi International Electronics, Communications and Photonics Conference. IEEE, 2013, pp. 1–6.
- [46] N. Nikbakht-Sardari, M. Ghiamy, M. E. Akbari, and A. Charmin, "Novel adaptive hard-switching based hybrid RF-FSO system architecture using two threshold values in the presence of atmospheric turbulence and pointing error," *Results in engineering*, vol. 17, p. 100813, 2023.

- [47] B. Bag, A. Das, I. S. Ansari, A. Prokeš, C. Bose, and A. Chandra, "Performance analysis of hybrid fso systems using FSO/RF-FSO link adaptation," *IEEE Photonics Journal*, vol. 10, no. 3, pp. 1–17, 2018.
- [48] A. Tahami, A. Dargahi, K. Abedi, and A. Chaman-Motlagh, "A new relay based architecture in hybrid RF/FSO system," *Physical Communication*, vol. 36, p. 100818, 2019.
- [49] S. Zhalehpour and M. Uysal, "Performance of multiuser scheduling in free space optical systems over atmospheric turbulence channels," *IET Optoelectronics*, vol. 9, no. 5, pp. 275–281, 2015.
- [50] J. Abouei and K. N. Plataniotis, "Multiuser diversity scheduling in free-space optical communications," *Journal of Lightwave Technology*, vol. 30, no. 9, pp. 1351–1358, 2012.
- [51] P. Puri, P. Garg, and M. Aggarwal, "Multiple user pair scheduling in TWR assisted FSO systems," *Journal of Optical Communications and Networking*, vol. 8, no. 5, pp. 290–301, 2016.
- [52] F. S. Vetelino, C. Young, L. Andrews, and J. Recolons, "Aperture averaging effects on the probability density of irradiance fluctuations in moderate-to-strong turbulence," *Applied optics*, vol. 46, no. 11, pp. 2099–2108, 2007.
- [53] L. C. Andrews, "Aperture-averaging factor for optical scintillations of plane and spherical waves in the atmosphere," *Journal of the Optical Society of America A*, vol. 9, no. 4, pp. 597–600, 1992.
- [54] X. Zhu and J. M. Kahn, "Free-space optical communication through atmospheric turbulence channels," *IEEE Transactions on communications*, vol. 50, no. 8, pp. 1293–1300, 2002.
- [55] J. Li and M. Uysal, "Optical wireless communications: system model, capacity and coding," in 2003 IEEE 58th Vehicular Technology Conference. VTC 2003-Fall (IEEE Cat. No. 03CH37484), vol. 1. IEEE, 2003, pp. 168–172.
- [56] E. J. Lee and V. W. Chan, "Part 1: Optical communication over the clear turbulent atmospheric channel using diversity," *IEEE journal on selected areas in communications*, vol. 22, no. 9, pp. 1896–1906, 2004.
- [57] W. O. Popoola, Z. Ghassemlooy, and V. Ahmadi, "Performance of sub-carrier modulated free-space optical communication link in negative exponential atmospheric turbulence environment," *International Journal of Autonomous and Adaptive Communications Systems*, vol. 1, no. 3, pp. 342–355, 2008.
- [58] P. D. Todorovic, B.Jaksic and M.Bandur, "Analysis of signal quality in FSO systems with PolSK modulation," *Serbian Journal of Electrical Engineering*, vol. 17, no. 2, pp. 171–186, 2020.

- [59] Piyush, N. Jayanthi, and M. Lakshmanan, "Closed form expressions of AC and SER for double GG fading distribution under EGC Scheme in FSO communication system," *Wireless Personal Communications*, vol. 127, no. 4, pp. 2935–2954, 2022.
- [60] O. S. Badarneh, F. El Bouanani, F. Almehmadi, and H. S. Silva, "FSO communications over doubly inverted Gamma-Gamma turbulence channels with nonzero-boresight pointing errors," *IEEE Wireless Communications Letters*, 2023.
- [61] Y. M. Shishter, R. Young, and F. H. Ali, "General statistical model of irradiance fluctuations in free space optics," *Journal of the Optical Society of America A*, vol. 40, no. 1, pp. 53–63, 2023.
- [62] A. A. Ibrahim, S. Özgür Ata, E. Erdoğan, and L. Durak-Ata, "Performance analysis of free space optical communication systems over imprecise Málaga fading channels," *Optics Communications*, vol. 457, p. 124694, 2020.
- [63] N. D. Chatzidiamantis, H. G. Sandalidis, G. K. Karagiannidis, S. A. Kotsopoulos, and M. Matthaiou, "New results on turbulence modeling for free-space optical systems," in *2010 17th International Conference on Telecommunications*. IEEE, 2010, pp. 487–492.
- [64] O. S. Badarneh, R. Derbas, F. S. Almehmadi, F. El Bouanani, and S. Muhaidat, "Performance analysis of FSO communications over  $\mathcal{F}$  turbulence channels with pointing errors," *IEEE Communications Letters*, vol. 25, no. 3, pp. 926–930, 2020.
- [65] S. N. Khalighi, Mohammad-Ali, N. Aitamer, and S. Bourennane, "Fading reduction by aperture averaging and spatial diversity in optical wireless systems," *Journal of optical communications and networking*, vol. 1, no. 6, pp. 580–593, 2009.
- [66] X. Li, X. Zhao, P. Zhang, and S. Tong, "BER performance of FSO communication system with differential signaling over correlated atmospheric turbulence fading," *China Communications*, vol. 17, no. 4, pp. 51–65, 2020.
- [67] M. Sharma, D. Chadha, and V. Chandra, "High-altitude platform for free-space optical communication: Performance evaluation and reliability analysis," *Journal of Optical Communications and Networking*, vol. 8, no. 8, pp. 600–609, 2016.
- [68] M. R. Bhatnagar and Z. Ghassemlooy, "Performance analysis of Gamma–Gamma fading FSO MIMO links with pointing errors," *Journal of Lightwave technology*, vol. 34, no. 9, pp. 2158–2169, 2016.
- [69] H. Singh and A. S. Sappal, "Moment-based approach for statistical and simulative analysis of turbulent atmospheric channels in FSO communication," *IEEE Access*, vol. 7, pp. 11 296–11 317, 2019.

- [70] K. Prabu and D. S. Kumar, "BER analysis of DPSK–SIM over MIMO free space optical links with misalignment," *Optik*, vol. 125, no. 18, pp. 5176–5180, 2014.
- [71] T. Singh, Sandhya, R. Srivastava, S. Yadav, M. Lakshmanan, S. Katiyar, and P. Jain, "Performance analysis of free space optical communication system over Double Generalized Gamma distribution with polarization shift keying modulation," in *Advances in Smart Communication and Imaging Systems: Select Proceedings of MedCom 2020.* Springer, 2021, pp. 211–220.
- [72] H. Kong, M. Lin, W.-P. Zhu, H. Amindavar, and M.-S. Alouini, "Multiuser scheduling for asymmetric FSO/RF links in satellite-UAV-terrestrial networks," *IEEE Wireless Communications Letters*, vol. 9, no. 8, pp. 1235–1239, 2020.
- [73] A. K. Mandpura and S. Prakriya, "Outage performance of scheduling in a distributed multiuser fixed-gain AF relay system with co-channel interference and noise," in 2016 International Conference on Signal Processing and Communications (SPCOM). IEEE, 2016, pp. 1–5.
- [74] M. A. Amirabadi and V. T. Vakili, "Performance of a relay-assisted hybrid FSO/RF communication system," *Physical communication*, vol. 35, p. 100729, 2019.
- [75] L. Yang, M. O. Hasna, and I. S. Ansari, "unified performance analysis for multiuser mixed  $\eta \mu$  and  $\mathcal{M}$  distribution dual-hop RF/FSO systems," *IEEE Transactions on Communications*, vol. 65, no. 8, pp. 3601–3613, 2017.
- [76] A. M. Salhab, "Performance of multiuser mixed RF/FSO relay networks with generalized order user scheduling and outdated channel information," *Arabian Journal for Science and Engineering*, vol. 40, pp. 2671–2683, 2015.
- [77] A. H. Abd El-Malek, A. M. Salhab, S. A. Zummo, and M.-S. Alouini, "Security-reliability trade-off analysis for multiuser SIMO mixed RF/FSO relay networks with opportunistic user scheduling," *IEEE Transactions on Wireless Communications*, vol. 15, no. 9, pp. 5904–5918, 2016.
- [78] —, "Physical layer security enhancement in multiuser mixed RF/FSO relay networks under RF interference," in 2017 IEEE Wireless Communications and Networking Conference (WCNC). IEEE, 2017, pp. 1–6.
- [79] V. K. Tonk, A. Upadhya, P. K. Yadav, and V. K. Dwivedi, "Mixed MUD-RF/FSO two way dcode and forward relaying networks in the presence of co-channel interference," *Optics Communications*, vol. 464, p. 125415, 2020.
- [80] I. Trigui, S. Affes, A. M. Salhab, and M.-S. Alouini, "Multi-user mixed FSO-RF systems with aperture selection under poisson field interference," *IEEE Access*, vol. 7, pp. 73764–73781, 2019.
- [81] A. Upadhya, V. K. Dwivedi, and G. Singh, "Multiuser diversity for mixed RF/FSO cooperative relaying in the presence of interference," *Optics Communications*, vol. 442, pp. 77–83, 2019.

- [82] A. Goel and R. Bhatia, "On the performance of mixed user diversity-RF/spatial diversity-FSO cooperative relaying AF systems," *Optics Communications*, vol. 477, p. 126333, 2020.
- [83] A. H. Abd El-Malek, A. M. Salhab, S. A. Zummo, and M.-S. Alouini, "Effect of RF interference on the security-reliability tradeoff analysis of multiuser mixed RF/FSO relay networks with power allocation," *Journal of Lightwave Technology*, vol. 35, no. 9, pp. 1490–1505, 2017.
- [84] K. O. Odeyemi and P. A. Owolawi, "On the performance of transmit antenna selection in multiuser asymmetric RF/FSO system under generalized order user scheduling," *Optik*, vol. 197, p. 163102, 2019.
- [85] K. S. Ahn and R. W. Heath, "Performance analysis of maximum ratio combining with imperfect channel estimation in the presence of cochannel interferences," *IEEE Transactions on Wireless Communications*, vol. 8, no. 3, pp. 1080–1085, 2009.
- [86] X. Li, Y. Li, X. Song, J. Li, and S. Zhao, "Physical layer security analysis of hybrid FSO/RF systems in SAGIN with channel imperfection and interference," *IEEE Transactions on Aerospace and Electronic Systems*, pp. 1–15, 2025.
- [87] Y. Zhuang and J. Zhang, "Secrecy performance analysis for a NOMA based FSO-RF system with imperfect CSI," *J. Opt. Commun. Netw.*, vol. 14, no. 7, pp. 500–510, 2022.
- [88] Z. Zhang, Q. Sun, M. López-Benítez, X. Chen, and J. Zhang, "Performance analysis of dual-hop RF/FSO relaying systems with imperfect CSI," *IEEE Transactions on Vehicular Technology*, vol. 71, no. 5, pp. 4965–4976, 2022.
- [89] H. Lei, H. Luo, K.-H. Park, I. S. Ansari, W. Lei, G. Pan, and M.-S. Alouini, "On secure mixed RF-FSO systems with TAS and imperfect CSI," *IEEE transactions on communications*, vol. 68, no. 7, pp. 4461–4475, 2020.
- [90] H. Lei, H. Luo, K.-H. Park, Z. Ren, G. Pan, and M.-S. Alouini, "Secrecy outage analysis of mixed RF-FSO systems with channel imperfection," *IEEE Photonics Journal*, vol. 10, no. 3, pp. 1–13, 2018.
- [91] E. Balti and M. Guizani, "Mixed RF/FSO cooperative relaying systems with cochannel interference," *IEEE Transactions on Communications*, vol. 66, no. 9, pp. 4014–4027, 2018.
- [92] E. Balti, M. Guizani, and B. Hamdaoui, "Hybrid Rayleigh and Double-Weibull over impaired RF/FSO system with outdated CSI," in *2017 IEEE International Conference on Communications (ICC)*. IEEE, 2017, pp. 1–6.
- [93] M. Petkovic, G. T. Djordjevic, and I. B. Djordjevic, "Analysis of mixed RF/FSO system with imperfect CSI estimation," in 2017 19th International Conference on Transparent Optical Networks (ICTON). IEEE, 2017, pp. 1–7.

- [94] A. M. Salhab, F. S. Al-Qahtani, R. M. Radaydeh, S. A. Zummo, and H. Alnuweiri, "Power allocation and performance of multiuser mixed RF/FSO relay networks with opportunistic scheduling and outdated channel information," *Journal of Lightwave Technology*, vol. 34, no. 13, pp. 3259–3272, 2016.
- [95] G. T. Djordjevic, M. I. Petkovic, A. M. Cvetkovic, and G. K. Karagiannidis, "Mixed RF/FSO relaying with outdated channel state information," *IEEE Journal on Selected Areas in Communications*, vol. 33, no. 9, pp. 1935–1948, 2015.
- [96] Y. Gu, S. S. Ikki, and S. Aissa, "Opportunistic cooperative communication in the presence of co-channel interferences and outdated channel information," *IEEE Communications Letters*, vol. 17, no. 10, pp. 1948–1951, 2013.
- [97] Y. Wu, G. Li, and D. Kong, "Performance analysis of relay-aided hybrid FSO/RF cooperation communication system over the generalized turbulence channels with pointing errors and Nakagami-*m* fading channels," *Sensors*, vol. 23, no. 13, p. 6191, 2023.
- [98] M. Siddharth, S. Shah, N. Vishwakarma, and R. Swaminathan, "Performance analysis of adaptive combining based hybrid FSO/RF terrestrial communication," *IET Communications*, vol. 14, no. 22, pp. 4057–4068, 2020.
- [99] K. O. Odeyemi and P. A. Owolawi, "Selection combining hybrid FSO/RF systems over generalized induced-fading channels," *Optics Communications*, vol. 433, pp. 159–167, 2019.
- [100] H. Khalid, S. S. Muhammad, H. E. Nistazakis, and G. S. Tombras, "Performance analysis of hard-switching based hybrid FSO/RF system over turbulence channels," *Computation*, vol. 7, no. 2, p. 28, 2019.
- [101] W. M. R. Shakir, "Performance evaluation of a selection combining scheme for the hybrid FSO/RF system," *IEEE Photonics Journal*, vol. 10, no. 1, pp. 1–10, 2017.
- [102] A. Touati, A. Abdaoui, F. Touati, M. Uysal, and A. Bouallegue, "On the effects of combined atmospheric fading and misalignment on the hybrid FSO/RF transmission," *Journal of Optical Communications and Networking*, vol. 8, no. 10, pp. 715–725, 2016.
- [103] T. Rakia, H.-C. Yang, M.-S. Alouini, and F. Gebali, "Outage analysis of practical FSO/RF hybrid system with adaptive combining," *IEEE Communications Letters*, vol. 19, no. 8, pp. 1366–1369, 2015.
- [104] M. Usman, H.-C. Yang, and M.-S. Alouini, "Practical switching-based hybrid FSO/RF transmission and its performance analysis," *IEEE Photonics journal*, vol. 6, no. 5, pp. 1–13, 2014.
- [105] P. S. Bithas, H. E. Nistazakis, A. Katsis, and L. Yang, "Hybrid FSO/RF communications in space–air–ground integrated networks: A reduced overhead link selection policy," *Electronics*, vol. 13, no. 4, p. 806, 2024.

- [106] H. Joshi and S. Gupta, "On the performance of dual-hop mixed RF and hybrid RF-FSO relaying," *Optical and Quantum Electronics*, vol. 55, no. 9, p. 803, 2023.
- [107] V. Bankey, S. Sharma, A. Madhukumar *et al.*, "Physical layer security of HAPS-based space—air—ground-integrated network with hybrid FSO/RF communication," *IEEE Transactions on Aerospace and Electronic Systems*, vol. 59, no. 4, pp. 4680–4688, 2022.
- [108] R. Deka, V. Mishra, I. Ahmed, S. Anees, and M. S. Alam, "On the performance and optimization of HAPS assisted dual-hop hybrid RF/FSO system," *IEEE Access*, vol. 10, pp. 80 976–80 988, 2022.
- [109] D. R. Pattanayak, V. K. Dwivedi, and V. Karwal, "On the physical layer security of hybrid RF-FSO system in presence of multiple eavesdroppers and receiver diversity," *Optics Communications*, vol. 477, p. 126334, 2020.
- [110] M. Torabi and R. Effatpanahi, "Performance analysis of hybrid RF–FSO systems with amplify-and-forward selection relaying," *Optics Communications*, vol. 434, pp. 80–90, 2019.
- [111] P. Chen, K. Buis, and X. Zhao, "A comprehensive toolbox for the Gamma distribution: The gammadist package," *Journal of Quality Technology*, vol. 55, no. 1, pp. 75–87, 2023.
- [112] I. S. Gradshteyn and I. M. Ryzhik, *Table of integrals, series, and products*. Academic press, 2014.
- [113] Wolfram, *The Wolfram functions site*. [Online]. Available: http://functions.wolfram.com.
- [114] X. Fan, J. Niu, J. Cheng, and J. Ma, "Few-mode fiber-based free-space optical communication with nonzero boresight pointing errors," *IEEE Photonics Technology Letters*, vol. 33, no. 10, pp. 519–522, 2021.
- [115] D. Wayne, "The PDF of irradiance for a free-space optical communications channel: A physics based model," 2010.
- [116] Z.-H. Yang and Y.-M. Chu, "On approximating the modified bessel function of the second kind," *Journal of inequalities and applications*, vol. 2017, no. 1, pp. 1–8, 2017.
- [117] Z. S. Guanjun Xu, "Performance analysis for mixed  $\kappa \mu$  fading and M-distribution dual-hop radio frequency/free space optical communication systems," *IEEE Transactions on Wireless Communications*, vol. 20, no. 3, pp. 1517–1528, 2020.
- [118] P. Puri, P. Garg, and M. Aggarwal, "Bi-directional relay-assisted FSO communication systems over strong turbulence channels with pointing errors," *International Journal of Communication Systems*, vol. 30, no. 4, p. e3027, 2017.

- [119] M. Siddharth, S. Shah, N. Vishwakarma, and R. Swaminathan, "Performance analysis of adaptive combining based hybrid FSO/RF terrestrial communication," *IET Communications*, vol. 14, no. 22, pp. 4057–4068, 2020.
- [120] J. Ding, X. Xie, L. Tan, J. Ma, and D. Kang, "Dual-hop RF/FSO systems over  $k-\mu$  shadowed and Fisher-Snedecor  $\mathcal F$  fading channels with non-zero boresight pointing errors," *Journal of Lightwave Technology*, vol. 40, no. 3, pp. 708–719, 2022.
- [121] O. M. S. Al-Ebraheemy, A. M. Salhab, A. Chaaban, S. A. Zummo, and M.-S. Alouini, "Precise performance analysis of dual-hop mixed RF/unified-FSO DF relaying with heterodyne detection and two IM-DD channel models," *IEEE Photonics Journal*, vol. 11, no. 1, pp. 1–22, 2019.
- [122] A. Bletsas, H. Shin, and M. Z. Win, "Cooperative communications with optimal opportunistic relaying," *IEEE Transactions on Wireless Communications*, vol. 6, no. 9, pp. 3450–3460, 2007.
- [123] A. K. Mandpura and S. Prakriya, "Outage performance of scheduling in a distributed multiuser fixed-gain AF relay system with co-channel interference and noise," in 2016 International Conference on Signal Processing and Communications (SPCOM). IEEE, 2016, pp. 1–5.
- [124] R. M. Corless, G. H. Gonnet, D. E. Hare, D. J. Jeffrey, and D. E. Knuth, "On the Lambert W function," *Advances in Computational mathematics*, vol. 5, pp. 329–359, 1996.
- [125] E. Nam, C. Jang, and J. H. Lee, "Performance analysis of CDF-based relay selection in dual-hop wireless networks," *IEEE Transactions on Vehicular Technology*, vol. 64, no. 6, pp. 2742–2748, 2014.
- [126] X. Ge, H. Jin, and V. C. Leung, "Cdf-based scheduling algorithm for proportional throughput fairness," *IEEE Communications Letters*, vol. 20, no. 5, pp. 1034–1037, 2016.
- [127] O. S. Badarneh, R. Derbas, F. S. Almehmadi, and M. Mansour, "Free-space optical communications over imperfect  $\mathcal{F}$  turbulence channels with pointing errors," *Telecommunication Systems*, vol. 83, no. 1, pp. 41–50, 2023.
- [128] A. P. Prudnikov, I. A. Brychkov, and O. I. Marichev, *Integrals and series: special functions*. CRC press, 1986, vol. 2.
- [129] E. Nam, C. Jang, and J. H. Lee, "Performance analysis of CDF-based relay selection in dual-hop wireless networks," *IEEE Transactions on Vehicular Technology*, vol. 64, no. 6, pp. 2742–2748, 2014.
- [130] P. K. Singya, N. Kumar, V. Bhatia, and M.-S. Alouini, "On the performance analysis of higher order QAM schemes over mixed RF/FSO systems," *IEEE Transactions on Vehicular Technology*, vol. 69, no. 7, pp. 7366–7378, 2020.

- [131] D. B. da Costa, H. Ding, and J. Ge, "Interference-limited relaying transmissions in dual-hop cooperative networks over Nakagami-m fading," *IEEE Communications Letters*, vol. 15, no. 5, pp. 503–505, 2011.
- [132] A. P. Prudnikov, J. A. Bryčkov, and O. I. Maričev, *Integrals and series. Vol. 1, Elementary functions.* Gordon and Breach, 1988.
- [133] P. Mittal and K. Gupta, "An integral involving generalized function of two variables," in *Proceedings of the Indian academy of sciences-section A*, vol. 75, no. 3. Springer, 1972, pp. 117–123.
- [134] World Weather Online. (2021) [Accessed: 28-Jul-2021]. [Online]. Available: https://www.worldweatheronline.com/lehweather-averages/jammu-and-kashmir/in.aspx
- [135] Z. Ghassemlooy, W. O. Popoola, and E. Leitgeb, "Free-space optical communication using subcarrier modulation in gamma-gamma atmospheric turbulence," in 2007 9th international conference on transparent optical networks, vol. 3. IEEE, 2007, pp. 156–160.
- [136] K. Peppas, H. E. Nistazakis, V. D. Assimakopoulos, and G. S. Tombras, "Performance analysis of SISO and MIMO FSO communication systems over turbulent channels," *Optical communication*, pp. 415–438, 2012.
- [137] R. Rani, N. Jayanthi, and A. Mandpura, "Power allocation & CAR optimization in multiuser dual-hop RF/FSO DF relaying systems with channel estimation error," *IEEE Transactions on Green Communications and Networking*, pp. 1–1, 2025.

## **Appendices**

## Appendix-I

## CDF of the RF link for CDF-based Scheduling Scheme with Perfect CSI

In this appendix, we explain the derivation of (4.22). The expression (4.21) is further evaluated by assuming  $U_m = F_{\Gamma_{m,r}}(x)$  which follows a uniform distribution in the range [0,1], leading to the following computation:

$$\mathbf{F}^{\mathrm{CDFS}}_{\Gamma_{m^*,r}}(\gamma_{th}) = \sum_{m=1}^{M} \mathrm{Pr}\Bigg(U_k^{\frac{1}{\upsilon_k}} < U_m^{\frac{1}{\upsilon_m}}, \forall \ k\epsilon 1, 2...M \bigcap \Gamma_{m,r} < \gamma_{th}\Bigg). \tag{I.1}$$

where,  $\Gamma_{m,r}=\frac{X_m}{Z+1}$  as defined in (4.2). Since, the range of  $U_m$  under the condition  $(\Gamma_{m,r}<\gamma_{th})$  is  $U_m\epsilon[0,F_{\Gamma_{m,r}}(\gamma_{th})]$  that leads to the following expression for the CDF of the RF link:

$$\mathbf{F}_{\Gamma_{m^*,r}}^{\text{CDFS}}(\gamma_{th}) = \sum_{m=1}^{M} \int_{0}^{F_{\Gamma_{m,r}}(\gamma_{th})} \prod_{\substack{k=1,2..M\\k \neq m}} F_{U_k}(u_m^{\frac{\upsilon_k}{\upsilon_m}}) f_{U_m}(u_m) du_m. \tag{I.2}$$

By considering  $U_k$  is an independent and uniformly distributed which is defined as  $F_{U_h}(x) = x$  in (I.2), then it becomes:

$$\mathbf{F}_{\Gamma_{m^*,r}}^{\text{CDFS}}(\gamma_{th}) = \sum_{m=1}^{M} \int_{0}^{F_{\Gamma_{m,r}}(\gamma_{th})} u_m^{\frac{1}{\upsilon_m} - 1} du_m. \tag{I.3}$$

Solving the integral and substituting (4.7) into (I.3) yields the closed-form expression of the RF link presented in (4.22).

## **Appendix-II**

## **Optimum Value of CAR with Perfect CSI**

The derivation of (4.36) is detailed in this appendix. Taking the first derivative of (4.35)and equate to zero. Further, simplify it into the form  $BA^x + x + c = 0$ , it becomes:

$$\begin{split} \frac{\lambda}{\ln\left(\frac{\gamma_{th}}{\gamma_{a}\Omega_{m,r}}\sum_{n=1}^{N}\gamma_{I_{n,r}}\Omega_{I_{n,r}}\right)} \left(\frac{\gamma_{th}}{\gamma_{a}\Omega_{m,r}}\sum_{n=1}^{N}\gamma_{I_{n,r}}\Omega_{I_{n,r}}\right)^{-\frac{1}{\upsilon_{m*}}} - \frac{1}{\upsilon_{m*}} \\ + \frac{1}{\ln\left(\frac{\gamma_{th}}{\gamma_{a}\Omega_{m,r}}\sum_{n=1}^{N}\gamma_{I_{n,r}}\Omega_{I_{n,r}}\right)} = 0. \quad \text{(II.1)} \end{split}$$

Further, using identity  $e^{\ln(x)} = x$  and multiply  $\left( \frac{\gamma_{th}}{\gamma_s \Omega_{m,r}} \sum_{n=1}^N \gamma_{I_{n,r}} \Omega_{I_{n,r}} \right)^{-\frac{1}{\ln\left(\frac{\gamma_{th}}{\gamma_s \Omega_{m,r}} \sum_{n=1}^N \gamma_{I_{n,r}} \Omega_{I_{n,r}}\right)}} \text{ on both sides, (II.1) is written as:}$ 

$$\begin{split} \frac{\lambda}{\ln\left(\frac{\gamma_{th}}{\gamma_{a}\Omega_{m,r}}\sum_{n=1}^{N}\gamma_{I_{n,r}}\Omega_{I_{n,r}}\right)} & \left(\frac{\gamma_{th}}{\gamma_{a}\Omega_{m,r}}\sum_{n=1}^{N}\gamma_{I_{n,r}}\Omega_{I_{n,r}}\right)^{-\frac{1}{\ln\left(\frac{\gamma_{th}}{\gamma_{a}\Omega_{m,r}}\sum_{n=1}^{N}\gamma_{I_{n,r}}\Omega_{I_{n,r}}\right)}} \\ & = \left(\frac{1}{v_{m^{*}}} - \frac{1}{\ln\left(\frac{\gamma_{th}}{\gamma_{a}\Omega_{m,r}}\sum_{n=1}^{N}\gamma_{I_{n,r}}\Omega_{I_{n,r}}\right)}\right) \\ & \times \left(e^{\ln\left(\frac{\gamma_{th}}{\gamma_{a}\Omega_{m,r}}\sum_{n=1}^{N}\gamma_{I_{n,r}}\Omega_{I_{n,r}}\right)}\right)^{\frac{1}{v_{m^{*}}} - \frac{1}{\ln\left(\frac{\gamma_{th}}{\gamma_{a}\Omega_{m,r}}\sum_{n=1}^{N}\gamma_{I_{n,r}}\Omega_{I_{n,r}}\right)}}. \end{split}$$
 (II.2)

Multiply both side by term,  $\ln\left(\frac{\gamma_{th}}{\gamma_s\Omega_{m,r}}\sum_{n=1}^N\gamma_{I_{n,r}}\Omega_{I_{n,r}}\right)$ , (II.2) is written as:

$$\begin{split} \lambda \left( \frac{\gamma_{th}}{\gamma_{a}\Omega_{m,r}} \sum_{n=1}^{N} \gamma_{I_{n,r}} \Omega_{I_{n,r}} \right)^{-\frac{1}{\ln\left(\frac{\gamma_{th}}{\gamma_{a}\Omega_{m,r}} \sum_{n=1}^{N} \gamma_{I_{n,r}} \Omega_{I_{n,r}}\right)}} = \\ \left( \frac{1}{\upsilon_{m^{*}}} - \frac{1}{\ln\left(\frac{\gamma_{th}}{\gamma_{a}\Omega_{m,r}} \sum_{n=1}^{N} \gamma_{I_{n,r}} \Omega_{I_{n,r}}\right)} \right) \ln\left(\frac{\gamma_{th}}{\gamma_{a}\Omega_{m,r}} \sum_{n=1}^{N} \gamma_{I_{n,r}} \Omega_{I_{n,r}}\right) \\ \times \left( e^{\ln\left(\frac{\gamma_{th}}{\gamma_{a}\Omega_{m,r}} \sum_{n=1}^{N} \gamma_{I_{n,r}} \Omega_{I_{n,r}}\right)} \right)^{\frac{1}{\upsilon_{m^{*}}} - \frac{1}{\ln\left(\frac{\gamma_{th}}{\gamma_{a}\Omega_{m,r}} \sum_{n=1}^{N} \gamma_{I_{n,r}} \Omega_{I_{n,r}}\right)}}. \end{split}$$
 (II.3)

Take the Lambert W on both side in (II.3) and utilize  $W(xe^x) = x$  provided by [124], it becomes:

$$\begin{split} W\left(\lambda\left(\frac{\gamma_{th}}{\gamma_{a}\Omega_{m,r}}\sum_{n=1}^{N}\gamma_{I_{n,r}}\Omega_{I_{n,r}}\right)^{-\frac{1}{\ln\left(\frac{\gamma_{th}}{\gamma_{a}\Omega_{m,r}}\sum_{n=1}^{N}\gamma_{I_{n,r}}\Omega_{I_{n,r}}\right)}}\right)\\ &=\left(\frac{1}{v_{m^{*}}}-\frac{1}{\ln\left(\frac{\gamma_{th}}{\gamma_{a}\Omega_{m,r}}\sum_{n=1}^{N}\gamma_{I_{n,r}}\Omega_{I_{n,r}}\right)}\right)\ln\left(\frac{\gamma_{th}}{\gamma_{a}\Omega_{m,r}}\sum_{n=1}^{N}\gamma_{I_{n,r}}\Omega_{I_{n,r}}\right). \end{split} \tag{II.4}$$

Therefore, (II.4) is solved for  $v_m^*$ , which results the required expression shown in (4.36).

## **Appendix-III**

## CDF of the RF hop for CDF based Scheduling with Imperfect CSI

In this appendix, we elaborate a detailed explanation of the steps involved in deriving (5.25). We evaluate the expression (5.24) by assuming  $\hat{U}_m = F_{\hat{\Gamma}_{m,r}}(x)$  where it follows a uniform distribution in the range [0,1]. This leads to the following computation:

$$\mathbf{F}^{\mathrm{CDFS}}_{\hat{\Gamma}_{m^*,r}}(\gamma_{th}) = \sum_{m=1}^{M} \mathrm{Pr}\Bigg(\hat{\boldsymbol{U}}_{k}^{\frac{1}{\upsilon_{k}}} < \hat{\boldsymbol{U}}_{m}^{\frac{1}{\upsilon_{m}}}, \forall \ k\epsilon 1, 2...M \bigcap \hat{\boldsymbol{\Gamma}}_{\mathrm{m,r}} < \gamma_{th}\Bigg). \tag{III.1}$$

where,  $\hat{\Gamma}_{\rm m,r}=\frac{\hat{X}_m}{\hat{Z}+1}$  as defined in (5.3). Since, the range of  $\hat{U}_m$  under the condition  $(\hat{\Gamma}_{\rm m,r}<\gamma_{th})$  is  $\hat{U}_m\epsilon[0,{\rm F}_{\hat{\Gamma}_{m,r}}(\gamma_{th})]$ , the CDF for the RF hop is expressed as:

$$\mathbf{F}^{\text{CDFS}}_{\hat{\Gamma}_{m^*,r}}(\gamma_{th}) = \sum_{m=1}^{M} \int_{0}^{\mathbf{F}_{\hat{\Gamma}_{m,r}}(\gamma_{th})} \prod_{\substack{k=1,2..M\\k\neq m}} F_{\hat{U}_k}(u_m^{\frac{v_k}{v_m}}) f_{\hat{U}_m}(u_m) du_m. \tag{III.2}$$

By considering  $\hat{U}_k$  is an independent and uniformly distributed which is defined as  $F_{\hat{U}_k}(x)=x$  in (III.2), it becomes :

$$\mathbf{F}^{\text{CDFS}}_{\hat{\Gamma}_{m^*,r}}(\gamma_{th}) = \sum_{m=1}^{M} \int_{0}^{\mathbf{F}_{\hat{\Gamma}_{m,r}}(\gamma_{th})} u_{m}^{\frac{1}{\upsilon_{m}} - 1} du_{m}. \tag{III.3}$$

Solving the above integral and substituting (5.8) into the expression yields the closed-form results given in (5.25) for the CDF based scheduling system.

## **Appendix-IV**

## Optimum Value of CAR with Imperfect CSI

The derivation of (5.40) is detailed in this appendix. Taking the first derivative of (5.39) and equate to zero. After simplify it into the form  $BA^x + x + c = 0$ , we yield:

$$\frac{\lambda}{\ln\left(\Lambda_{m,r}\right)} \left(\Lambda_{m,r}\right)^{-\frac{1}{\upsilon_{m^*}}} - \frac{1}{\upsilon_{m^*}} + \frac{1}{\ln\left(\Lambda_{m,r}\right)} = 0. \tag{IV.1}$$

Using Lambert W function, represented as  $W(xe^x) = x$  [124] in the above expression, it can be expressed as:

$$\frac{\lambda}{\ln\left(\Lambda_{m,r}\right)} = \left(\frac{1}{\upsilon_{m^*}} - \frac{1}{\ln\left(\Lambda_{m,r}\right)}\right) \left(\Lambda_{m,r}\right)^{\frac{1}{\upsilon_{m^*}}}.$$
 (IV.2)

Further, using identity  $e^{\ln(x)}=x$  and multiply  $\left(\Lambda_{m,r}\right)^{\frac{-1}{\ln(\Lambda_{m,r})}}$  on both sides, we get:

$$\frac{\lambda}{\ln\left(\Lambda_{m,r}\right)} \left(\Lambda_{m,r}\right)^{-\frac{1}{\ln(\Lambda_{m,r})}} = \left(\frac{1}{v_{m^*}} - \frac{1}{\ln\left(\Lambda_{m,r}\right)}\right) \left(e^{\ln(\Lambda_{m,r})}\right)^{\frac{1}{v_{m^*}} - \frac{1}{\ln(\Lambda_{m,r})}}.$$
(IV.3)

Multiplying both sides by  $\ln (\Lambda_{m,r})$ , we can written (IV.3) as:

$$\lambda \left( \Lambda_{m,r} \right)^{-\frac{1}{\ln(\Lambda_{m,r})}} = \left( \frac{1}{\upsilon_{m^*}} - \frac{1}{\ln\left(\Lambda_{m,r}\right)} \right) \ln\left(\Lambda_{m,r}\right) \left( e^{\ln(\Lambda_{m,r})} \right)^{\frac{1}{\upsilon_{m^*}} - \frac{1}{\ln(\Lambda_{m,r})}}. \tag{IV.4}$$

Now taking the Lambert W on both sides in (IV.4), we obtain:

$$W\left(\lambda\left(\Lambda_{m,r}\right)^{-\frac{1}{\ln\left(\Lambda_{m,r}\right)}}\right) = \left(\frac{1}{\upsilon_{m^*}} - \frac{1}{\ln\left(\Lambda_{m,r}\right)}\right)\ln\left(\Lambda_{m,r}\right). \tag{IV.5}$$

Further, solve (IV.5) for  $v_m^*$  which is the obtained expression as given in (5.40).

### **Appendix-V**

### **Proof of Equation (6.17)**

In this appendix, we elaborate a detailed explanation of the steps involved in deriving the equation as presented in (6.17). The expression for CDF-based scheduling is calculated by assuming  $F_{\Gamma_{SR}^{SR}}(x)$  follows a uniform distribution in the range [0,1] as given by [137]:

$$\mathbf{F}_{\Gamma_{m^*,r}^{\text{SR}}}^{\text{CDFS}}(\gamma_{th}) = \sum_{m=1}^{M} \upsilon_m \left( \mathbf{F}_{\Gamma_{m,r}^{\text{SR}}}(\gamma_{th}) \right)^{\frac{1}{\upsilon_m}}. \tag{V.1}$$

On the substitution of (6.9) in (V.1), the CDF of first-hop becomes:

$$\begin{split} \mathbf{F}_{\Gamma_{m^*,r}^{\mathrm{SR}}}(\gamma_{th}) &= \sum_{m=1}^{M} \upsilon_m \bigg(1 - \sum_{l=0}^{m_{\mathrm{m,r}}-1} \sum_{k=0}^{l} \binom{l}{k} \frac{\Gamma(k+m_{\mathrm{I}})}{l! \Gamma(m_{\mathrm{I}})} \bigg(\frac{\gamma_{\mathrm{I}} \Omega_{\mathrm{I}}}{m_{\mathrm{I}}}\bigg)^k \bigg(\frac{m_{\mathrm{m,r}}}{\gamma_{\mathrm{s}} \Omega_{\mathrm{m,r}}} y\bigg)^l \\ &\times e^{-\frac{m_{\mathrm{m,r}}}{\gamma_{\mathrm{s}} \Omega_{\mathrm{m,r}}} y} \frac{1}{\bigg(1 + \frac{m_{\mathrm{m,r}} \gamma_{\mathrm{I}} \Omega_{\mathrm{I}}}{m_{\mathrm{I}} \gamma_{\mathrm{s}} \Omega_{\mathrm{m,r}}} y\bigg)^{\frac{1}{\upsilon_m}}. \end{split} \tag{V.2}$$

To calculate the CDF of second-hop for hybrid FSO/RF system, substitute CDFs of (6.10) and (6.11) into (6.12), it is calculated as:

$$\begin{split} \mathbf{F}_{\Gamma^{\mathrm{RD}}_{\mathrm{hybrid}}}(x) &= \frac{\omega^2}{\Gamma(a)\Gamma(b)} G_{3,3}^{2,2} \left( \frac{a\omega^2}{(b-1)(1+\omega^2)} \sqrt{\frac{x}{\bar{\gamma}^{\mathrm{FSO}}_{\mathrm{r,d}}}} \middle| 1-b,1,1+\omega^2 \right) \\ &\qquad \qquad \left( 1 - \frac{\Gamma(m_{\mathrm{r,d}},\frac{m_{\mathrm{r,d}}}{\gamma^{\mathrm{RF}}_{\mathrm{r}}\Omega_{\mathrm{r,d}}}x)}{\Gamma(m_{\mathrm{r,d}})} \right). \quad \text{(V.3)} \end{split}$$

On substituting equations (V.2) and (V.3) into (6.15) and performing the required simplifications, we derive the final expression given in (6.17).

## **Appendix-VI**

## Optimum Value of CAR for Dual-hop MU-Hybrid FSO/RF System

The detailed steps leading to (6.33) are presented in this appendix. Taking the first derivative of (6.31) and equate to zero. After simplifying into the form  $XY^k + k + l = 0$ , we can obtained as follows:

$$\frac{\lambda}{\ln{(Z_{\rm m,r})}} \left(Z_{\rm m,r}\right)^{-\frac{1}{\upsilon_{m^*}}} - \frac{1}{\upsilon_{m^*}} + \frac{1}{\ln{(Z_{\rm m,r})}} = 0. \tag{VI.1}$$

By emplying the Lambert W function, defined as  $W(xe^x) = x$  in [124], the above expression can be expressed as:

$$\frac{\lambda}{\ln\left(Z_{\rm m,r}\right)} = \left(\frac{1}{\upsilon_{m^*}} - \frac{1}{\ln\left(Z_{\rm m,r}\right)}\right) \left(Z_{\rm m,r}\right)^{\frac{1}{\upsilon_{m^*}}}. \tag{VI.2}$$

Further, using identity  $e^{\ln(x)}=x$  and multiply  $(Z_{\mathbf{m,r}})^{\frac{-1}{\ln(Z_{\mathbf{m,r}})}}$  on both sides, we get:

$$\frac{\lambda}{\ln{(Z_{\rm m,r})}} (Z_{\rm m,r})^{\frac{-1}{\ln{(Z_{\rm m,r})}}} = \left(\frac{1}{\upsilon_{m^*}} - \frac{1}{\ln{(Z_{\rm m,r})}}\right) \left(e^{\ln{(Z_{m,r})}}\right)^{\frac{1}{\upsilon_{m^*}} - \frac{1}{\ln{(Z_{\rm m,r})}}}. \tag{VI.3}$$

Multiplying both sides by  $\ln(Z_{m,r})$ , we can written (VI.3) as:

$$\lambda \left( Z_{\rm m,r} \right)^{-\frac{1}{\ln(Z_{\rm m,r})}} = \left( \frac{1}{\upsilon_{m^*}} - \frac{1}{\ln\left( Z_{\rm m,r} \right)} \right) \ln \left( Z_{\rm m,r} \right) \left( e^{\ln(Z_{\rm m,r})} \right)^{\frac{1}{\upsilon_{m^*}} - \frac{1}{\ln(Z_{\rm m,r})}}. \tag{VI.4}$$

Now taking the Lambert W on both sides in (VI.4), we obtain:

$$W\left(\lambda\left(Z_{\rm m,r}\right)^{-\frac{1}{\ln\left(Z_{\rm m,r}\right)}}\right) = \left(\frac{1}{\upsilon_{m^*}} - \frac{1}{\ln\left(Z_{\rm m,r}\right)}\right)\ln\left(Z_{\rm m,r}\right). \tag{VI.5}$$

Therefore, (VI.5) is solved for  $v_m^*$  which is the desired expression given in (6.33).

#### Thesis Publications

Based on the work done in this thesis, the following publications have been produced:

#### SCI/SCIE Journal Publications

- R. Rani, N. Jayanthi, Anup Mandpura, "Performance Analysis of Free Space Optical System Over Inverse Gaussian Gamma Turbulence Channel," Transactions on Emerging Telecommunications Technologies, vol. 35, no. 11, 2024. (IF 2.5) (doi.org/10.1002/ett.70009)
- **R. Rani**, N. Jayanthi, Anup Mandpura, "Power Allocation and CAR Optimization in Multiuser Dual-hop RF/FSO DF Relaying Systems with Channel Estimation Error," IEEE Transactions on Green Communications and Networking, 2025. (IF 6.7) (doi.org/10.1109/TGCN.2025.3535523).
- R. Rani, N. Jayanthi, Anup Mandpura, "Outage Probability of CDF based Scheduling in Dual-hop Multiuser RF and hybrid FSO/RF system with Co-channel Interference," IEEE Transactions on Green Communications and Networking, 2025. (IF 6.7) (doi.org/10.1109/TGCN.2025.3619088).
- **R. Rani**, N. Jayanthi and A. Mandpura, "Optimal Power allocation and CAR in Multiuser Dual-hop RF/FSO DF Relaying Systems with CDF based Scheduling," International Journal of Communication Systems, vol. 38, no. 16, 2025. (IF 1.8) (doi.org/10.1002/dac.70280).

#### **Conference Publications**

- **R. Rani** and Gurjit Kaur, "Design and Analysis of MIMO FSO System and WDM FSO System for Leh (Ladakh), India under Worst Weather Conditions," IEEE International Conference on Signal Processing and Communication (ICSC), pp. 31–36, 2021. (doi.org/10.1109/ICSC53193.2021.9673278)
- R. Rani, N. Jayanthi and A. Mandpura, "Outage Performance Analysis and Power Allocation in Multiuser RF/FSO Relaying System with Proportional Fair Scheduling," IEEE International Conference on Computing Communication and Networking Technologies (ICCCNT), pp. 1–6, 2024. (doi.org/10.1109/ICCCNT61001.2024.10724598)
- R. Rani, N. Jayanthi and A. Mandpura, "Outage Analysis of Dual-hop Multiuser RF and Hybrid FSO/RF System with Proportional Fairness User Scheduling," IEEE International Conference on Computing Communication and Networking Technologies (ICCCNT), 2025. (Accepted)

#### **Paper Submitted**

• **R. Rani**, N. Jayanthi and A. Mandpura, "Joint Optimization of Power Allocation and CAR for Multiuser Dual-hop RF/FSO DF Relaying Systems with CDF based Scheduling," **communicated** in AEU - International Journal of Electronics and Communications.

## turnitin Page 1 of 151 - Cover Page

## main.pdf



Delhi Technological University

#### **Document Details**

Submission ID

trn:oid:::27535:103007396

**Submission Date** 

Jun 30, 2025, 1:12 PM GMT+5:30

Download Date

Jun 30, 2025, 1:17 PM GMT+5:30

File Name

main.pdf

File Size

7.7 MB

139 Pages

41,177 Words

196,618 Characters



Page 1 of 151 - Cover Page

Submission ID trn:oid:::27535:103007396



## 8% Overall Similarity

The combined total of all matches, including overlapping sources, for each database.

#### Filtered from the Report

- Bibliography
- Small Matches (less than 9 words)

#### **Exclusions**

▶ 1 Excluded Source

#### **Match Groups**

216Not Cited or Quoted 6%

Matches with neither in-text citation nor quotation marks

54 Missing Quotations 2%

Matches that are still very similar to source material

**2** Missing Citation 0%

Matches that have quotation marks, but no in-text citation

• 0 Cited and Quoted 0%

Matches with in-text citation present, but no quotation marks

#### **Top Sources**

4% 🌐 Internet sources

6% **Publications** 

4% Land Submitted works (Student Papers)

#### **Integrity Flags**

0 Integrity Flags for Review

No suspicious text manipulations found.

Our system's algorithms look deeply at a document for any inconsistencies that would set it apart from a normal submission. If we notice something strange, we flag it for you to review.

A Flag is not necessarily an indicator of a problem. However, we'd recommend you focus your attention there for further review.





## DELHI TECHNOLOGICAL UNIVERSITY

(Formerly Delhi College of Engineering) Shahbad Daulatpur, Main Bawana Road, Delhi-42

#### PLAGIARISM VERIFICATION

	Control and a final fina
)	
)	Title of the Thesis Design and Performance Analysis of impro- free Space Optical Communication system for Tuebulent At
)	Title of the Thesis Design and Performance Analysis of improfesse Space Optical Communication system for Turbulent At Total Pages 139 Name of the Scholar Ms. Rekhar Lauri
)	Supervisor (s)  Name of the Scholar 18 Ketha Coun
ン つ	
ノー	(1) Dr. N. Jayanthi (2) Dr. Arup Mandpuea
)	(3)
)	Department Electorice and Communication Engineering
)	0 1
	This is to report that the above thesis was scanned for similarity detection. Process and outcome is given below:
)	octow.
)	Software used: Turntin Similarity Index: 870, Total Word Count: 41,177
)	
)	Date: 30. June. 2025.
7	
√ \	
) \	
)	Lethe Leun'
)	Candidate's Signature Signature of Supervisor(s)
)	
)	

#### Rekha Rani

Department of Electronics and Communication Engineering

Email: rekhaaggarwalece@gmail.com

**Phone**: +91-9654272674

Orcid ID: orcid.org/0000-0002-3394-5989



#### **Profile**

Eight years of rich experience in teaching and research at various reputed institutions as an assistant professor. Expertise in Wireless Communication, Information Theory and Coding, Machine learning for 5G and 6G, MATLAB, OptiSystem, Mathematica, Mendeley, and Latex. Guided more than 40 B.Tech students with their major projects. Took additional responsibility of class coordinator, NBA committee member, External practical coordinator, Industrial visit coordinator, Project coordinator, and other duties performed.

#### **Academic Qualifications**

Year	Degree	Institute	CGPA/Percentage
2020-Present	Ph.D	Delhi Technological University, Delhi	9.5/10
2011	Master in Engineering	Thapar University, Patiala	9/10
2008	Bachelor of Technology	Punjab Technical University, Jalandhar	77%

#### **Work Experience**

• Visiting Faculty, ECE – Netaji Subhas University of Technology, Delhi	July' 25 – Present
Visiting Faculty, ECE – Bennett University, Greater Noida	Aug' 24 – May' 25
• Assistant Professor, ECE – Galgotia College of Engineering and Technology, Greater Noida	Aug' 17–Sep 23
• Assistant Professor, ECE – Sai College of Engineering and Technology, India	July 12 – Oct'13
• Lecturer, ECE – KCT College of Engineering and Technology, India	Sep' 11 – June 12

#### **Technical Skills**

- **Programming Languages:** MATLAB, Python, and related Libraries (TensorFlow, NumPy, Keras, Scikit-learn, Pytorch, Pandas, Matplotlib)
- Research-Oriented Software: Optisystem, LaTeX, Mendeley, Mathematica

#### **Relevant Courses**

Wireless and Mobile Communication	Digital Communication
Information Theory and Coding	Signal and System
Machine Learning for 5G and 6G wireless communication- IISc Bangalore	Advances in Optical Communications - IIIT Delhi
AI for Everyone - Coursera	Digital Circuits and Systems -NPTEL

#### Membership

- Life membership (AM-501420) of the Institution of Electronics and Telecommunication Engineers (IETE).
- Life membership (AM101000581299) of the Universal Association of Computer and Electronics Engineers.
- Life membership (No. 205465) of the International Association of Engineering (IAENG).

#### **Journal Publications**

- *Rekha Rani*, N. Jayanthi, Anup Mandpura, "Outage Probability of CDF based Scheduling in Dual-hop Multiuser RF and hybrid FSO/RF system with Co-channel Interference," IEEE Transactions on Green Communications and Networking. (IF 6.7) (doi.org/10.1109/TGCN.2025.3619088)
- *Rekha Rani*, N. Jayanthi, Anup Mandpura, "Power Allocation and CAR Optimization in Multiuser Dual-hop RF/FSO DF Relaying Systems with Channel Estimation Error," IEEE Transactions on Green Communications and Networking. (IF 6.7)(doi.org/10.1109/TGCN.2025.3535523)
- *Rekha Rani*, N. Jayanthi, Anup Mandpura,"Performance Analysis of Free Space Optical System Over Inverse Gaussian Gamma Turbulence Channel," Transactions on Emerging Telecommunications Technologies. (IF 2.5) (doi.org/10.1002/ett.70009)
- R. Rani, N. Jayanthi and A. Mandpura, "Optimal Power allocation and CAR in Multiuser Dual-hop RF/FSO DF Relaying Systems with CDF based Scheduling," International Journal of Communication Systems, vol. 38, no. 16, 2025. (IF 1.8) (doi.org/10.1002/dac.70280).
- M Lakshmanan, Rekha Rani, N. Jayanthi, "Unified Performance Analysis of Dual-Hop Radio Frequency/Free Space Optical

- System," Wireless Personal Communications. (IF 2.2)(doi.org/10.1007/s11277-024-11646-7)
- *Rekha Rani*, M Lakshmanan, Anup Mandpura, N. Jayanthi,"Pointing error influence on the performance of dual-hop radio frequency/wireless optical communication system over Nakagami-m/Fisher-Snedecor Turbulence channels," Photonic Network Communications. (IF 1.7) (doi.org/10.1007/s11107-025-01028-9)
- *Rekha Rani*, Gurjit Kaur, "Bidirectional transmission of High-Speed 704 Gbps using 64 Channels for Long reach DWDM-PON-PDCF System," in Telecommunications and Radio Engineering.(**Scopus**) (doi.org/10.1615/TelecomRadEng.2022038599)
- *Rekha Rani*, "Analytical Performance of LDPC Codes with OC in the Presence of Interferers," in International Journal of Engineering Trends and Technology. (Scopus)(doi.org/10.14445/22315381/IJETT-V12P225)

#### **Conference Publications**

- *Rekha Rani*, N. Jayanthi, Anup Mandpura, "Outage Analysis of Dual-hop Multiuser RF and Hybrid FSO/RF System with Proportional Fairness User Scheduling," in 2025 16th International Conference on ICCCNT, IIT Indore.
- *Rekha Rani*, N. Jayanthi, Anup Mandpura, "Outage Performance Analysis and Power Allocation in Multiuser RF/FSO Relaying System with Proportional Fair Scheduling," in 2024 15th International Conference on ICCCNT, IIT Mandi. (doi.org/10.1109/ICCCNT61001.2024.10724598)
- *Rekha Rani*, Gurjit Kaur, "Design and analysis of MIMO FSO system and WDM FSO system for Leh (Ladakh), India under worst weather conditions." in 2021 International Conference on signal processing and communication (ICSC). (doi.org/10.1109/ICSC53193.2021.9673278)
- Deepesh Joshi, Deergh Sharma, Himanshu Singh, Rachit Agrawal, *Rekha Rani*, AS Mohammed Shariff, "Performance Analysis of Mixed FSO-UWOC Dual-Hop Transmission System." in 2024 IEEE International Conference on Computing, Power and Communication Technologies (IC2PCT).(doi.org/10.1109/IC2PCT60090.2024.10486428)
- Abhishek Gupta, Kunjan Chauhan, Abhishek Yadav, *Rekha Rani*, Abhishek Jain, Lakshmanan M, "Performance Analysis of Adaptive Combining Based Hybrid FSO/RF Communication System with Pointing Errors Over F-Distribution/ Nakagamim Channel Models." in 2023 2nd International Conference on Vision Towards Emerging Trends in Communication and Networking Technologies (ViTECoN). (dx.doi.org/10.1109/ViTECoN58111.2023.10157930)
- Pranjal Tiwari, Ketan Rai, Naman Kumar Shukla, , Nitish Malik, Lakshmanan M, *Rekha Rani*, "Performance Enhancement of WDM-RoFSO Communication System under Different Weather Conditions." in 2023 2nd International Conference on Vision Towards Emerging Trends in Communication and Networking Technologies (ViTECoN). (doi.org/10.1109/ViTECoN58111.2023.10157005)
- *Rekha Rani*, Abhishek Tiwari, Aman Tiwari, Akshay Singh, Adarsh Singh, Lakshmanan M, "Outage Performance of Hybrid FSO/RF-FSO Communication System with single threshold," in 2023 2nd International Conference on Vision Towards Emerging Trends in Communication and Networking Technologies (ViTECoN). (doi.org/10.1109/ViTECoN58111.2023.10157466)
- *Rekha Rani*, Gurjit Kaur, Shubham Gautam, M Lakshmanan, Shubham Kumar, "Performance Analysis of Dual-Hop Mixed RF/FSO System over Nakagami-m/Fisher Snedecor Fading Channels," in 2023 International Conference on Artificial Intelligence and Smart Communication (AISC). (doi.org/10.1109/AISC56616.2023.10085239)
- Shreyanshi Agrawal, Siddharth Saini, Tushar Sharma, *Rekha Rani*, M Lakshmanan, "BER Analysis of Hybrid LPPM-POLSK-SIM Over Double Generalized Gamma Distribution Incorporating Zero Boresight Pointing Error," in 2022 4th International Conference on Advances in Computing, Communication Control and Networking (ICAC3N). (doi.org/10.1109/ICAC3N56670.2022.10074537)
- *Rekha Rani*, Gurjit Kaur, Sirhan Maheshwari, Vikash Kumar Pandey, Sneha Porwal, "Outage probability analysis of RF/FSO System Over Nakagami-m Fading and Fisher-Snedecor Distribution with Pointing Error," in 2022 International Conference on Advances in Computing, Communication and Materials (ICACCM). (doi.org/10.1109/ICACCM56405.2022.10009180)
- Mansi Gupta, Gagan Agrawal, Namrata Kumari, *Rekha Rani*, "Bit error rate analysis for indoor optical wireless communication system," in Advances in Smart Communication and Imaging Systems: Select Proceedings of MedCom 2020. (10.1007/978-981-15-9938-5\_40)
- Akshit Chaurasia, Mayank Sharma, Abhinav Garg, *Rekha Rani*, "Statistical analysis of SNR and optical power distribution in an indoor VLC System," in Journal of Physics: Conference Series. (doi.org/10.1088/1742-6596/1706/1/012067)

#### **Book Chapters**

- *Rekha Rani*, Gurjit Kaur, "Performance evaluation of high-speed 320Gb/s bidirectional transmission for long reach DWDM-PON system," in Recent Trends in Communication and Electronics, CRC Press.
- *Rekha Rani*, Gurjit Kaur, Prabhjot Singh, "Smart Soil Monitoring System for Smart Agriculture," in Artificial Intelligence and IoT-Based Technologies for Sustainable Farming and Smart Agriculture, IGI Global.(10.4018/978-1-7998-1722-2.ch013)
- *Rekha Rani*, Gurjit Kaur, "Hybrid Wireless Optical Broadband Network (HWOBAN)", in Green optical communication systems, green communication Technologies for future networks: An energy-efficient perspective, CRC Press.